Final Report

FDOT Contract Number: BDV24-977-33

Prediction Model of Vibration-Induced Settlement due to Pile Driving

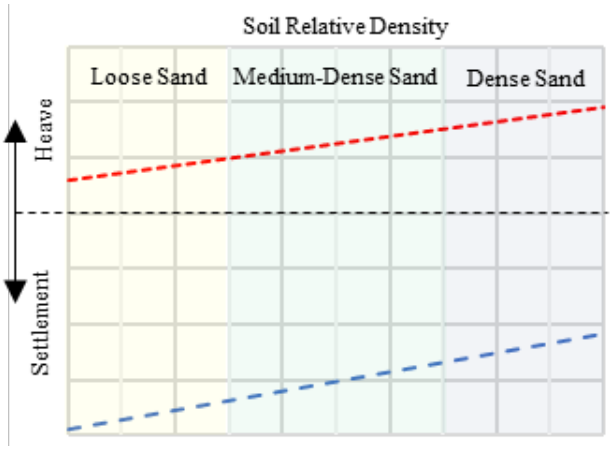

Principal Investigators: Luis G. Arboleda-Monsalve, Ph.D., Assistant Professor
Boo Hyun Nam, Ph.D., Associate Professor

Project Manager: Larry Jones

Graduate Students: Jorge E. Orozco-Herrera, Ph.D. Student
Berk Turkel, Ph.D. Candidate
Sergio Marin, Ph.D. Candidate

University of Central Florida
Department of Civil, Environmental and Construction Engineering
College of Engineering and Computer Science
Orlando, Florida 32816

February 2022

DISCLAIMER

The opinions, findings, and conclusions expressed in this publication are those of the authors and not necessarily those of the State of Florida Department of Transportation.

METRIC CONVERSION

APPROXIMATE CONVERSION TO SI UNITS

Symbol	When You Know	Multiply By	To Find	Symbol
		Length		
in	inches	25.4	millimeters	mm
ft	feet	0.305	meters	m
yd	yards	0.914	meters	m
mi	miles	1.61	kilometers	km

Symbol	When You Know	Multiply By	To Find	Symbol
		Area		
in^2	square inches	645.2	square millimeters	mm^2
ft^2	square feet	0.093	square meters	m^2
yd^2	square yard	0.836	square meters	m^2
ac	acres	0.405	hectares	ha
mi^2	square miles	2.59	square kilometers	km^2

Symbol	When You Know	Multiply By	To Find	Symbol
		Volume		
fl oz	fluid ounces	29.57	milliliters	mL
gal	gallons	3.785	liters	L
ft^3	cubic feet	0.028	cubic meters	m^3
yd^3	cubic yards	0.765	cubic meters	m^3

Symbol	When You Know	Multiply By	To Find	Symbol
		Mass		
oz	ounces	28.35	grams	g
lb	pounds	0.454	kilograms	kg
T	short tons (2000 lb)	0.907	megagrams (or "metric ton")	Mg (or "t")

Symbol	When You Know	Multiply By	To Find	Symbol
		Temperature (exact degrees)		
^oF	Fahrenheit	5 (F-32)/9 or (F-32)/1.8	Celsius	^oC

Symbol	When You Know	Multiply By	To Find	Symbol
		Force and Pressure or Stress		
lbf	poundforce	4.45	newtons	N
lbf/in^2	poundforce per square inch	6.89	kilopascals	kPa

TECHNICAL REPORT DOCUMENTATION PAGE

1. Report No.	2. Government Accession No.	3. Recipient's Catalog No.
Final Report		

4. Title and Subtitle	5. Report Date
Prediction Model of Vibration-Induced Settlement due to Pile Driving	February 2022
	6. Performing Organization Code
7. Author(s)	8. Performing Organization Report No.
Luis G. Arboleda-Monsalve, Boo Hyun Nam, Jorge E. Orozco-Herrera, and Berk Turkel	
9. Performing Organization Name and Address	10. Work Unit No. (TRAIS)
Department of Civil, Environmental, and Construction Engineering University of Central Florida 12800 Pegasus Drive, Suite 211 Orlando, Florida 32816-2450	11. Contract or Grant No. BDV24-977-33
12. Sponsoring Agency Name and Address	13. Type of Report and Period Covered
Florida Department of Transportation 605 Suwannee Street, MS 30 Tallahassee, FL 32366 – 6580	Final Report May 2019 –February 2022
	14. Sponsoring Agency Code

15. Supplementary Notes

16. Abstract

This report presents a method for predicting ground deformations caused by impact pile driving, which accounts explicitly for the attenuation characteristics of Central Florida-specific soil conditions. Currently, vibration limits are not linked to the amount of pile driving-induced deformations that soils will experience due to vibrations, which is important when repetitive and cumulative loadings are applied in predominantly sandy soils. The most important variables for the ground response due to impact pile driving operations of the most common deep foundation type in Florida (i.e., 18" to 30" square prestressed concrete piles) are considered: rated energy of the hammer, distance from the pile, pre-drilling, and soil relative density. Field data obtained from different construction sites in Central Florida are used to show ground deformations and their relationships with ground vibration levels. Common construction practices in the area are also analyzed from the reported field data. The analyses were conducted using a combination of field measurements and numerical analyses using with GRLWEAP and PLAXIS 2D. A continuous pile driving modeling approach, in which the pile is installed with a continuous time series of hammer impacts up to the target installation depth, was adopted in the numerical analyses based on comparisons of numerical modeling approaches performed for this report. An advanced constitutive soil model capable of reproducing changes in the void ratio of the soil during pile driving is used in the analyses. Numerical studies of the effects of impact pile driving installation methods on expected ground vibrations and deformations are presented. It is concluded that in cases where vibration levels did not exceed the limit defined by the Florida Department of Transportation (i.e., peak particle velocities not exceeding 0.5 in/s), ground deformations can still occur depending on the above-mentioned site-specific variables. Equations and charts useful for estimating ground deformation envelopes are proposed to provide guidance for researchers and practitioners relating ground deformations, peak particle velocities (PPV), rated energy of impact hammers, and distance away from the pile.

17. Key Word	18. Distribution Statement
Pile Driving, Vibrations, Ground Deformations.	No Restrictions

19. Security Classif. (of this report)	20. Security Classif. (of this page)	21. No. of Pages	22. Price
Unclassified	Unclassified	189	

ACKNOWLEDGEMENTS

The researchers would like to thank the Florida Department of Transportation for the financial support to conduct this research and the guidance from the project manager, Larry Jones. The authors also appreciate the help of FDOT District 5 Engineers Michael Byerly and Tharwat Hannadawod in coordinating the field-testing sites and providing relevant information about them. The field visits that the researchers performed would not have been possible without the help of Chris Briggs and Jose Medina at Jacobs, Arnaldo Larrazabal at RS&H, and Roger Gobin at WSP. The support of students Sergio Marin and Jaime Mercado at UCF was greatly appreciated.

EXECUTIVE SUMMARY

Impact pile driving is commonly used for the installation of deep foundations that support the loads transferred from civil engineering structure to the bearing soils. This installation method is common in Central Florida due to the soil conditions in the area consisting mainly of sandy soil deposits that allow a relatively fast pile installation. As a result, vibrations are generated in the surrounding soils, which might potentially trigger ground deformations and possible damage to nearby infrastructure. It is common practice in current designs and construction standards to focus mainly on pile driving-induced ground vibrations quantified in terms of peak particle velocities (PPVs). The Florida Department of Transportation (FDOT) limits construction-induced vibrations to 0.5 in/s (FDOT, 2021a). This limit is not formally linked to the amount of settlement or heave that soils will experience due to pile driving-induced vibrations which could trigger additional damage in nearby structures. This report includes a comprehensive analysis of current state of the art in terms of pile driving-induced ground deformations and a combination of field measurements, mostly performed in Central Florida, and numerical analyses to elucidate the effects of the most important variables that trigger those ground deformations: peak particle velocities (PPVs), rated energy of impact hammers, distance away from the pile, and relative density of soil.

A total of eleven bridge construction sites in the region of Central Florida is presented in this report. Four projects were located in Lake County (i.e., Sites A1, A2, B, and C), six in Orange County (i.e., Sites D, Z.1, Z.2, Z.3, Z.4, and Z.6), and one in Volusia County (i.e., Site A3). These sites were selected because dynamic tests were routinely conducted on prestressed concrete piles using impact hammers in these locations. This provided the opportunity to perform measurements on undisturbed ground as well as to take advantage of acceleration and strain measurements within the pile that are normally performed during these tests. Information corresponding to the field sites given in this report consists of: (i) type and size of piles, (ii) type of hammer and driving appurtenances used, (iii) pile driving sequence and procedure, and (iv) soil conditions. The subsurface conditions were characterized for most of the sites as sandy soils with varying relative densities ranging from loose to medium-dense. Field measurements in terms of ground deformations and vibrations performed at each project site are included. Ground deformations were measured by using survey equipment to track ground movements during impact pile driving. Ground vibration measurements were also performed by installing vertical geophones to measure particle velocities at different points away from the pile. PPVs were obtained from velocity time histories in order to compare with the existing FDOT limit of 0.5 in/s.

A series of finite element (FE) analyses were performed in the software PLAXIS 2D to model different pile driving scenarios that reflect the most common conditions found at the surveyed construction sites. An idealized soil profile consisting of a sandy soil layer with varying relative density was modeled based on the existing soil profiles encountered in the region of Central Florida during the field visits. The UBC3D-PLM model was used to investigate the geotechnical mechanisms due to liquefaction of the highly disturbed zone close to the pile, and the hypoplasticity model for sands was selected to model the ground deformation behaviors of the soils because it provides the possibility to track changes in void ratios (or relative densities) as the

pile is driven into the ground. A parametric study was performed to analyze the effect of the variables involved on the problem of pile driving-induced ground deformations.

The following items describe the contents of this report and summarize the main findings:

1. A comprehensive technical literature review was conducted to analyze previously reported case histories that involved ground deformation and vibration measurements around the world. A database of approximately 76 pile driving case histories is included in this report alongside a survey conducted of practitioners in the state of Florida. This allowed the authors to understand the conditions of the state of the practice in the state of Florida and the perception of practitioners on ground deformations induced by impact pile driving. It was shown that approximately 60% of the respondents had experienced construction problems (i.e., damages) associated with ground surface settlements induced by pile driving and that the principal type of pile that causes this issue is large-displacement prestressed concrete piles when they were driven through sands below the water table.

2. Field measurements were performed at 11 bridge construction sites. Field visits allowed the authors to become familiar with pile driving procedures (i.e., typical hammer and pile types, driving criteria, etc.) in the region of Central Florida as well as to identify predominant soil conditions in the area. Ground deformation time histories are presented herein to analyze the evolution of deformations as prestressed concrete piles are driven into the ground. Ground vibration measurements are used to verify FDOT vibration limits followed during pile driving operations.

3. A robust numerical modeling approach based on finite element analyses is presented to accurately model the conditions encountered during the field visits. Selection of model parameters and soil geometry are explained in this report. The analyses include the use of advanced constitutive soil models capable of reproducing changes in the void ratio of the soil (or relative densities) during impact pile driving. Validation of the numerical model was performed by comparing ground deformations measured at a specific site (i.e., Site A1) versus those computed by modeling the site-specific conditions as close to reality as possible.

4. An evaluation of the main variables that influence the pile driving-induced ground deformations is presented. The variables include the rated energy of the driving hammer, distance away from the pile, soil density, and pre-drilling depths. It was concluded that higher rated energies might generate larger ground deformations. The study of the soil density on the pile driving-induced ground deformations was used to conclude that larger settlements occurred when driving piles through loose soils than in medium-dense to dense soils. The same study showed greater heave is expected when driving piles in dense sandy layers than in loose sandy layers as a function of the phenomenon of volumetric expansion. It was also concluded that pre-drilling was beneficial to reduce ground deformations and vibrations because it increases the radial distance between the ground surface and the pile tip; this conclusion was confirmed during field observations.

5. Equations and charts that summarize approximately 140 numerical analyses performed in this research are proposed. These design equations and charts are presented to predict maximum ground deformations related to the considered soil relative densities for those conditions when PPVs satisfied the FDOT limit of 0.5 in/s. It was concluded that even if the reference value of PPV equal to 0.5 in/s is satisfied, there is still potential of ground deformations to be developed.

6. Maximum ground deformation equations related to the scaled distance away from the pile (i.e., distance away from the pile normalized with respect to the square root of the rated energy of the hammer) are also presented in this report. These equations are presented to provide practical guidelines on design envelopes of pile-driving induced ground deformations.

CONTENTS

LIST OF FIGURES

LIST OF TABLES

1. INTRODUCTION

Deep foundations represent a compelling alternative in the geotechnical engineering practice because they allow structural loads to be transferred to deep competent strata. Deep foundations installed using impact driving methods are very common in the region of Central Florida because the soil conditions in the area consist mainly of medium-dense sandy soils underlain by a competent limestone bedrock. However, it has been shown in previous studies that pile driving-induced vibrations can cause ground deformations that might potentially damage structures. Massarsch and Fellenius (2014) defined four types of damage categories due to pile driving. The first category consists of static movements caused by differential settlements and the heave commonly seen after installation of large piles in cohesive soils. The second category is associated with ground distortions generated by the propagation of surface waves that generates cycles of hogging and sagging movements in the structures. The third category is linked to the ground deformations caused by dynamic effects in the soil due to ground vibrations and cyclic effects, which is problematic in loose granular materials (this is the case of most sites in Central Florida). The final category involves the damage type directly associated with vibrations in the structure and their dynamic effects. Currently, most standards and specifications focus on this last category. This implies that vibration limits are not linked to the amount of settlement that soils will experience due to vibrations, which is important when repetitive and cumulative loadings are applied in predominantly sandy soils. The Florida Department of Transportation (FDOT) already specifies vibration limits in terms of peak particle velocity (PPV) for values less than 0.5 in/s (FDOT, 2021a).

A survey was conducted for the purpose of this report to ask consultants in the state of Florida about their experience with ground deformations and damage induced by pile driving (see Appendix A for more details). It was concluded that approximately 60% of the respondents have experienced damage associated with this problem. Additionally, 50% of the respondents consider that modeling this problem is an important issue during the design stage. The purpose of this research was to propose a method to predict ground deformations caused by pile driving, accounting explicitly for the attenuation characteristics of Central Florida soil conditions.

This report presents the summary of field data and measurements of ground vibrations and deformations due to pile driving performed at different construction sites in Central Florida. Data relevant to the pile driving activities are also presented, including type of hammers used, energy transmitted to the piles, and the relationship between vertical pile penetration and cumulative applied hammer blows. Construction details of selected projects are presented in this report: geometry and structural characteristics of the bridges, in situ soil profiles, field and laboratory tests, and type and dimensions of the piles.

The study was primarily conducted at locations where test piles via dynamic methods were also conducted. Data were collected from test dynamic test piles not only on the ground response in terms of ground deformations and vibrations caused by impact pile driving but also the applied force/stress and energy that the driving hammer transmitted to the pile and the way the pile responded. This report also introduces selected past field data because there have been similar case histories in the technical literature in Central Florida that measured the above-mentioned variables (e.g., Bayraktar et al. 2013; Heung et al. 2007). The field data presented herein are discussed and used to define and compare numerical models capable of predicting ground vibrations, deformations, and pile displacements during pile driving activities. The finite element (FE)

software PLAXIS 2D was used to perform the numerical analyses presented in this report. The wave equation analysis software GRLWEAP was also used to compute the force applied to the pile in the FE model.

A study analyzing the influence of the variables involved in this problem, such as the properties of the surrounding soils, pre-drilling depth, type of hammer, peak particle velocities, and distance away from the pile are also presented in this report. For the analysis, field data collected from various projects served as a baseline to determine the ranges of variation of those variables around Central Florida projects. Conclusions are drawn for the specific soil conditions in terms of ground movements and vibrations due to impact pile driving. Finally, charts and equations are presented that can be used to predict ground deformations using the following input variables: relative density of the soils, rated energy of the hammer, and distance away from the pile.

1.1. OBJECTIVES AND SCOPE OF WORK

The following are the of primary objectives of this research report:

1. To understand the mechanisms of near-field and far-field ground vibrations during pile driving and determine the critical distance from near-field to far-field deformation zones. This applied to primarily loose to medium-dense sands to silty sand conditions.

2. To investigate relationships among three major components: vibration-induced ground deformation, distance away from the pile, and ground vibration quantified in terms of PPV. Affecting parameters such as soil strength, pile installation method, type of pile-hammer system, relative density of the soil, and energy source will be considered in the development of correlations, equations, and charts. Field experiments and numerical modeling will be used to develop the correlations of those major components.

3. To develop pile driving induced dynamic settlement charts (or correlations or equations) as a function of PPV, relative density of the soil, distance from the source, soil shear strain, and input energy.

In order to accomplish the research objectives, the research was composed of 5 main tasks as listed below:

1. Conduct a comprehensive technical literature review of the current methods for the determination of ground deformations from field tests and numerical methods. Chapter 2 includes a detailed literature review conducted by the authors that includes a summary of existing ground deformation prediction methods. A compilation of case histories that involve both ground vibrations and deformations induced by pile driving is included in this chapter. Numerical modeling approaches reported in the literature are also included.

2. Survey to practitioners and district geotechnical engineers. Appendix A includes the survey results conducted in this research. The survey asked questions related to current practice in dealing with ground deformations induced by pile driving.

3. Field testing at several pile driving sites. The field data collected by the authors is presented in Chapter 3. This field data includes ground deformations, vibrations, and forces computed at the top of the pile. The results are analyzed in terms of site-specific conditions of each site and possible geotechnical mechanisms causing the measured ground responses.

4. Develop numerical models of pile driving induced ground deformations. Chapters 4 and 5 present the development and results of the numerical modeling framework conducted in this research. A detailed description of the modeling assumptions is presented in those chapters alongside a parametric study to analyze the effect of the variables that affect the final ground response.

5. Develop empirical prediction correlations for pile-driving induced ground deformations. Chapter 7 presents a summary of the charts and equations developed in this study to predict ground deformations caused by pile driving.

2. LITERATURE REVIEW

There are three main sections in this chapter. The first section presents a summary of reported methods for the estimation of ground deformations induced by pile driving. The second part of the chapter is oriented to describe reported case histories of pile driving induced settlements and vibrations. The third section describes numerical strategies adopted in the literature to study numerically and parametrically the variables involved in the problem.

Several case histories involving ground vibration and dynamic deformations during pile driving are presented in this chapter. Details of case histories such as vibration sources, soil properties, and site conditions were reviewed and included. Each case history was analyzed to understand the procedures adopted for instrumentation and field tests of pile driving projects. A literature review on numerical analyses for pile driving is also presented so that conclusions can be drawn from each case to summarize the most important lessons learned.

This chapter is presented for the most part in terms of imperial units. However, some figures and tables were collected from internationally published research that use SI units. The authors decided to report herein both unit systems, first the imperial followed by SI units in parenthesis, in order to link the text with the provided figures and tables that at times are presented in their original form in SI units.

2.1. VIBRATION-INDUCED GROUND DEFORMATION ESTIMATION METHODS

This section presents a summary of settlement risk assessment methods associated with pile-driving. The methods used to develop settlement estimation approaches ranged from empirical methods to laboratory-based methods and/or semi-empirical methods. This section introduces three classical and simplified methods to estimate pile driving-induced ground settlements that can be found in the technical literature. These methods are later used to compare the numerical results obtained from the FE simulations conducted in this research. The methods used to develop deformation estimation approaches due to pile driving operations have been derived from empirical methods, laboratory-based methods, or semi-empirical methods.

2.1.1 Method Proposed By Massarsch (2004)

Massarsch (2004) presented a simplified empirical method developed from several soil compaction projects. The author assumed that the sand densification process occurs within a zone of three times the diameter of the pile (i.e., 3D) and the total affected area will extend up to a distance of 3D+L/2 from the center of the pile with a maximum settlement (S_{max}) at the center of the pile. The maximum settlement (S_{max}) and the average settlement (S_{avg}) within the influence zone can be estimated as:

$$S_{max} = \alpha(L + 6D) \tag{2-1}$$

$$S_{avg} = \frac{\alpha(L + 6D)}{3} \tag{2-2}$$

where, L is the effective length of the pile (i.e., length in the compressible layer), D is the diameter of the pile, and α is a compression factor that can be estimated from Table 2-1. The driving energy input value depends on the pile installation method and the pile type and is quantitatively categorized as low, average, or high. The displaced volume of the installed pile was neglected in this method, thus its effects on the final ground surface settlement were not considered. Settlements can occur outside the influence zone, but they are often negligible.

Table 2-1. Compression factors for different ground conditions and driving energies (after Massarsch, 2004).

Driving Energy	Low	Average	High
Soil Density		Compression factor, α	
Very Loose	0.02	0.03	0.04
Loose	0.01	0.02	0.03
Medium	0.005	0.01	0.02
Dense	0.00	0.005	0.01
Very dense	0.00	0.00	0.005

2.1.2 Method Proposed By Drabkin et al. (1996)

This method consists of a polynomial model of vibration-induced settlements in sands that was validated with five case histories around the world (see Section 2.2 for details on the case histories). According to Drabkin et al. (1996) the model was developed based on several laboratory tests varying the following factors:

- Vibration amplitude
- Deviatoric stress
- Confining pressure
- Soil gradation
- Number of cycles
- Relative density
- Moisture content

The model of vibration-induced settlements for small to intermediate vibration levels is presented in Eq. (2-3).

$$\ln Y = 2.27 + 1.19x_1 - 0.71{x_1}^2 + 0.49x_2 - 0.68{x_2}^2 - 0.8x_3 + 1.09{x_3}^2 - 0.46x_4 + 0.06{x_4}^2 + 0.45x_5 - 0.38{x_5}^2 - 0.19x_6 - 0.10x_7 \quad (2\text{-}3)$$

where, Y is the settlement expressed in 1/1000 in. (0.0254 mm) and the variables x_i are the major factors affecting the settlements. The testing ranges used for each variable are shown in Table 2-2. The tests conducted for the development of the mathematical model were performed by placing the soil sample under drained conditions in a triaxial cell that was placed on a shaking table with a vibratory frame.

Table 2-2. Considered factors, tested ranges, and coding values for predicting the mathematical model (modified from Drabkin et al., 1996).

Factor	Factor Code	Tested Ranges	Coding of Factors
Peak Particle Velocity (PPV)	x_1	0.1-0.7 in/s	$x_1 = -1 + \frac{PPV - 0.1}{0.3}$
Deviatoric Stress (s)	x_2	2-15 psi	$x_2 = -1 + \frac{s - 2}{6.5}$
Confining Pressure (p)	x_3	10-30 psi	$x_3 = -1 + \frac{p - 10}{10}$
Sand Mixture	x_4	Coarse, Medium, or Fine	x_4 ranges from -1 for coarse sand to 1 for fine sand
Number of vibration cycles (N)	x_5	60-500,000 cycles	$x_5 = -1 + \frac{N - 60}{26{,}997}$
Moisture content	x_6	Dry, Saturated	x_6 ranges from -1 for dry sand to 2 for saturated sand
Initial relative density	x_7	Loose, Medium Dense	x_7 ranges from -1 for loose sand to 2 for medium sand

The polynomial model was developed by testing 5.9 in. (150 mm) thick soil specimens, thus it needs to be extrapolated to be applicable to thicker soil layers. Drabkin et al. (1996) assumed that the settlement (Δ) of a layer with thickness H_t (in mm), is directly proportional to the settlement y (in mm) of the tested specimen as follows:

$$\Delta = \frac{y}{150} H_t \tag{2-4}$$

where input values are in millimeters. Additionally, at construction sites where the *in-situ* soil conditions are highly non-homogeneous, the authors proposed dividing the vulnerable layers into 10 equal thickness layers.

2.1.3 Method Proposed By Mohamad and Dobry (1987)

This method consists of an approach to estimate the susceptibility of cohesionless soils to vibration-induced settlements. The authors used a similar methodology to the one used to evaluate the liquefaction potential of soils presented by Dobry et al. (1982). A maximum cyclic shear strain (γ_{max}) induced by the vibrating source is calculated and then it is compared with a threshold strain

(γ_t) below which no densification of dry granular soils takes place. For most sands, the value of γ_t is 0.01%. Equation (2-5) was presented by Mohamad and Dobry (1987) to calculate the shear strain induced by pile driving vibrations:

$$\gamma = m \cdot \frac{PPV}{V_s} \tag{2-5}$$

where, γ is the shear strain; *PPV* is the peak particle velocity; V_S is the shear wave velocity; and *m* is a shear strain factor. The value of *m* depends on the Poisson's ratio and the depth of analysis as shown in Figure 2-1.

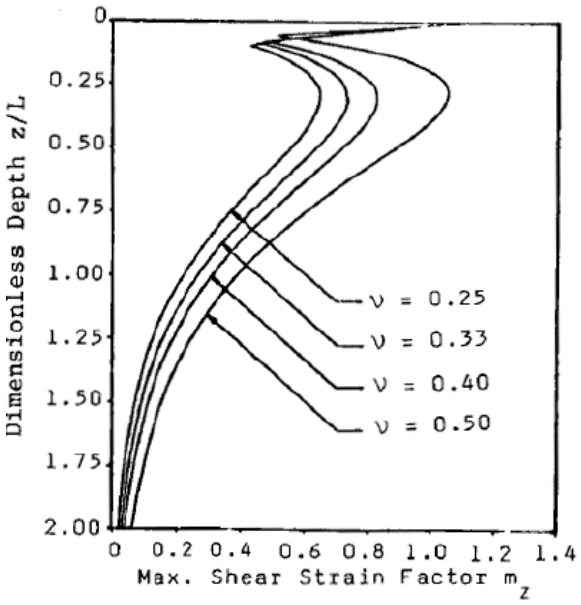

Figure 2-1. Shear strain factor to be used with the vertical peak particle velocity (from Mohamad and Dobry, 1987).

The non-linearity of the soil was considered by Mohamad and Dobry (1987) by using the concept of shear modulus degradation at a given shear strain level. This was estimated in terms of the maximum shear modulus (G_{max}) at very small strains. Thus, the shear wave velocity of the soil at a certain strain level ($V_{s\gamma}$) is given by Equation (2-6):

$$V_{S\gamma} = V_S \sqrt{\frac{G}{G_{max}}} \tag{2-6}$$

The maximum induced cyclic shear strain can be calculated by substituting Eq. (2-6) into (2-5):

$$\gamma_{max} = m \cdot \frac{PPV}{V_s\sqrt{G/G_{max}}} \quad (2\text{-}7)$$

where, γ_{max} is the maximum shear strain; *PPV* is the peak particle velocity measured at the site, V_S is the shear wave velocity at small strains; *m* is the maximum shear strain factor; and (G/G_{max}) is the effective modulus reduction factor of the soil at cyclic strain, γ_{max}. If a certain threshold shear strain, γ_t, is defined, it can be substituted into Equation (2-7) to calculate the limit peak particle velocity, PPV_t. This PPV threshold value can then be compared to the measured PPVs in the field to define the zone of influence of the pile driving activities.

$$PPV_T = \frac{\gamma_t V_s\sqrt{G/G_{max}}}{m} \quad (2\text{-}8)$$

2.2. CASE HISTORIES ON PILE DRIVING-INDUCED GROUND DEFORMATIONS AND VIBRATIONS

A summary of pile driving-induced ground deformations and vibrations reported in the literature is presented in this section. A total of 76 case histories reported in 55 papers were reviewed by the authors. Case histories where ground deformations were reported are presented in detail in this section. Additionally, ground vibration measurements are presented in cases where the soil conditions consisted mainly of granular soils (i.e., expected conditions in Central Florida). A summary of the entire dataset of the case histories is presented in Appendix B. In addition to the case histories presented in this report, the dataset includes case histories reported by Lambe and Horn (1965), Brenner and Viranuvut (1977), Mallard and Bastow (1980), Moore et al. (1995), Wong and Chua (1999), Kim and Lee (2000), Athanasopoulos and Pelekis (2000), Thandavamoorthy (2004), Shen et al. (2005), Massarsch and Fellenius (2008), Brandenberg et al. (2009), Seo et al. (2014), and Massarsch and Fellenius (2015).

2.2.1 Reported Ground Deformations

It was mentioned in Section 2.1.2 that Drabkin et al. (1996) used four case histories to validate the vibration-induced settlement prediction method. Two of these projects were located in New York City, and the rest of them were in Boston, Wantagh (NY), and Northern Spain.

The first project was located at the Back Bay section in Boston. It consisted of the driving of 180 14.2 ft (360 mm) square precast concrete piles by using an ICE 640 diesel hammer (rated energy of 40 kip-ft or 54 kN-m). The piles were driven up to depths ranging from 95 to 128 ft (29 to 39 m). Figure 2-2 presents the site-specific soil conditions, the measured PPV, and settlements. The measuring plan consisted of vibration measurements at two adjacent buildings and settlement measurements at different site locations on the ground surface and the top of the sandy layer. Notice that the peak particle velocity ranged from 0.25 to 0.6 in/s (6.4 to 15.0 mm per second), and the corresponding measured settlements ranged from 0.7 to 2.1 in (18 to 54 mm), demonstrating that even values of PPV less than the limit of 0.5 in/s (12.5 mm/s) can generate

significant settlements. The observed settlements occurred only during pile driving but did not continue once driving ended.

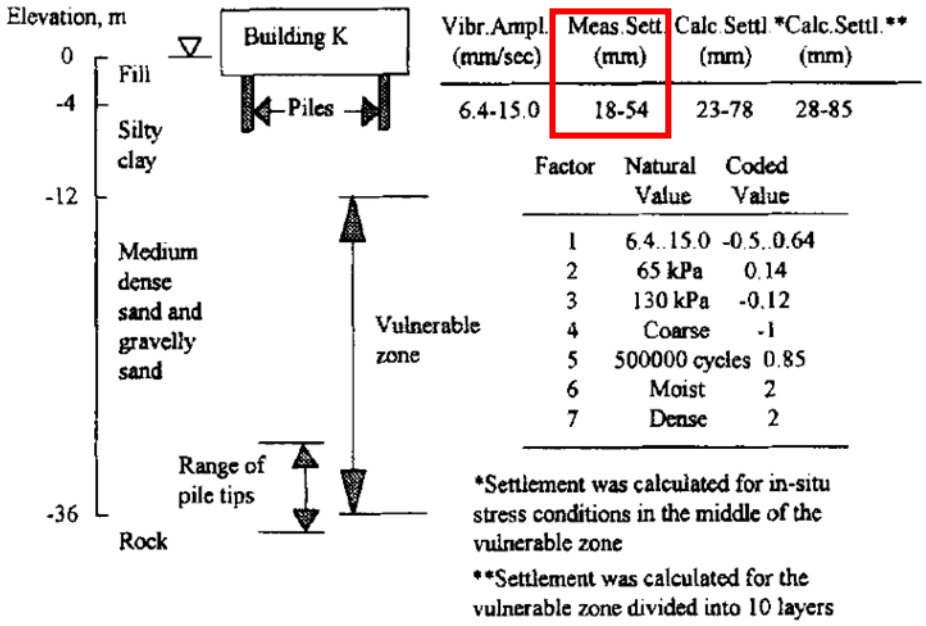

Figure 2-2. Project soil conditions and vibration-induced settlement at Back Bay Section in Boston (after Drabkin et al., 1996).

The second project was located in Southern Brooklyn in New York City. This case history consists of vibration-induced differential settlement measurements of 16.4 ft (5 m) tall, and 262.5 ft (80 m) wide aeration tanks supported on timber piles. Figure 2-3 presents the site-specific soil conditions, the measured PPV, and settlements. The settlements occurred during driving of 100 close-ended 10.7 in. (273 mm) pipe piles. The pipe piles were driven more than 131 ft (40 m) through a medium dense, fine to coarse sand by using a Vulcan 08 impact hammer. During the pile driving activities, the aeration tanks experienced a settlement greater than 1 in. (25 mm). All the tanks were emptied afterwards to reduce those settlements. However, the settlement continued up to 2.8 in. (70 mm) and the contractor decided to change the remaining pipe piles to auger cast-in-place piles (ACIP). The values of PPV were always less than 0.1 in./sec (2.5 mm/sec) on the structure and ranged from 0.1 to 0.9 in./sec (2.5 to 23 mm/sec) on the ground surface.

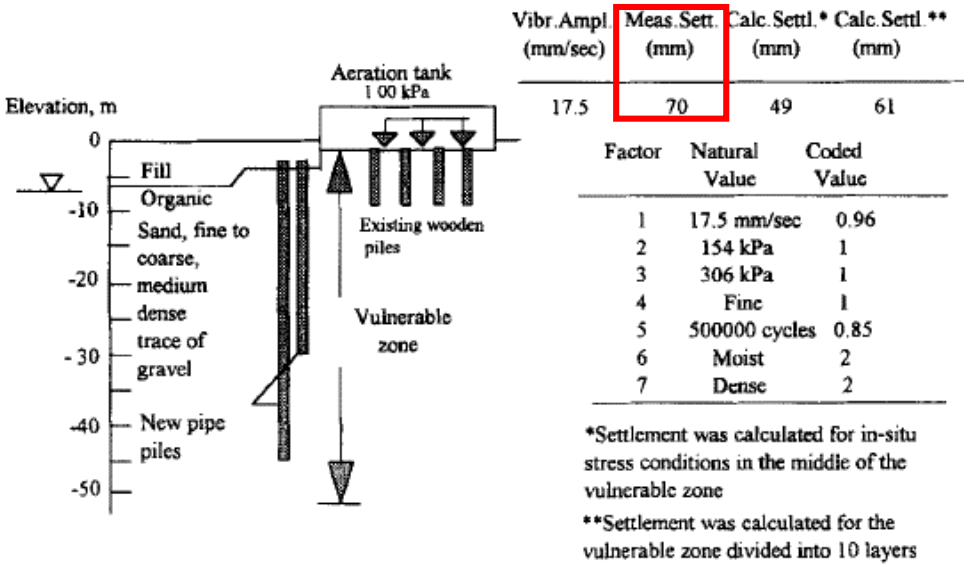

Figure 2-3. Project soil conditions and vibration-induced settlement at Southern Brooklyn Site in New York City (after Drabkin et al., 1996).

The third case history presented by Drabkin et al. (1996) consists of pile-driving induced settlements in Northern Spain. The settlements occurred on cast-in-place concrete piers of 3.5 ft (1.08 m) diameter embedded to a depth of approximately 66 ft (20 m) while H-piles were being driven up to the bedrock. Figure 2-4 presents the site-specific soil conditions, the measured PPV, and settlements. One of the pier foundations settled 10 in. (250 mm) during the H-pile driving. Static tests (i.e., field plate-load test), pier-load tests, and laboratory consolidation tests were performed at the site evaluate the causes of settlement. It was concluded based on static load test that the cause might have been dynamic compaction on the sandy layer since negligible settlement was measured during static loading.

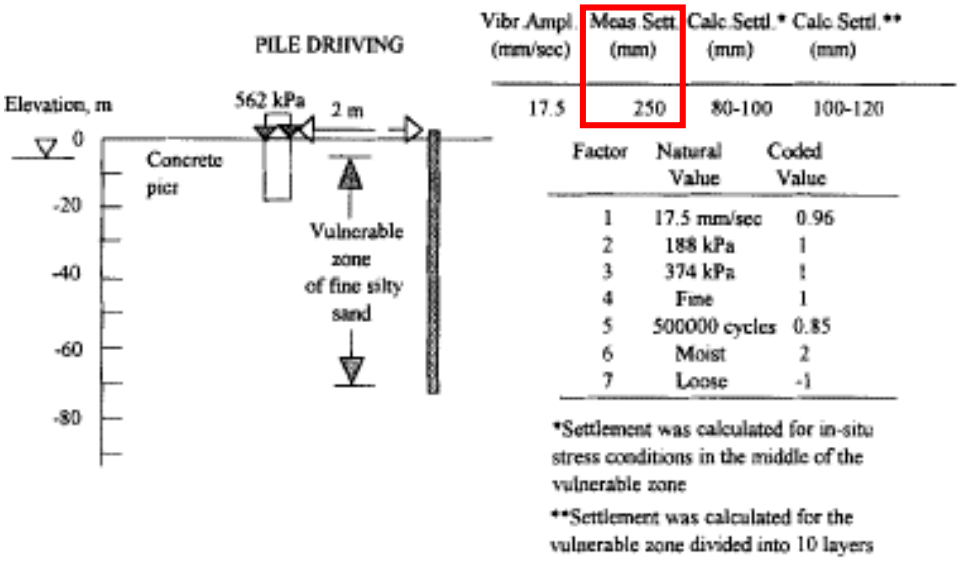

Vibr.Ampl. (mm/sec)	Meas.Sett. (mm)	Calc.Settl.* (mm)	Calc.Settl.** (mm)
17.5	250	80-100	100-120

Factor	Natural Value	Coded Value
1	17.5 mm/sec	0.96
2	188 kPa	1
3	374 kPa	1
4	Fine	1
5	500000 cycles	0.85
6	Moist	2
7	Loose	-1

*Settlement was calculated for in-situ stress conditions in the middle of the vulnerable zone

**Settlement was calculated for the vulnerable zone divided into 10 layers

Figure 2-4. Project soil conditions and vibration-induced settlements at the Lesaka site, Northern Spain (after Drabkin et al., 1996).

The fourth case history involves pile driving-induced settlements due to the construction of the 52-story residential Tri-Beca tower in Manhattan, New York. The foundation of the tower consisted of open-ended pipe piles with an outside diameter and length of 7 in. and 100 ft (178 mm and 30 m), respectively. Figure 2-4 presents the site-specific soil conditions, the measured PPV, and settlements. The soil was characterized mainly as a medium compact sand. Vibrations and settlements on a 2-story historical building in the nearby are presented as well. Settlements ranging from 1.5 in to 2.7 in. (38 mm to 69 mm) were observed at the 2-story building.

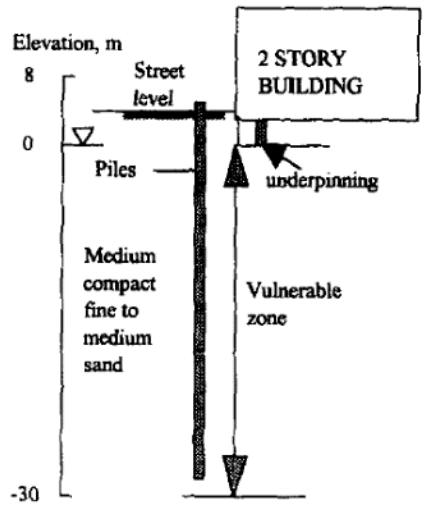

Vibr.Ampl. (mm/sec)	Meas.Sett. (mm)	Calc.Settl.* (mm)	Calc.Settl.** (mm)
5-13	38-69	12-49	18-65

Factor	Natural Value	Coded Value
1	5..13	-0.67..0.37
2	53 kPa	-0.13
3	106 kPa	-0.46
4	Fine	1
5	500000 cycles	0.85
6	Moist	2
7	Dense	2

*Settlement was calculated for in-situ stress conditions in the middle of the vulnerable zone

**Settlement was calculated using 10-layers extrapolation scheme

Figure 2-5. Project soil conditions and vibration-induced settlements at Tri-Beca tower in Manhattan, New York (after Drabkin et al., 1996).

Chen et al. (1997) presented the results of a full-scale driving test performed at the Chang-Hua Coastal Industrial Park near the Taichung Harbor in Central Taiwan without the presence of any surrounding structure (i.e., free-field test). The test consisted of driving five 31.5-in (800 mm) precast concrete piles to a depth of approximately 79.0 ft (24.0 m). A KOBELO 80 diesel hammer was used to drive the five precast concrete piles. The soil conditions at the site consisted of a 13.0-ft-thick (4.0 m) man-made loose gravely and sandy fill underlain mainly by sandy soils interbedded with some silty sand layers. Figure 2-6 presents the ground surface settlements induced by the driving of the first three piles (i.e., P1, P2, and P3). These settlements were measured along an axis parallel to the line of the piles (X-axis) and perpendicular to the piles (Y-axis). Most of the settlement occurred during driving of pile P3 (i.e., closest pile to the settlement points). The settlement does not become negligible for distances up to 16.5 ft (5.0 m). Chen et al. (1997) also presented results in terms of pore water pressure build-up due to pile driving, measured by three piezometers installed at different depths. It was observed that most of the excess pore water pressure was generated when the tip of the pile was above the piezometers. This indicated that the effects of the spherical waves emanating from the tip of the pile are the main triggering factor compared with the conical wavefront emanating from the shaft.

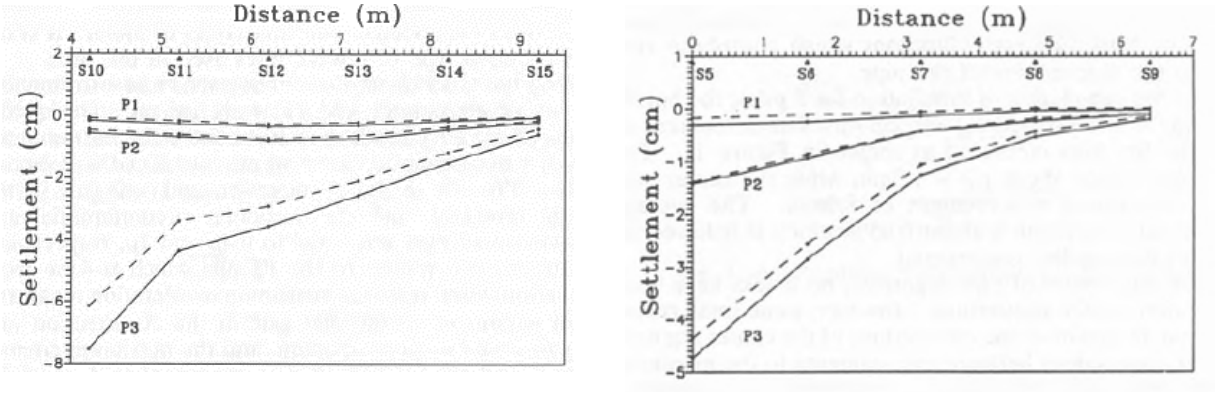

(a) (b)

Figure 2-6. Ground settlements due to driving of piles P1, P2, and P3 along two perpendicular axes: (a) X-axis and (b) Y-axis (after Chen et al.,1997).

Lewis and Davie (1993) presented a case history where structural response due to pile driving was measured at a U.S government facility. The project consisted of the installation of square precast prestressed concrete piles with a side of 14 in. (355 mm) by using an ICE 640 closed-ended diesel hammer with a rated energy of 40 kip-ft (54.2 kN-m). The site was located in the coastal plain of the eastern United States. The soil conditions consisted of alternating layers of loose to very dense fine sand and silty fine sand. The depths between -59 and -88.5 ft (-18 and -27 m) was the bearing stratum for the piles. Figure 2-7 presents the ground deformations measurements performed around each pile as well as for a five-pile group during the load test. Ground deformations ranged from 0.5 in. (12.7 mm) of heave to 3 in. (76 mm) of settlement. No movement was recorded at distances beyond the length of the piles.

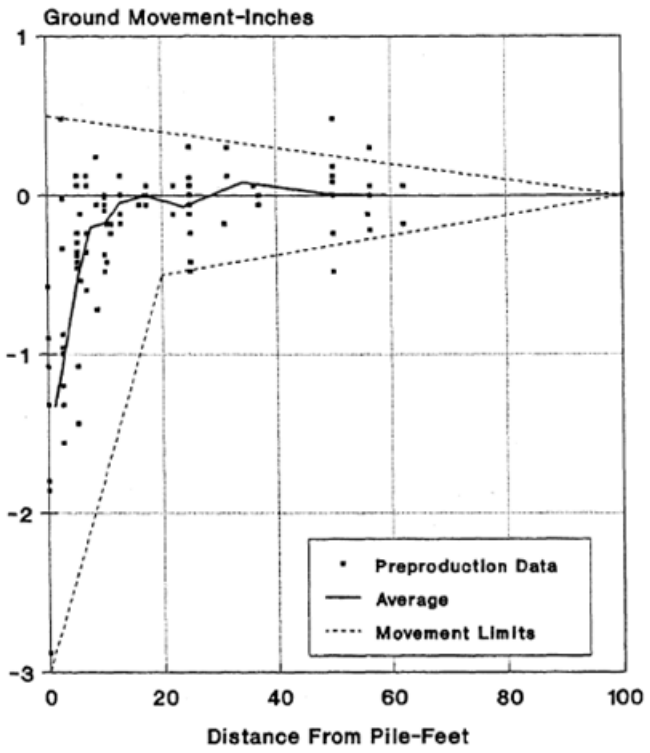

Figure 2-7. Ground displacement versus distance from the pile (after Lewis and Davie, 1993)

Linehan et al. (1992) the response of a pressurized natural gas pipeline located near the driving of piles for the construction of a railroad bridge foundation. Both vibratory sheet pile driving and impact H-pile driving were performed at the site. The 20 ft (6.0 m) long PZ40 sheet piles were driven up to a depth of 15 ft (4.5 m) using a vibratory hammer with transmitted energy of 333 ft-lb (451 N-m). The HP 14x73 piles with a length of 58 ft (18.0 m) were driven by a diesel impact hammer with a transmitted energy ranging from 231,000 to 30,000 ft-lb (313,193 to 40,674 N-m). The site consisted of a surficial layer of soft organic soils underlain by very dense sandy and gravelly soils. Figure 2-8 presents settlements induced in the pipeline by the different construction activities. It can be seen that the driving of the sheet piles caused a maximum settlement of about 0.5 in (12.5 mm). It was caused by vibration-induced densification of the foundation soils. After driving the HP-piles for the center pier, an additional settlement of 0.75 in. (19.0 mm) occurred. HP-pile driving in the east abutment induced settlements ranging from 0.5 to 1.0 in. (12.5 to 25.0 mm). A maximum total settlement along the pipeline of approximately 2.0 in. (50.0 mm) was recorded after construction. The authors highlighted the importance of extensive monitoring programs when pile driving is performed near sensitive structures. Linehan et al. (1992) also emphasized that if construction-induced ground vibrations were a concern, ground displacements should probably be a greater concern because there are fewer documented failures from vibration effects than from excessive displacements.

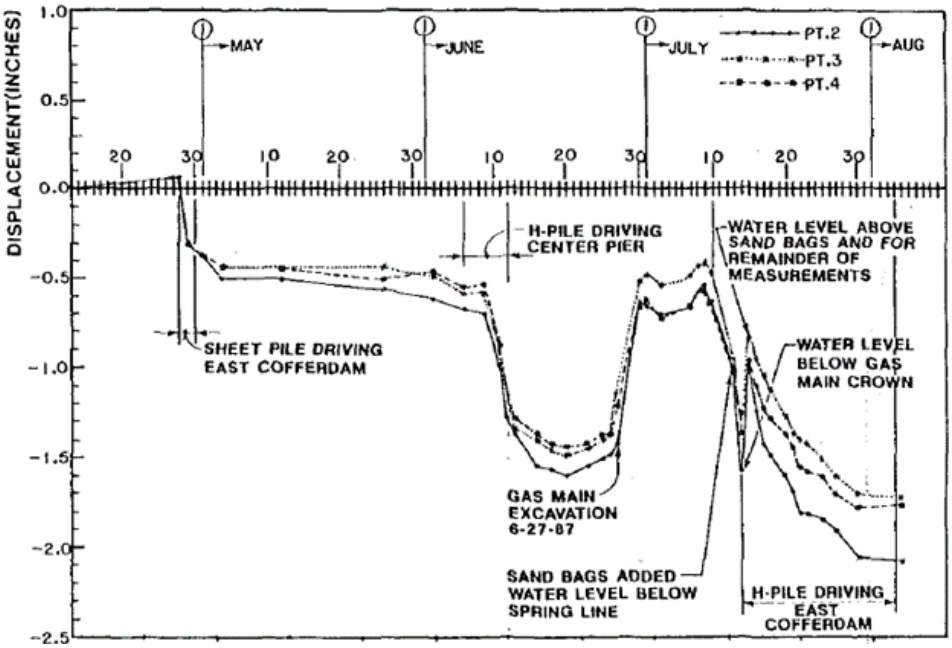

Figure 2-8. Vertical displacements of the pipeline during construction (from Linehan et al.,1992).

Hwang et al. (2001) presented several field measurements from full-scale pile driving tests at the Chiayi-Taipo County in Taiwan. The measured ground responses included porewater pressures, lateral movements, settlements, and ground vibrations. The project consisted of 13 bored concrete piles and 13 precast driven piles with diameters of 4.9 ft and 2.6 ft (1.5 m and 0.8 m), respectively. The bored piles and the driven piles had a spacing 14.8 ft and 7.9 ft (4.5 m and 2.4 m), respectively. The study only focused on the driving of the first three driven piles (i.e., DP1, DP2, and DP3) and their effect on the bored piles. The soil profile consisted mainly of medium-dense to dense sandy soils interbedded by some soft clay layers up to a depth of 131 ft (40.0 m). Figure 2-9a presents the final radial (i.e., horizontal) displacements after driving of pile DP1 at distances of 3d, 6d, and 9d from the center of pile DP1. Notice that the radial displacement at 3d was the greatest of the three inclinometers with an average value of 0.8 in (2 cm), which is approximately 2.5% of pile diameter. Vertical displacements during driving of DP1, DP2, and DP3 piles (e.g., DP1-9M means that DP1 pile reached 9.0 m below the ground surface) at each settlement post are presented in Figure 2-9b. Notice that most of the settlement posts experienced heave during the driving of the three piles, which might indicate that for dense sandy soils and/or clayey soils heave can be expected rather than settlement.

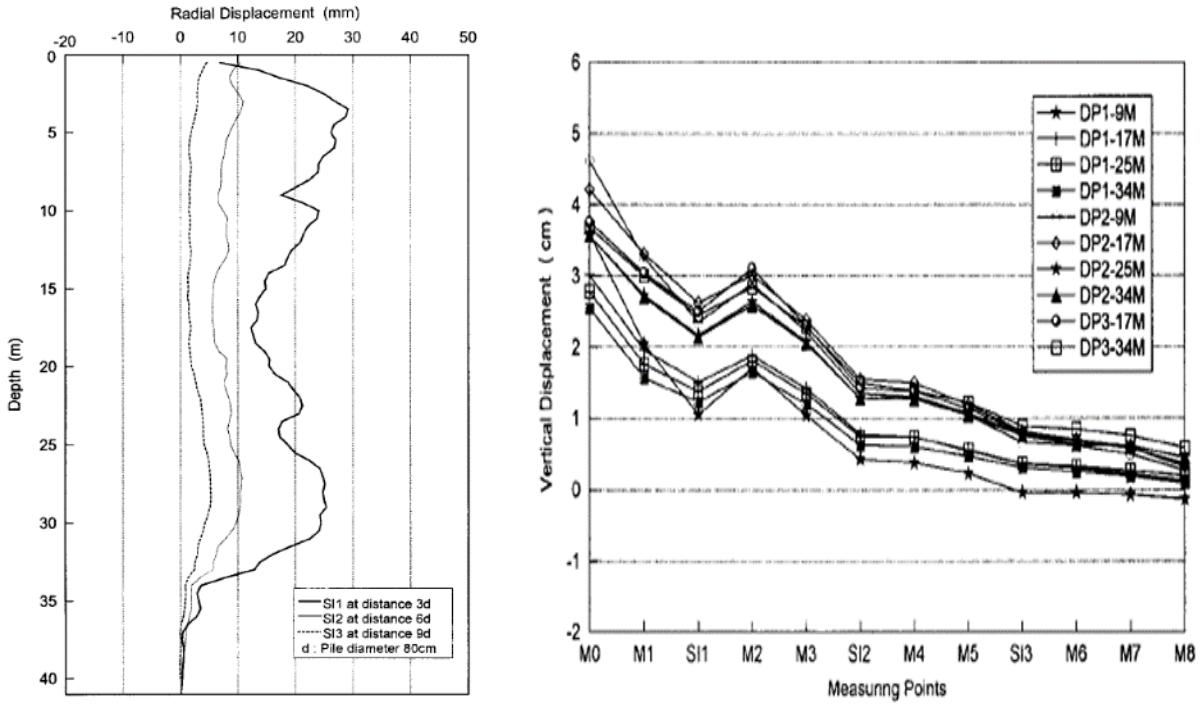

(a) (b)

Figure 2-9. Measurements at Chiayi-Taipo County in Taiwan: (a) horizontal displacements after driving DP1 pile and (b) vertical displacements after driving of DP1, DP2, and DP3 piles (after Hwang et al., 2001).

Clough and Chameau (1980) presented a case history that consisted of sheet pile driving in the proximity of San Francisco Bay. Extensive measurements were conducted at two sites (i.e., E1 and E2), including peak particle accelerations and settlements at various distances from the piles. A surficial 9 ft (3 m)-thick loose to medium dense rubble fill made up of dune sands was underlain by sand pockets up to a depth of 29.5 ft (9 m). Below the sand pocket, soft bay muds followed by alternating layers of dense sand and firm clay were found. Figure 2-10 presents the settlement measured at both sites. The maximum measured settlement was approximately 12.7 cm at a distance from the pile of 1.0 m. Approximately at a distance of 11 ft (3.4 m) from the pile no settlement was measured. This corresponds to a distance of approximately the length of the piles.

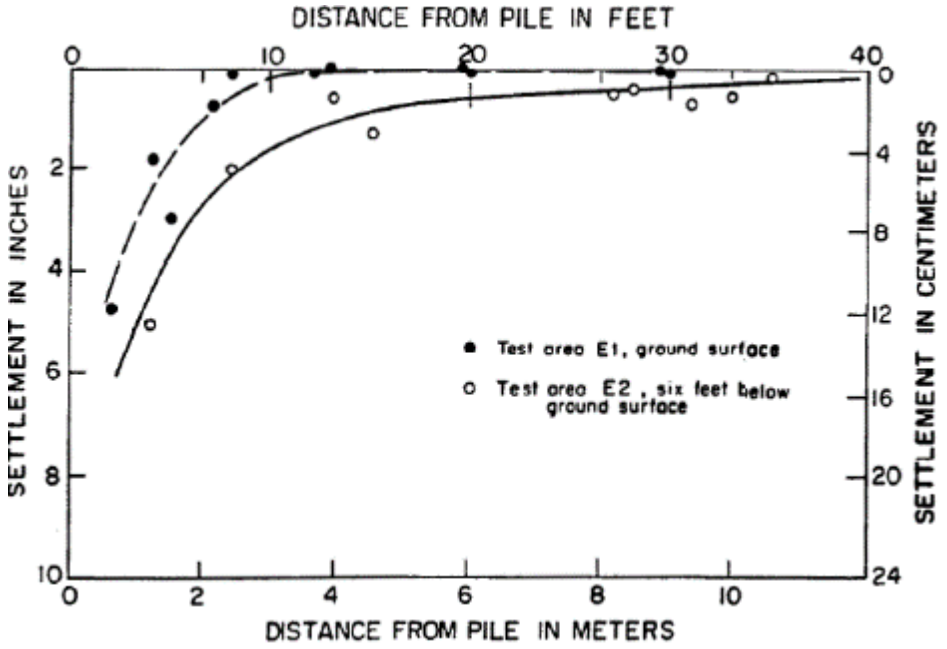

Figure 2-10. Measured settlements due to vibratory sheet pile driving (from Clough and Chameau, 1980).

Bozozuk et al. (1978) presents soil disturbance of sensitive marine clays caused by driving of two groups of 116 concrete piles, at a project located in Contrecoeur, Quebec. Soil disturbance was established in terms of porewater pressure, soil heave, lateral movements, soil strength, compressibility, and consistency limits measured prior to the construction and three months afterwards. The piles were standard Herkules H800 precast concrete piles that supported a massive reinforced concrete octagon-shaped foundation. The pile diameter was 1 ft (30 cm) with a cross-sectional area of 124 in.^{2} (800 cm^2) and an average length of 85 ft (26 m). The pile spacing ranged from 5 to 6 times the diameter. Soil displacements were recorded by using surface heave and below-hose gauges and inclinometers along the instrumentation lines. Figure 2-11 presents the variation of soil heave caused by pile driving with the distance from the piling area and depth in terms of “equi-heave lines”. The average soil heave at 10 ft (3.0 m) outside the pile group was about 4.3 in. (110 mm). Notice that for distances from the edge of the piling area greater than 39 ft (12 m) no ground surface heave was observed.

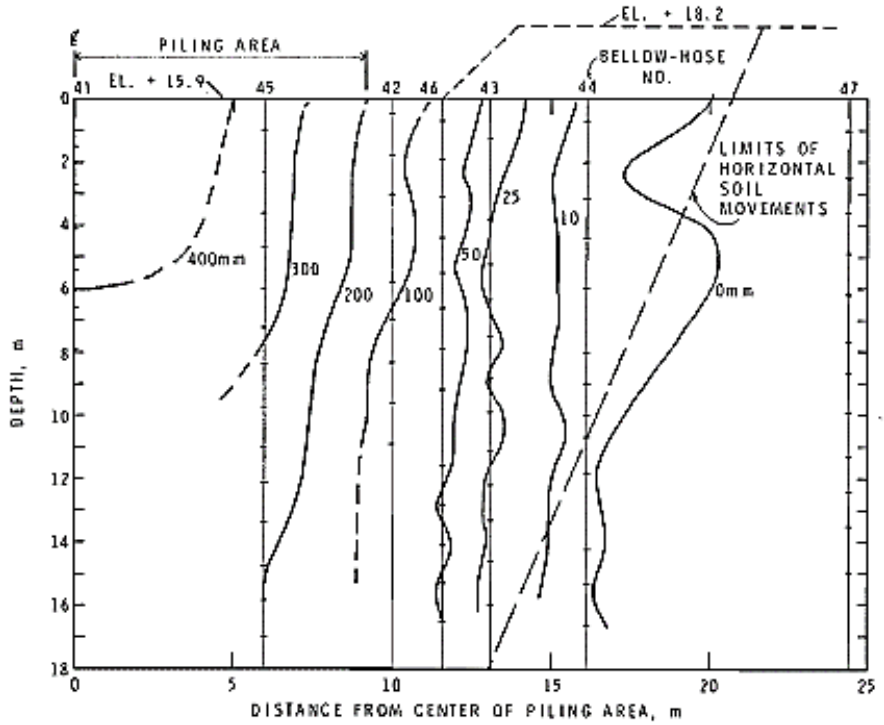

Figure 2-11. Soil heave contours due to pile driving (from Bozozuk et al., 1978)

2.2.2 Reported Ground Vibrations

Most of the studies in the literature that present ground vibrations measurements focus mainly on providing expressions and coefficients to fit already established Peak Particle Velocity (PPV) attenuation curves to field data. Different PPV attenuation equations can be used for that purpose. Hendricks (2002) proposed Equation (2-9) to predict vibration levels based on the distance from the pile (D):

$$PPV = PPV_0 \left(\frac{D_0}{D}\right)^k \tag{2-9}$$

where PPV is the peak particle velocity at a distance D from the pile, PPV_0 is the peak particle velocity at a reference distance D_0, and k is a soil attenuation parameter that must be determined experimentally for site-specific conditions. Bornitz (1931) proposed Equation (2-10) to account for both soil and geometric damping for the attenuation of the PPV induced by pile driving:

$$PPV = PPV_0 \left(\frac{D_0}{D}\right)^n e^{-\alpha(D-D_0)} \tag{2-10}$$

where n is the geometric damping coefficient and α is the material damping coefficient. The coefficient n depends on the type of waves generated from the source of vibrations. Equations (2-9) and (2-10) only express the PPV attenuation depending on the distance from the pile. It has been found that there is a better correlation between predicted and measured data when the distance from the pile is normalized by the energy of the hammer. Wiss (1981) introduced the concept of the scaled distance to account for this normalization:

$$PPV = k\left(\frac{D}{\sqrt{W_r}}\right)^{-n} \quad (2\text{-}11)$$

where D is the distance from the pile, W_r is the energy of the source, k is the value of the PPV at a unit value of scaled distance $(D/\sqrt{W_r})$ and n is the soil attenuation factor. For sites where there is no information about wave propagation, it can be assumed that the coefficient n lies between 1.0 and 2.0.

Lewis and Davie (1993) presented several vibration measurements at different sites where various pile types and pile hammers had been used. According to authors, vibration damage is not a common concern unless the piles are installed adjacent to existing structures. Table 2-3 presents a summary of the site conditions, pile type, and hammer specifications for each project site. The soil conditions at the sites consisted mostly of sandy soils with varying densities interbedded by clay layers. Vibration measurements at sites 2 to 7 we14re performed by seismographs and at site 1 accelerometers and velocity transducers were used.

Table 2-3. Case histories summary (modified from Lewis and Davie, 1993)

Site	Pile Type	Driven Length (ft)	Hammer Type	Rated Energy (ft-kip)	Soil Conditions
1	14-in Square Concrete Pile	80	ICE 640	40.00	Loose to dense sands and silty sands
2	Raymond Step Taper	78	Vulcan 80c	24.45	Fill, Soft Clayey Silt and medium clayey Sand
3	PZ-27 Sheet Pile	30	DELMAG D-15	27.00	Medium to dense sands
4	Raymond Step Taper	40	Vulcan 80c	24.45	Fill, Soft Silts and clay, dense to medium dense sands
5	Close-end Pipe pile 10.75 in x 0.219 in	30	Vulcan 06	19.50	Loose to Medium Sand, Soft clay, very dense sand
6	H-Pile 14x117	30	Vulcan 06	19.50	Medium dense to dense sand
7	Raymond Step Taper	80	Vulcan 06	19.50	Loose sand, soft clayey silt, and medium dense to dense sand

Ground vibration measurements performed by Lewis and Davie (1993) are presented in Figure 2-12. Equation (2-11) was used to develop the PPV attenuation curves. The charts were developed using the transmitted energy to the pile with the assumption that it was approximately 30% to 40% of the rated energies of the hammers. An average transmitted energy of 10,000 lbf-ft was used. Notice that the attenuation coefficients n and k from Equation (2-11) were computed as 1.0 and 0.1, respectively. For distances greater than 10 ft (3.0 m) the peak particle velocity was less than 2 in./sec and no structural damage was reported.

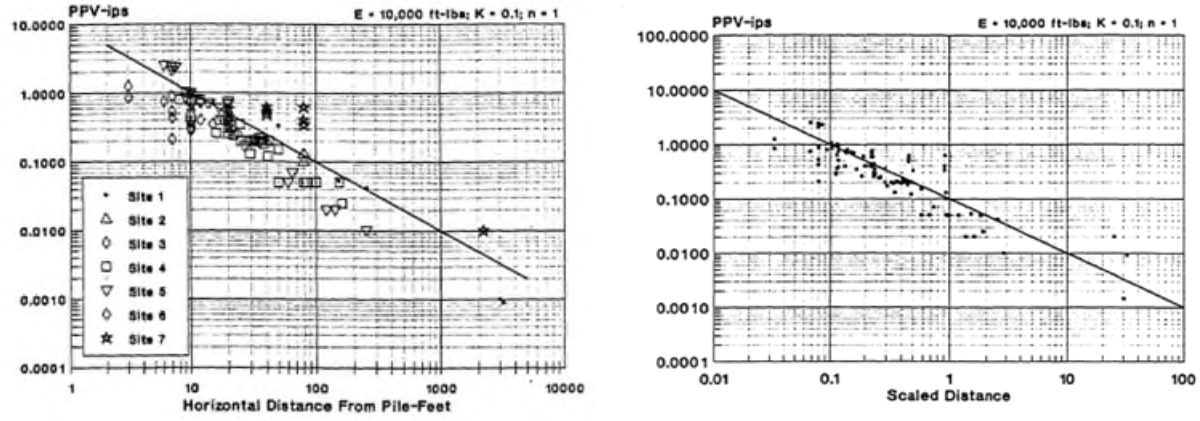

(a) (b)

Figure 2-12. Peak particle velocity measurement versus (a) distance, and (b) scaled distance (from Lewis and Davie, 1993)

Brunning and Joshi (1989) monitored the ground vibrations due to driving of six HP-piles in a construction project in Calgary, Italy. The 36 ft (11 m) long piles were driven within a horizontal spacing of 6.5 ft (2 m) at a distance of 7 ft (2.1 m) from an existing 16-inch (400-mm) gas pipeline lying at depth of 3.3 ft (1 m) below the ground surface. The D-22 diesel hammer used to drive the piles had a rated energy of 40 kip-ft/blow (54 kJ/blow). The study analyzed the effects of pile driving vibrations on the adjacent pipeline. The soil conditions consisted of a loose silty sand and gravelly fill underlain by a very dense coarse gravel mixed with boulders. The deepest stratum was defined as a low plasticity very stiff clay found at a depth ranging from 20 ft (6 m) and 26 ft (8 m). below the ground surface. Figure 2-13a presents the variation of peak particle velocity with pile penetration at the gas pipeline during driving of piles 97, 99 and 100. It can be seen that no vibration was induced when the piles penetrated the loose granular fill, whereas the maximum PPV occurred when the piles reached 3.3 ft (1 m) of penetration through the dense gravel layer. The values of peak particle velocity ranged from 0.75 in./sec (19 mm/sec) to 0.87 in./sec (22 mm/sec), which were significantly less than the PPV limit of 0.5 in./sec for Florida FDOT standards. During driving of the remaining two piles (i.e., piles 100 and 102) ground vibrations were measured at a distance of 4 ft (1.2 m) and 5 ft (1.5 m), respectively, and the resultant PPV versus the pile penetration depth is shown in Figure 2-13b. The maximum PPV of 2.8 in./sec (70 mm/sec) and 2.3 in./sec (59 mm/sec) were measured when the piles penetrated through the dense gravel layer.

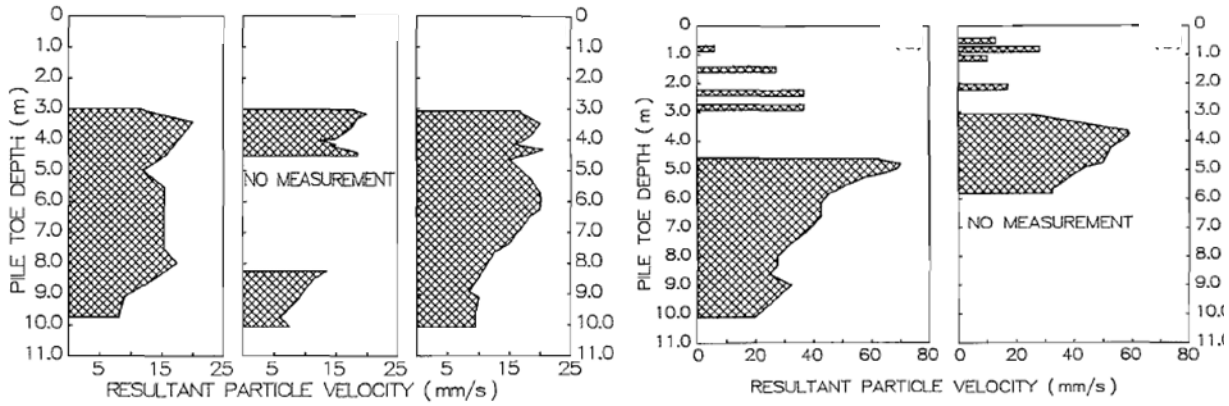

Figure 2-13. Vibration levels: (a) at the pipeline during driving of piles 97, 99, and 100; and (b) at the ground surface during driving of piles 100 and 102 (after Brunning and Joshi, 1989).

Grizi et al. (2016) presented ground vibration measurements during driving of steel H-piles using diesel hammers in loose granular soils in the state of Michigan. The measurements were made at different depths below the ground surface and at different distances from the piles. A Pileco D30-32 and a Delmag D30-32 diesel hammer were used to drive the 55.1 ft-long H-piles. Penetration depths varied between 53.1 ft and 43 ft. The soil conditions consisted of predominantly loose sands underlain by layers of medium dense to very dense sands. A comparison between ground vibrations and depth of pile penetration at the buried sensors is presented in Figure 2-14. When the pile penetrated below the sensor depth, ground vibrations started to increase significantly. This observation validated the hypothesis that the sensors only measure spherical body waves when the pile tip is above them, but when the pile tip is below the sensor depth, it can record the spherical body waves from the pile tip as well as the cylindrical shear waves from the shaft. When the pile tip was far from the sensor ground response started to decrease.

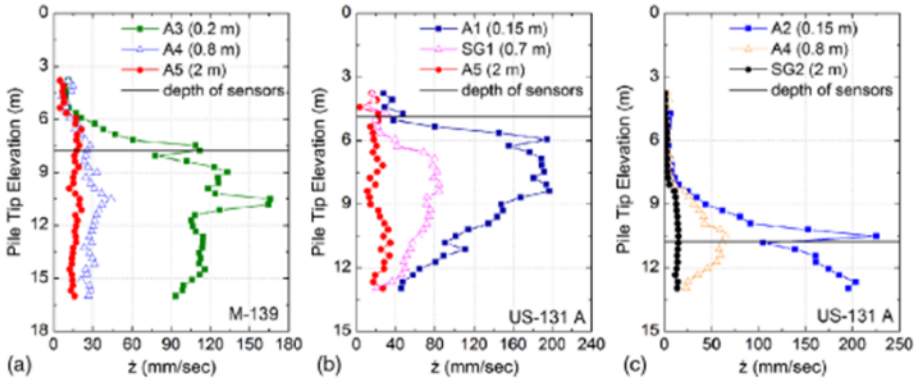

Figure 2-14. Peak particle velocity versus pile penetration depth at depths of (a) 7.8 m, (b) 4.9 m, and (c) 10.8 m (after Grizi et al., 2016).

Figure 2-15 shows the subsurface vibrations induced by pile driving and the attenuation curves fitted by using (2-10). A high rate of attenuation was observed near the pile, but it decreased dramatically when the distance from the pile increased.

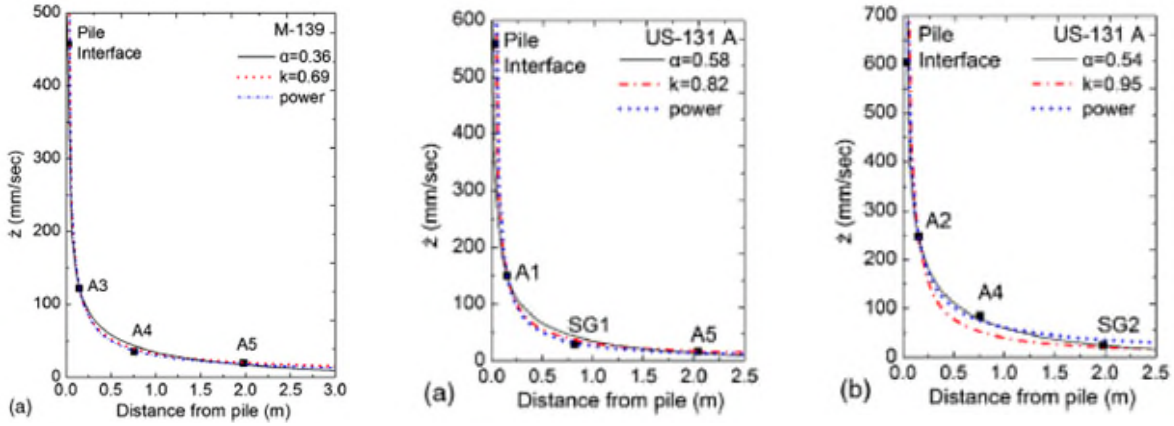

(a) (b) (c)

Figure 2-15. Attenuation curves fitted to in-depth measurements at depths of (a) 7.8 m, (b) 4.9 m, and (c) 10.8 m (after Grizi et al., 2016).

Cleary et al. (2015) presents the investigation of ground vibrations induced by pile driving near the Mobile River in Mobile, Alabama. The objectives of that research were: (i) to study the parameters that affect the level of vibrations during construction process, such as distance from the source, site specific conditions, and pile installation method, and (ii) to develop a vibration prediction equation to use for the Alabama Department of Transportation (ALDOT) projects. The project consisted of driving one 35 in-precast concrete pile, one HP-14X117 pile, and one HP 12X53 pile, which are commonly used by ALDOT. The pile lengths were 88 ft (27 m), 105 ft (32 m), and 69 ft (21 m), respectively. The soil conditions consisted of loose to medium and medium dense sands interbedded by a thin stiff to very stiff clay layer. geophones were located at distances from the piles of 50 ft, 69 ft, 100 ft, and 150 ft (15 m, 21 m, 30 m and 45 m) to obtain an attenuation distribution of ground vibrations. Figure 2-16 presents the PPV attenuation curves for both precast concrete pile and H-Piles. Equation (2-9) was used to obtain the regression lines from the field data. Note that the soil attenuation parameter (k) was the same for both equations with a value of 1.6, since the soil had similar properties for both cases. Notice that higher vibration levels are expected when precast concrete piles are driven than in the case of the H-pile due to the volume displaced by the piles and the effort required to drive them into the ground.

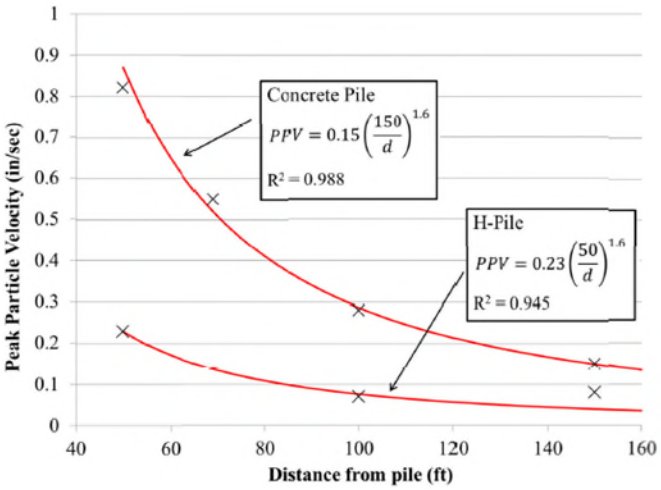

Figure 2-16. Peak particle velocity relationships for precast concrete pile and H-piles (after Cleary et al., 2015).

2.3.NUMERICAL MODELING OF PILE DRIVING

This report aims to combine measured data in the region of Central Florida with robust numerical models capable of simulating field conditions in order to analyze the effect of different variables on pile driving-induced ground deformations. This section presents different pile driving numerical modeling approaches reported in the literature. This allowed the authors to decide the most suitable approach to model the pile driving through various soil conditions in a FE environment.

Pile driving is a complex dynamic soil-structure interaction problem. Vibrations and deformations are induced in surrounding soils that might potentially damage infrastructure. Numerical models must be capable of reproduce accurately the pile and soil dynamics so that the response of soil during the pile installation can be properly assessed. There are two main modeling approaches found in the literature. The first approach (referred to as "discontinuous" modeling approach herein) consists of installing the pile at different "wished-in-place" depths and applying a single hammer blow at the top of the pile for each depth. It has been used to understand ground vibration levels and excess pore water pressure build-up. The second approach (referred to as "continuous" modeling approach herein) consists of a continuous pile penetration, in which the pile is driven without any interruption to a final depth. The main use of this approach is to analyze vibrations generated as the pile is driven.

2.3.1 Discontinuous Modeling Approach

Grizi et al. (2018) presented HP-pile driving-induced vibrations in a reduced-scale laboratory test at the University of Michigan. The test results were validated with a numerical model in Plaxis 3D by using a discontinuous approach. The laboratory test consisted of the installation of a 8.2-ft-long (2.5 m) S 3x5.7 beam by using a steel fence post driver with a weight of 44 lbs (20 kg) as the driving hammer. The soil used for the test was silica sand compacted into a cylindrical sandpit. The soil was modeled by using the Hardening Soil (HS) model. A material data set for the pile-soil interface with reduced parameters was employed to avoid issues with the default interface

elements in PLAXIS 3D. This interface was extended in a cylindrical shape with a diameter of 0.5 ft around the pile and 0.5 ft below the pile tip. Most of the parameters were reduced by a factor of R=0.5, excluding the shear velocity, which was reduced by a factor of R_S= 0.2. A total of seven hammer blows at seven different penetration depths were selected. Figure 2-17 presents both experimental measurements and numerical results in terms of PPV at different radial distances located at a depth of 0.6 m. For a radial distance of 0.36 ft (0.11 m) from the center of the pile, which corresponded to the reduced parameter zone, there was good agreement between calculated and measured data. However, Plaxis overestimated ground motions when the tip was located below 3.6 ft (1.1 m). For distances from the center of the pile between 1 ft (0.3 m) and 2.3 ft (0.7 m), Plaxis underestimated the peak particle velocity. It should be noted that the authors recognized that this approach cannot capture changes in stresses and strains during pile driving, thus it is unfeasible to get soil deformations by using discontinuous pile driving.

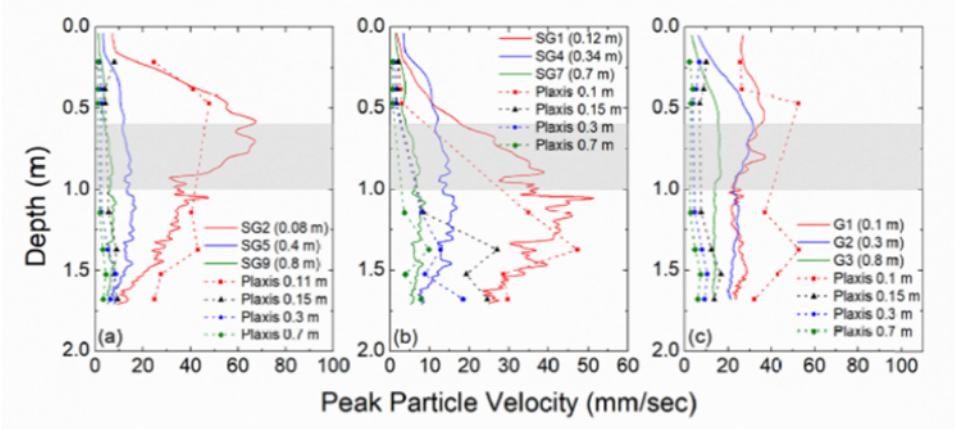

Figure 2-17. Comparison between measured data and numerical analysis at depths of (a) 0.6 m; (b) 1.2 m; and (c) at the ground surface (after Grizi et al., 2018).

Mabsout et al. (1995) presented a simulation of the driving response of a concrete pile below a pre-bored hole using a Lagrangian formulation. The soil selected was an undrained, normally consolidated clay, and was simulated by using non-linear finite elements. The model selected to represent soil conditions was a bounding-surface plasticity model for isotropic cohesive soils developed by Kaliakin and Dafalias (1989). The first soil consisted of a laboratory-prepared kaolin clay and the second one consisted of a softer clay. A linear elastic formulation was used to model the pile by assuming that it was subjected to small deformations. A slide-line formulation was used to model the soil-pile interface. This allows large relative sliding between pile and soil and separation when tension occurs. The authors analyzed the difference between a pre-bored pile and a driven pile in terms of pile tip displacement. This comparison can be considered as a comparison of a discontinuous with a continuous modeling approach. Figure 2-18 shows pile tip displacement for a pre-bored pile at a depth of 55.8 ft (17.0 m) driven by eight hammer blows (B8-D17) up to a penetration of 1 ft (0.33 m), and pile tip displacement at a depth of 59.1 ft (18.0 m) for 1 hammer blow (B1-D18). Ground responses for both cases were similar and therefore it can be expected that if the D17 pile was driven to 59.1 ft (18.0 m) depth it would have exhibited a stiffer response than

the first blow of D18. Thus, a discontinuous analysis under a single blow could lead to more flexible and unrealistic responses than an analysis under multiple blows.

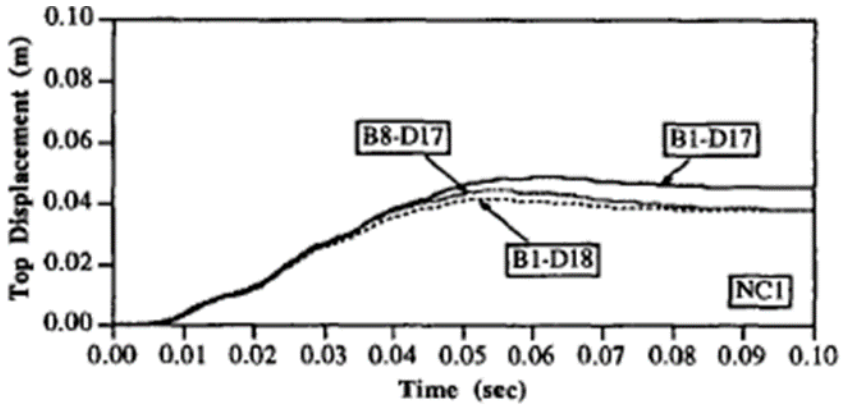

Figure 2-18. Comparison of pile tip displacements for the cases of 1 and 17 blows at a depth of 17.0 m and 1 blow at a depth of 18.0 m (after Mabsout et al., 1995).

2.3.2 Continuous Modeling Approach

Khoubani and Ahmadi (2014) presented an axisymmetric FE model with an adaptive arbitrary Langrangian-Eulerian (ALE) mesh method using the commercial code *Abaqus*. This model simulates a continuous pile penetration to a desired depth from the ground surface. A 35 in (0.5 m) diameter pile with a length of 30 ft (10 m) was driven in the model. A small gap of 0.4 in (10 mm) was placed between the pile and the soil on the axis of symmetry for a more realistic simulation. The gap caused the pile to push the soil elements sideways and downwards avoiding excessive distortion of the soil elements. The non-linearity of the soil was modeled using the Mohr-Coulomb model considering wave dissipation due to plastic deformations in the soil around the pile shaft. The Coulomb friction model was used to model the soil-pile interaction. This model allows the interface to take shear stresses up to a certain magnitude before it starts to slide. Figure 2-19a presents the vertical velocity of a point at 16.4 ft (5.0 m) from the center of the pile on the ground surface against the pile tip depth (d). As the pile penetrated the soil, ground vibrations increased reaching a maximum value at a depth of 15.7 ft (4.8 m). The concept of critical depth of vibration was introduced in Figure 2-19b in order to calculate the depth of pile penetration that causes the maximum level of vibration at a certain distance from the pile. For any distance greater than 16.4 ft (5.0 m) from the center of the pile, the critical depth of vibration tends to be approximately the same.

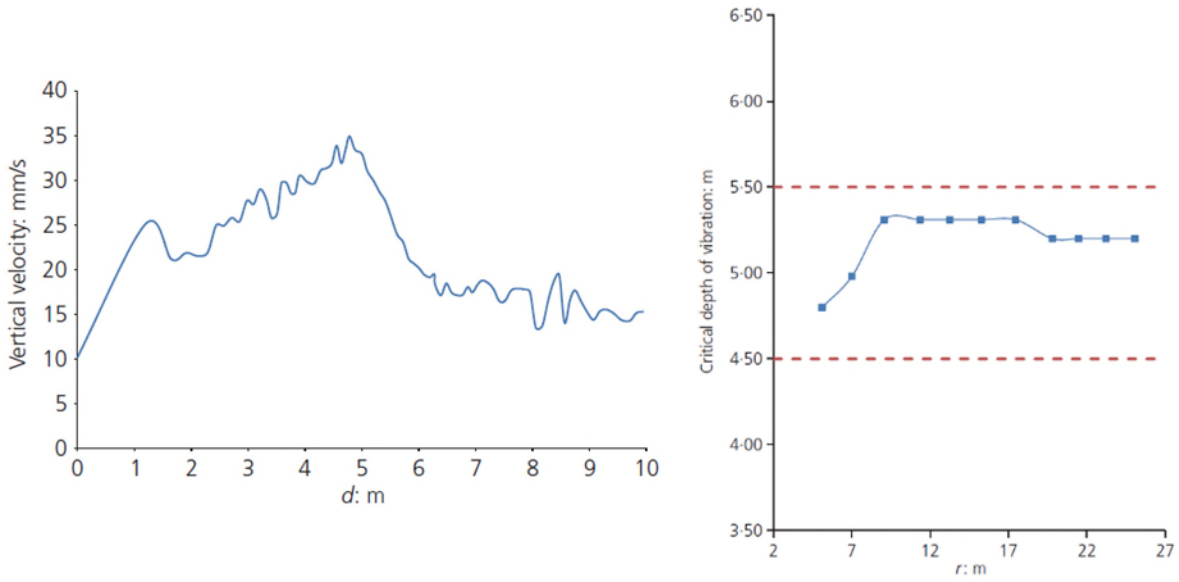

(a) (b)

Figure 2-19. (a) Vertical velocity of ground surface at a distance of 5 m from the center of pile against depth of pile penetration, d; (b) critical depth of vibration against distance from the pile (from Khoubani and Ahmadi, 2014).

Farshi Homayoun Rooz and Hamidi (2017) modeled an axisymmetric and continuous pile driving using an Arbitrary Lagrangian-Eulerian (ALE) adaptive mesh in the FE software *Abaqus* to predict ground vibrations induced by pile driving in sandy clay soil. The results were compared with previously published field data by Wiss (1981). A parametric study was conducted to analyze the influence of the impact hammer force, pile diameter, tip angle and damping ratio on the ground response. The 1.6-ft (0.5-m) diameter concrete pile with a length of 32.8 ft (10 m) was modeled as an elastic material. The Mohr-Coulomb failure criterion was used to model the sandy clay. The model used an artificial boundary technique at the right boundary as proposed by Liu and Jerry (2003) to prevent wave reflection. Different clusters with varying soil damping ratios were introduced in the model. Figure 2-20 presents the comparison between calculated and measured data in terms of the attenuation of PPV with the distance from the center of the pile on the ground surface. The model accurately predicted the measured data presented.

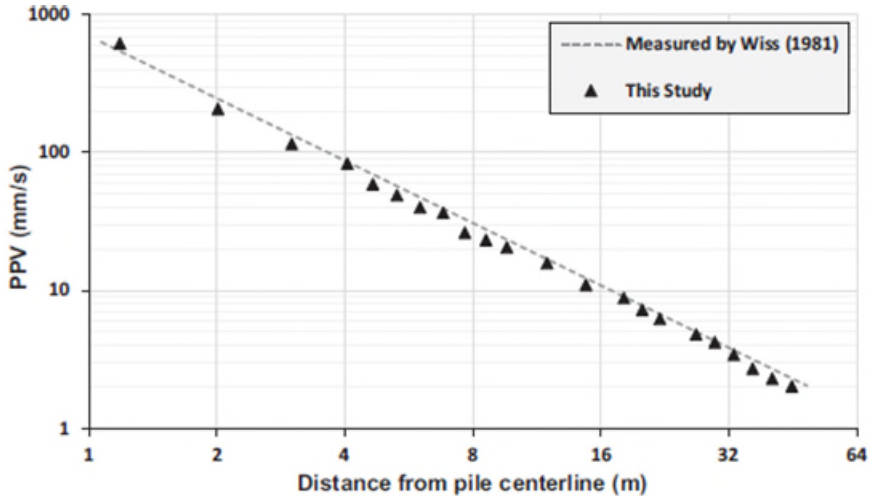

Figure 2-20. Comparison of calculated and measured field data in terms of peak particle velocity (PPV) versus distance from the center of the pile (from Farshi Homayoun Rooz and Hamidi, 2017).

Farshi Homayoun Rooz and Hamidi (2017) performed a parametric study to evaluate the influence of pile parameters, soil parameters, and pile-soil interaction parameters on the final ground response. The six pile parameters were hammer impact force, elastic modulus, diameter of the pile, and Poisson's ratio. The soil parameters were friction angle, cohesion intercept, elastic modulus, damping ratio, density, Poisson's ratio, and dilatancy angle. The effect of different friction coefficients between the soil and pile materials was also assessed. Figure 2-21 presents the factors that affect the most the ground response in terms of ground vibrations. Notice that a decrease in the hammer impact force (Figure 2-21a) from 8 to 6 MN (i.e., 25% reduction) and from 8 to 4 MN (i.e., 50% reduction) decreased the PPV to approximately 18 and 36%, respectively. It was concluded by the authors that the most significant factors that affect the response of the soil due to pile driving were impact hammer force, pile diameter, soil friction angle and damping ratio.

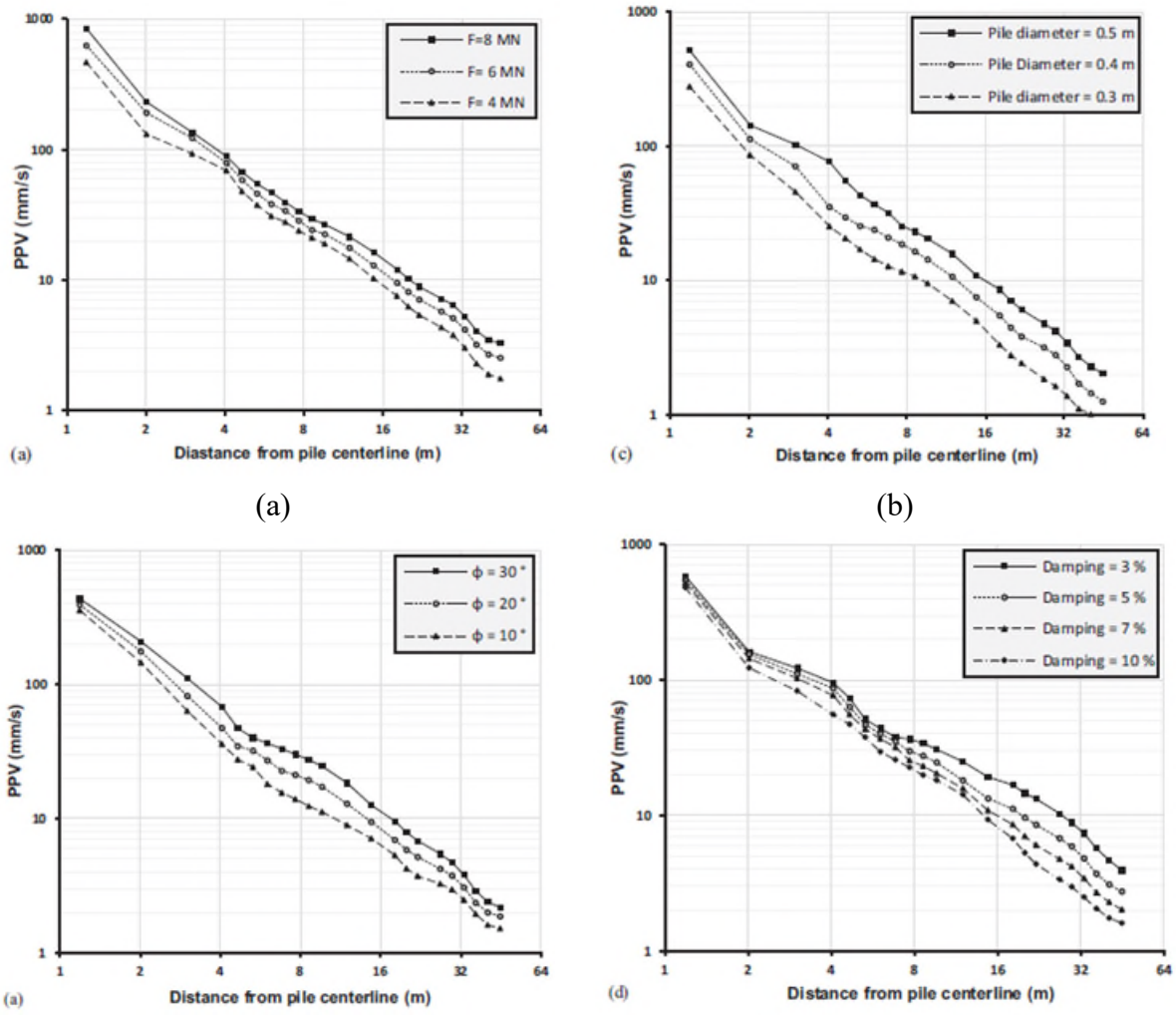

Figure 2-21. Evaluation of the parameters that largely affect the ground response in terms of vibrations: (a) impact hammer force, (b) pile diameter, (c) friction angle of the soil, and (d) damping ratio of the soil (from Farshi Homayoun Rooz and Hamidi, 2017).

3. FIELD DATA ON IMPACT PILE DRIVING

This chapter presents the field testing program designed to measure both ground displacements and ground vibrations induced by impact pile driving operations at project sites in Central Florida. An overall description of each project, details of the testing equipment, and procedures used to install the piles are also presented. A total of eleven bridge construction sites in Central Florida are included in this chapter. The field data collected are used in the following chapters to build and compare numerical models and to study the interactions among the variables involved in this problem (i.e., type of hammer, type, size and length of pile, and soil properties) and to issue recommendations on the prediction of ground surface deformations and vibration levels for similar geotechnical conditions.

3.1. DESCRIPTION OF FIELD EQUIPMENT

3.1.1. Geophones and Data Acquisition System

Ground vibrations measurements were conducted using single component (i.e., vertical axis) geophones manufactured by *Sercel Ltd.* The technical specifications for these geophones are shown in Table 3-1. The geophones had a natural frequency of 5 Hz and worked under a wide range of temperatures. A total of 18 geophones were used in this research. This number of sensors allowed measurements close to the piles and at approximately free-field conditions to define ground attenuation characteristics.

Table 3-1. Technical specifications of the geophones used in the field.

Model	SG-5
Natural Frequency	5 Hz
Coil Resistance	1850 Ω
Harmonic Distortion	<0,1%
Sensitivity	80 V/m/s (2.03 V/in/s)
Moving Mass	22.7 g (0.05 lb)
Spurious Resonance	> 150 Hz
Diameter	32 mm (1.26 in)
Length	43 mm (1.69 in)
Weight	170 g (0.37 lb)
Operating Temperature	-40°C to 80°C (-40° F to 176°F)

The data acquisition unit was the multi-channel system RAU *eX-3* manufactured also by *Sercel Ltd*. Each RAU unit is equipped with three slots for geophones, thus six acquisition units were used in this project for the 18 geophones. Table 3-2 presents the technical specifications of the acquisition system. These units were selected because they provided a wireless system offering flexibility when deploying sensors to the field, provided a good sampling rate, and a wide operational temperature range.

Table 3-2. Technical specifications of the data acquisition system used in the field.

Number of channels	3
Memory autonomy (2 ms sampling)	310 h
Timing accuracy	better than 20 μs
Operational temperature	-40 °C to +60°C (-40 °F to +140°F)
Acquisition gain	0 dB or 12 dB

3.1.2. Survey Equipment

Ground deformations were measured during pile driving by using DT209 Theodolites manufactured by *Topcon Ltd*. Table 3-3 presents the technical specifications of the DT209 model. Three theodolites were available to perform ground deformation measurements during pile driving. The location of the 18 geophones and 8 inch-long survey nails manufactured by *Bernsten International* were used to collect deformation points in the field during the pile driving.

Table 3-3. Technical specifications of the survey equipment used in the field.

Angle Measurement	Accuracy	9 seconds
	Method	Absolute reading
	Min. Reading	20 seconds
Telescope	Magnification	26x
	Minimum Focus	0.9 m (3.0 ft)
	Sighting Collimator	Double
Optical Plummet	Magnification	3x
	Field of view	3°
Operating Time	Theodolite and Laser	170 h
Operating Temperature		-20°C to 50°C (-4°F to 122°F)

3.2. PROJECT SITE DESCRIPTIONS

Figure 3-1 presents the location of the bridges considered in this research. Sites are numbered from north to south. Dynamic load tests were performed on piles at Sites A through D. Direct measurements were taken during the tests in terms of ground deformations, ground vibrations, and pile strains near the top of the pile (i.e., forces on top of the pile were calculated based on these strains). Site A is located between Lake and Volusia Counties in Florida. Sensors were deployed to the site to measure ground surface deformations and peak particle velocities (PPVs) caused by pile driving operations at Piers 2, 3, and Bent 11 (i.e., Sites A1, A2, and A3, respectively). Sites B and C are located in Lake County nearby the city of Sorrento. Peak particle velocities and ground surface deformations were collected during pile installations at the project sites. Site D is a connection ramp bridge at a highway intersection located in Orange County. The soil profile and field data were provided by District 5 engineers at the FDOT. Sites Z.1 through Z.5 correspond to sites previously studied by Bayraktar et al. (2013). These sites are located relatively close to Site

D (i.e., 2.0 miles from Site Z.1 and 19.0 miles from Site Z.5), thus these measurements were considered valuable for this project. Even though measurements of ground deformations were not reported by Bayraktar et al. (2013), PPV measurements and information regarding the input energy are used in the following chapters to compare the proposed numerical models.

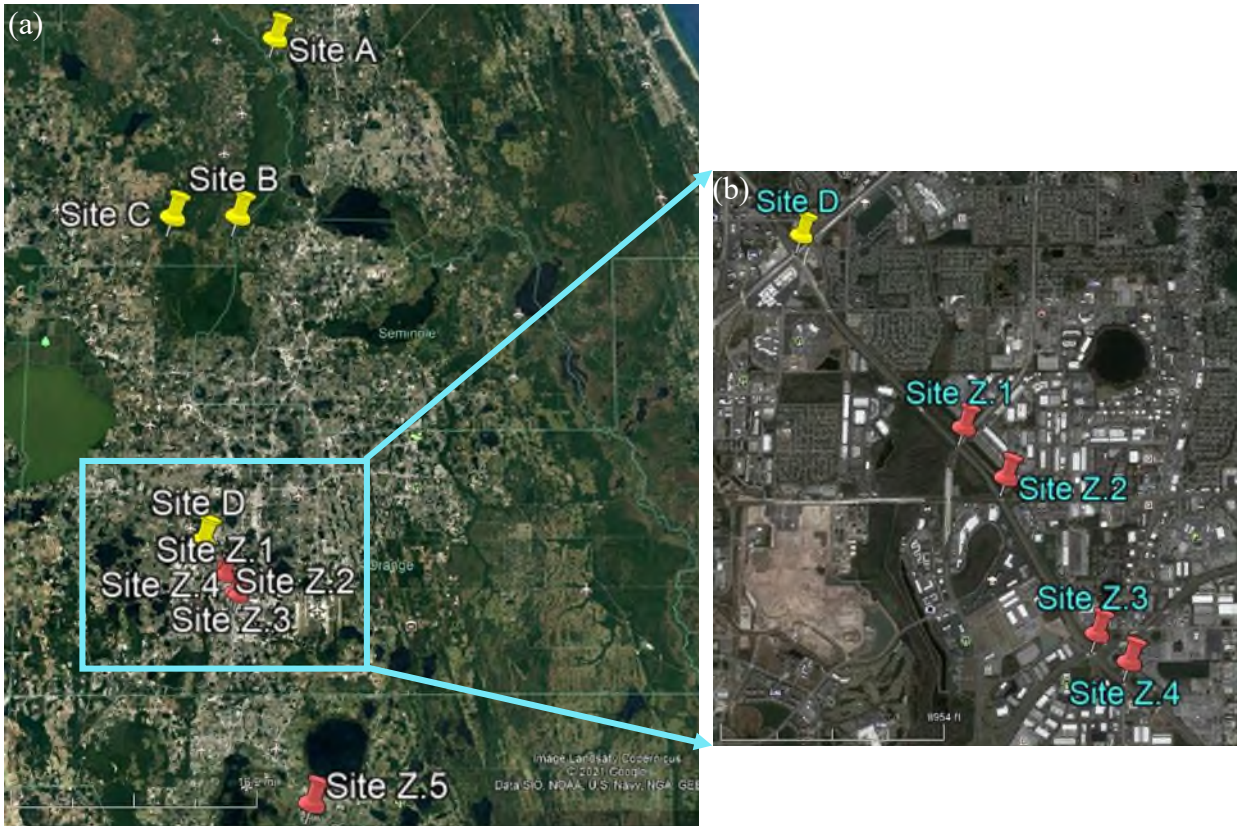

Figure 3-1. Location of the project sites: (a) overall location and (b) zoom-in view of projects in Orange County, Florida (Map data © 2020 Google).

Table 3-4 presents a summary of the measurements obtained from each project site. Ground deformation measurements were performed at Sites A, B, and C. Force time history on top of the pile for a single blow was computed from Embedded Data Collectors (EDC) at Sites A and C and from Pile Driving Analyzer (PDA) tests at Sites B and D. PDA measurements performed at Site D were used to apply forces at the top of pile in the numerical analyses. The PPV measurements performed by Bayraktar et al. (2013) at Sites Z.1 to Z.5 are also presented.

Table 3-4. Summary of project site locations and measurements performed at the sites in FDOT's District 5.

Site	Location	Measurements		
		PDA /EDC	PPV	Ground Deformation
A1	Lake County	X	X	X
A2	Lake County	X	X	X
A3	Volusia County	X	X	X
B	Lake County		X	X
C	Lake County	X	X	X
D	Orange County	X		
Z.1	Orange County[a]		X	
Z.2	Orange County[a]		X	
Z.3	Orange County[a]		X	
Z.4	Orange County[a]		X	
Z.5	Osceola County[a]		X	

[a] Measurements previously reported by Bayraktar et al. (2013).

3.2.1. Site A1

This project consists of a two-lane bridge over a river in Lake County, Florida (see Figure 3-2). The information about this project was provided by FDOT district 5 including soil borings and structural drawings. Figure 3-2 also presents the location of the soil borings (B1 through B3) and a nearby cone penetration test performed at the site (CPT-177).

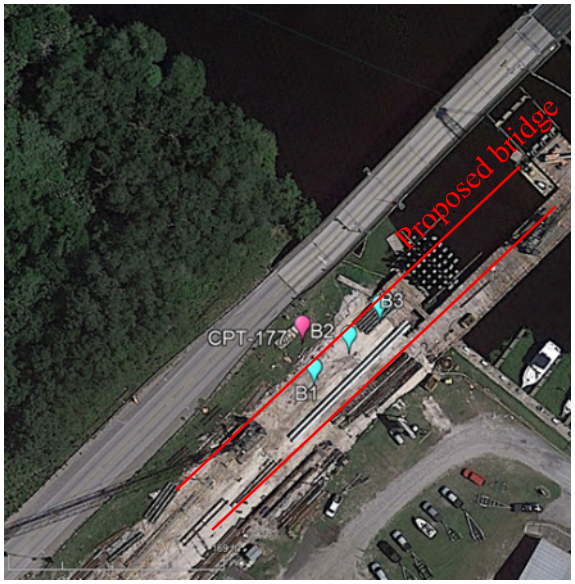

Figure 3-2. Location of soil borings relative to construction sites A1 and A2 (Map data © 2021 Google).

Sites A1 and A2 correspond to Piers 3 and 2, respectively. These piers belong to the same two-lane bridge over a river in Lake County. Figure 3-3a presents the foundation layout for the bridge. A detailed view of the foundation layout for both piers is shown in Figure 3-3b. The piers consisted of groups of twenty-two 24 in. square prestressed concrete piles with a length of approximately 125 ft. Piles 10 and 13 were used as the test piles for Site A1.

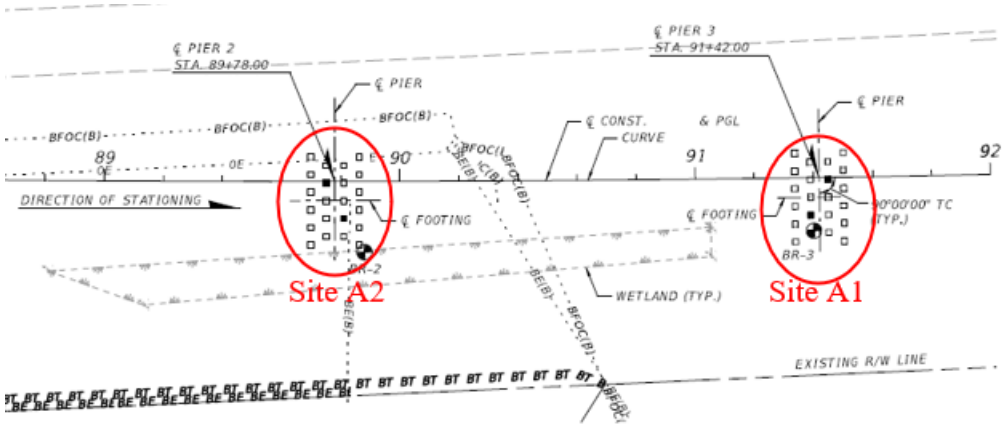

(a)

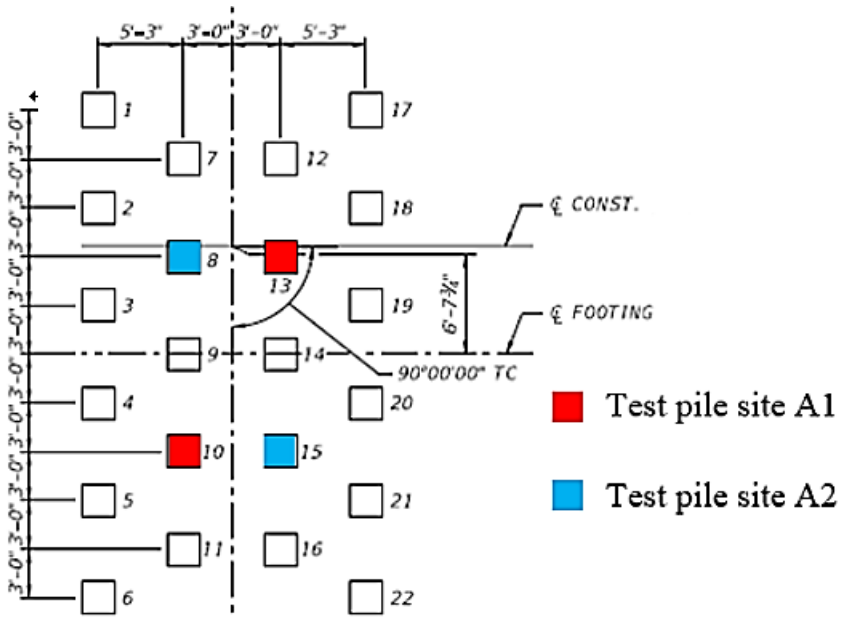

(b)

Figure 3-3. Foundation layout at sites labeled herein as A1 and A2: (a) overall plan view with location of test piles and (b) detailed typical plan view of foundation layout.

A shallow sheet pile was installed only for construction purposes around pile 10 prior to driving both piles. Figure 3-4 presents the sheet piles installed in the field. Notice that the sheet piles were located only around pile 10 and no structural elements were installed around pile 13. Figure 3-5 presents a graphical explanation of the driving process of both piles. An APE D50-52 hammer with a rated energy of 124.0 kips-ft was used to drive the piles approximately 105 ft into the ground as shown in Figure 3-5b. Piles 10 and 13 were predrilled up to a depth of 35 ft and 22 ft, respectively. Pile driving operations of pile 13 were conducted first. Installation of pile 10 was conducted on the following day. EDC was installed prior to driving the test piles to perform the dynamic test and obtain the pile capacity, stresses within the pile, transferred energy, and hammer stroke. Piles 10 and 13 were the first piles installed at the site. This allowed the researchers to measure ground deformations that occurred during the initial pile driving operations, which is beneficial since the surrounding soil was not subjected at the time to any previous dynamic loading.

(a) (b)

Figure 3-4. Location of test piles and sheet piles installed around pile 10 at Site A1 for construction purposes: (a) general view and (b) close-up view.

(a) (b) (c)

(d) (e) (f)

Figure 3-5. Pile driving process at Site A1: (a) hoisting of pile 13, (b) APE D50-52 used for driving piles 10 and 13, (c) installation of plywood cushion, (d) hammer in leads before pile driving of pile 13 and (e) pile 10, and (f) ending of driving.

3.2.2. Site A2

Site A2 is located at the same project as Site A1 (see section 3.2.1) but corresponds to the field measurements performed during driving of test piles at Pier 2. The test piles selected for this site were piles 8 and 15. Figures 3-6 and 3-7 present the photographic records of the pile driving process that occurred at the pier. An APE D50-52 diesel hammer with a rated energy of 124.0 kips-ft was used to drive the 135 ft long prestressed concrete piles up to a penetration depth of 110 ft. Piles 8 and 15 were predrilled at depths of 28 ft and 24 ft, respectively. The driving sequence started with pile 8 followed by driving of pile 15. EDCs to conduct the dynamic tests were installed prior to driving the test piles. The cushion was changed during driving of pile 8 due to excessive driving stresses in the pile according to the dynamic testing logs. Piles 8 and 15 were the first piles installed at this site allowing to perform ground deformation measurements on a soil which was not disturbed by pile driving.

(a) (b) (c)

Figure 3-6. Driving process of pile 8 at Site A2: (a) prior to installation, (b) during installation, and (c) end of installation.

(a) (b) (c)

Figure 3-7. Driving process of pile 15 at Site A2: (a) pile hoisting, (b) hammer in leads, and (c) hammer impact acting on the pile.

3.2.3. Site A3

Site A3 is located on the other side of the river as Sites A1 and A2. However, it is located in Volusia County, Florida. This site corresponds to Bent 11 of the bridge, where measurements were performed during driving of test pile. The information about this project was also provided by FDOT district 5 including soil borings and structural drawings. Figure 3-8 presents the location of the soil borings (B9 and B9) and a nearby cone penetration test performed at the site (CPT-178).

Figure 3-8. Location of soil borings relative to construction Site A3 (Map data © 2021 Google).

Site A3 corresponds to Bent 11 of the same bridge as Sites A1 and A2. Figure 3-9 presents a detailed view of the foundation layout. The bent consisted of a group of seven 24 in. square prestressed concrete piles with a length of approximately 160 ft. The piles were arranged in a linear array and the spacing between them was 8.75 ft. Pile 4 was used as the test pile for Site A3.

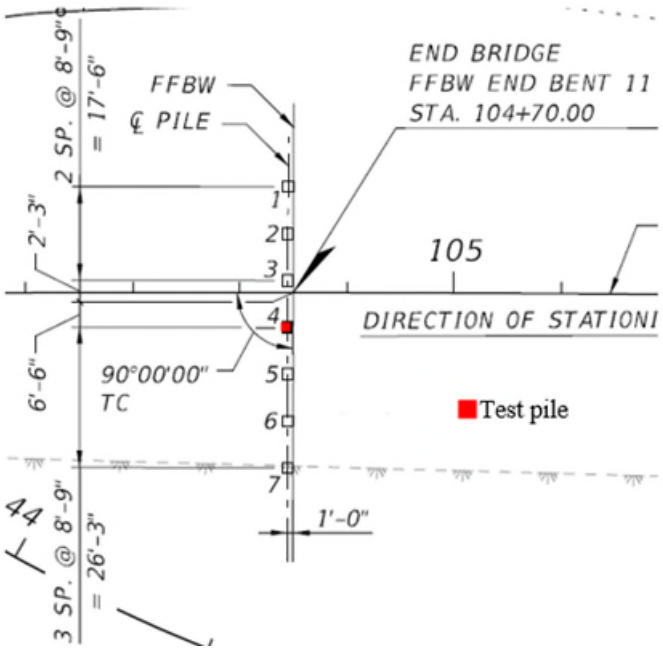

Figure 3-9. Detailed typical plan view of foundation layout at site labeled herein as A3.

Figure 3-10 present the photographic records of the pile driving process that occurred at the site. An APE D70-52 diesel hammer with a rated energy of 173.6 kips-ft was used to drive the 160 ft long prestressed concrete piles up to a penetration depth of 136 ft. Pile 4 was predrilled at a depth of 28 ft. The pile was spliced into two 80 ft-long segments. Both pile segments were driven in consecutive days. According to the contractor, it was not possible to drive the pile completely in a single day due to curing of the epoxy that is commonly applied to the EDC sensors. The first segment was driven up to a depth of 76 ft. Pile 4 was the first pile installed at this site.

(a) (b) (c)

(d) (e) (f)

Figure 3-10. Driving process of pile 4 at Site A3: (a) initial conditions before driving, (b) pile penetration before splicing, (c) second pile segment placement, (d) final pile penetration, (e) used plywood cushion, and (f) APE D70-52 hammer used to drive the pile.

3.2.4. Site B

Site B consisted of a bridge crossing over the Wekiva River in Lake County, Florida. Figure 3-11 presents the foundation layout of the project and a detailed foundation layout of a typical pier. A total of 3 bridges were projected at this site. Pile 12 located at Pier 5 was selected as the test pile for the field measurements. Pier 5 consists of a group of 14 square prestressed concrete piles with a width of 24 in. Pile 12 was 65 ft long. Figure 3-12 presents the conditions at the site prior to installation of pile 12. A sheet pile cofferdam was built by the contractor around the pile group due to the ground water regime and soil conditions at the site. The effects of this cofferdam around the pile group on the pile driving induced vibrations and ground movements are discussed in further sections in light of the measurements taken during the driving process. Photographic records taken during the pile driving operations, including pile hoisting, hammer in leads, and ending of the pile driving are shown in Figures 3-13 and 3-14. Notice that piles were already driven at this site, thus the soil was already disturbed by previous pile driving activities when the researchers arrived.

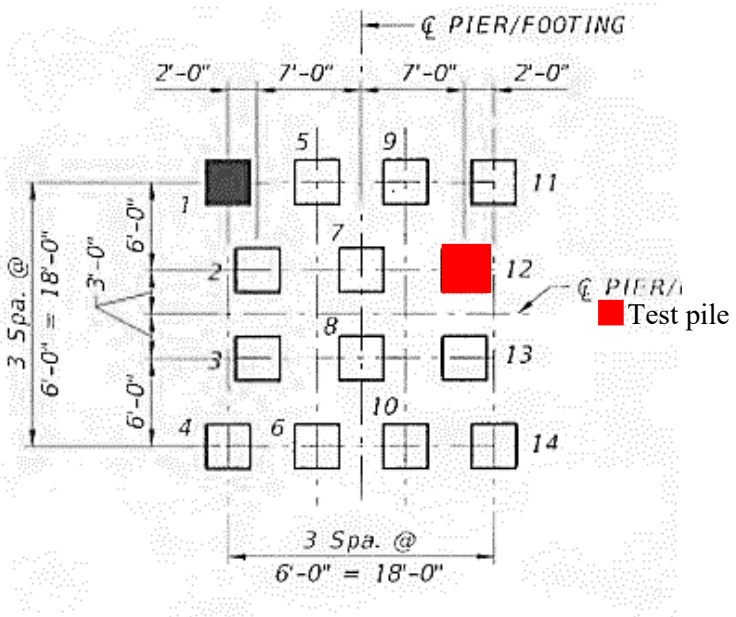

Figure 3-11. Typical plan view of foundation layout at Site B.

(a) (b) (c)

Figure 3-12. Conditions prior to pile driving process: (a) prestressed concrete test pile cross-section, (b) accelerometer installation for PDA test, and (c) cofferdam built around pier 5 at Site B.

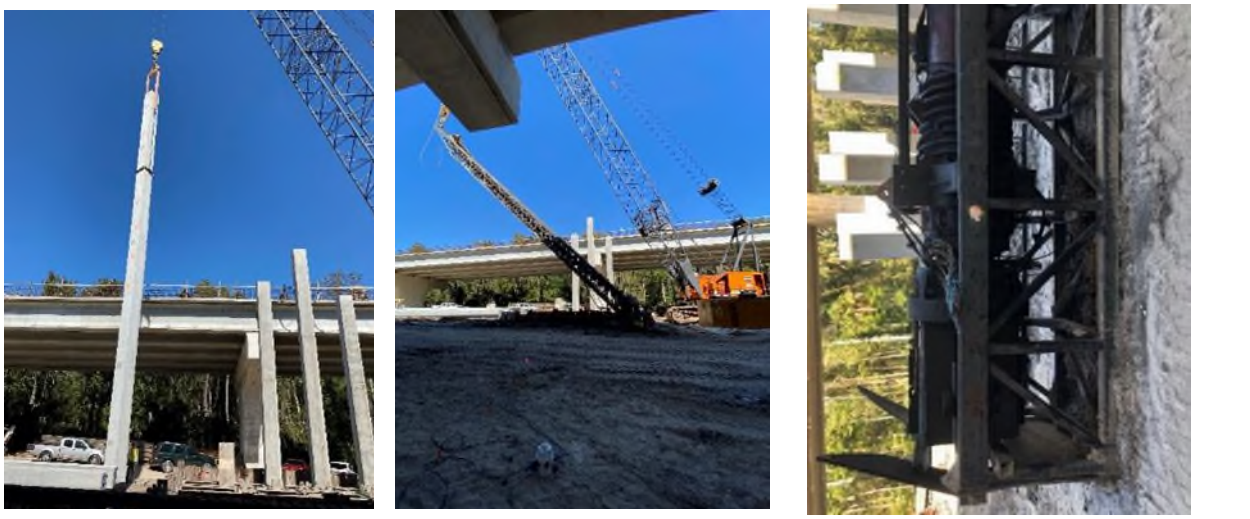

(a) (b) (c)

Figure 3-13. Pile driving process at Site B: (a) prestressed concrete pile hoisting, (b) hammer in leads, and (c) APE hammer used for pile driving operation.

(a) (b) (c)

Figure 3-14. Pile driving process at Site B: (a) beginning, (b) pile at final penetration depth, and (c) driving hammer during the installation of the prestressed concrete test pile.

3.2.5. Site C

Site C consisted of a bridge over a wildlife crossing (WLC) near the town of Sorrento, Florida. Figure 3-15 presents the foundation layout of the project. The field measurements were taken for the driving activities of piles at Bent 4. The bent consisted of a group of seven 24 in. square prestressed concrete piles spaced at 8.7 ft. The length of the piles was 110 ft. The soil borings performed at the project site are also shown in the figure. Borings S4 and B8 are used in this report to define the soil profile at the site.

Figure 3-16 presents a graphical description of the driving process observed during the field visit. An APE D70-52 hammer with a rated energy of 173.6 kips-ft was used to drive the piles up to a penetration depth of 90 ft. Piles 1 and 7 were already driven prior to the day the research team performed the field measurements. Piles 4 and 5 were not driven up to the specified depth due to practical refusal in terms of the number of blows applied to the pile. Pile 3 was not driven completely on the day of the field visit due to the large number of blows required to drive the pile; structural concerns about the pile integrity were reported by the contractor. The installation sequence started with the driving of pile 6 followed by driving of piles 5, 4, 3, and 2.

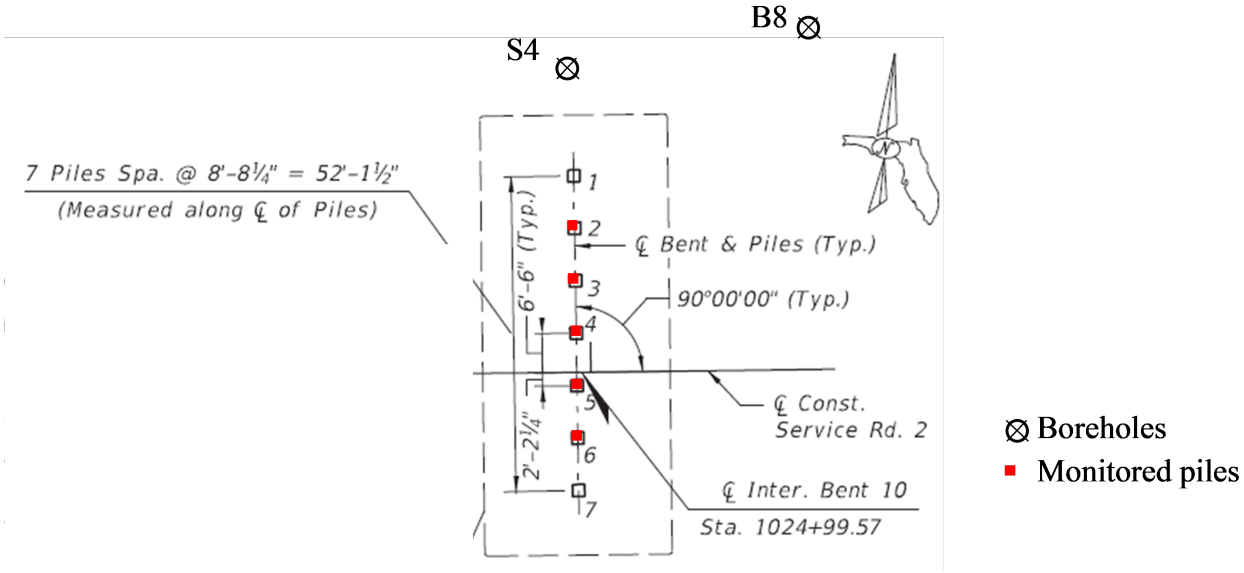

Figure 3-15. Detailed view of Bent 4 foundation layout at Site C.

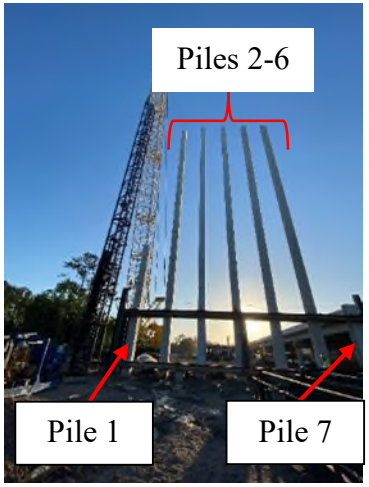

(a)

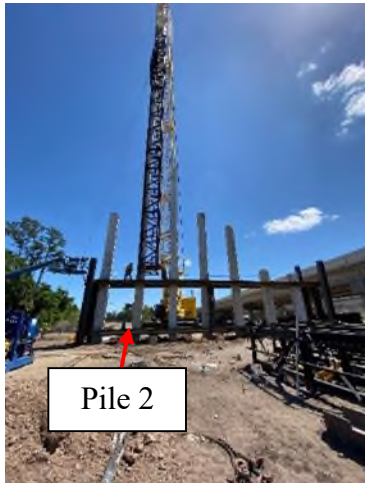

(b)

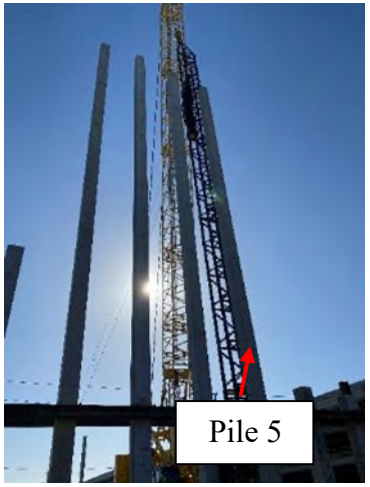

(c)


(d)


(e)


(f)

Figure 3-16. Pile driving process at Site C: (a) initial conditions at beginning of driving, (b) driving of pile 2, (c) hammer in leads for driving of pile 5, (d) end of driving of piles 2 through 6, (e) plywood cushion with a thickness of 20 inches used for driving (placed on its side), and (f) impact hammer.

3.2.6. Site D

The project for Site D involved the construction of a connection ramp bridge at a highway intersection in Central Florida. The information provided by FDOT about this project included driving records from several test piles, soil borings, and structural drawings. The location of the soil borings performed at the project site (TB-63) and at nearby locations (B1 through B7) is presented in Figure 3-17.

Figure 3-17. Location of soil borings relative to the construction site at Site D (Map data © 2021 Google).

The foundation system for the structure consisted of groups of 12 precast prestressed concrete piles. A dynamic test conducted at pile 1 of pier 11RT was selected for the analyses. The 90.0 ft long, 24 in square prestressed concrete pile was pre-drilled at a depth of 32.0 ft before the pile driving operations started. The pile was installed by using an APE D70-52 open-ended diesel (OED) hammer with a ram weight of 15.4 kips and a maximum rated energy of 173.6 kip-ft. A 15 in. thick plywood pile cushion was used but it was later modified during the driving process for an 18 in thick plywood. The hammer cushion consisted of 2 layers of 1 in. thick Micarta and 3 layers of 0.5 in thick aluminum materials.

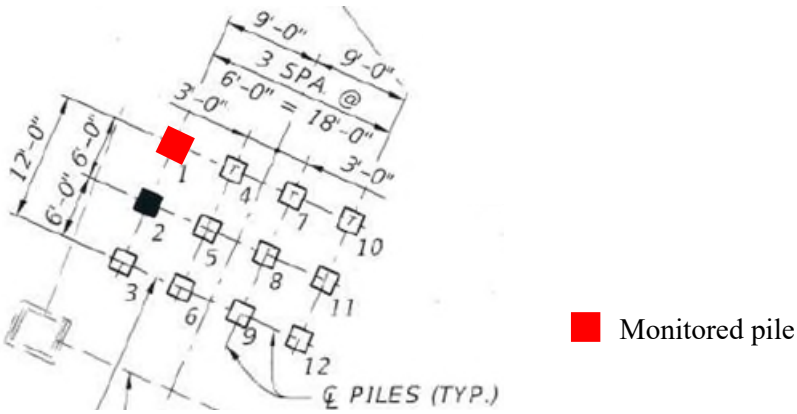

Figure 3-18. Detailed view of Pier 11 RT foundation layout at Site D.

3.3. SOIL CONDITIONS AT THE SITES

The soil conditions at the sites were defined based on SPT, CPTs, and index properties: fine contents, water contents (w), liquid limits (LL), and plastic limits (PL). The relative density (D_r) of the sand layers and the undrained shear strength (S_u) of interbedded clay layers were determined by using correlations with blow counts presented by Kulhawy and Mayne (1990). In summary, the soil conditions in the area were characterized by the presence of mostly poorly graded sands and silty sands (i.e., SP and SM based on USCS soil classification) of relative densities in the medium-dense range.

3.3.1. Sites A1 and A2

Figure 3-19 presents the results of the subsurface exploration data collected at project Site A. The summarized soil conditions shown in the figure consist of a surficial 10 ft-thick muck layer which was removed before the pile driving operations started according to the contractor. Beneath this stratum, a silty sand layer was observed to a depth of approximately 60 ft. This layer presented a gradual increase in relative density from approximately 20% at the shallow portion to approximately 60% at a depth of 60 ft where the soil transitioned to a fat clay layer (CH) with a thickness of 10 ft. This clay layer was underlain by a 40 ft thick medium-dense sand stratum. Unlike the topmost silty sand layer, this medium-dense sand presented more uniform values of SPT blow counts with depth. At the bottom of the soil profile, a weathered limestone was found until the end of the boring depth of approximately 190 ft was reached. The figure also shows the approximate location of a shallow groundwater table encountered at the project site.

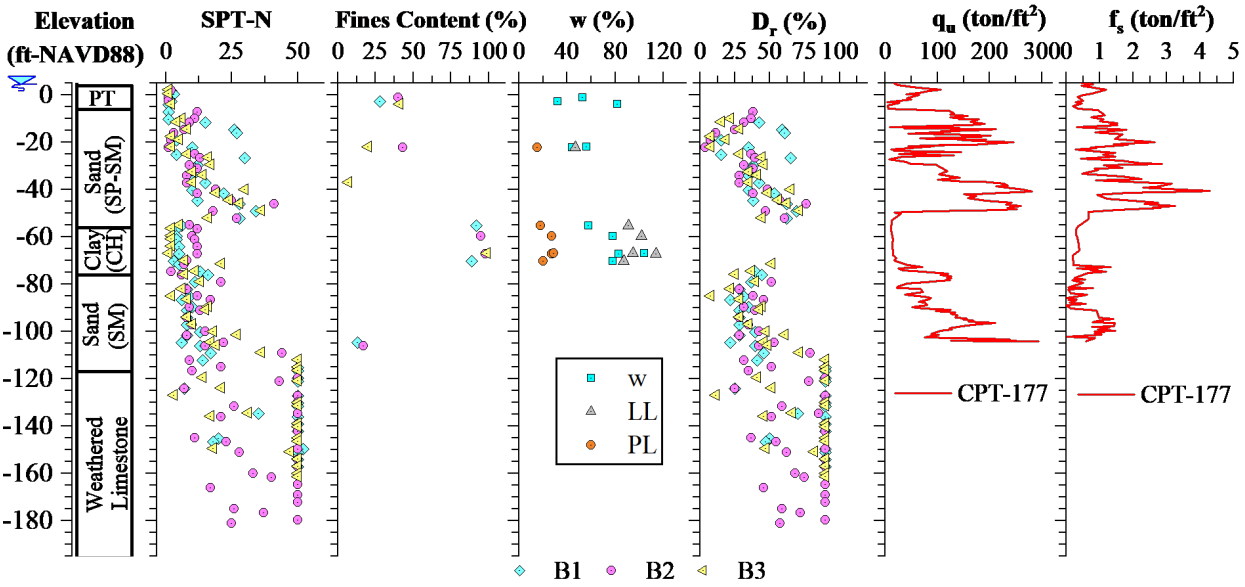

Figure 3-19. Summarized subsurface conditions at Sites A1 and A2.
Note: NAVD88= National American Vertical Datum of 1988.

3.3.2. Site A3

Figure 3-20 presents the results of the subsurface exploration data collected at project Site A3. The summarized soil conditions shown in the figure consist of a surficial 24 ft-thick fine silty sand layer with some organic material. This stratum is underlain by a 15 ft-thick sandy fat clay layer interbedded with a brown muck (PT). The underlying layer of fine sand with silts extends up to a depth of approximately 60 ft. Relative densities ranging from 30% to 75% were observed in this layer. Some lenses of the overlying fat clay layer were observed in this stratum as well. A thick fat clay layer was encountered up to a depth of 95 ft. Notice how the cone tip resistance (q_u) as well as the blow counts decreased significantly through this layer. The weathered limestone, typical of the Central Florida region, was reached at a depth of approximately 125 ft. The figure also shows the approximate location of a shallow groundwater table encountered at the project site.

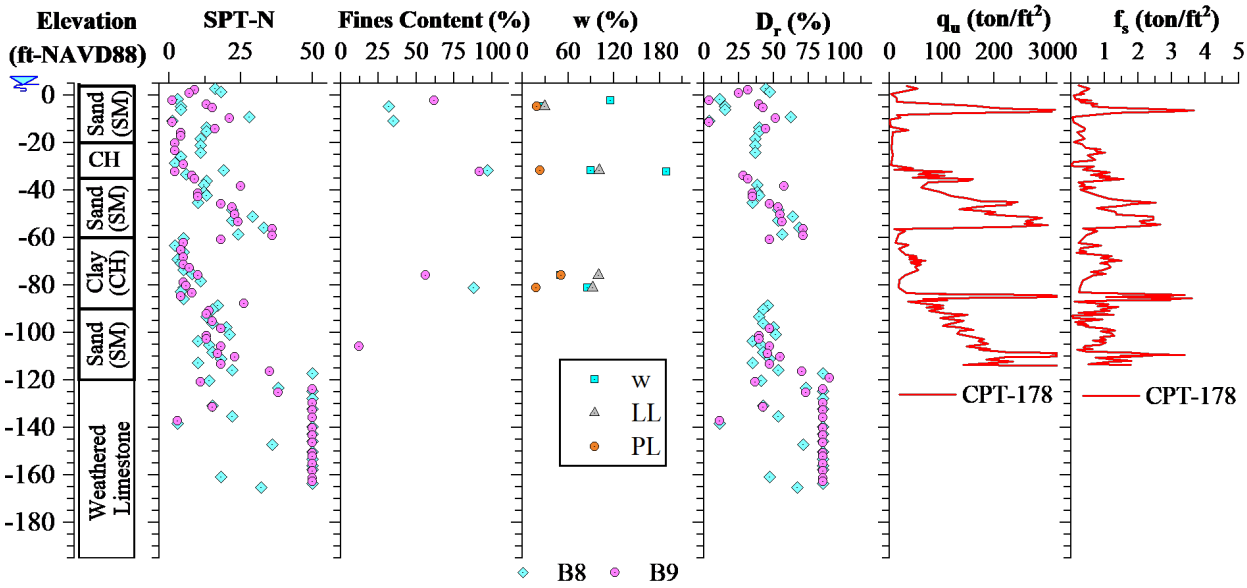

Figure 3-20. Summarized subsurface conditions at Site A3.
Note: NAVD88= National American Vertical Datum of 1988.

3.3.3. Site B

Soil conditions at Site B were not provided by the contractor of the project. The soil conditions in the area were defined based on information obtained from the FDOT soil borings database and consisted of a surficial loose to medium dense sand and silty sand up to a depth of 20 ft underlain by a 15 ft-thick sandy clay layer. A gray weathered dolostone with phosphates was found at the bottom of the borings which occurred at an approximate depth of 75 ft. The groundwater table was found approximately at the ground surface.

3.3.4. Site C

Figure 3-21 presents the results of the subsurface exploration data collected at project Site C. The summarized soil conditions shown in the figure consist of a surficial 40 ft thick poorly graded sand with silts (SP-SM) with relative densities varying between the loose and medium-dense state.

Some traces of clay were also found in this layer. The topmost sand layer was underlain by a 25 ft thick severely weathered gray dolomitic limestone with interbedded layers of SP-SM soils. The change in stratum can be observed in the sudden increase in the blow counts where practical refusal (i.e., more than 50 blows per foot) was reached. The bottom layer consisted of a silty sand (SM) layer with interbedded limestone lenses extending from a depth of 65 ft up to the bottom of the borings at a depth of 140 ft. Relative densities in this layer varied from medium-dense to dense.

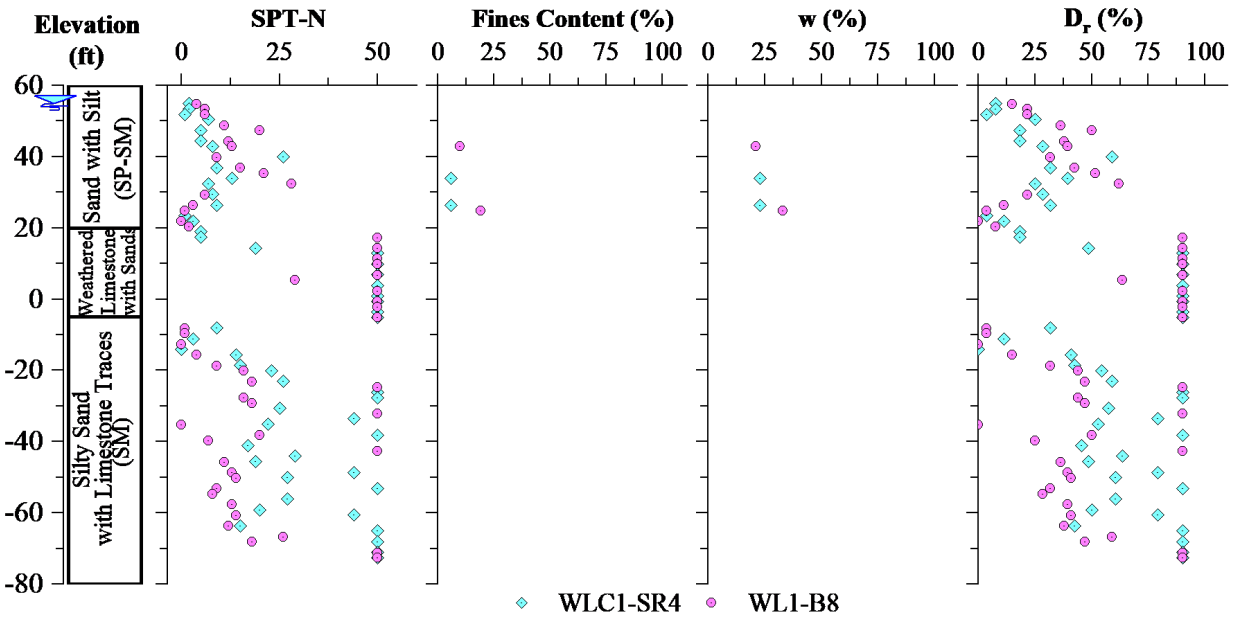

Figure 3-21. Summarized subsurface conditions at Site C.

3.3.5. Site D

Figure 3-22 presents the summarized subsurface conditions at Site D. The medium dense sand layer, which extends from the ground surface level to a depth of 20 ft, is underlain by a 23 ft thick medium stiff clay layer. A 49 ft thick loose to medium dense sand with a 45% relative density is followed by a dense sand of 85% in relative density. The predominant soil conditions at Site D consist mainly of medium dense sands, except for the 23 ft thick interbedded fat clay layer (very typical of the greater area defined for this study) and some transitional zones from silty clays to silty sands of relative densities lower than 40%. The figure also shows the approximate location of the shallow groundwater table found at the project site.

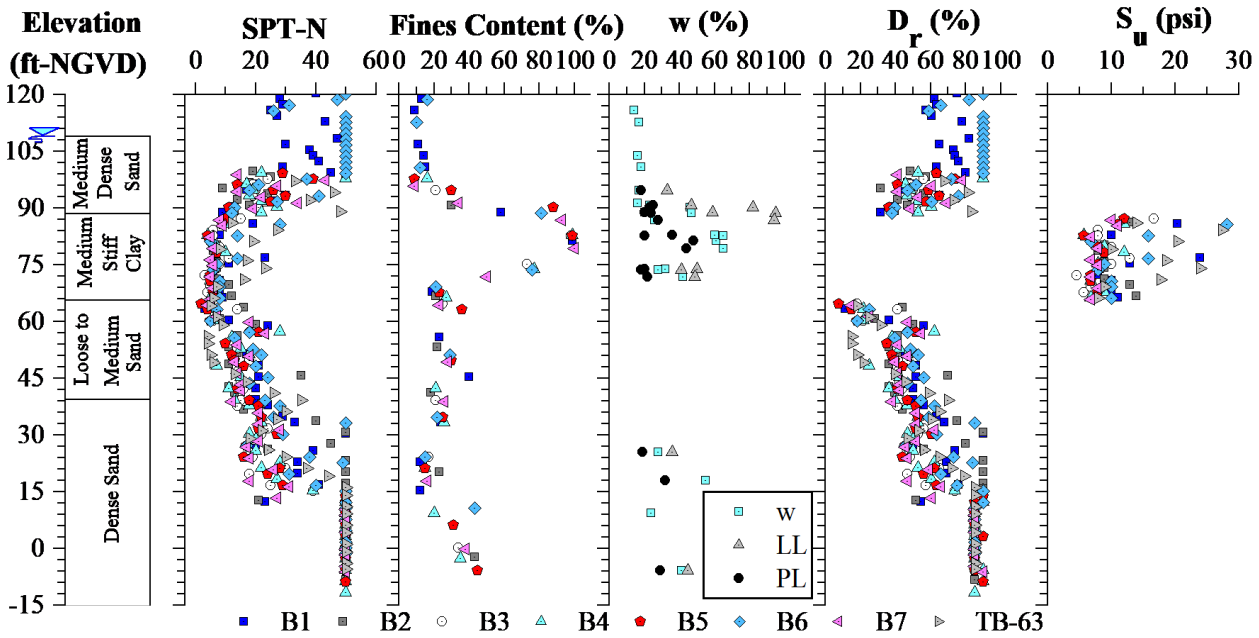

Figure 3-22. Summarized subsurface conditions at Site D (after Turkel et al., 2021).
Note: NGVD= National Geodetic Vertical Datum.

3.4. FIELD TESTING PROCEDURE

This section presents details of the field equipment installation at Sites A, B, and C used to measure ground deformations and vibrations during pile driving. As shown in Table 3-4, Sites A, B, and C were the projects selected in this research to collect data.

3.4.1. Site A1

The field measurements at Site A1 consisted of ground deformations measured with the survey equipment and ground vibrations measured with the geophones. The measurements during pile driving operations of pile 10 were performed by tracking the vertical position of survey nails at the locations of the geophones. Figure 3-23 shows the equipment installed at Site A1 during installation of pile 10. A survey nail was installed very close to the sheet piles to measure the effects of this temporary structure around pile 10.

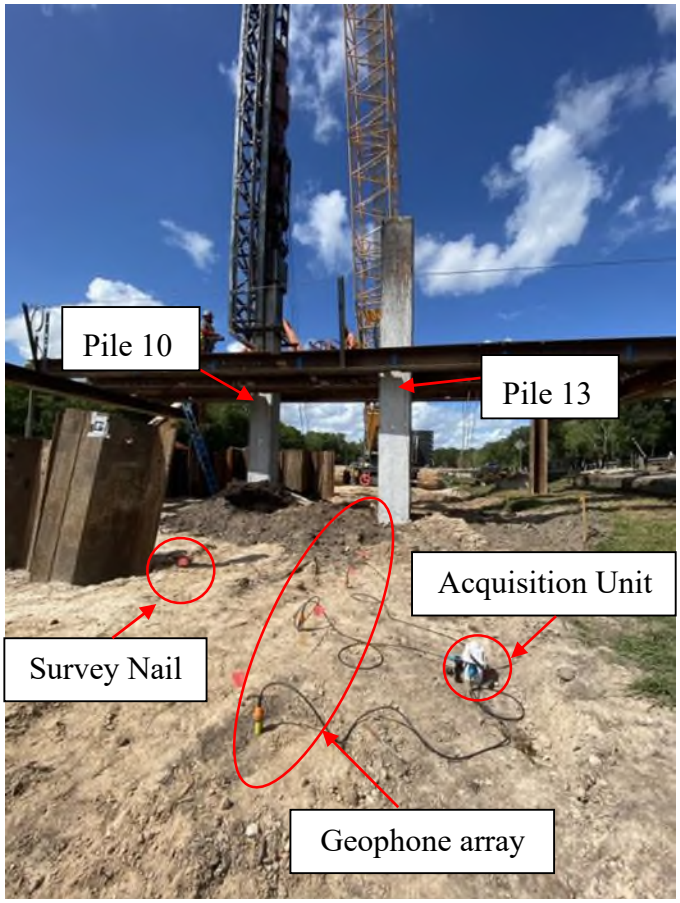

Figure 3-23. Field equipment installed during driving of Pile 10 at Site A1.

Figure 3-24a presents the survey equipment layout during driving of pile 13. The ground deformations were measured at the location of the nine geophones. The closest geophone (G1) was located 11 ft away from the center of test pile 13. Geophones G1 through G6 were spaced at 5 ft. Three geophones (i.e., G7 through G9) were placed 57 ft away from the pile to capture vibrations and deformations on the free-field zone. Figure 3-24b presents the survey equipment layout during driving of pile 10. The survey nails were located in front of pile 13 due to the restrictions from the sheet pile installed around pile 10. The closest survey nail was placed 7.9 ft away from the center of pile 13 and 17.2 ft away from the center of pile 10, which corresponds to 8.6 times the width of the 24-in prestressed concrete pile.

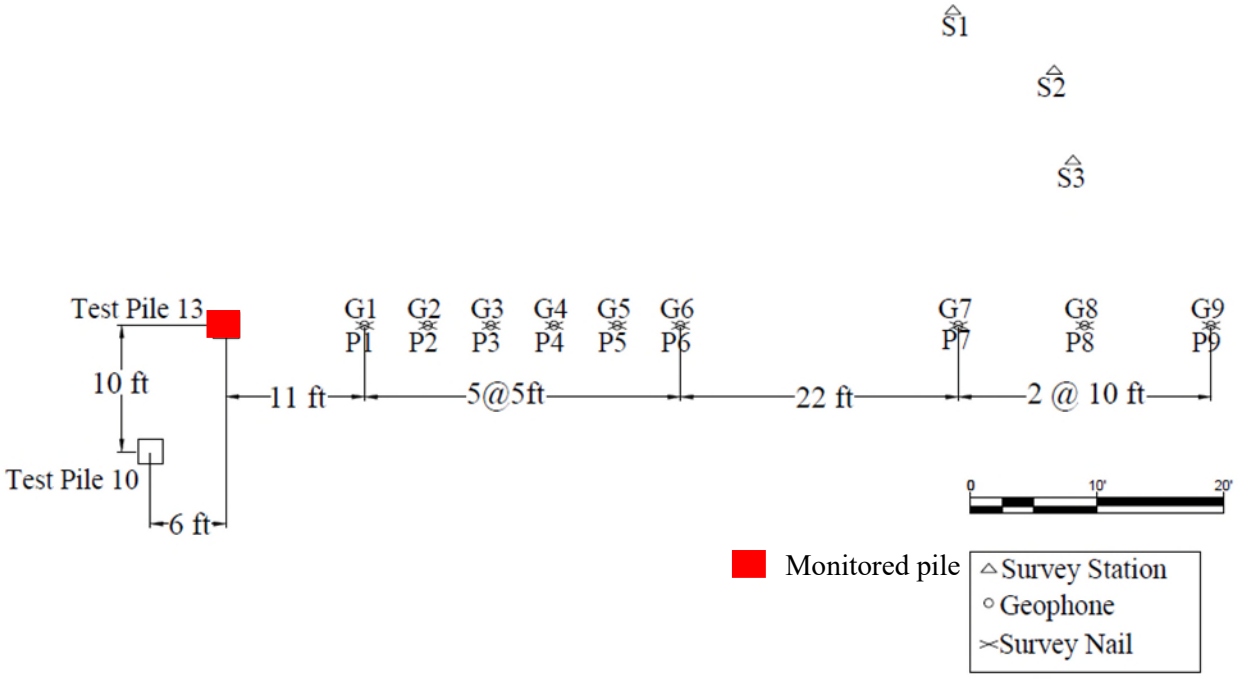

(a)

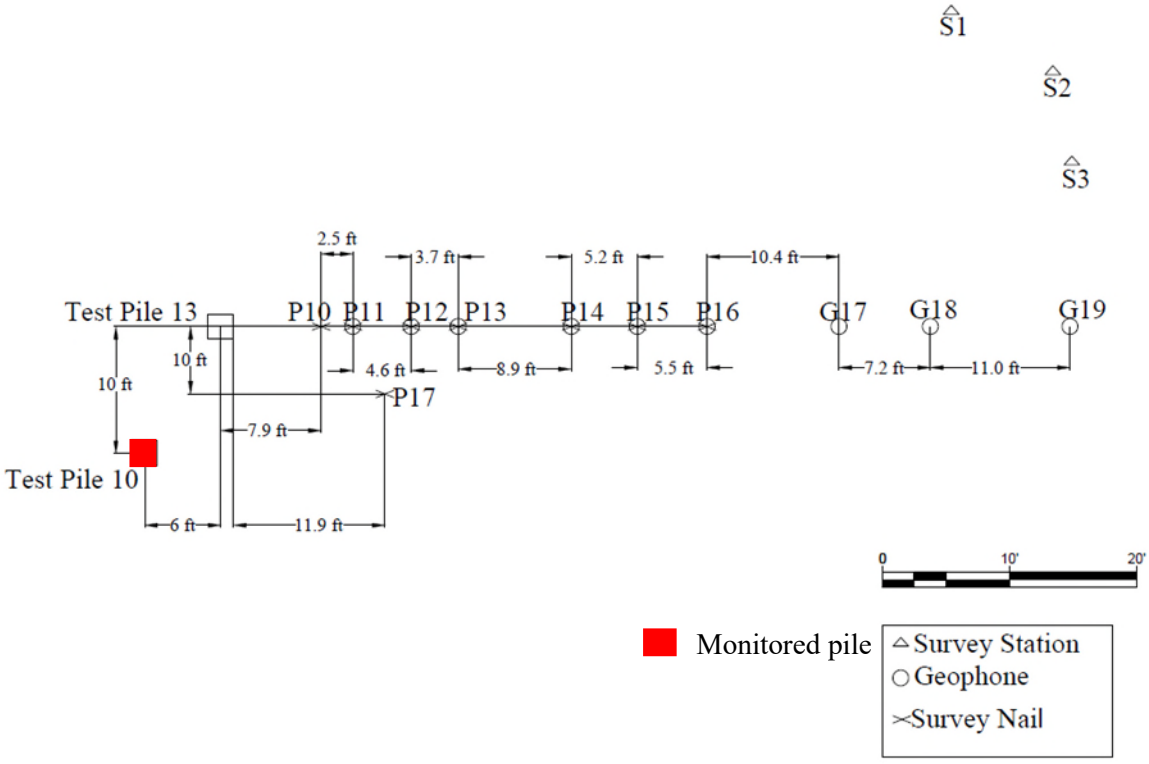

(b)

Figure 3-24. Plan view of the instrumentation layout showing location of geophones, survey nails, and survey stations used to collect data during driving of: (a) pile 13 and (b) pile 10 at Site A1.

3.4.2. Site A2

The field measurements at Site A2 consisted of ground deformations measured with the survey equipment and ground vibrations measured with the geophones. The measurements conducted during pile installations were performed using survey nails at the locations of the geophones. Figure 3-25 shows the equipment installed at Site A2 during driving of piles 8 and 15. The equipment was installed in front of each pile and around an idle hydraulic hammer power pack. Sheet piles were not installed near this pier like one shown for Site A1.

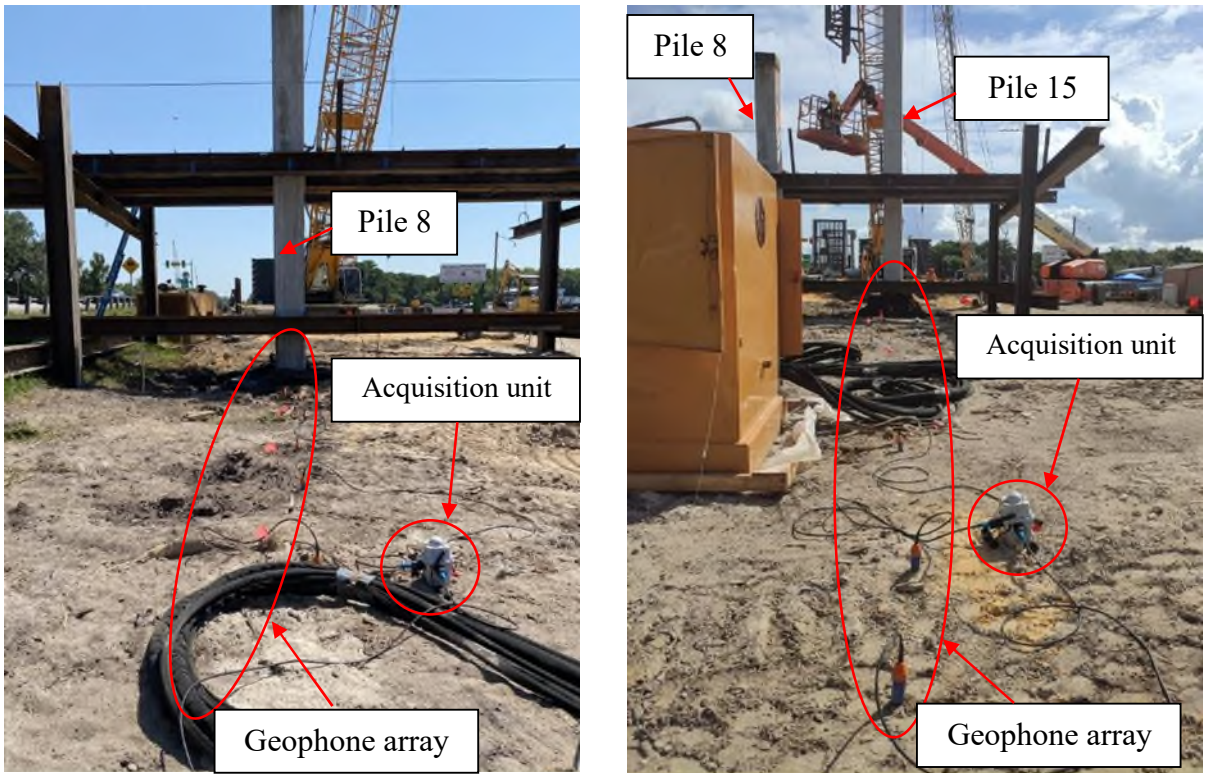

(a) (b)

Figure 3-25. Field equipment installed at Site A2 during driving of: (a) pile 8 and (b) pile 15.

Figure 3-26a presents the equipment layout during installation of pile 8. The first survey nail (P1) was installed 4.2 ft away from the center of test pile 8. The rest of the survey nails were located 11 ft away from the center of the pile at an approximate spacing of 5 ft. Geophones were located next to survey nails P2 through P6. In order to analyze ground vibrations in the far-field zone, three geophones spaced at 5 ft were located at 52 ft away from the pile. Figure 3-26b presents the equipment layout during driving of pile 15. The first survey nail for ground deformation measurements was located 11 ft away from the pile with the remaining four survey nails spaced at 5 ft. Five geophones were located next to the survey nails to measure PPVs at the same location as the deformation measurements. Three geophones were located at 54.5 ft away from the center of pile 15 to measure ground vibrations in free-field conditions.

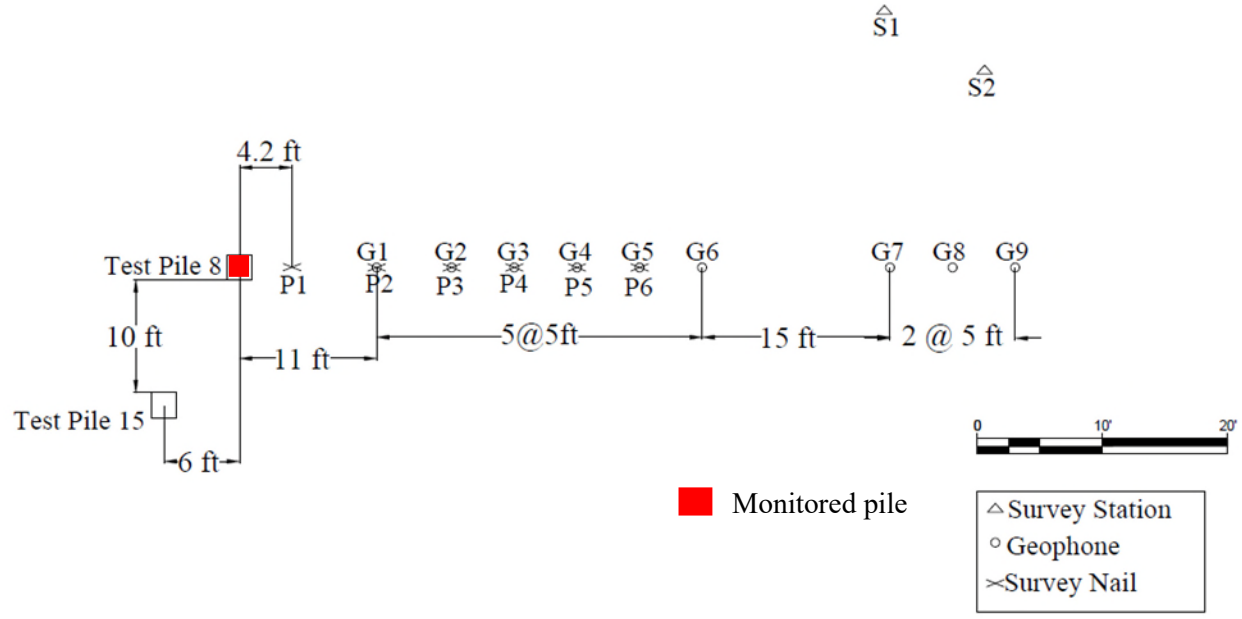

(a)

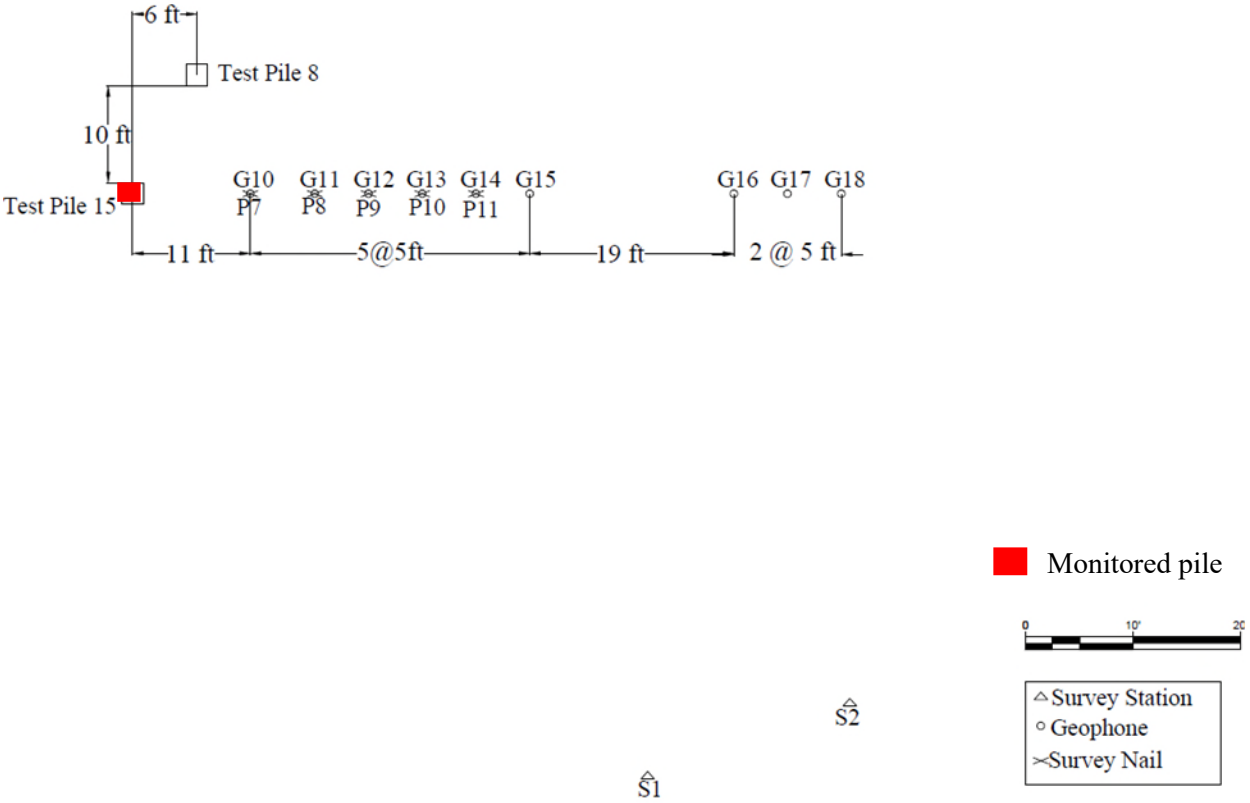

(b)

Figure 3-26. Plan view of the instrumentation layout showing location of geophones, survey nails, and survey stations used to collect data during driving of: (a) pile 8 and (b) pile 15 at Site A2.

3.4.3. Site A3

The field measurements at Site A3 consisted of ground deformations measured with the survey equipment and ground vibrations measured with the geophones. The measurements during pile driving operations of pile 4 were performed by tracking the vertical position of survey nails at the locations of the geophones. Figure 3-27 shows the equipment installed at Site A3 during installation of pile 4. Recall that the pile was driven in two days since it was spliced into two 80 ft-long segments. Figure 3-27a shows the equipment installed during driving of the first segment while Figure 3-27b presents the equipment installed during driving of the second pile segment. Survey nails were installed at the same location in both days in order to track ground deformations during the entire installation of pile 4.

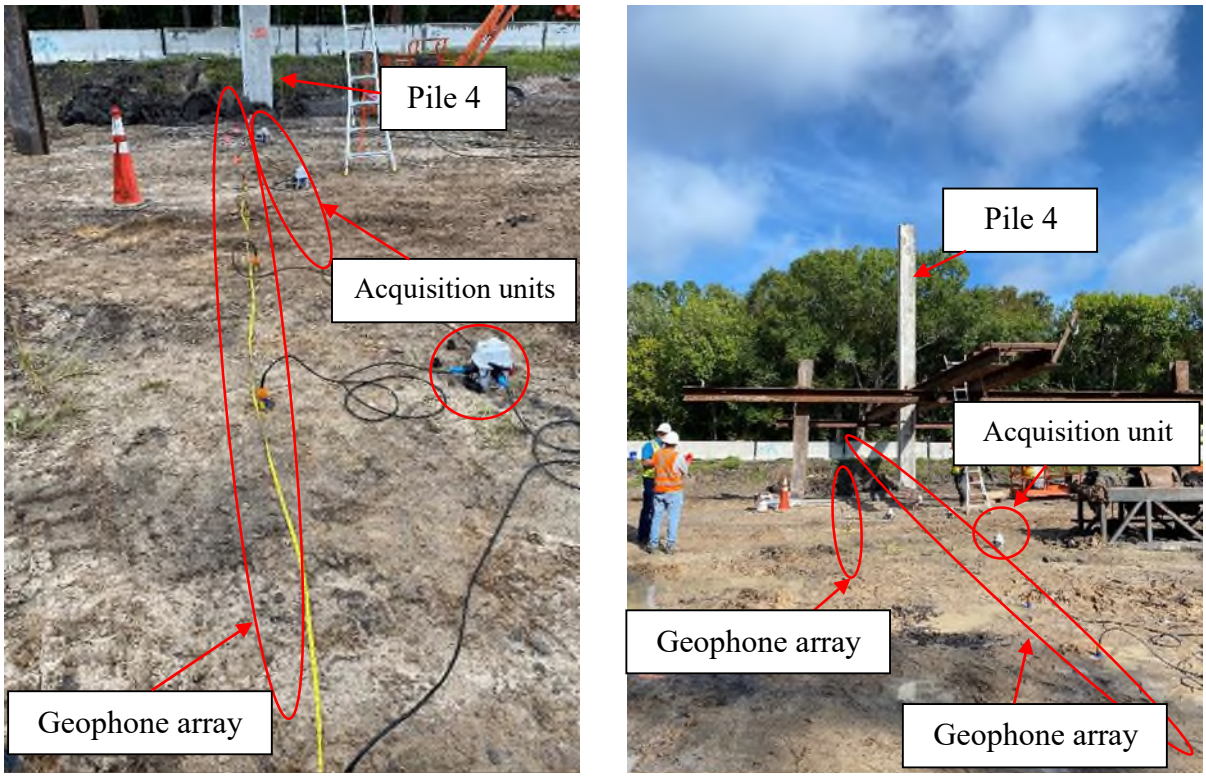

(a) (b)

Figure 3-27. Field equipment installed at Site A3 during driving of pile 4: (a) first segment and (b) second segment.

Figure 3-28 presents the equipment layout during installation of pile 4. Figure 3-28a shows the equipment layout during driving of the first pile segment. A total of five survey nails were used in the field. The first survey nail (P1) was installed 11 ft away from the center of the pile. The rest of the survey nails were spaced at 5 ft. Geophones were installed at a spacing of 5 ft as well from a distance of 11 ft to 51 ft away from the pile to a distance up to 51 ft away from the pile. Figure 3-28b presents the equipment layout during installation of the second pile segment. The location of the survey nails remained the same as for the previous day. Two arrays of geophones were installed during installation of the second pile segment (i.e., L1 and L2). The geophone array L1

consisted of a total of 12 geophones spaced at 5 ft. Geophone array L2 consisted of 6 geophones spaced at 5 ft as well.

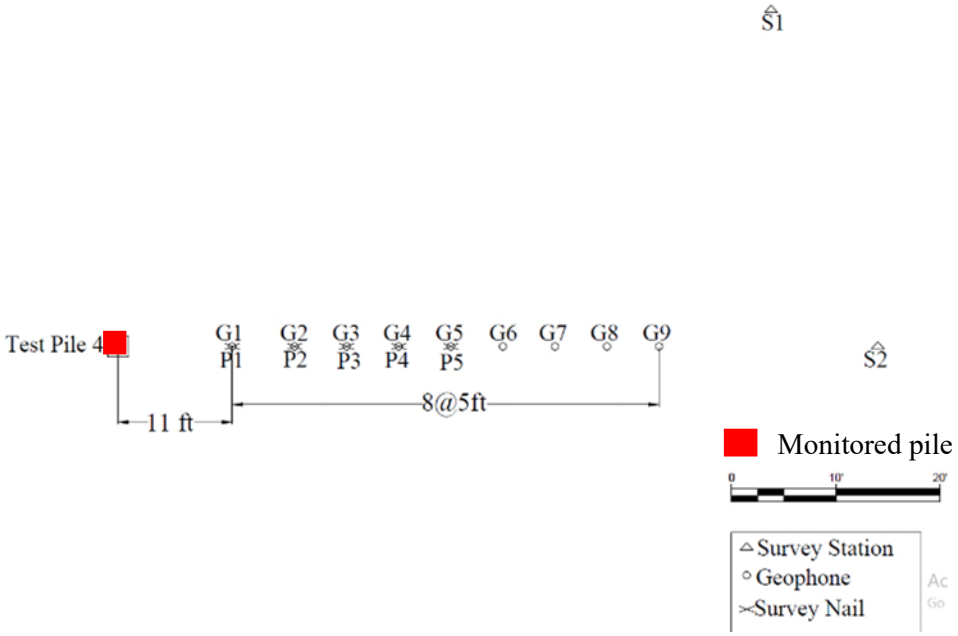

(a)

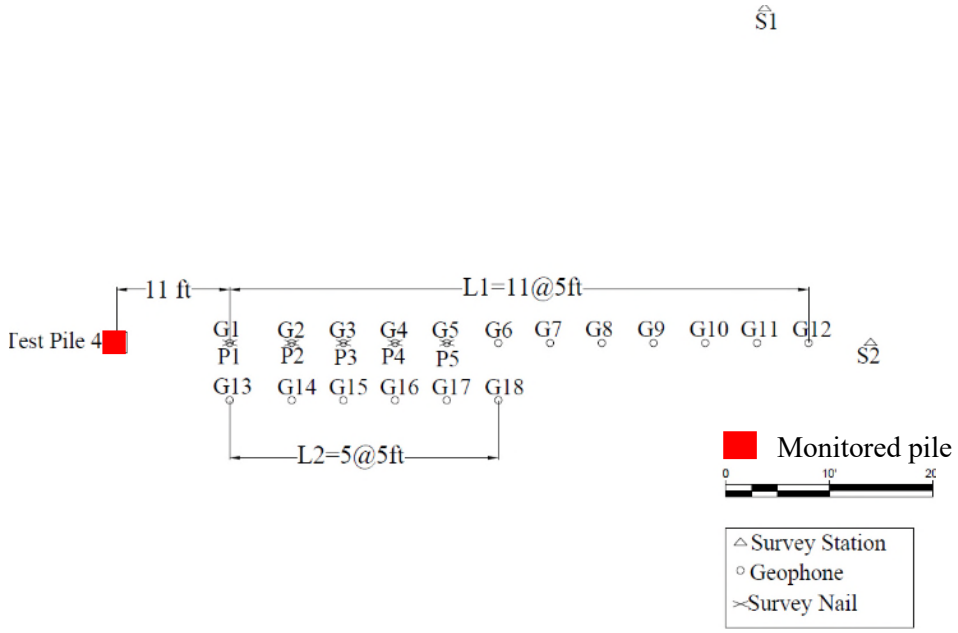

(b)

Figure 3-28. Plan view of the instrumentation layout showing location of geophones, survey nails, and survey stations used to collect data during installation of pile 4 for: (a) first segment before splicing and (b) final stage after splicing.

3.4.4. Site B

The nine 5.0 Hz geophones described in Section 3.1.1 were used to measure ground vibration levels outside the cofferdam installed at Site B for the construction of the pier. The locations of the geophones were also used as settlement points to control the ground movements with the 3 survey equipment stations (see Figure 3-29a). Additionally, a settlement plate was located at the same distance as the first geophone (i.e., G1) to control ground surface deformations as close as possible to the cofferdam (see Figure 3-29b). Those settlement points were controlled with survey equipment stations shown in the figure.

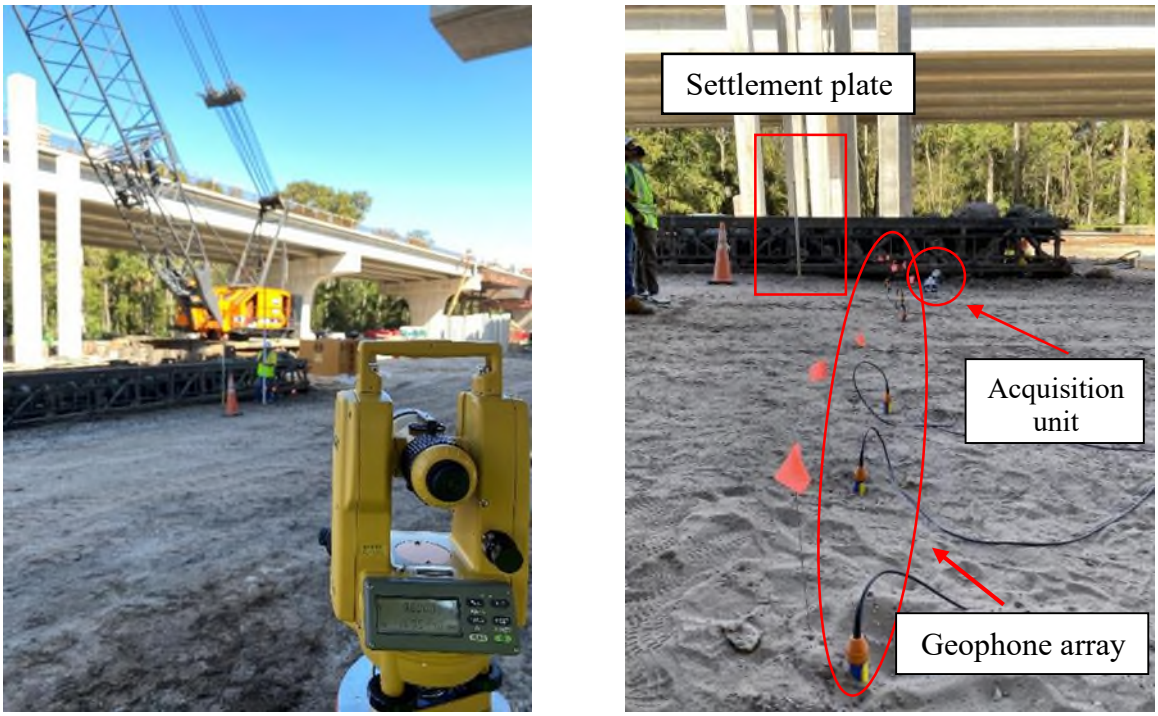

(a) (b)

Figure 3-29. Field equipment installed at Site B: (a) survey station and (b) settlement plate and geophones installed in the field.

Figure 3-30 presents the layout of the geophones installed in the field. The cofferdam was located approximately 10 ft to 15 ft away from the test pile. The closest location that the geophones were allowed to be installed was 11.3 ft from the face of the cofferdam to satisfy safety requirements by the contractor. The remaining geophones in the array were placed at a separation of either 3.0 ft or 8.0 ft from each other. The spacing of 8 ft was necessary to allow construction trucks and equipment to drive through the project site prior to the pile driving process.

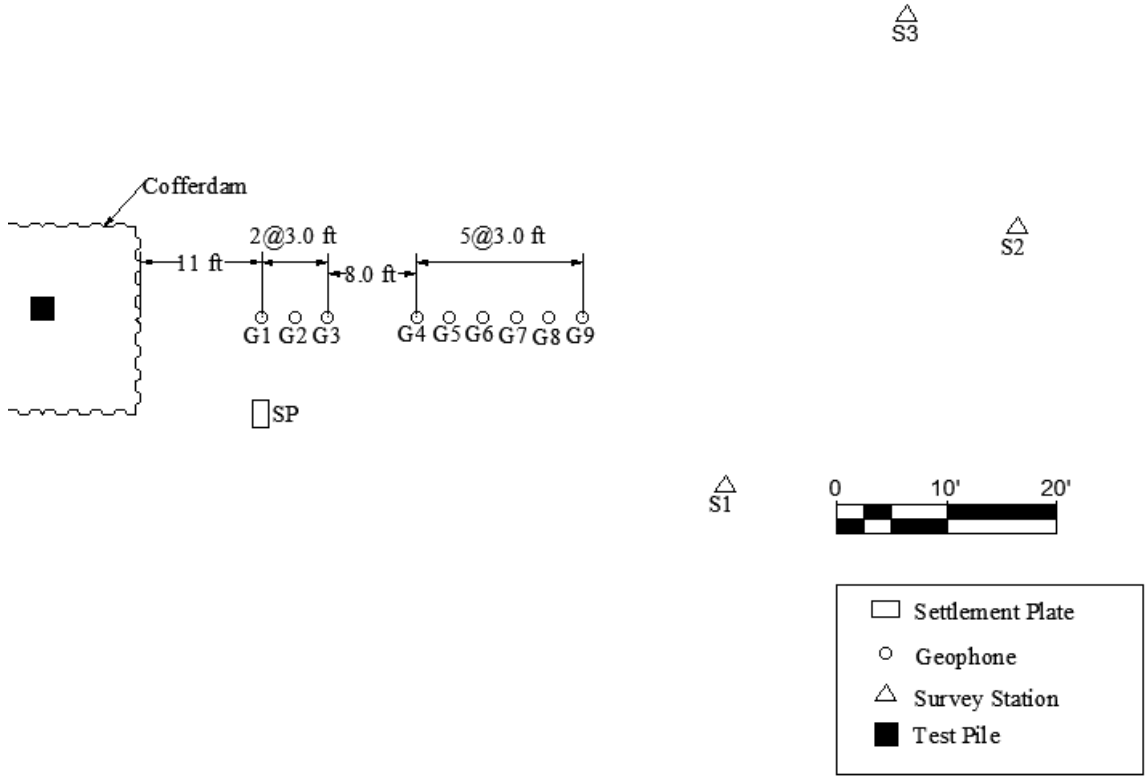

Figure 3-30. Plan view of the instrumentation layout showing location of geophones, survey nails, and survey stations used to collect data during driving of pile 12 at Site B.

3.4.5. Site C

Field measurements of ground deformations and vibrations were performed during installation of piles 2 through 6 at Site C. Figure 3-31a shows the geophones installed in the field to measure ground vibrations. The geophone array was located perpendicular to bent 4 and between piles 3 and 4. Figure 3-31b shows a survey station used for ground deformation measurements. The ground deformations were measured at the location of geophones shown in the figure.

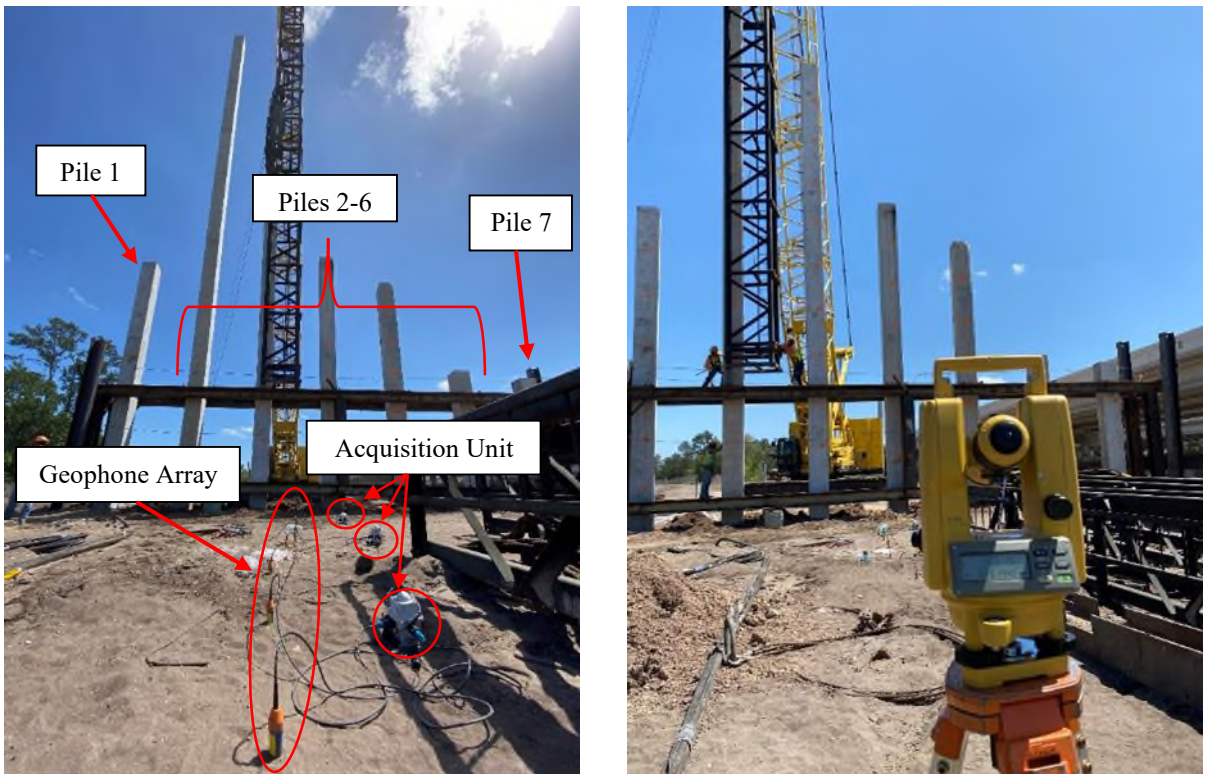

(a) (b)

Figure 3-31. Field equipment installed at Site C: (a) vertical geophones and (b) survey station.

Figure 3-32 presents the field equipment layout during installation of piles 2 through 6. The closest geophone (i.e., G1) was located 11 ft away from the center of the pile (i.e., 5.5 times the width of the pile). The rest of the geophones were equally spaced at 3 ft. Therefore, the last survey nail and geophone (i.e., G9) were located 35 ft away from the center of the pile corresponding to 17.5 times the width of the 24-in square prestressed concrete pile.

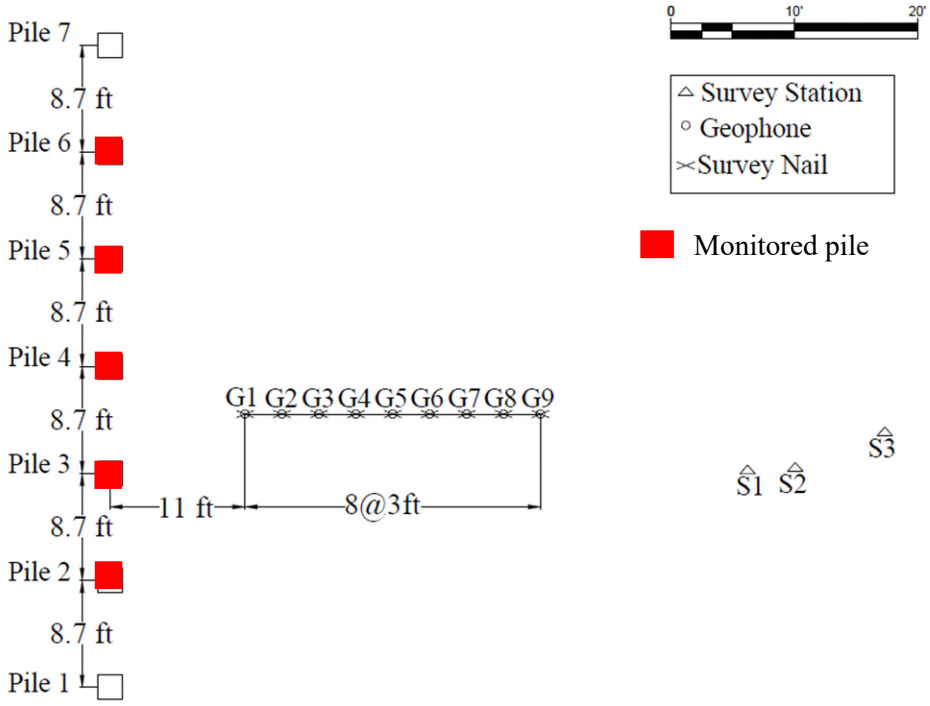

Figure 3-32. Plan view of the instrumentation layout showing location of geophones, survey nails, and survey stations used to collect data during driving of piles 2 through 6 at Site C.

3.5. DYNAMIC TEST PILE MEASUREMENTS

For this research, it was important to accurately quantify the force applied to the pile by the hammer since it has been shown that this variable largely affects the pile dynamics and the adjacent soil response in terms of ground deformations and vibrations. The force time history that a single hammer blow applies to the top of the pile for the different sites is the main input variable in the numerical models presented in further sections. EDC measurements were performed at Sites A1 and A2 during installation of the test piles. PDA tests were also performed at Sites B and D. PDA data were obtained from District 5 at FDOT for the construction of the bridge at Site D. The force applied on top of the pile was obtained from PDA results during the dynamic test pile for a single hammer blow as shown in Figure 3-33. The peak applied force was approximately 1600 kips and a complete hammer blow was applied in approximately 125 milliseconds.

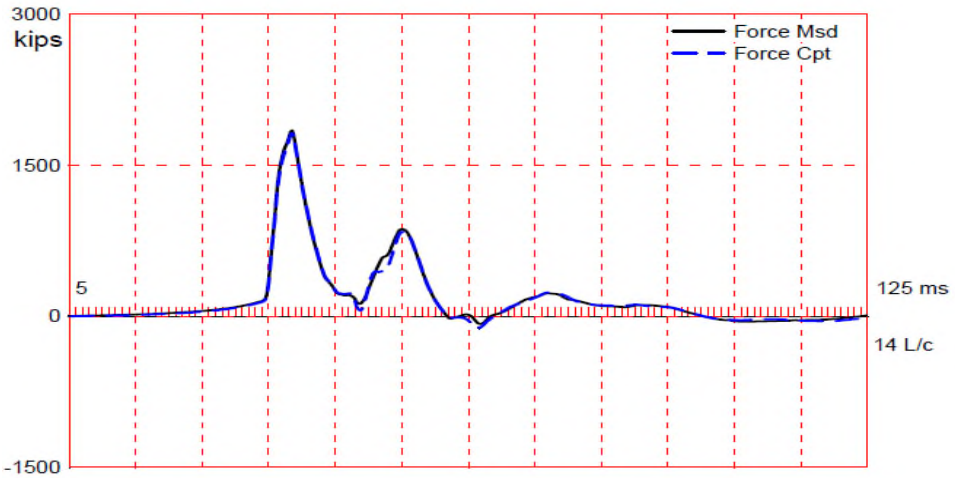

Figure 3-33. Typical measured impact force using APE D70-52 hammer at the top of pile 1 of pier 11RT for the 180th hammer blow at a penetration depth of 88.9 ft at Site D.

Pile penetration versus cumulative applied hammer blows from the different sites are also used in further sections to compare numerical models by varying different types of hammers and driving conditions. Figure 3-34 presents the measured pile penetration during the installation process for test pile 1 at Site D obtained from the driving logs. Only the pile penetration due to the applied hammer blows is presented, thus the pre-drilled length of 32 ft is not shown (i.e., initial pile penetration value set to zero). Notice that after 1173 hammer blows and a penetration depth of approximately 46.0 ft the driving effort changed due to a change in the fuel settings in the hammer. This is evidenced by the change in slope at approximately 1173 hammer blows. A total of 1822 blows were necessary to drive the pile 56.0 ft below the pre-drilled depth.

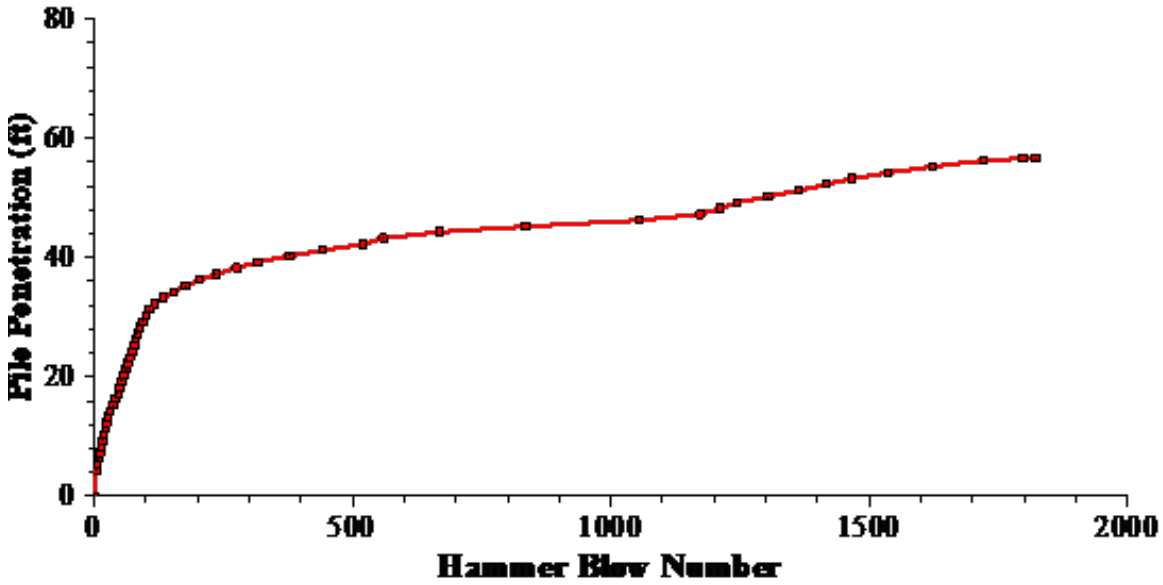

Figure 3-34. Vertical pile penetration versus cumulative hammer blows on top of the pile at pile 1, pier 11RT, Site D showing the hammer blows necessary to reach a penetration depth below the pre-drilled value.

3.6. MEASUREMENTS OF GROUND DEFORMATIONS

3.6.1. Site A1

Figure 3-35 presents the ground deformation time history during installation of pile 13 at each control point (i.e., P1 through P9). Positive values express heave while negative values represent settlement. Notice that a maximum settlement of approximately 1.2 in occurred at the location of P1 and P2 which are located at distances from the center of the pile of approximately 11 ft and 16 ft (i.e., 5.5 and 8.0 times the width of the pile), respectively. The settlement decreased after that point since heave occurred as the pile penetrated deeper into the ground.

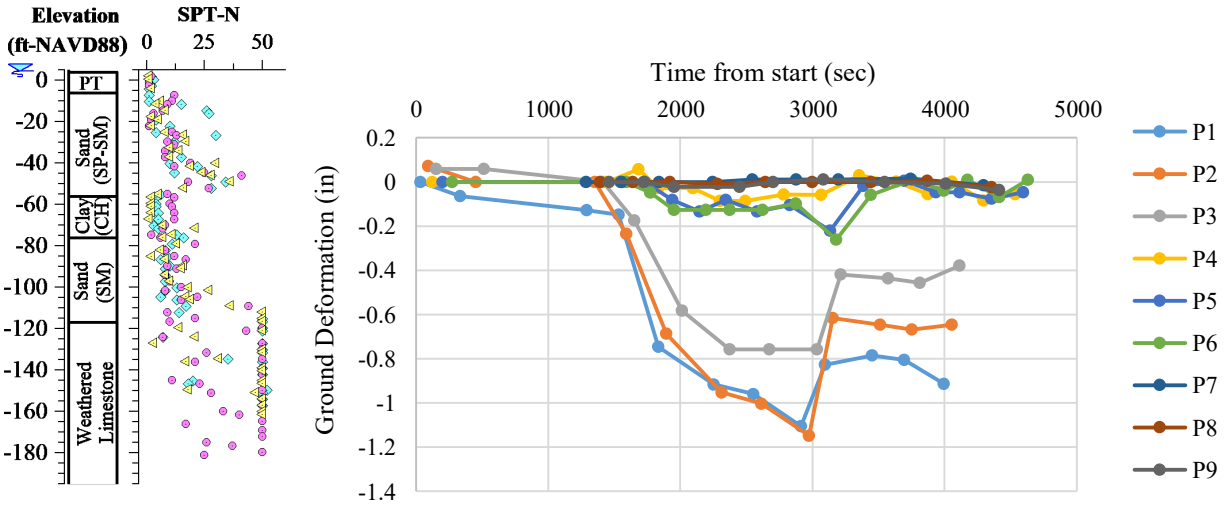

Figure 3-35. Ground deformations time histories during installation of pile 13 at Site A1.

Figure 3-36 presents the final ground deformations measured after installation of pile 13. Notice that close to the pile a final settlement of approximately 0.8 in occurred. Settlements are negligible at approximately 26 ft (i.e., 13 times the pile width). The attenuation properties of the soil in terms of deformations at the site are significant. Recall that the predominant soil conditions at this site are sandy soil layers with varying relative densities and that the pile was predrilled 22 ft below the ground surface.

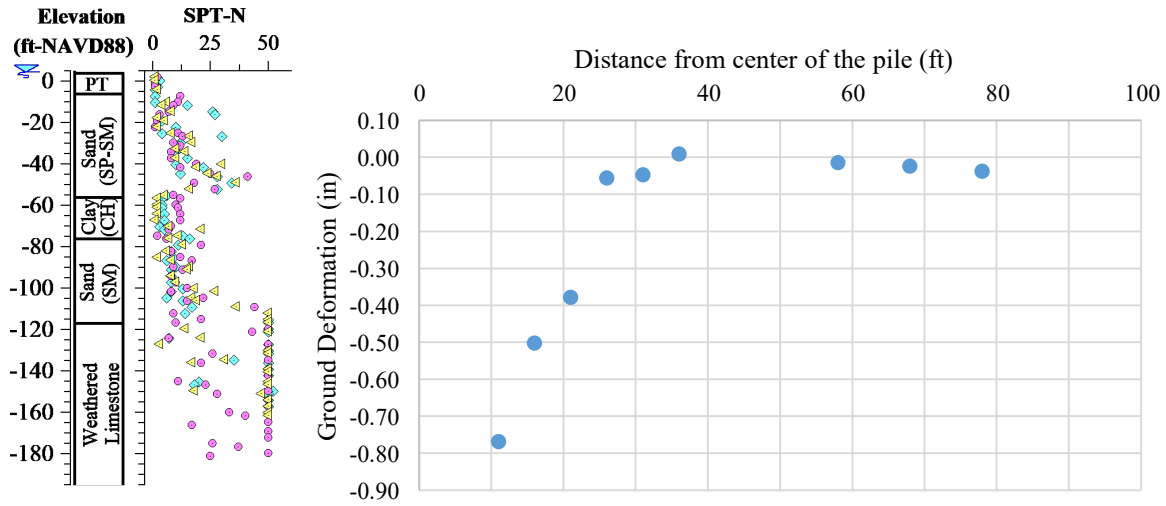

Figure 3-36. Final ground deformations induced by driving of pile 13 at Site A1.

Figure 3-37 presents the ground deformation time history for pile 10 measured at the survey nails. Installation of pile 10 at pier 3 occurred after pile 13 was driven. First, single hammer blows were applied every 2 or 3 minutes up to 1500 seconds. This change in the hammer blow application rate can be observed in the figure at approximately 1500 to 1600 s from the start of driving. The

hammer cushion was changed at approximately 4000 s, which can be noticed in the sudden increase in the magnitude of heave for settlement point P13 and P14 which are approximately 27.4 ft and 35.6 ft away from the center of the pile (i.e., 13.7 and 17.8 times the width of the pile), respectively. Mostly ground surface settlements were measured at P17 (i.e., survey nail close to the sheet piles) with a maximum settlement of approximately 0.2 in for this pile. This can be attributed to the relative position of the settlement point P17 with respect to the sheet piles and their attenuation characteristics.

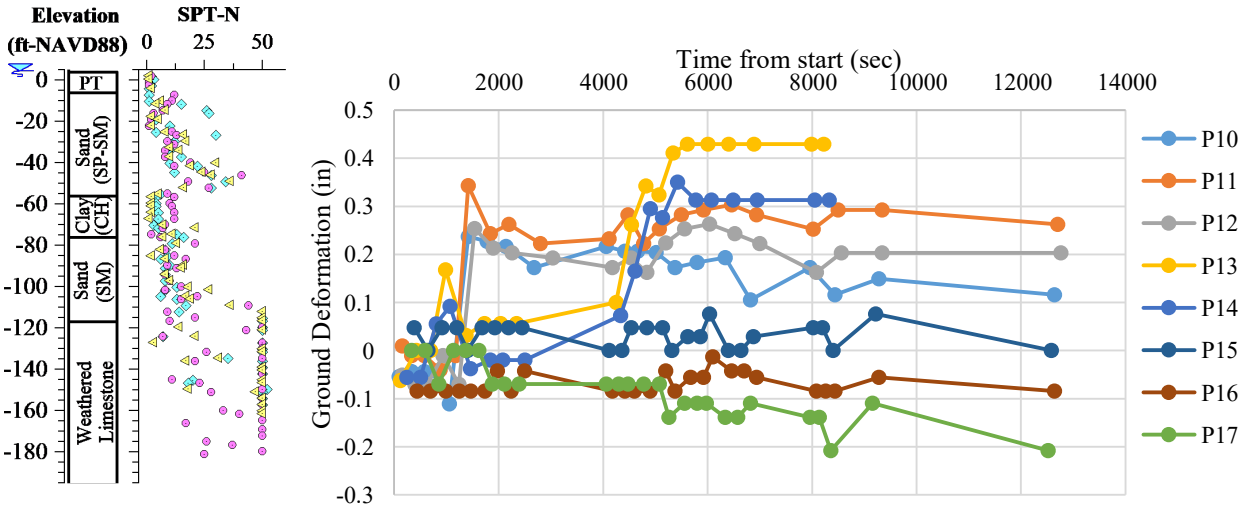

Figure 3-37. Ground deformations time histories during driving of pile 10 at Site A1.

Figure 3-38 presents the final ground deformation profile (i.e., after driving pile 10), which represents "residual" vertical displacements at the end of the pile installation. A maximum heave of approximately 0.4 in occurred at 27.4 ft away from the center of the pile (i.e., 13.7 times the pile width). Installation of pile 10 caused mostly heave at the ground surface in relation to the ground deformations during installation of the first pile 13. This can be attributed to the densification process of medium-dense sandy soils caused after installation of pile 13, thus causing volumetric expansion during installation of pile 10.

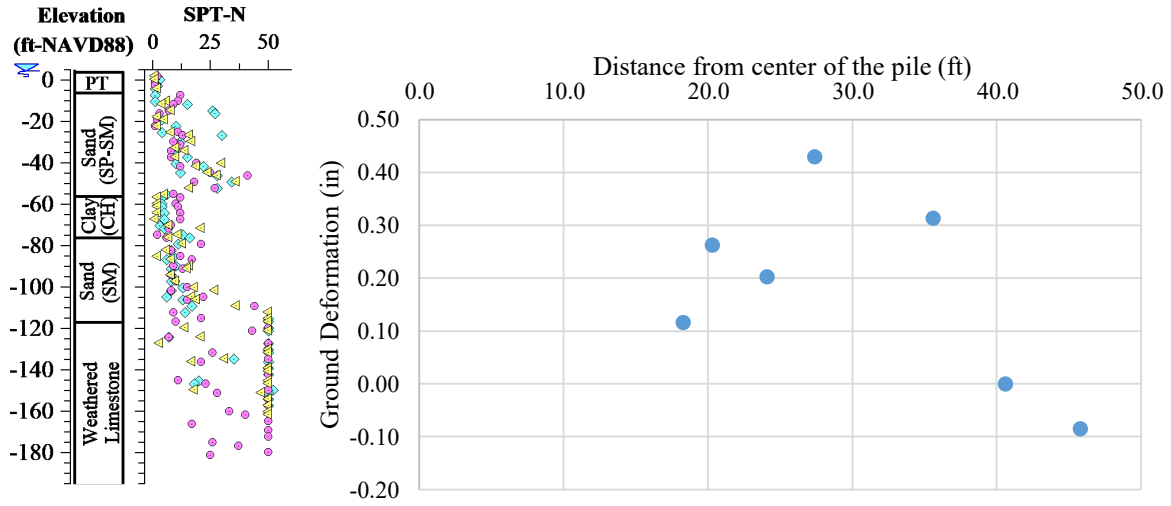

Figure 3-38. Final ground deformations induced by driving of pile 10 at Site A1.

3.6.2. Site A2

Figure 3-39 presents the ground deformation time history during installation of pile 8 at Site A2. Ground deformation measurements were performed after changes in the driving accessories due to excessive transmitted energy, thus the pile driving process had already started and larger ground deformations could have been measured. The hammer blows applied prior to the change in the driving accessories were 1215 out of the total 3169 applied hammer blows. Notice how the deformations tend to reach a plateau after the pile driving was performed for a certain period. This occurred when the pile tip reached large depths, causing less impact in the deformations measured at the ground surface.

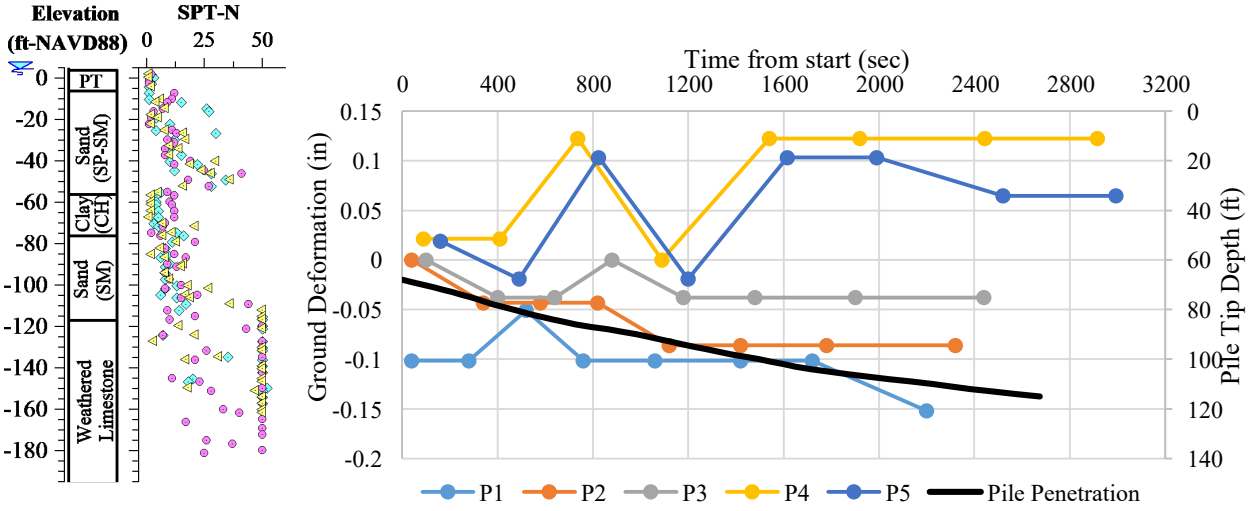

Figure 3-39. Ground deformation time history during driving of pile 8 at Site A2. Dual axis showing pile penetration.

Figure 3-40 presents the final ground deformations after installation of pile 8 at Site A2. The installation of this pile was characterized by a combination of settlement and heave depending on the location of the settlement point and the time in the installation sequence. A maximum settlement of only 0.15 in was measured at a distance from the pile of 4.2 ft (i.e., 2.1 times the width of the pile). A maximum heave of 0.12 in was measured at 22.3 ft away from the pile. Notice that the ground deformations are smaller compared with values measured at Site A1, since the measurements were taken after the driving accessories were changed. This highlights the importance of estimating the transmitted energy in order to accurately predict ground deformations.

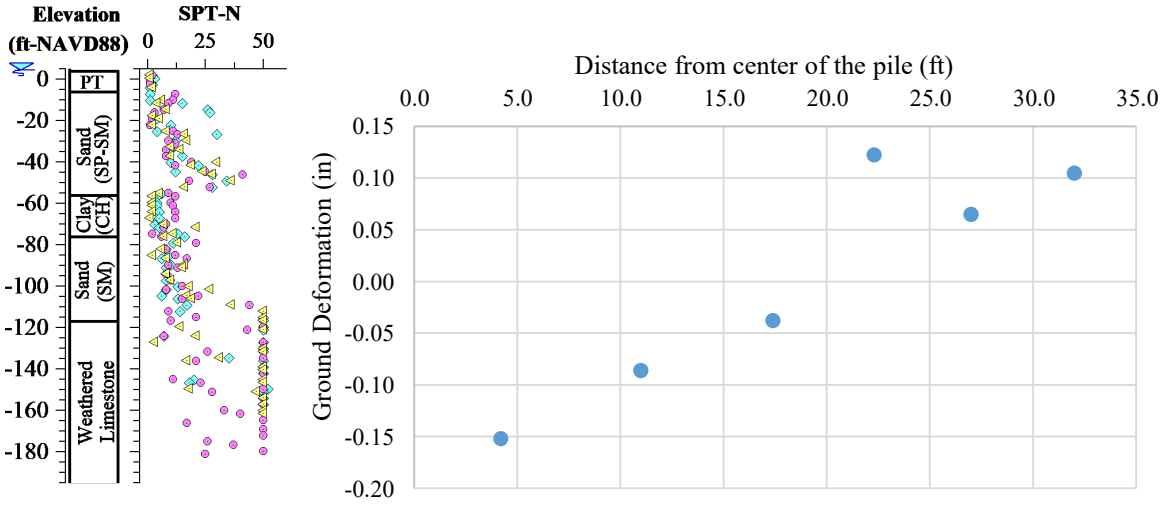

Figure 3-40. Final ground deformations induced by driving of pile 8 at Site A2.

Figure 3-41 presents the ground deformation time history at each survey nail due to installation of pile 15 at Site A2. A maximum heave of 0.2 in was measured at the beginning of the driving process at the closest point to the pile (i.e., P7). Notice that for survey nails P7 through P9 the ground deformations started with a maximum value and then attenuated during driving. This can also be attributed to the depth of the pile tip as the driving process occurs.

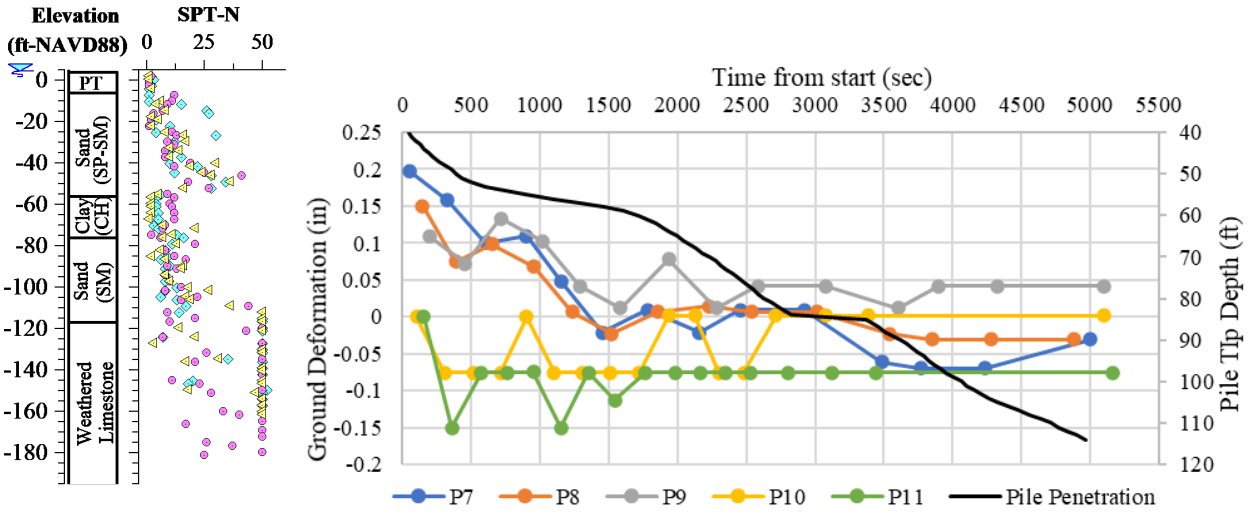

Figure 3-41. Ground deformation time history during driving of pile 15 at Site A2. Dual axis showing pile penetration.

Figure 3-42 presents the final ground deformations after installation of pile 15 at Site A2. In this case, the ground deformations were negligible since they were within the accuracy of settlement measurements with survey equipment of approximately 1/8 in. Similar to the case of Site A1, the ground deformations induced by driving of the second test pile were smaller than the deformations measured during driving of the first test pile. This confirms that there is a densification process during the first pile installation that affects the ground response during driving of the second test pile.

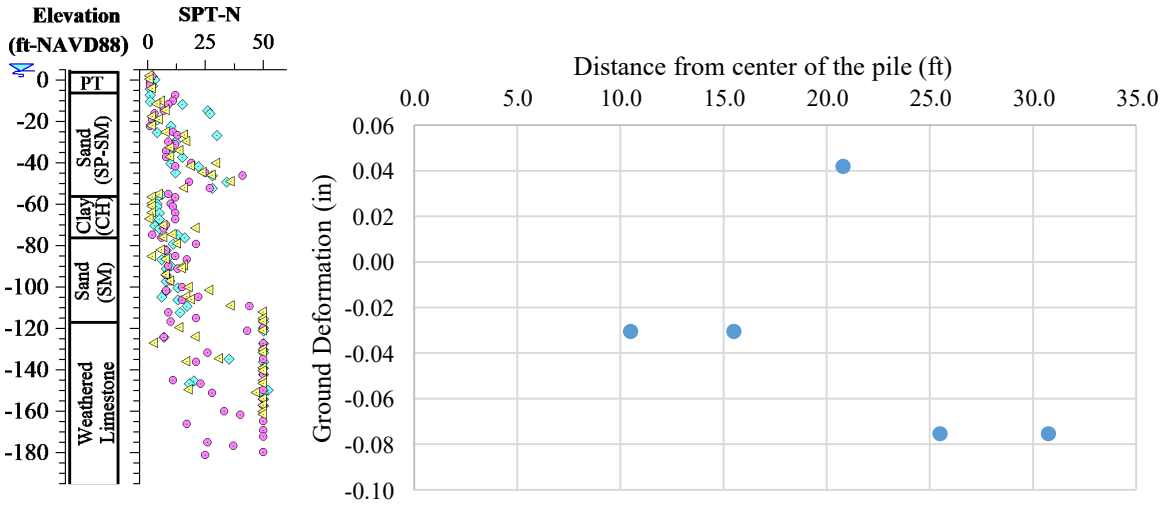

Figure 3-42. Final ground deformations induced by driving of pile 15 at Site A2.

3.6.3. Site A3

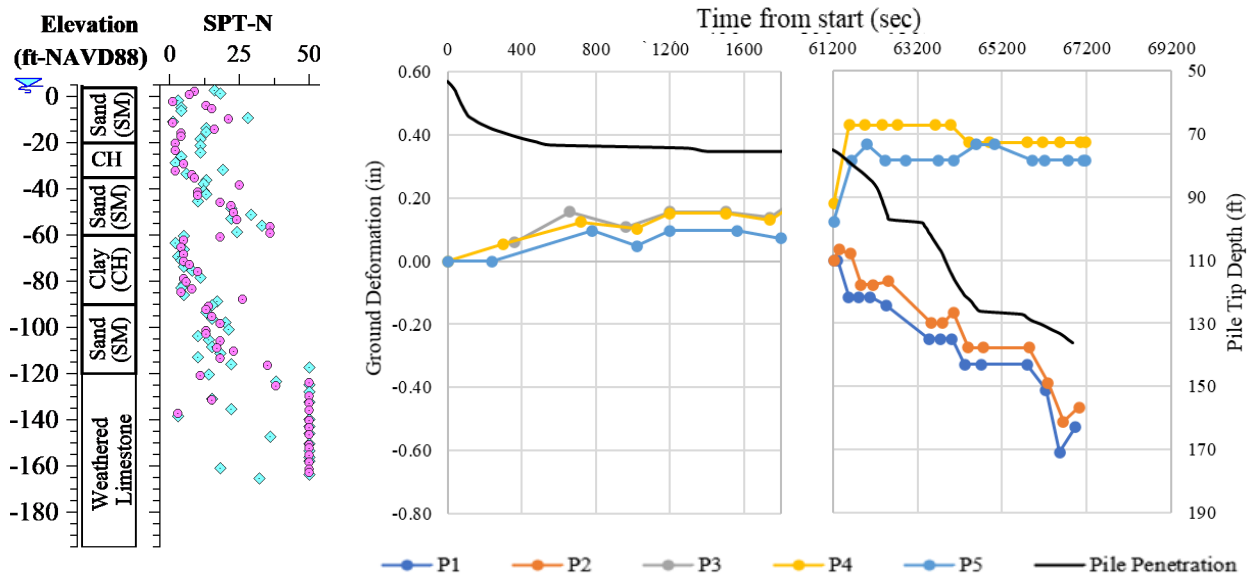

Figure 3-43Figure 3-43 presents the ground deformation time history at each survey nail due to installation of pile 4 at Site A3. The ground deformations triggered before and after the splicing of the test pile are shown in the figure. Notice that a maximum heave of approximately 0.40 in was measured at survey nail P4, which was located at 26 ft away from the pile (i.e., 13 times the diameter of the pile). Measurements before the splicing of the pile are not shown in the figure for P1 and P2 (i.e., closest survey nails to the pile) since they were moved during the first stage of driving due to external construction activities close to the pile. A maximum settlement of approximately 0.6 in was measured at the survey nail P1, which was located at 11 ft away from the pile (i.e., 5.5 times the size of the pile).

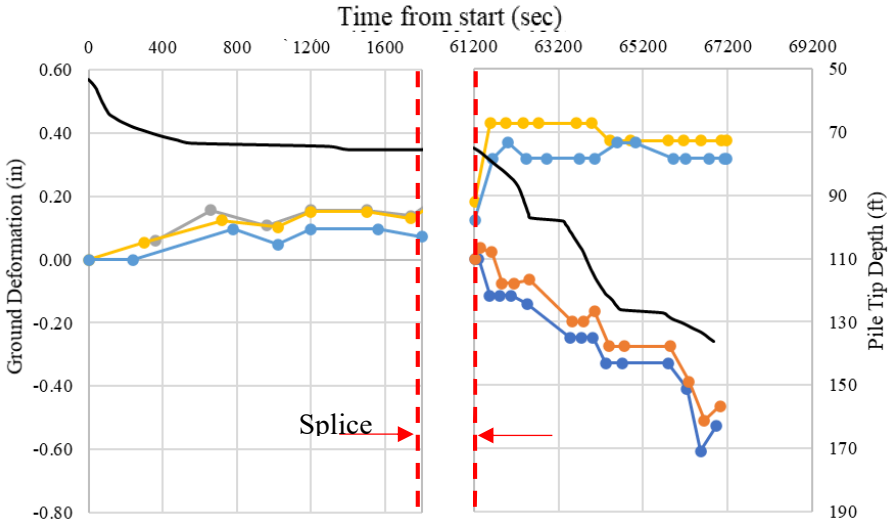

Figure 3-43. Ground deformation time history during driving of pile 4 at Site A3. Dual axis showing pile penetration.

Figure 3-44 presents the final ground deformations after installation of pile 4 at Site A3. Notice that settlement was measured at distances close to the pile while heave was observed further away from the pile. Maximum settlement and heave of approximately 0.53 and 0.37 in were measured, respectively. This variation between heave and settlement depending on the distance away from the pile where the measurements were taken highlights the importance of developing a robust model capable of tracking changes in soil density as the pile is installed and accurately predicting able to predict both types of ground deformations (i.e., heave and settlements) instead of just settlements.

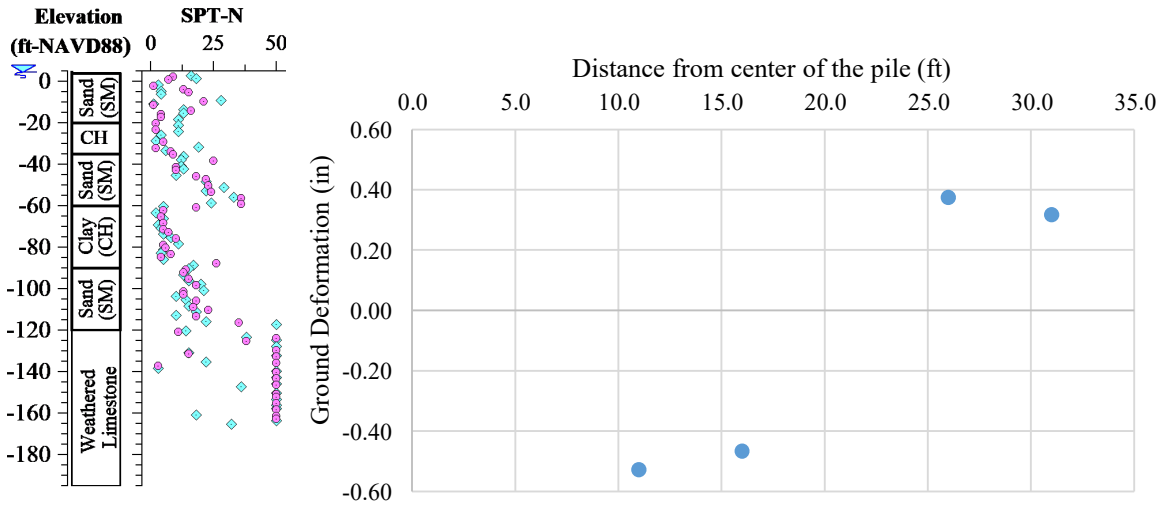

Figure 3-44. Final ground deformations induced by driving of pile 4 at Site A3.

3.6.4. Site B

Ground deformation measurements were conducted at Site B at the location specified in Section 3.4.2. For that project, negligible measurements of ground surface deformations (i.e., heave or settlement) were recorded. This was attributed to the presence of the cofferdam installed prior to the beginning of the pile driving process. The cofferdam around the pier not only densified the soil during its installation but also provided a protection barrier that caused energy absorption of the cylindrical and spherical waves emanating from the pile. This result is also consistent with the measurements of peak particle velocities conducted at the project site.

3.6.5. Site C

Figure 3-45 presents the ground deformation time history at each settlement point during installation of piles 2 through 6 at bent 4. Recall that the soil conditions at this site were characterized mainly by the presence of medium-dense silty sand layers with interbedded weathered limestone layers. As mentioned before, the driving sequence started with the installation of pile 6 followed by installation of piles 5, 4, 3, and 2. Notice that a maximum heave of 0.44 in was measured at settlement point G1 during installation of pile 4, which was the closest pile to the geophone and settlement point array. The time histories of ground deformations were characterized by relatively uniform ground deformations after certain time of starting the installation process of each pile and as the pile tip reached greater depths.

Figure 3-46 summarizes the final ground deformations after installation of piles 6 through 2. Maximum heave of 0.36 in occurred at a distance of 17 ft away from the axis of the bent (i.e., 8.5 times the width of the pile). Notice that the largest ground deformations occurred during installation of pile 4 followed by driving of piles 5 and 6. The relative position of the instrumentation in relation to the pile group affected the final ground deformations because the survey array was located close to pile 4. Ground deformations due to installation of pile 6 were large considering that this was the furthest pile to the settlement points. Pile 6 was the first pile in the driving sequence, thus the soil was not subjected to many vibration cycles and soil densification could have occurred. Ground deformations induced by installation of piles 2 and 3 (i.e., last piles driven during the field visit) were small compared with deformations induced during driving piles 5 and 4. This can also be explained with the fact that the soil was already subjected to numerous vibration cycles and soil densification occurred prior to installation of piles 2 and 3.

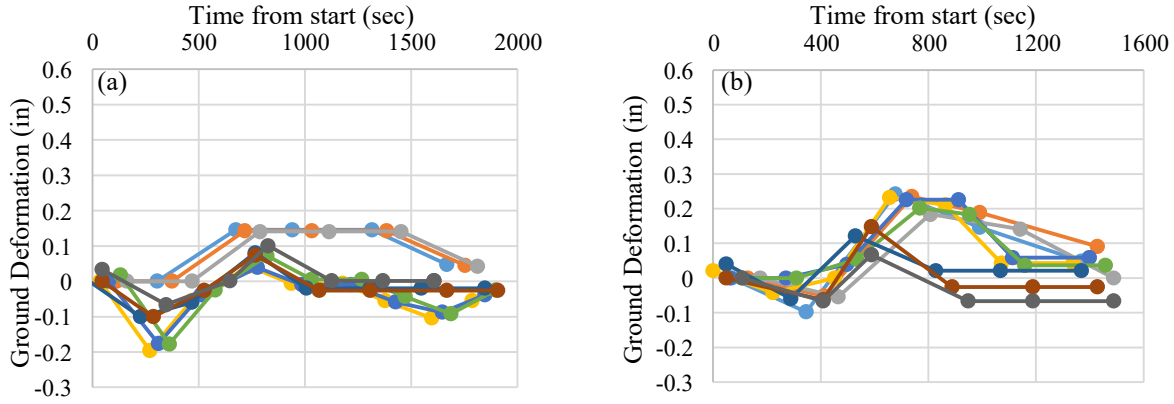

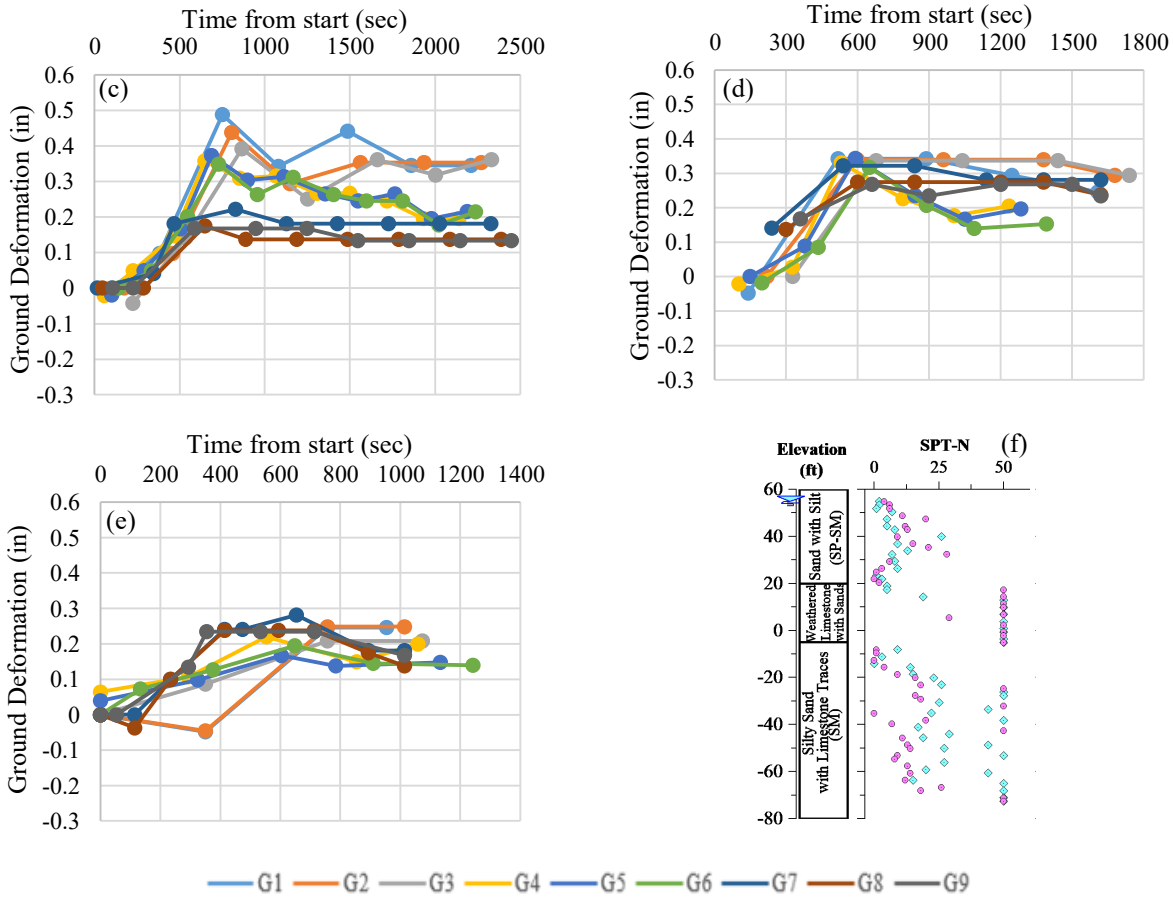

Figure 3-45. Ground deformation time histories at Site C during driving of (a) pile 2, (b) pile 3, (c) pile 4, (d) pile 5, (e) pile 6. (f) Representative soil boring.

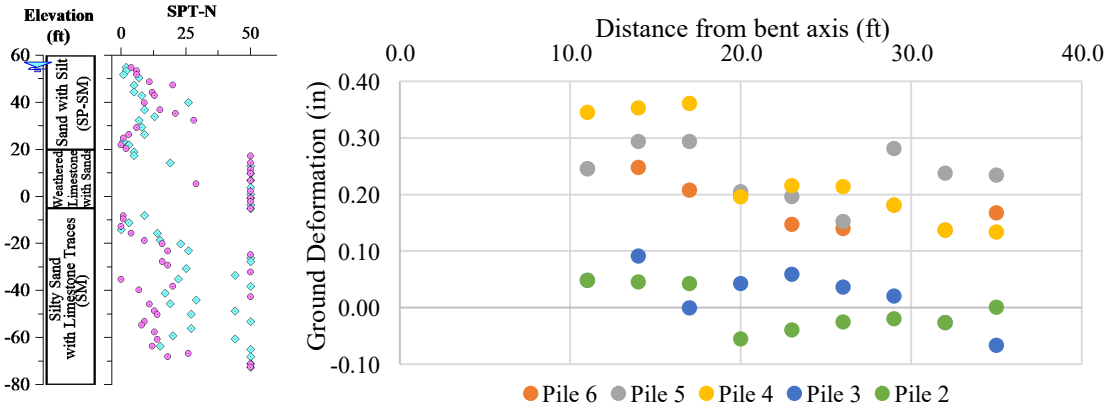

Figure 3-46. Final ground deformations after driving of piles 2 through 6 at Site C.

3.7. MEASUREMENTS OF GROUND VIBRATIONS

This section presents PPV measurements performed at Sites A and B during pile driving operations. The ground vibrations were measured by using the 18 5 Hz vertical geophones

available for this project (see Section 3.1.1). Vibrations reported by Bayraktar et al. (2013) are also presented in this section for Sites Z.1 through Z.5 to supplement the data collected from the test sites in this project.

3.7.1. Site A1

Figure 3-47 presents the PPV measurements performed during driving of piles 10 and 13 at Site A1. Notice that PPVs at distances up to 36 ft from the center of the pile are not reported. During PPV data collection, the geophones malfunctioned and adjusted sensor gains below that value, thus limiting the maximum recorded values. The data confirms that for distances beyond 36 ft the PPV values did not reach the limit defined by FDOT of 0.5 in/s. Notice how the recorded PPV values were larger during driving of pile 13 than during driving of pile 10. This indicates changes in the soil attenuation characteristics (i.e., changes in volumetric contractive or dilative responses of soils) due to consecutive pile driving installations.

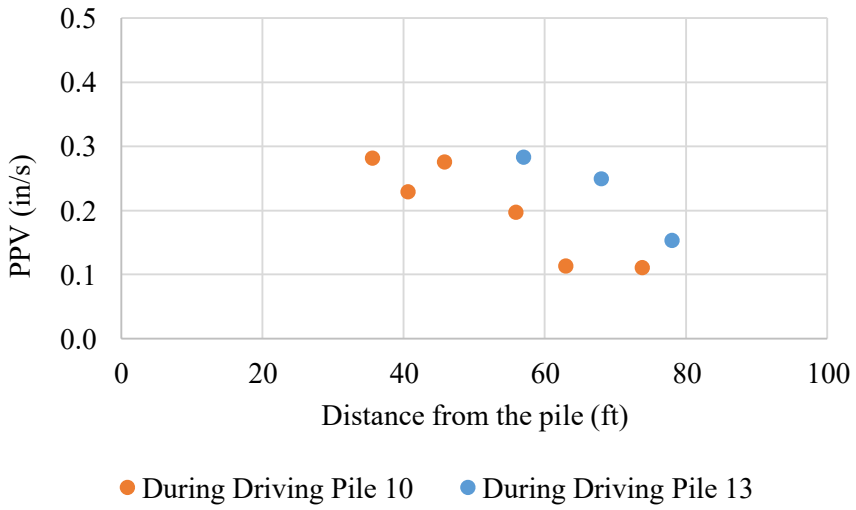

Figure 3-47. PPV measurements at Site A1 during driving of piles 10 and 13.

3.7.2. Site A2

Figure 3-48 presents the PPV measurements performed during installation of piles 8 and 15 at Site A2. Temporarily the FDOT limit of 0.5 in/s was exceeded during driving of pile 8 up to a distance of approximately 23.0 ft. Notice how the vibration levels during driving of pile 15 are lower than during driving of pile 8. This is consistent with the ground vibrations measured during pile driving operations at Site A1 and confirms changes in the soil attenuation characteristics due to pile driving vibrations.

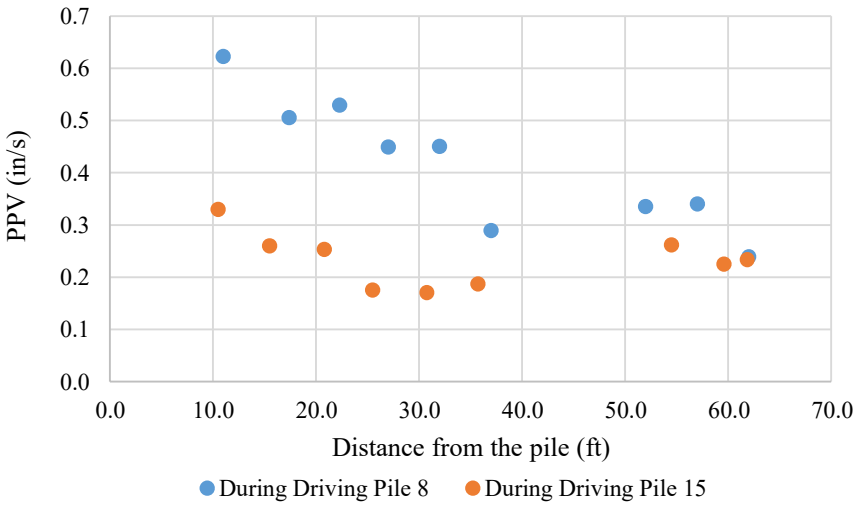

Figure 3-48. PPV measurements at Site A2 during installation of piles 8 and 15.

3.7.3. Site A3

Figure 3-49 presents the PPV measurements performed during installation of pile 4 at Site A3. Measurements during driving of the first pile segment as well as two different geophone arrays measurements (i.e., L1 and L2) during driving of the second pile segment are included in the figure. Notice that higher PPV values were measured before the pile splicing for most of the geophones (i.e., for distances ranging from 16 ft to 41 ft away from the pile). This can be attributed to the distance of the pile tip with respect to the sensors (i.e., the deeper the pile tip the lower the vibration levels). The opposite occurs for distances close to the pile where higher PPV values were measured after the pile splicing (i.e., the pile tip was deeper than before the pile splicing). This might be attributed to the concept of critical depth of vibration given by Khoubani and Ahmadi (2014) in Section 2.3.2.

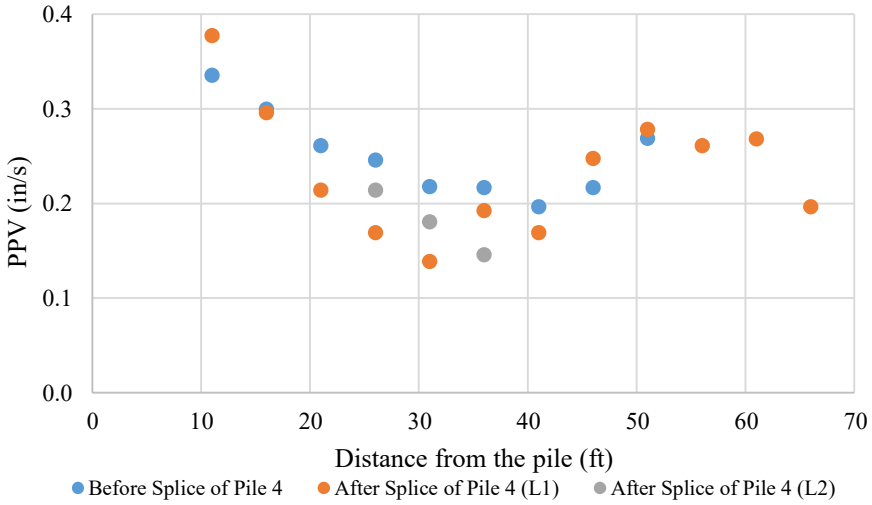

Figure 3-49. PPV measurements at Site A3 during installation of pile 4 including measurements before and after the pile was spliced.

3.7.4. Site B

Figure 3-50 presents typical measurements of velocity time histories with the geophones during the pile driving process. The driving process was divided into two stages since the contractor stopped the process to adjust driving settings, thus the results are presented in two figures. Most of the driving process occurred during the first stage (see Figure 3-50a) than the second stage (see Figure 3-50b). The maximum recorded velocity value is also shown in the figures. Notice that higher velocity values were measured during the second stage due to changes in the fuel settings.

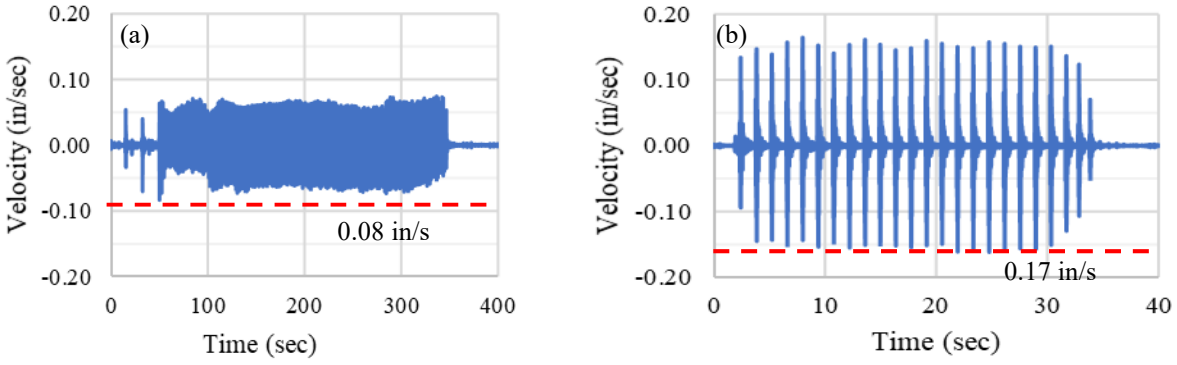

Figure 3-50. Typical velocity time history for: (a) first pile driving stage at geophone (G1) and (b) second pile driving stage at geophone (G6).

Figure 3-51 presents the PPV measured at different distances from the face of the cofferdam during the two installation stages. The PPV values were calculated based on the maximum velocity

in the time history for each geophone (e.g., in Figure 3-50a the PPV value is 0.08 in/s). The maximum vibration level in terms of PPV for the first driving sequence was approximately 0.08 in/s, measured at a distance of 11.3 ft from the face of the cofferdam (i.e., G1). In the second driving sequence, the maximum recorded value was approximately 0.17 in/s at a distance of approximately 30.0 ft from the cofferdam (i.e., G6). Larger PPV values were experienced during the second stage of the driving process due to changes in the hammer settings. The recorded measurements at this Site D did not exceed the PPV limit of 0.5 in/s established by FDOT. The pre-drilling operation and the presence of the cofferdam had a major attenuation effect on the final measured vibration response and ground surface deformations generated by the pile driving process at this site. The presence of cofferdams or other underground geostructures have a major impact on the vibrations and settlements induced by pile driving operations.

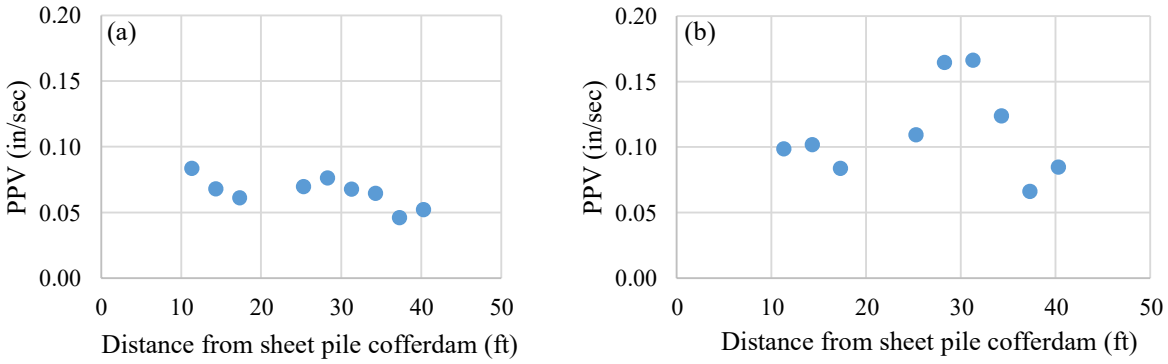

Figure 3-51. PPV measurements for the (a) first and (b) second part of the driving process at site B.

3.7.5. Site C

PPV measurements were performed during driving of pile 2 through 6 of bent 4 at Site C. During PPV data collection, the geophones malfunctioned and adjusted sensor gains below that value, thus limiting the maximum recorded values to 0.3 in/s. Vibration levels higher than 0.3 in/s could be expected up to a distance of 35 ft away from the bent axis.

3.7.6. Sites Z.1 to Z.5

Bayraktar et al. (2013) used Eq.(2-11), originally proposed by Wiss (1981), to represent the PPV attenuation curves for each project surveyed in that report. Table 3-5 presents the rated and transferred energies of the hammers used as well as the coefficients *k* and *n* found for each project. Note that the ratio between transferred and rated energy (i.e., energy efficiency) is low and varied between 10% and 32%.

Table 3-5. Input rated and transferred energy and attenuation coefficients for selected projects in Central Florida (Adapted from Bayraktar et al., 2013).

Site	Rated Energy (kip-ft)	Transferred Energy (kip-ft)	Energy Efficiency (%)	k	n
Z.1	161.5	16.8	10.4	1.4	1
Z.2	100.0	18.0	18.0	1.3	1
Z.3	80.0	21.2	26.5	3.4	1
Z.4	100.0	16.8	16.8	3.3	1
Z.5	84.1	26.9	32.0	6.7	1

Figure 3-52 presents some measured PPV values and PPV attenuation curves derived for each project and presented by Bayraktar et al. (2013). These curves represent the upper limits for the PPV values measured at each project. The scaled distance in the horizontal axis was defined using the transfer energy instead of the rated energy of the hammer. Notice that the project with the largest transfer energy of 26.9 kip-ft (i.e., Site Z.5) presented the attenuation curve with the highest PPV values. Direct proportionality between rated energy and PPV was found.

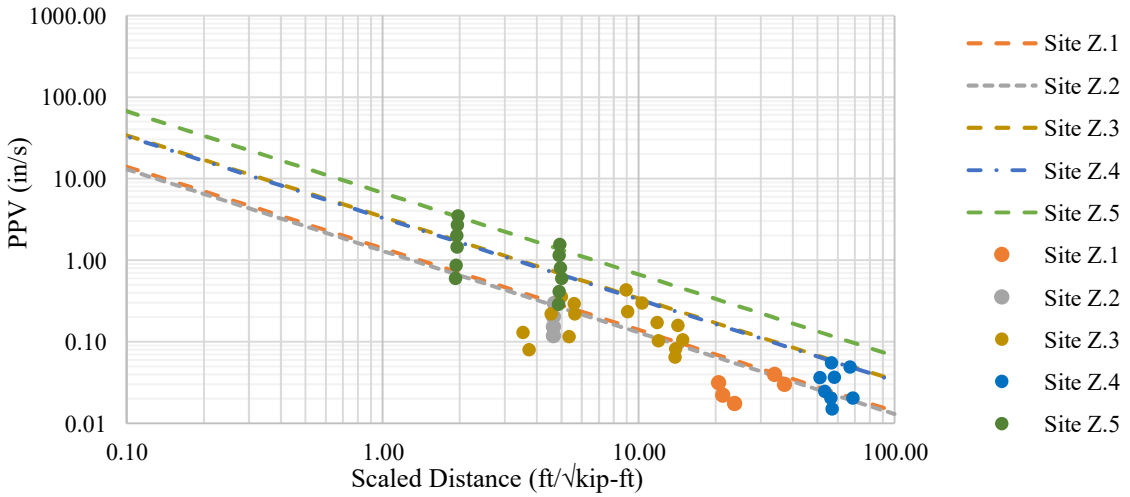

Figure 3-52. Peak particle velocity attenuation curves measured in selected Florida's Turnpike projects corresponding to Sites Z.1 through Z.5. (Adapted from Bayraktar et al., 2013).

4. COMPARATIVE ANALYSIS OF PILE DRIVING NUMERICAL MODELING APPROACHES

This chapter consists of a numerical model conducted for pile driving at Site D (see Section 3.2.6) in order to compare continuous and discontinuous modeling approaches. As defined in the literature review (see Section 2.3), a discontinuous modeling approach consists of installing the pile at different depths and applying a single hammer blow at each depth to compute ground vibrations in the soil continuum. A continuous modeling approach consists of driving the pile without interruption until the final penetration depth is achieved.

The selection of the most adequate numerical and constitutive models to study ground deformations arising from pile driving and the understanding via wave equation analysis of soil-pile interactions and dynamics are the main goals of this section. Software such as GRLWEAP and CAPWAP use wave equation analyses to estimate engineering demands generated during the pile driving and are also used to analyze dynamic testing of piles for the determination of in situ bearing capacity of piles. The wave equation analysis originally proposed by Smith (1960) improved the analysis and design of deep foundations by incorporating in the design process the production of bearing graphs, driveability studies, and enhanced the understanding of pile dynamics in terms of velocities, forces, and displacements that occur as a result of the driving. The pile driving demands applied to the models (i.e., force time history for a single hammer blow applied at the top of the pile) were numerically simulated using the wave equation analysis program GRLWEAP. Despite having numerous positive features that can be used to guide deep foundation designs and installation processes, wave equation-based programs such as GRLWEAP still cannot provide insight into the effects of pile driving on the surrounding soil or nearby structures because engineering demands such as ground deformations, ground vibrations, pore water pressures, etc. cannot be retrieved from those type of programs. GRLWEAP only allows the calculation of a detailed time history of displacements, velocities, forces, and energies in the pile for a single hammer blow. Hence, to overcome this issue, the pile driving at Site D was also modeled in the finite element (FE) platform PLAXIS 2D to draw conclusions about the relationships between input energy, ground deformations, peak particle velocities, distance from the source, and soil properties. PDA data were used to model the continuous pile driving approach in PLAXIS 2D for the analysis and the results were compared with the reported pile driving records. The discontinuous model presented herein was modeled at a selected depth to compute pile penetration and induced PPV caused by a single hammer blow. The FE models were validated with CAPWAP/iCAP and GRLWEAP program outputs for a single blow to compare computed pile dynamics. Input parameters for the PLAXIS 2D model presented herein were estimated from subsurface exploration data and processed using GRLWEAP.

4.1. GRLWEAP PILE DRIVING MODEL FOR DRIVING AT SITE D

In the wave equation analysis program GRLWEAP, the soil profile was generated based on SPT-N values for each stratum obtained from the borings near the project site, as presented in Figure 3-22. Soil parameters such as quake for the shaft and toe (0.22 in. and 0.26 in., respectively) and damping for the shaft and toe resistances (0.21 s/ft and 0.09 s/ft, respectively) were obtained from the CAPWAP results presented in the project foundation reports. The hammer model and pile dimensions used in the analyses were defined from actual pile driving conditions and as-built

dimensions. Since the PDA measurement during the dynamic test was performed for the 1810th blow (i.e., 88.9 ft penetration depth), then the properties for the pile cushion were assigned as "used" plywood material to model the thickness reduction in the cushion at the end of driving according to the GRLWEAP manual. A thickness of 1.5 in for the hammer cushion and 15 in for the pile cushion were used.

A GRLWEAP wave equation analysis was performed for a penetration depth of 88 ft for the pile with a load-bearing capacity of 1823 kips in order to obtain a force time history similar to the measured force with the PDA shown in Figure 3-33. Figure 4-1 presents a comparison between the GRLWEAP model and the field measurements of applied stress versus time processed by CAPWAP. This input demand was applied in terms of a uniformly distributed stress acting on top of the pile and was computed by dividing the measured and computed force by the area of the pile (i.e., 4 ft^2). Since the applied stress history at the top of the pile obtained with GRLWEAP matched well the one measured with PDA, especially in terms of peak magnitude and overall shape, the force time history was converted into a stress function to be distributed on top of the pile in PLAXIS 2D.

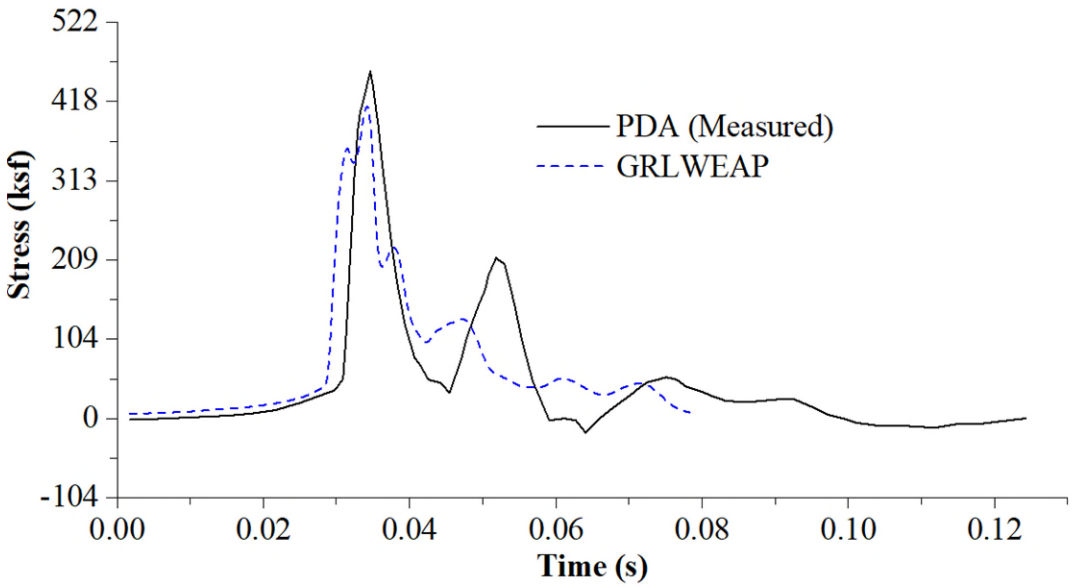

Figure 4-1. Stress function time history applied at the top of the pile.

A second wave equation analysis was performed in GRLWEAP to compare the results of the discontinuous model with the continuous pile driving analysis. In order to define the "wished-in-place" pile penetration depth, the 667th hammer blow was selected, which corresponds to a penetration depth of 76 ft with an ultimate capacity of 250 kips. This pile penetration depth was modeled in GRLWEAP and PLAXIS 2D to compare the results of pile dynamics in light of the measured field data.

4.2. FINITE ELEMENT MODEL FOR DRIVING AT SITE D

The numerical model in PLAXIS 2D was performed under axisymmetric conditions to model the driving of the test pile 11 at Pier 11RT at Site D. Figure 4-2a shows the model geometry, indicating the groundwater table and the soil profile used for the continuous model. The model mesh had a height and width of 145.0 ft and 177.2 ft, respectively. Boundary conditions in the model were defined as normally fixed for the right and left boundaries and fully fixed for the bottom. Viscous boundaries were placed at the right and bottom ends to avoid wave reflections. Fifteen-node triangular elements and a medium-mesh option were used.

The concept of a "plastic zone" with reduced stiffness and strength was introduced around the pile to model the continuous process of pile installation. The soil-pile interaction was modeled by introducing a plastic zone around the pile with reduced strength (R) and shear wave velocity (R_s) parameters instead of defining an interface element between soil and pile. This method was proposed by Grizi et al. (2018) to overcome issues with interface elements in PLAXIS 2D when a dynamic stage is conducted. The radius of the plastic zone was defined to be twice the diameter of the pile (i.e., 4.0 ft for a 24-in prestressed concrete pile), which is the same ratio used by Grizi et al. (2018) that used a plastic zone of 0.50 ft for a laboratory test performed in a pile of 0.25 ft in diameter. However, instead of defining an R value of 0.5 and an R_s of 0.2 as suggested by Grizi et al. (2018), this study used factors of 0.4 and 0.12 for R and R_s, respectively.

Figure 4-2b presents a detailed view of the pile for the continuous model and the "plastic zone" clusters, which were defined to represent the soil-pile interaction. Since the pile was first pre-drilled up to a depth of 32.0 ft before the pile driving started, the pile cluster was activated in the model at that depth instead of beginning the driving from the ground surface. The water table was placed at the ground surface. For the discontinuous model, the only parameter that changed was the initial depth of pile penetration from 32.0 ft to 76.1 ft.

The HS small model available in PLAXIS 2D was used as the constitutive soil model since it provides small-strain soil stiffness, adequate hysteretic soil behavior and it has been successfully used in various types of soils (Grizi et al. 2018; Obrzud 2010). Correlations with the D_r of the sand layers presented by Brinkgreve et al. (2010a) were used to calculate the HS small parameters of the granular layers. The parameters for the clay layer that underlies the top sand layer were based on an S_u of 2297 psf corresponding to a medium-stiff clay. HS small soil parameters for similar soils have been proposed in the technical literature (Likitlersuang et al. 2013; Surarak et al. 2012).

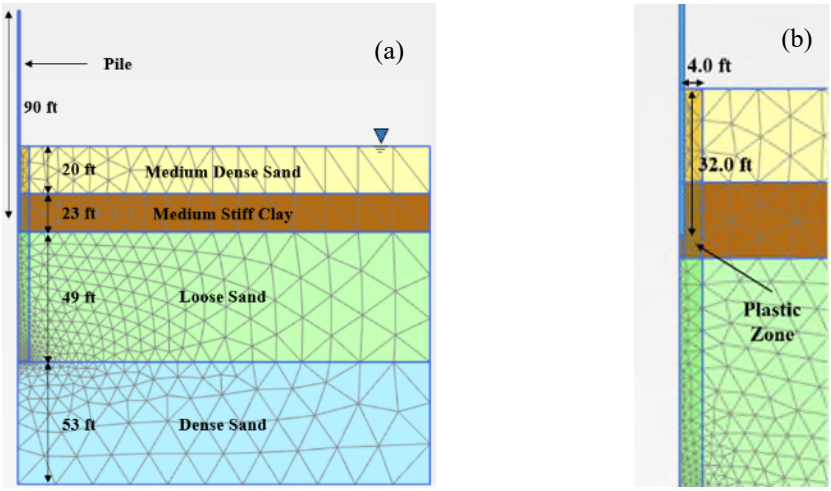

Figure 4-2. Continuous pile driving model in PLAXIS 2D: (a) model geometry and (b) detailed view of the pile initial penetration depth.

Table 4-1 presents the input parameters used in the model for both the plastic zone and the zone of soil continuum away from the plastic zone as it approaches free field conditions, labeled as "free-field zone." Only the strength and stiffness parameters of the plastic zone were affected by the reduction factors. Rayleigh damping was also applied to both zones in terms of the Rayleigh mass (α) and stiffness (β) proportional damping coefficients. These parameters were defined for each layer to introduce a uniform damping ratio (ξ) of 5% throughout the model and supplement the constitutive model hysteretic damping. As proposed by (Hudson et al. 1994), α and β were determined by estimating the natural frequency of the soil layers.

Table 4-1. Soil layer properties used for the HS small model in PLAXIS 2D.

Parameter	Units	Free-Field Zone				Plastic Zone		
		Medium Dense Sand	Medium Stiff Clay	Loose Sand	Dense Sand	Medium Dense Sand	Medium Stiff Clay	Loose Sand
Thickness	ft	20	23	49	53	20	23	49
SPT-N	-	30.0	10.0	20.0	50.0	30.0	10.0	20.0
D_r	(%)	60.0	-	45.0	85.0	60.0	-	45.0
R	-	-	-	-	-	0.4	0.4	0.4
R_s	-	-	-	-	-	0.12	0.12	0.12
γ_{sat}	pcf	127	121	125	130	127	121	125
ϕ'	º	35.5	28.0	33.6	38.6	14.2	11.2	13.5
ψ	º	5.5	-	3.6	8.6	2.2	-	1.5
c'	psf	-	240	-	-	-	240	-
S_u	psf	-	2297	-	-	-	919	-
E_{50}^{ref}	ksf	751.9	198.4	563.9	1065.2	10.8	2.9	8.1
E_{oed}^{ref}	ksf	751.9	250.6	563.9	1065.2	10.8	3.6	8.1
E_{ur}^{ref}	ksf	2255.6	626.6	1691.7	3195.5	32.5	9.0	24.4
G_0^{Ref}	ksf	2255.6	1462.0	1892.2	2460.3	30.3	21.1	27.3
m	-	0.5	0.7	0.6	0.4	0.5	0.7	0.6
ν'_{ur}	-	0.3	0.2	0.3	0.3	0.3	0.2	0.3
$\gamma_{0.7}$	$x10^{-4}$	1.40	9.95	1.55	1.15	1.40	9.95	1.55
α	-	2.7	2.6	1.9	2.0	0.7	0.6	0.3
β	$x10^{-4}$	9.4	9.2	6.7	6.9	2.6	1.9	1.0
R_f	-	0.9	1.0	0.9	0.9	0.9	1.0	0.9

The force time history that was obtained from GRLWEAP was input as the stress function on top of the pile in PLAXIS 2D (see Figure 4-1). The continuous pile driving analysis consisted of three stages in PLAXIS 2D. The first stage was applied to initialize the stress field of the soil layers so that representative K_0-conditions in the field can be simulated before the pile driving started. In the second stage, the pile cluster was activated at the pre-drilling elevation described in the foundation reports. The third stage included the activation of the plastic zone and the application of a total of 1824 hammer blows at the top of the pile using the stress function. A time interval of 1 second between blows was implemented in the analysis. For the discontinuous model, the first two stages remained the same but instead, the installation depth was defined at 76 ft since it was the selected installation depth for the GRLWEAP analysis. However, the third stage only involved a single hammer blow.

4.3. NUMERICAL MODEL RESULTS FOR SITE D

The results obtained at the end of the GRLWEAP and PLAXIS 2D numerical analyses of the pile driving are presented in this section. Since pile driving records from the foundation reports present the pile penetration corresponding to the hammer blow number (see Figure 3-34), the influence of the plastic zone on the pile driving was first parametrically investigated. Table 4-2 presents four different sets of reduction factors (R and R_s) defined in this study to investigate the influence of the plastic zone on the pile driving. Model A is considered as a baseline model in this comparative study. In order to analyze the separate effects of R and R_s, models B and C were

created by varying each factor separately. *Model D* used the same reduction factors presented by Grizi et al. (2018).

Table 4-2. Reduction factors for the plastic soil adjacent to the pile.

PLAXIS 2D Model	Strength Reduction Factor (R)	Shear Wave Velocity Reduction Factor (R_s)
Model A	0.40	0.12
Model B	0.40	0.20
Model C	0.50	0.12
Model D	0.50	0.20

The continuous numerical model was validated by comparing the results versus the actual pile driving records from the foundation reports in terms of vertical displacements at the top of the pile as a result of 1824 hammer blows. Figure 4-3a presents the computed and measured number of blows versus pile penetration. As mentioned in Section 3.5, the measured data show after 1173 blows that the penetration depth increased suddenly due to changes in the fuel settings of the hammer reported in the pile driving record log of the project. However, the input force time history in the numerical models was not modified to allow for changes in the fuel setting affecting the stress function to perfectly match the measured pile penetration process. A comparison of the numerical results is presented in terms of pile penetration for the different sets of parameters adopted for the plastic zone. This is to highlight its importance in the numerical modeling framework, in particular when a model like hardening soil with small strain is used. Later in the report, the authors will discuss ways to overcome these issues with more advanced soil models. It is observed that the model A, selected as the base model, matches very well the measured data up to the point of change in the fuel setting. As expected, it is found that as the reduction factors increased, the pile penetration decreased. Comparing model D with models B and C, it was concluded that the shear wave velocity factor had a greater effect on the driveability of the pile than the strength reduction factor.

Figure 4-3b presents parametrically the influence of the size of the plastic zone (r) on the pile penetration process. The reduction factors for model A were used for further comparisons since they matched well the field measurements. Observe in the figure how an increase in the width of the plastic zone increased the pile penetration as well. The assumption of having a plastic zone radius of twice the diameter of the pile is in good agreement with the measured penetration and also matches the values proposed by Grizi et al. (2018). The definition of the properties and size of this plastic zone is key in the study of pile driving-induced geotechnical mechanisms (e.g., ground deformations, excess pore water pressures, peak particle velocities, etc.) that occur in the soil continuum because the actual pile penetration process needs to be properly characterized in the numerical model. The selection of numerical input parameters for this highly disturbed zone near the pile, idealized in this first finite element model as a plastic zone, must be performed as a function of the type of soil, pile properties (i.e., geometric and material), and characteristics of the input source.

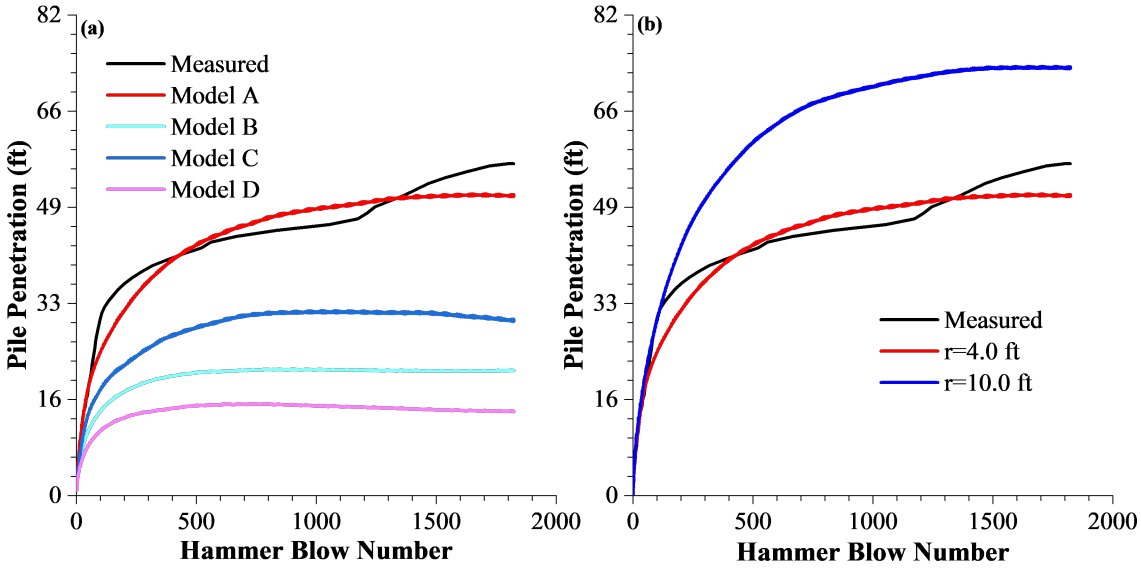

Figure 4-3. Effects of: (a) plastic zone parameters on the pile penetration and (b) size of the plastic zone on the pile penetration.

After the continuous model was validated using the driving records in the foundation reports (see Figure 4-3), the discontinuous model was also performed in PLAXIS 2D at the desired depth of 76 ft. In this analysis, the same set of parameters corresponding to *model A* and the size of the plastic zone of 4.0 ft were used. The comparison between the two modeling approaches in PLAXIS 2D in relation to the results computed with GRLWEAP for a single blow applied at the top of the pile is presented in Figure 4-4. The time history of vertical velocities at the top of the pile for the 667th hammer blow is shown in Figure 4-4a. The three approaches have approximately the same peak velocity of 99 in/s at the top of the pile. However, a better representation of the signal computed with GRLWEAP was obtained using the continuous modeling approach as opposed to the discontinuous model. Figure 4-4b presents the vertical displacement time history computed with GRLWEAP and both modeling approaches in PLAXIS 2D. Only the continuous model was able to represent the magnitude of residual vertical displacements as a result of a single hammer blow. These differences in the discontinuous approach accumulate and ultimately provide misleading results when the entire pile penetration is modeled (e.g., 1824 blows for the pile in this report). Despite differences in the shape of the time history results of vertical displacements, the continuous model provides very similar results that GRLWEAP in terms of both displacements and velocities. This is attributed to the accuracy in the numerical representation of the state of stresses generated during the pile driving when continuous pile driving models are used.

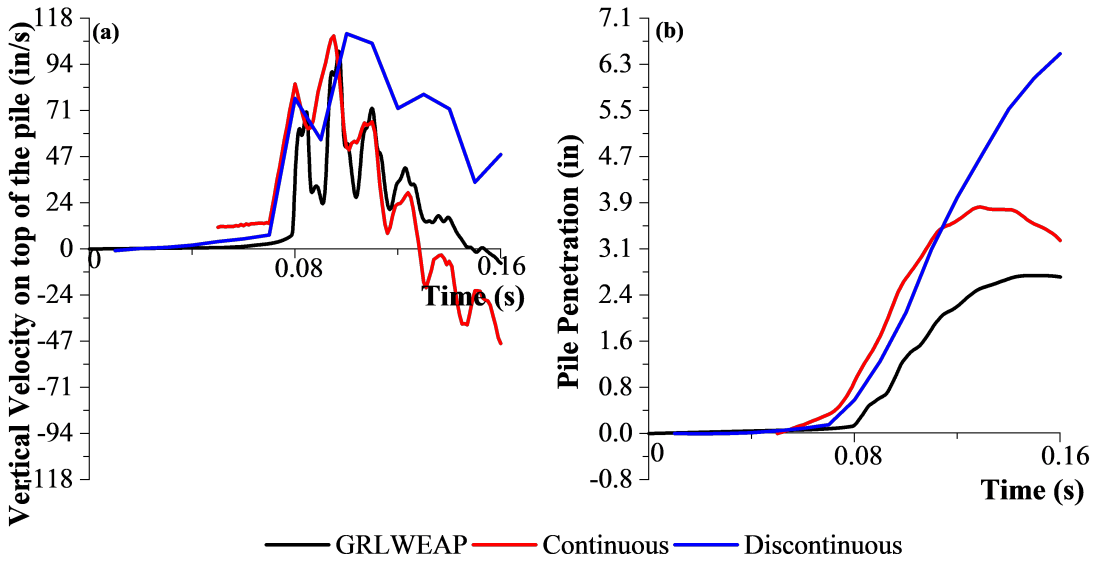

Figure 4-4. Comparison of the continuous and discontinuous numerical approaches compared with results from GRLWEAP in terms of: (a) vertical velocity at the top of the pile and (b) vertical displacement at the top of the pile.

Figure 4-5 presents the PPV values at various distances on the ground surface away from the pile obtained with the continuous numerical analysis. This data is compared with the historical records of PPV data collected by Bayraktar et al. (2013) which were presented in Section 3.7.6. Note that PPV values are presented in terms of scaled distance (ft/√kips-ft). All the PPV values computed from the model were within the same range as the upper boundaries provided by Bayraktar et al. (2013).

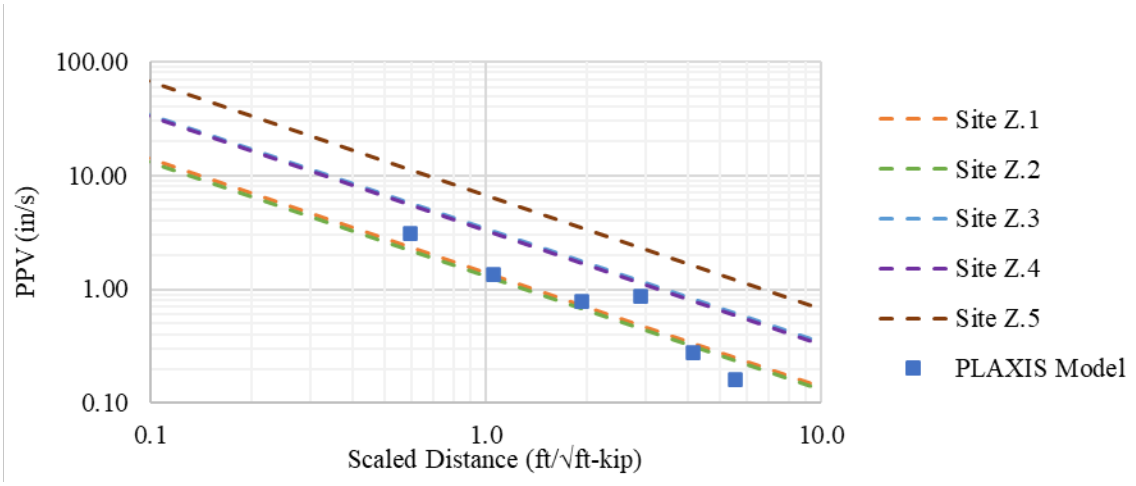

Figure 4-5. Peak particle velocity attenuation curves measured along selected Florida's Turnpike projects corresponding to Sites Z.1 to Z.5 (Adapted from Bayraktar et al., 2013).

5. NUMERICAL MODELING OF PILE DRIVING

A study regarding the effects of the main variables involved in pile-driving induced ground deformations (i.e., soil properties, peak particle velocities, distance from the pile, and input energy) are drawn in this project after gathering information from the projects visited by the research team and conducting the numerical simulations proposed in this research. The analyses were performed to investigate the predominant soil conditions and commonly used driving hammers that cause ground deformations and vibrations in Central Florida granular soils arising from pile driving operations. During field visits to different construction sites, it was observed that the considered soils are mainly characterized by the presence of granular materials with relative densities varying from loose to medium dense. A parametric study was performed to investigate the effect of various relative densities for these sandy soils and various hammer types commonly used in Florida on the continuous pile driving of the most common deep foundation type in Florida, prestressed concrete piles. The analyses are presented using a combination of numerical runs conducted in GRLWEAP and PLAXIS 2D by following the same procedure presented in Chapter 4. The force time histories applied at the top of the pile by the various hammers and appurtenances were obtained using GRLWEAP. The pile driving was modeled in PLAXIS 2D by adopting the continuous pile driving modeling approach (see Section 4.2 for details) in the numerical analyses since it was concluded in Chapter 4 that it is capable of accurately representing the accumulation of stresses in the soil and track changes in void ratio (or relative densities) in the soil as the pile driving progresses (Turkel et al., 2021). Subsequently, conclusions about the relationships between input energy, ground deformations, peak particle velocities, distance from the source, and soil properties were created.

Information regarding typical hammers used in Florida was collected for the analysis of the input energy during the considered pile driving operations to estimate sources of energies and applied forces/stresses in the numerical models. A total of 25 pile driving projects along Florida's Turnpike were collected by Heung et al. (2007) and used in this research to characterize the input energies. Information regarding hammer type and the number of projects where the hammer was used are presented in Table 5-1. It is important to note that most of the case histories involved the use of large-displacement prestressed concrete piles (PCP) with sizes ranging from 18 in to 30 in. Only two projects used small-displacement piles (i.e., H-piles) as shown in the table. The information of the rated energy, pile cushions, or any other appurtenances used during the pile driving operations was not reported by Heung et al. (2007).

Table 5-1. Typical hammer types used in Florida projects summarized from data presented by Heung et al. (2007).

Hammer Type	Number of Projects	Rated Energy (kip-ft) [a]	Type of Pile
APE D36-32	7	89.30	PCP
ICE 120-S	4	120.00	PCP
ICE 100-S	3	100.00	PCP
ICE 80-S	3	80.00	PCP and H-pile
DELMAG D30-02	3	66.20	PCP
DELMAG D36-32	2	90.56	PCP
DELMAG D46-32	2	122.19	PCP
ICE I-19	1	43.24	H-pile

[a] Rated energies obtained from GRLWEAP hammer database.

5.1. GRLWEAP PILE DRIVING MODEL

Before running the FE models, wave equation analyses for the pile were first conducted on GRLWEAP to obtain forces applied at the top of the pile by the various hammers and appurtenances corresponding to an ultimate capacity of approximately 1800 kips. The installation process of a 24 in-wide square precast concrete pile was modeled starting from a penetration depth of 30 ft corresponding to a pre-drilling depth. The total length of the pile was 90 ft. A hammer cushion consisting of 2 layers of 1 in Micarta and 3 layers of 0.5 in aluminum materials was used. A "used" plywood pile cushion with a thickness of 15 in was used to account for cushion thickness reduction after a considerable amount of hammer blows were applied. These accessories were selected based on published reports and field trips made by the research team. The soil profile for the final correlations and charts presented herein was idealized in GRLWEAP using two layers consisting of a 100 ft thick granular stratum and an underlying 175 ft thick very dense competent granular soil stratum. Forces at the top of the piles were obtained for selected hammer types in Florida. Figure 5-1 presents those forces generated in GRLWEAP at the top of the pile by a single hammer blow of the selected hammers at a penetration depth of 30 ft corresponding to the pre-drilling depth. Based on these analyses, the APE D70-52 and ICE I-19 hammers apply the highest and lowest peak forces at the top of the pile, respectively. Table 5-2 presents the rated energies obtained from GRLWEAP for the selected hammer types used by the research team for the final set of analyses and correlations presented in this research.

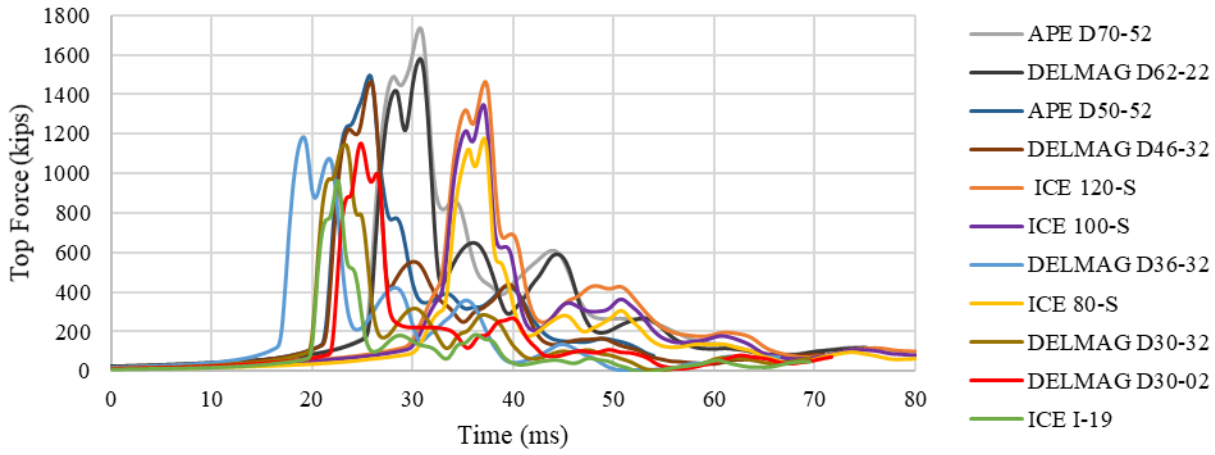

Figure 5-1. Analysis of force-time histories applied at the top of the pile for hammers used in Florida.

Table 5-2. Selected hammer types for the parametric studies including their rated energies.

Hammer Type	Rated Energy (kips-ft)
APE D70-52	173.6
DELMAG D62-22	164.6
APE D50-52	124.0
DELMAG D46-32	122.2
ICE 120-S	120.0
ICE100-S	100.0
DELMAG D36-32	90.6
ICE80-S	80.0
DELMAG D30-32	75.4
DELMAG D30-02	66.2
ICE I-19	43.2

5.2. FINITE ELEMENT MODEL OF PILE DRIVING

The selected hammers and their respective force time histories (see Figure 5-1) were used to conduct finite element analyses in PLAXIS 2D and investigate the pile-driving induced effects on the surrounding soils in terms of ground surface deformations and vibrations. It was concluded from the field trips that the predominant subsurface conditions investigated herein were mainly characterized by the presence of granular materials with relative densities ranging from loose to medium dense. The numerical study results and conclusions presented in this report are based on the investigation of the effect of relative densities, D_r, of the soils defined as: 25%, 40%, 50%, 55%, 60%, 70%, and 75% on pile-driving induced ground deformations. The hypoplasticity model for sands developed by von Wolffersdorff (1996) and enhanced with the intergranular strain

concept by Niemunis and Herle (1997) was used for the proposed analyses. This constitutive soil model is selected because accurate relationships between the variables involved can be established given its capabilities to perform dynamic analyses (Gudehus et al., 2008). The formulations of the hypoplasticity model consider the influence of the void ratio (e), which is closely related to the relative density concept, that enhances the computational capabilities to study the geomechanical response of soils to dynamic loadings for a wide range of relative densities and confining pressures (Wichtmann et al., 2019).

Figure 5-2a shows the geometric configuration of the numerical model, indicating the location of the groundwater table and the idealized soil profile selected for the analyses. The finite element model geometry was defined to match the conditions used in the GRLWEAP model. The layer thicknesses defined in the GRLWEAP model were defined for the idealized sand layer with variable relative densities and a very dense competent deep sand layer. A relative density of approximately 90% was assigned to the very dense sand layer. A high relative density was selected for the bottom layer to represent a firm bearing stratum where the pile driving was completed. The finite element mesh had a height and width of 275 ft and 310 ft, respectively. This was selected to avoid reflection and prevent boundary effects of emanating waves from the pile driving. Normally fixed boundary conditions were defined for the right and left boundaries and fully fixed for the bottom boundary. Viscous boundaries were also placed at the right and bottom ends to avoid wave reflections and an input Rayleigh damping ratio of 5% was defined throughout the analyses.

Fifteen-node triangular elements were used and a soil cluster with a refined mesh having a height of 70 ft and width of 65 ft was created around the pile to improve the accuracy of the numerical results close to the pile. Figure 5-2b presents a detailed view of this refined soil cluster which had a mesh coarseness factor of 0.25 in PLAXIS 2D. The mesh coarseness factor describes the ratio of the mesh refinement at the given soil cluster to the overall mesh coarseness of the model. The large deformation of the mesh given the continuous nature of the pile driving process was modeled by enabling the *updated mesh* option in PLAXIS 2D. Enabling this option in the analysis allows the finite element model to consider the influence of the geometry change of the mesh on the equilibrium formulation. This is very important when soils are loose and large deformations occur (Brinkgreve et al., 2010b). This procedure does not only update the nodal coordinates as the analysis proceeds but it runs the analysis based on an updated Lagrangian formulation (Bathe, 1982; Van Langen and Vermeer, 1991) to account for large deformations. A staged construction process similar to the one explained in Section 4.2 consisting of three main stages was followed in this parametric study. The first stage was applied to initialize the stress field of the soil layers so that representative K_0-conditions of the *in situ* conditions can be simulated before the pile driving started. In the second stage, the pile cluster was activated at a pre-drilling depth of 30 ft before starting the driving operation. In the last stage, the pile driving operation was initiated by applying a time history consisting of a total of approximately 1400 hammer blows applied at the top of the pile. The stress time history function was applied with a time interval of 1 s between blows. The analyses were finalized when the pile reached the bottom competent stratum or because of the large computational effort when approximately 1400 blows were applied. The results will show that the pile driving process was completed at a different total number of hammer blows depending on the considered relative densities assigned to the topmost soil layer. The water table was kept constant at the ground surface during the entire simulations.

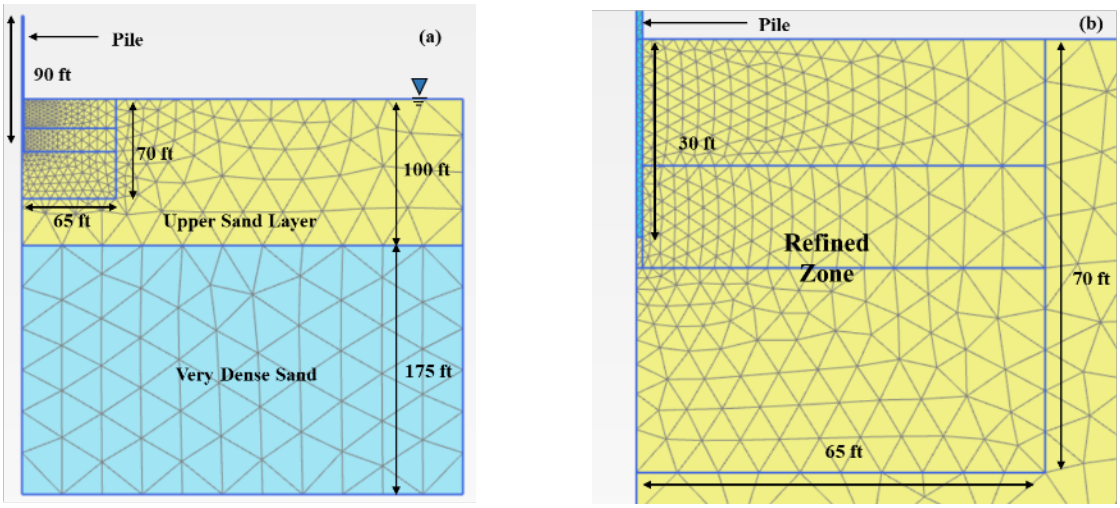

Figure 5-2. Pile driving model used in the parametric study in PLAXIS 2D: (a) model geometry and (b) detailed view of the refined mesh zone and initial pile penetration depth (i.e., pre-drilling depth).

5.2.1. Definition of Soil Parameters

A relative density varying between 25% and 75% was assigned to the upper soil layer in this numerical study. This was based on predominant relative densities observed in soil profiles after field visits conducted by the authors to different construction sites. Void ratios at zero pressure (i.e., e_0 for hypoplasticity model) were calculated corresponding to the selected relative densities (D_r) (i.e., 25%, 40%, 60%, and 70%) using Eq. (5-1). A maximum void ratio (e_{max} or e_{d0} in the model) of 1.10 and a minimum void ratio (e_{min} or e_{c0} in the model) of 0.58 were defined for similar soil conditions in terms of relative densities and critical state void ratios based on the research works by Lade et al. (1998) and Zapata-Medina et al. (2019) since Nevada and South Carolina sands (both poorly graded sands based on USCS) summarized in these studies have similar grain size distribution, angularity, and coefficient of uniformity (C_u) as the soils found in selected Central Florida sites (Arboleda-Monsalve and Chopra, 2020). Table 5-3 summarizes the relationship between e_0 and relative density.

$$e_0 = e_{max} - \frac{D_r}{100\%} * (e_{max} - e_{min}) \tag{5-1}$$

Table 5-3. Calculated e_0 values corresponding to each relative density.

D_r (%)	e_0
25	0.97
40	0.89
50	0.84
55	0.81
60	0.79
70	0.73
75	0.71

The methodology presented by Kim (2011) was followed to calculate the secant shear modulus degradation curves (or modulus reduction curves) of the upper sand layer on numerically simulated monotonic triaxial tests for each considered relative density. The nonlinear behavior of the upper sand layer at the laboratory scale level was studied to computationally match expected dilative or contractive responses of the soil in the field. Stress-controlled undrained triaxial compression tests consolidated to K_0 conditions (CK_0U-TXC) on the soil test module available in PLAXIS 2D were conducted to determine hypoplasticity model parameters. An initial cell pressure of 2089 psf and a K_0 of 0.5 were applied following similar monotonic undrained triaxial tests conducted by Hyodo et al. (1994) on saturated loose Toyoura sands. Thus, a mean normal confining pressure (p_s) of 2778 psf was applied. Numerically simulated triaxial test results using the selected parameter dataset are presented in Figure 5-3. Deviatoric stress (Δq) and excess pore water pressures (Δu) are presented versus axial strains (ϵ_a) for the considered relative densities in this study. A dilative response to shearing was the main characteristic of the medium-dense sands (i.e., D_r= 60% and 70%). A more contractive response was computed for the loose sands (i.e., D_r= 25% and 40%). The overall computed sand response to shearing investigated herein generally matches the results of CK_0U-TXC tests on similar sands that were conducted by Hyodo et al. (1994).

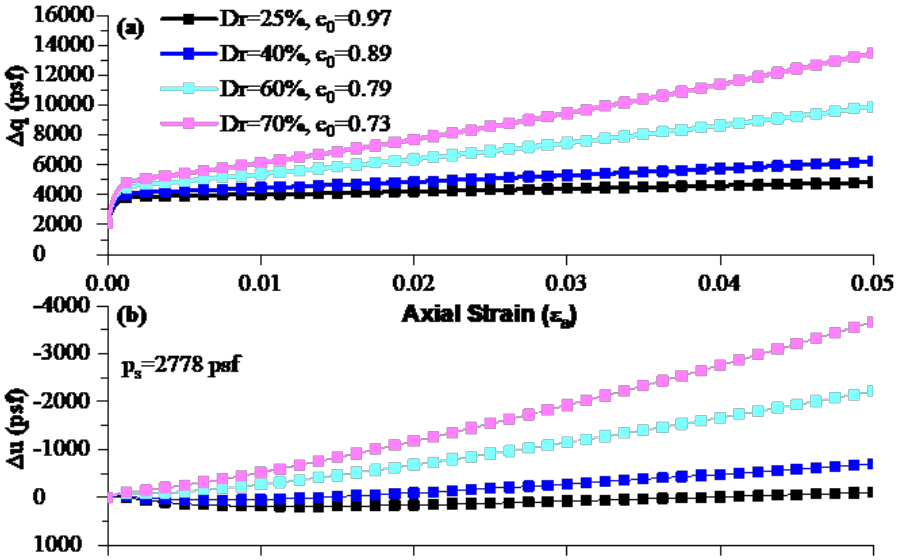

Figure 5-3. Computed triaxial test soil responses ($CK_0U - TXC$): (a) Δq versus ϵ_a and (b) Δu versus ϵ_a.

Figure 5-4 presents the computed secant shear modulus degradation curves with the selected parameters for the upper sand layer at the selected relative densities (i.e., 25%, 40%, 60%, and 70%). Based on the numerically simulated triaxial test results using the hypoplasticity sand model for the upper sand layer, the secant shear modulus degradation curves for each relative density were computed and are shown in the figure. The definition of soil parameters was conducted so that the computed secant shear modulus degradation curves for each void ratio (or relative density) matched other published shear stiffness degradation curves presented for example by Hardin and Drnevich (1972) and Seed and Idriss (1970). Since the void ratio at the specified p_s is required to plot the reference stiffness degradation curves, Eq. (5-2) developed by Bauer (1996), which is based on the granular hardness (h_s) of the soil and an exponent for the grain skeleton (n), was used to calculate the void ratio-applied pressure relationships.

$$e = e_0 * \exp\left[-(3 * p_s/h_s)^n\right] \tag{5-2}$$

The adopted set of parameters for the upper sand layer based on the numerically simulated triaxial tests are listed in Table 5-4. The same reference values at zero pressure proposed by Lade et al. (1998) and Zapata-Medina et al. (2019) for minimum void ratio (e_{d0}), critical void ratio (e_{c0}), and maximum void ratio (e_{i0}) were used. The remaining basic hypoplastic model parameters (i.e., h_s, n, α, β), and the size of the elastic range (R_{max}) and material constant representing stiffness degradation (β_r) were obtained by fitting the secant shear modulus degradation curves to the reference curves. The remaining intergranular strain concept parameters (i.e., m_R, m_T, χ) were also proposed by Zapata-Medina et al. (2019) and selected to match widely accepted secant shear modulus degradation curves published in the technical literature.

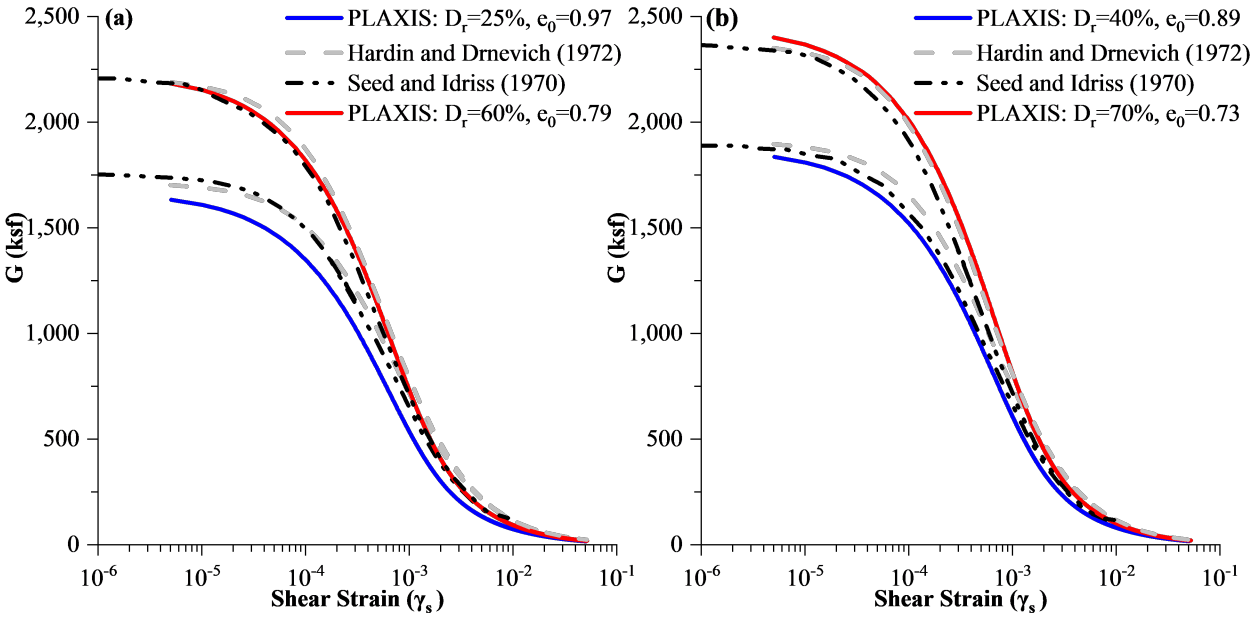

Figure 5-4. Soil secant shear stiffness degradation curves for the relative densities of (a) 25% and 60% and (b) 40% and 70%.

Table 5-4. Soil properties used for the Hypoplasticity sand model in PLAXIS 2D. Target relative densities are controlled with e_0 parameter.

No.	Parameter	Description	Value	Unit
1	ϕ_c	Critical state friction angle	31	°
2	pt	Shift of the mean stress due to cohesion	0	psf
3	h_s	Granular hardness	25062	ksf
4	n	Exponent for pressure sensitive of a grain skeleton	0.37	-
5	e_{d0}	Minimum void ratio at zero pressure (ps = 0)	0.58	-
6	e_{c0}	Critical void ratio at zero pressure (ps = 0)	1.096	-
7	e_{i0}	Maximum void ratio at zero pressure (ps = 0)	1.315	-
8	α	Exponent for transition between peak and critical stresses	0.05	-
9	β	Exponent for stiffness dependency on pressure and density	1.4	-
10	m_R	Stiffness increase for 180° strain reversal	5	-
11	m_T	Stiffness increase for 90° strain reversal	2	-
12	R_{max}	Size of elastic range	5.00×10^{-5}	-
13	β_r	Material constant representing stiffness degradation	0.1	-
14	χ	Material constant for evolution of intergranular strains	1.0	-

The constitutive soil model used for the deep very dense sand-bearing layer was Hardening Soil (HS) small. Correlations with the D_r presented by Brinkgreve et al. (2010a) were used to calculate HS small parameters of this bearing stratum. The selected parameters are given in Table 5-5.

Table 5-5. HS small constitutive soil parameters used for the very dense sand in PLAXIS 2D.

Parameter	ϕ' (°)	Ψ (°)	c' (psf)	E_{50}^{ref} (10^3 ksf)	E_{oed}^{ref} (10^3 ksf)	E_{ur}^{ref} (10^3 ksf)	G_0^{ref} (10^3 ksf)	m	ν'_{ur}	$\gamma_{0.7}$ ($x10^{-4}$)	R_f
Value	39.3	9.3	21	1.13	1.13	3.38	2.53	0.42	0.3	1.1	0.89

Figure 5-5 presents the results of changes in the void ratio of the upper sand layer as the pile driving advances which were computed for a selected numerical simulation presented in this report. The figure is shown during pile driving operation of square prestressed concrete pile installed using a DELMAG D36-32 for an initial relative density of 25% of the upper sand layer. Figures 10a, 10b, and 10c present the void ratio contours for the initial conditions and after the application of 500 and 1400 hammer blows, respectively. The red values represent initial void ratios of 0.97. Observe how the soil around the pile densifies (i.e., void ratio reduces) as the pile is driven. The zone of soil densification is extended as the pile penetrates which provides an indication of the influence zone caused by pile driving. These results highlight the importance of selecting a robust constitutive soil model like hypoplasticity, since it provides a realistic variation of the void ratio (or relative density) of the soil. The model considers this parameter as a state variable used to control the behavior of the material based on the classical formulation of critical state soil mechanics. Other constitutive soil models like Mohr-Coulomb, Drucker Prager, or Hardening Soil cannot track this evolution.

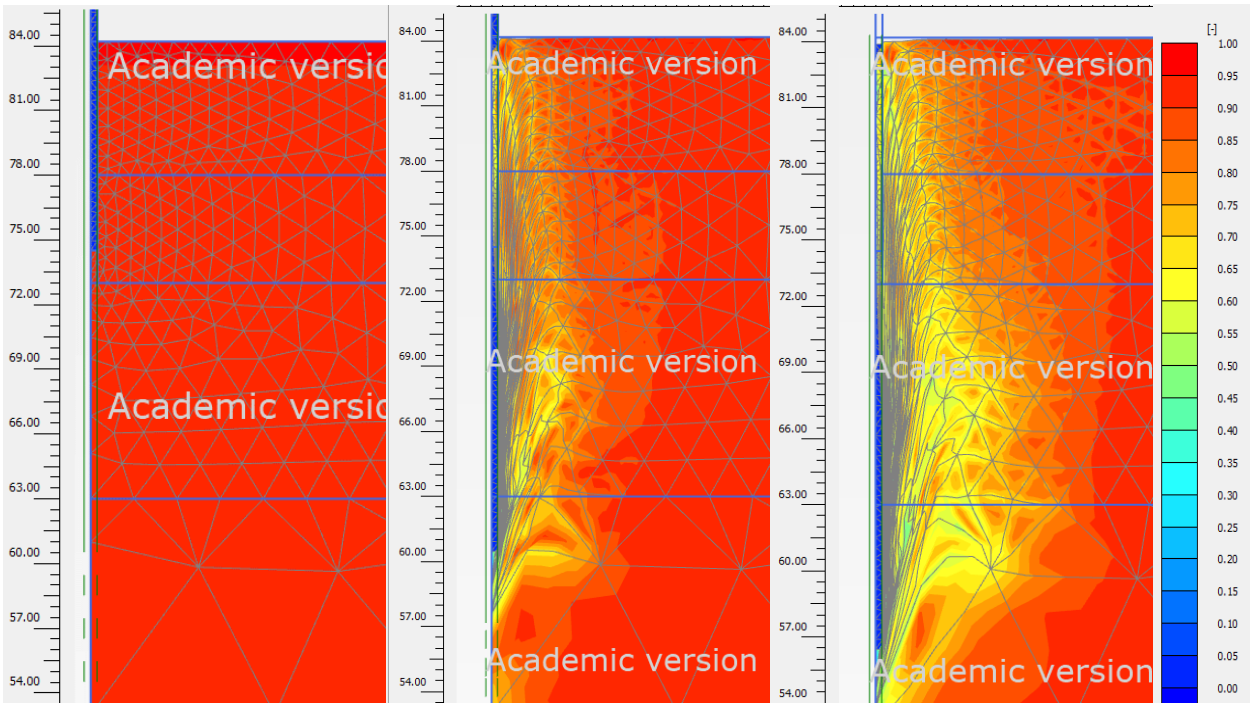

(a) (b) (c)

Figure 5-5. Void ratio contours during pile driving in the upper sand layer for a soil with 25% relative density. Pile installed using a DELMAG D36-32 hammer. Void ratios at (a) initial conditions and after applying (b) 500 and (c) 1400 hammer blows.

5.2.2. Description of FE Numerical Analyses

This section provides an overall description of the numerical analyses performed during the parametric studies finalized in this research so that the effects of the following variables on the pile-driving induced ground response can be elucidated: (i) soil density, (ii) hammer force time history and its rated energy, and (iii) pre-drilling depth. Table 5-6 presents a summary of the analyses performed herein. A total of 140 numerical simulations were performed for the purposes of this research accounting for a total of 3500 hours of computational effort. Three geometrical configurations were simulated. The baseline model corresponds to the initial model explained in Section 5.2. Models M1, M2, and M3 correspond to the analysis of different pre-drilling depths that were simulated in order to study the effect of this variable on the final pile-driving induced ground response. Hammers APE D70-52, ICE 120-S, and DELMAG D36-32 were selected for all configurations (i.e., baseline, M1, M2, and M3 models). The remaining set of hammers (see Table 5-2) were considered only for the analyses developed with the baseline model.

Table 5-6. Summary of the numerical analyses performed to conclude on pile driving-induced mechanisms on ground responses.

MODEL GEOMETRY				ANALYSIS IDENTIFICATION NUMBER						
				Relative Density (%)						
Model	**Pile Length (ft)**	**Pre-Drilling Depth (ft)**	**Hammer Type**	**25**	**40**	**50**	**55**	**60**	**70**	**75**
Baseline	90	30	APE D70-52	1	2	3	4	5	6	7
			ICE 120-S	8	9	10	11	12	13	14
			DELMAG D36-32	15	16	17	18	19	20	21
			DELMAG D62-22	22	23	24	25	26	27	28
			APE D50-52	29	30	31	32	33	34	35
			DELMAG D46-32	36	37	38	39	40	41	42
			ICE 100-S	43	44	45	46	47	48	49
			DELMAG D30-32	50	51	52	53	54	55	56
			ICE 80-S	57	58	59	60	61	62	63
			DELMAG D30-02	64	65	66	67	68	69	70
			ICE I-19	71	72	73	74	75	76	77
M1	90	23	APE D70-52	78	79	80	81	82	83	84
			ICE 120-S	85	86	87	88	89	90	91
			DELMAG D36-32	92	93	94	95	96	97	98
M2	130	40	APE D70-52	99	100	101	102	103	104	105
			ICE 120-S	106	107	108	109	110	111	112
			DELMAG D36-32	113	114	115	116	117	118	119
M3	130	46	APE D70-52	120	121	122	123	124	125	126
			ICE 120-S	127	128	129	130	131	132	133
			DELMAG D36-32	134	135	136	137	138	139	140

5.3. SOIL RESPONSE CLOSE TO THE PILE

A modified non-associative Drucker-Prager plastic potential function and a three-dimensional Mohr-Coulomb yielding criterion based advanced soil constitutive model UBC3D-PLM was used in PLAXIS 2D to investigate the geotechnical mechanisms due to soil liquefaction of the highly disturbed zone in the close proximity to the pile. The model was originally introduced by Puebla et al. (1997) and Beaty and Byrne (1998) as UBCSAND model and further reformulated by implementing a three-dimensional code in PLAXIS by Tsegaye (2010) and enhanced with a correction in model capabilities by Galavi et al. (2013). The UBC3D-PLM model was preferred in this section since the model can potentially captures soil liquefaction caused by pile-driving induced buildup of excess pore water pressures.

The same model geometry and mesh refinement described in Figure 5-2 was used for this analysis. Only the upper sand layer was modeled with the UBC3D-PLM model instead of hypoplasticity model. The UBC3D-PLM model requires an input of 15 constitutive parameters and the adopted set of parameters are given in Table 5-7. Arboleda-Monsalve et al. (2017) correlated these parameters for a loose to medium-dense sand deposit having a relative density of approximately 40% using the correlations given by Beaty and Byrne (2011).

Table 5-7. Upper sand layer properties used for the UBC3D-PLM model in PLAXIS 2D.

No	Definition	Parameter	Value	Unit
1	Friction angle at constant volume	ϕ_{cv}	34	°
2	Peak friction angle	ϕ_p	34.8	°
3	Cohesion intercept of Mohr-Coulomb envelope	c	0	psf
4	Elastic shear moduli at the reference pressure	K_G^{*e}	867.4	-
5	Drained plastic shear modulus	K_G^{*p}	266.54	-
6	Elastic bulk moduli at the reference pressure	K_B^{*e}	607.18	-
7	Elastic shear moduli exponent	n_e	0.5	-
8	Elastic bulk moduli exponent	m_e	0.5	-
9	Plastic shear moduli exponent	n_p	0.4	-
10	Failure ratio	R_f	0.81	-
11	Reference pressure	p_{ref}	2100	psf
12	Tension cut-off	σ_t	0	psf
13	Densification factor	f_{dens}	0.45	-
14	Corrected SPT value	$(N_1)_{60}$	8	-
15	Post-liquefaction stiffness degradation	$f_{E_{post}}$	0.1	-

The numerical model was performed under undrained axisymmetric conditions only for 200 hammer blows to compute the liquefaction occurrence around the pile under the predetermined soil conditions. The force time history created for a single hammer blow of APE D50-52 (see Figure 5-1) was used to perform the analysis. The numerical model consisted of four stages. Figure 5-6 presents the plastic points that occurred at the end of the stages. Figure 5-6a presents the initial stage in which the pile was placed at the predrilling depth. Figure 5-6b presents the plastic points

at the end of the second stage after 100 hammer blows were applied. Subsequently, a consolidation stage was defined to dissipate pile-driving induced excess pore water pressures. After consolidation was performed for a target excess pore water pressure of 20 psf, ground deformations are triggered and purple points indicating soil liquefaction fade (see Figure 5-6c). Observe in Figure 5-6d that liquefaction points expand again up to a distance of approximately 15 ft (i.e., a scaled distance 1.3 $ft/\sqrt{kips-ft}$) away from the pile when the second set of 100 hammer blows were applied at the top of the pile similar to Figure 5-6b. This additional set was defined to simulate cycles of impact hammer application followed by pauses in construction (either due to changes in fuel settings, cushion replacements, etc.) where excess pore water dissipation occurred in the zone in very close contact with the driven pile causing very localized highly disturbed zones in the proximity to the pile.

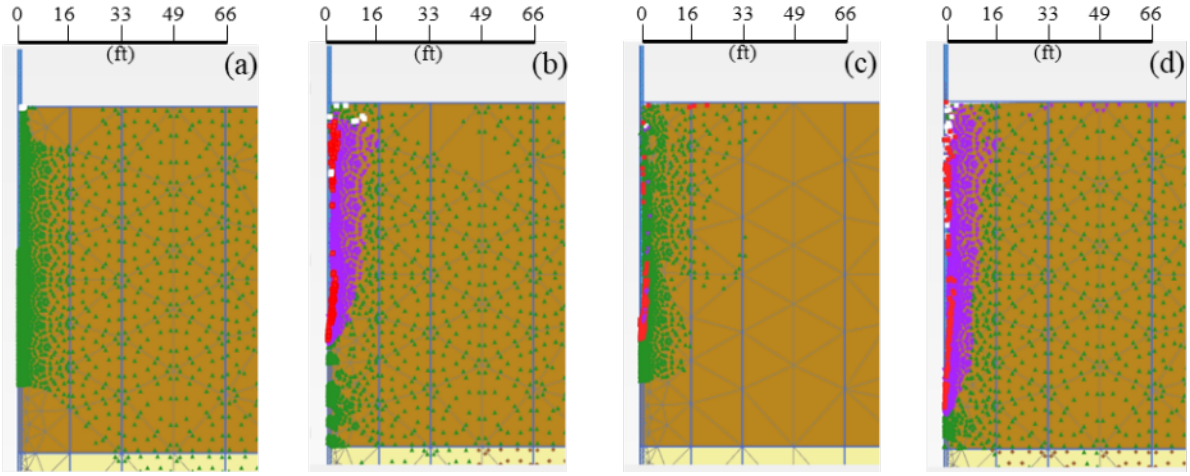

Figure 5-6. Plastic points after: (a) initial stage, (b) 100 hammer blows were applied at the top of the pile, (c) the consolidation stage, and d) after 200 hammer blows were applied at the top of the pile. Note: Liquefaction, hardening, and failure points are shown in purple, green, and red, respectively.

The change in excess pore water pressures throughout the analysis were further investigated to better understand the occurrence of liquefaction points and the behavior of the soils very close to the pile. Figure 5-7 presents pile-driving induced excess pore water pressure contours after each stage. Observe how excess pore water pressures built up to 8400 psf at the tip of pile and approximately 1000 psf about 15 ft away from the pile at the end of the analysis.

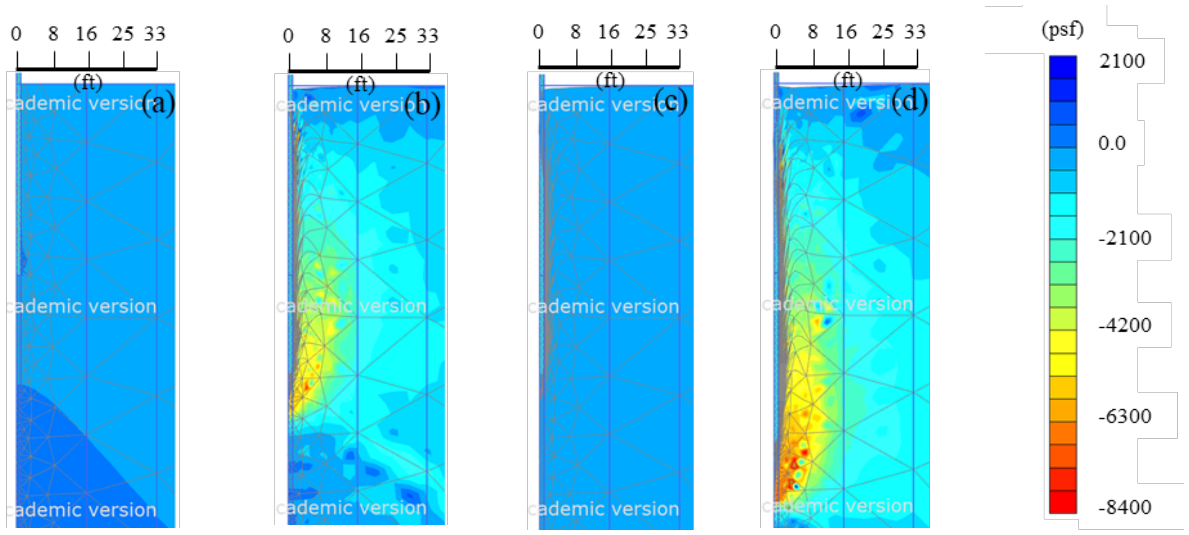

Figure 5-7. Contours showing excess pore water pressure buildup for the first 33 ft from the pile: (a) initial stage, (b) after 100 hammer blows, (c) consolidation stage, and (d) after 200 hammer blows. Note: The scale is given in terms of psf. Countours change between -8400 psf and 2100 psf, negative sign representing compression in pore water and positive sign representing tension.

The UBC3D-PLM model tracks soil liquefaction by using excess pore water pressure ratio (r_u) as a state variable in the dynamic undrained effective stress analysis. The calculation of r_u is given in Equation (5-3) representing the excess pore water pressure ratio in terms of vertical effective stress. In the equation, σ_v' stands for the vertical effective stress at the end of the calculation and σ_{v_0}' for the vertical effective stress at the initial condition. Observe how r_u reaches 1.0 close to the pile and varies between 0.4 and 0.8 at about 15 ft away from the pile after 100 and 200 hammer blows. It is considered that the liquefied state is reached when the state variable reaches 1.0 and it is to be liquefied when it is greater than 0.7 (Brinkgreve et al., 2010b). Beaty and Perlea (2012) asserted that liquefaction can be reached even if r_u is greater than 0.85. Due to the excess water pressure occurrence computed up to a distance of approximately 15 ft away from the pile, the scaled distance for the highly disturbed zoned surrounding the pile can be defined to be approximately 1.0 to 1.5 $ft/\sqrt{kips-ft}$ away from the pile based on the rated energy of APE D50-52 hammer (see Table 5-2). This zone will be labeled as "highly disturbed zone" in the subsequent chapters and charts. Very large pile driving-induced deformations and peak particle velocities will occur within 1.0 to 1.5 $ft/\sqrt{kips-ft}$ away from the pile and will represent a very critical zone where damage will happen to any type of urban infrastructure placed in loose to medium-dense sands.

$$r_u = 1 - \frac{\sigma_v'}{\sigma_{v_0}'} \tag{5-3}$$

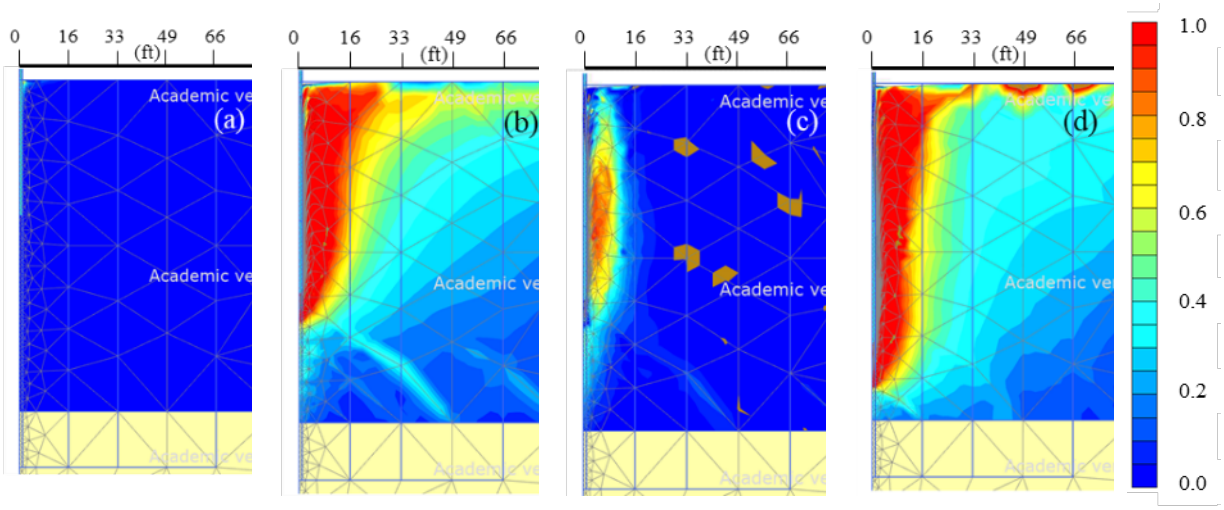

Figure 5-8. State variable r_u after: (a) initial stage, (b) 100 hammer blows, (c) consolidation stage, and (d) 200 hammer blows. Note: Contour scales are between 0 and 1.

5.4. NUMERICAL MODEL VALIDATION WITH MEASUREMENTS FROM SITE A1

The installation of pile 13 at Site A1 (see Section 3.3.1) was selected for the purpose of numerical validation. Before the finite element analysis was performed, the 125-ft-long, 24-in-wide prestressed concrete pile was modeled in GRLWEAP to obtain the force time history for a single hammer blow applied by the APE D50-52 hammer at the top of the pile. The soil profile summarized in Section 3.3.1 was idealized in GRLWEAP using three layers consisting of a 50-ft-thick medium-dense granular stratum underlain by 60-ft-thick loose sand and a very dense competent granular soil stratum. A hammer cushion consisting of 2 layers of 1-in Micarta and 3 layers of 0.5-in aluminum materials was used. Driving of pile 13 started with a new plywood pile cushion with a thickness of 18 in, which was replaced with a new cushion after 2257 hammer blows were applied in the field. The pile cushion was modeled both as "used" and "new" in GRLWEAP to compare the effect of the condition of the pile cushion on the force time history for a single hammer blow applied at the top of the pile. Figure 5-9 presents a comparison of the measured force time history obtained by EDC for the last hammer blow and the force time histories obtained as a result of the GRLWEAP models. Observe how the cushion condition affects the magnitude of the force time history. The magnitude of the force time history applied at the top of the pile varied throughout the installation. The magnitude of the peak force in the analysis with the "new" cushion is approximately the two thirds of the magnitude of the peak force in the analysis with a "used" cushion. When the pile cushion was modeled as "used", the applied force time history obtained from GRLWEAP matched well the one measured in the field, especially in terms of peak magnitude and overall shape. This is attributed to the fact that the force time history shared in the EDC report corresponded to the last hammer blow, and due to that, the pile cushion was already degraded. In the numerical analysis, the force time history obtained by using a "used" pile cushion was applied at the top of the pile, but it was varied throughout the numerical analysis based on the condition of the cushion to better match the field conditions.

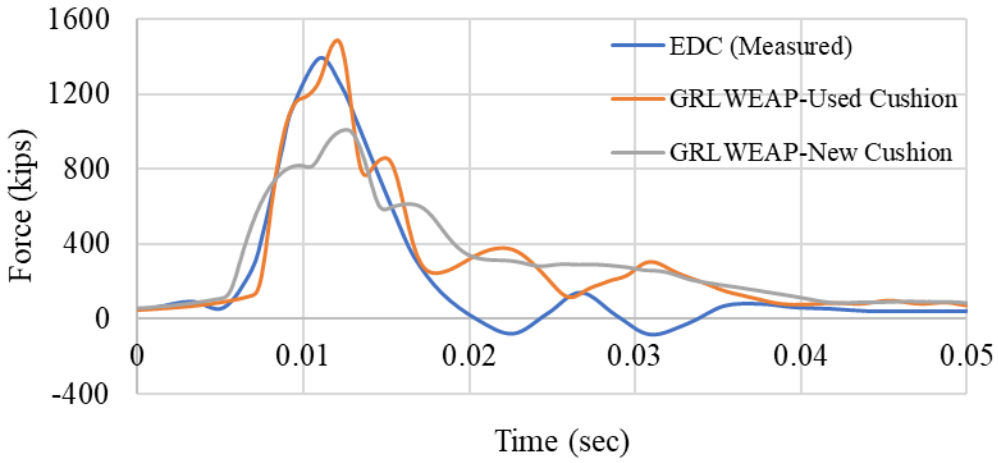

Figure 5-9. Force time history for a single hammer blow at the top of the pile.

The model described in Figure 5-2 was used in the numerical validation analysis of the pile performed in PLAXIS 2D. The relative density of the upper sand layer in the model was simplified as 40% based on the summarized soil conditions of the site. The computation was performed up to 1000 hammer blows due to large computation effort. Figure 5-10 presents a comparison of measured and computed vertical pile penetrations starting from the predrilling depth versus hammer blows during installation of the pile. The correlation between the vertical penetration at the top of the pile and the hammer blows were created by accumulating hammer blows based on the pile driving logs. From that information provided by the contractor, the numerical validation was performed by matching the progression of vertical pile penetration based on the accumulated number of hammer blows. Observe in the figure how the computed pile tip depth matched well the field data up to 1000 hammer blows.

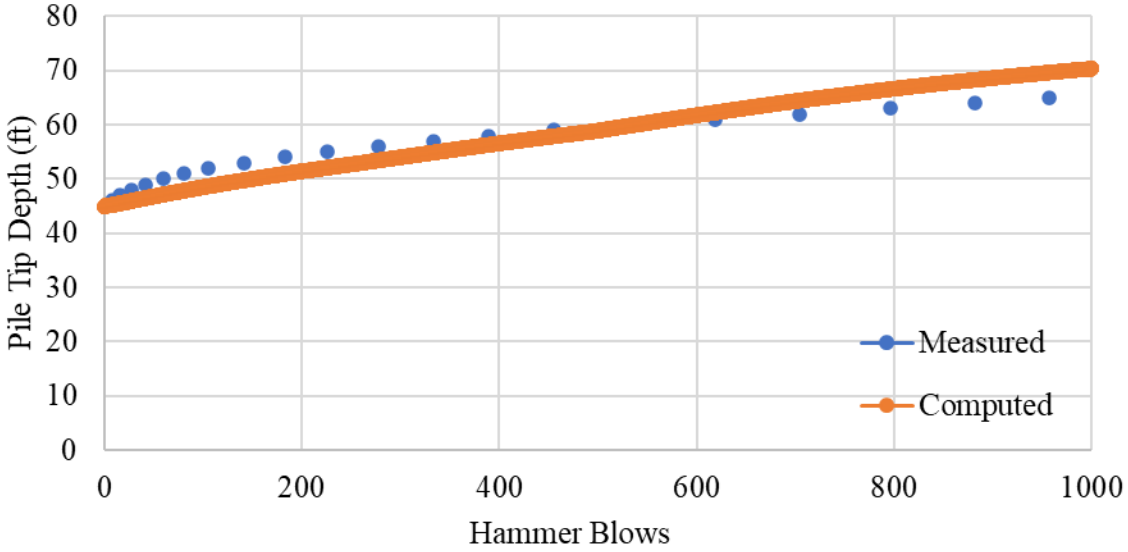

Figure 5-10. Comparison of measured and computed pile tip depth versus hammer blows during driving of pile 13 at Site A1.

Figure 5-11 presents a comparison of measured and computed PPVs during installation of pile 13. Since vibration measurements were also taken during the installation of pile 10 at the same site, measured PPVs are also presented for pile 10 in the chart as another reference value. The results are presented in terms of scaled distance in "$ft/\sqrt{kips-ft}$" and they are given beyond the highly disturbed zone defined in the previous section as 1.0 $ft/\sqrt{kips-ft}$. Observe how measured and computed values matched well beyond a scaled distance of 3.0 $ft/\sqrt{kips-ft}$. Measurements were not presented in the chart inside a scaled of distance 3.0 $ft/\sqrt{kips-ft}$ since geophone installations that close to the piles were not advised by the contractor for most cases given the proximity to the construction operations and when that was possible they malfunctioned during the data collection since the adjusted sensor gains were below a value of 0.3 in/s, thus limiting the maximum recorded values. Even though PPVs above 0.3 in/s could not be measured, it is possible to observe that the computations and measurements showed a similar trend, which implies that at least from the PPV standpoint the numerical model provides accurate results.

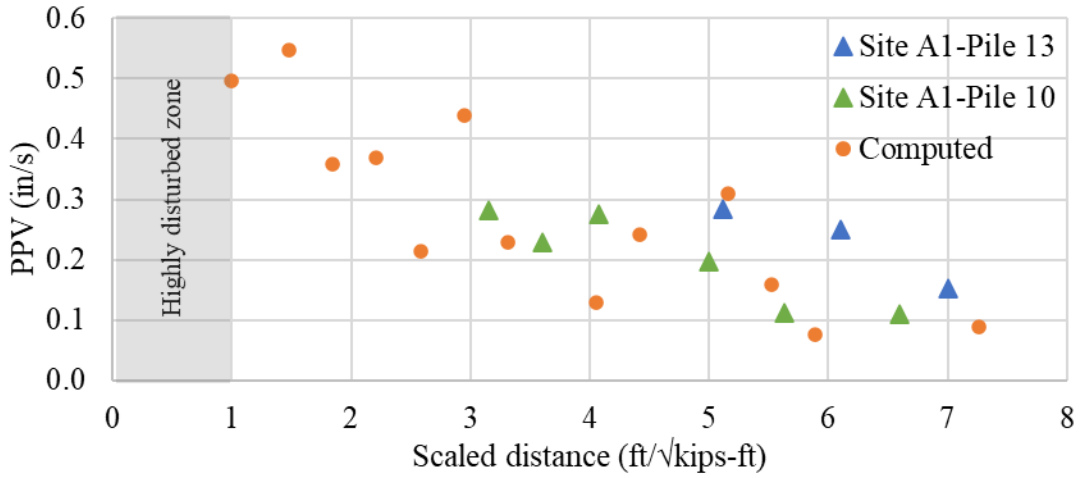

Figure 5-11. A comparison of measured and computed PPVs versus scaled distance in $ft/\sqrt{kips-ft}$ for Site A1 used for validation.

Figure 5-12 presents a comparison of measured and computed maximum settlements. The results are given in terms of scaled distance in "$ft/\sqrt{kips-ft}$". The maximum settlements are also plotted beyond the highly disturbed zone of 1.0 $ft/\sqrt{kips-ft}$, similar to those reported for PPVs. Observe in the figure how computed maximum settlements matched well those measured values at a scaled distance from approximately 1.0 to 2.0 $ft/\sqrt{kips-ft}$ and were slightly conservative with respect to those measured in the range from 2.0 to 5.0 $ft/\sqrt{kips-ft}$. This degree of conservatism of the numerical model is desirable since some recommendations, charts, and equations proposed in this report are derived from parametric analyses presented in further chapters. Note that maximum settlements became approximately negligible both in the field and in the numerical models at a scaled distance beyond 5.0 $ft/\sqrt{kips-ft}$. Based on the computed results, when PPVs met the 0.5 in/s FDOT limit in Figure 5-11, maximum settlements in Figure 5-12 were approximately 1.2 in. Both measured and computed results in this report show that significant amount of ground deformations can occur even if the FDOT PPV limit is satisfied,

hence the importance of studying in great detail ground deformations caused by impact pile driving.

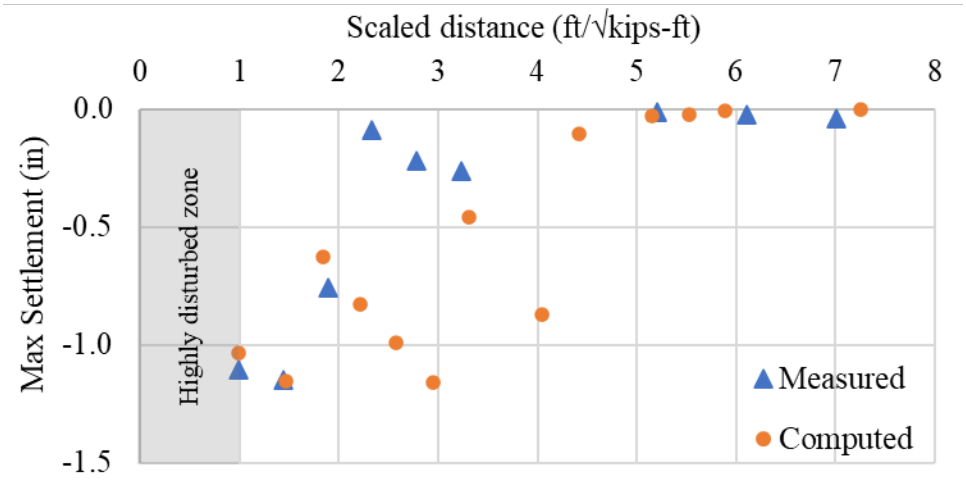

Figure 5-12. A comparison of measured and computed maximum settlements versus scaled distance in $ft/\sqrt{kips-ft}$ for Site A1 used for validation.

5.5. CLASSICAL METHODS FOR PILE DRIVING-INDUCED GROUND DEFORMATIONS

The authors used two classical simplified methods described in the technical literature (see Section 2.1) to compare versus the pile driving-induced ground settlements proposed in this research. These methods consist of an empirical method presented by Massarsch (2004) and a laboratory-based method developed by Drabkin et al. (1996). The former can be used as a quick estimate of the expected ground deformations due to its simplicity, whereas the latter requires knowledge of several input variables to obtain a more accurate estimate of ground surface settlements. Table 5-8 presents the average settlement within the influence zone proposed by Massarsch (2004) computed for the soil densities described as loose, medium, or dense. These settlements were computed for a pile penetration of 60 ft. According to this method and as expected, the looser the material the larger the computed settlements.

Table 5-8. Average settlements computed for soil density ranges using the method proposed by Massarsch (2004).

Loose	Medium	Dense
in	**in**	**in**
8.6	5.8	2.9

Table 5-9 presents the computed settlements for the relative density ranges considered herein (i.e., loose, medium-dense, and dense sand) obtained with the method proposed by Drabkin et al. (1996). PPV values of 0.7 and 0.5 in/s were selected to consider both the maximum possible computed settlements with the method and the settlements corresponding to the FDOT limit,

respectively. A layer thickness of 100 ft was used based on the thickness of the upper sand layer as it was defined in Section 5.2. Additionally, a saturated coarse soil mixture was assumed as the grain size distribution of the soil to consider the most critical condition evaluated in this research, and therefore add some degree of conservatism to the computed envelopes of pile-driving induced deformations studied in this project. Settlements computed at both vibration levels (i.e., PPVs of 0.5 and 0.7 in/s) will be compared versus those computed with the proposed equations and charts as a result of this project.

Table 5-9. Maximum computed pile driving-induced settlement for the proposed relative density ranges and vibration levels of 0.5 and 0.7 in/s computed using Drabkin et al. (1996) method.

Density	**PPV (in/s)**	**Settlement (in)**
Loose Sand	0.5	3.7
Loose Sand	0.7	4.5
Medium Sand	0.5	3.4
Medium Sand	0.7	4.0
Dense Sand	0.5	2.8
Dense Sand	0.7	3.3

6. RESULTS OF THE NUMERICAL MODELS INCLUDING PARAMETRIC STUDIES

This chapter presents the final results from the numerical analyses of the variables involved in pile driving-induced ground deformations and vibrations: hammer type and driving accessories (i.e., contained in the rated energy and forces applied at the top of the pile), relative density of the soils, distance from the vibration source, and vibration levels in terms of PPVs. The effects of these variables are analyzed in terms of the vertical pile penetration, ground vibrations (i.e., PPV), and maximum ground deformations (either settlement or heave depending on the relative density of the soils).

6.1. EFFECT OF SOIL RELATIVE DENSITY

The type of soil and *in situ* state of stresses and density play a crucial role in this problem. This section shows the effect of the relative density of the sand on the ground response during pile driving. As mentioned before, relative densities ranging from 25% to 70% (specifically 25%, 40%, 55%, 60%, and 70%) were selected in order to analyze loose, medium dense, and dense behaviors. Three different scenarios representing three different driving hammers (i.e., diesel hammer APE D70-50, ICE 120-S, and DELMAG D36-32) were modeled.

6.1.1. Vertical Pile Penetration

Figure 6-1 presents the computed vertical penetration tracked at the top of the pile as the hammer blows are applied for each combination of relative densities and hammers. The vertical penetrations computed by using an APE D70-52, ICE 120-S, and DELMAG D36-32 hammers are presented in Figures 6-1a, 6-1b, and 6-1c, respectively. Since the pre-drilling depth of 30 ft was used in all the models, that "offset" is not included in the charts (i.e., resetting the vertical penetration to start from zero). It can be seen that as D_r increases, the driving effort also increases (i.e., more hammer blows required to reach the same level of penetration). This feature is captured accurately by the numerical models since the pile driving process is modeled in a continuous form under a large deformation "updated mesh" framework and the constitutive soil model employed is capable of tracking changes in relative density as the pile is installed.

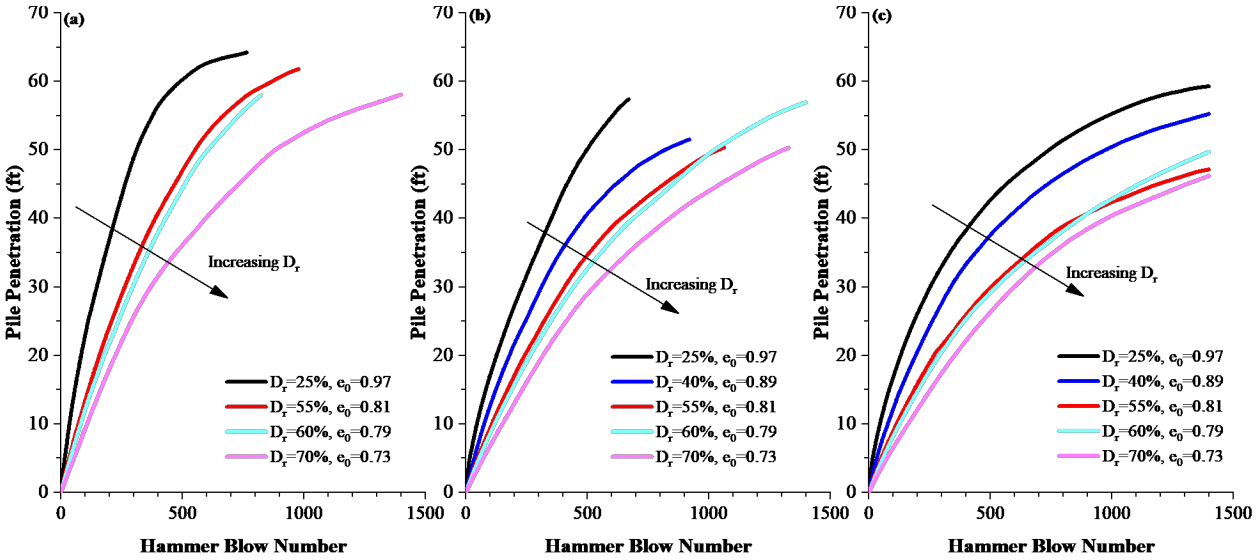

Figure 6-1. Effect of relative density of the sandy soils on the computed vertical pile penetration by using hammer types: (a) APE D70-52, (b) ICE 120-S, and (c) DELMAG D36-32.

6.1.2. Pile Driving-Induced Ground Vibrations (PPVs)

Figure 6-2 presents the attenuation of PPVs computed at the ground surface with the scaled distance from the center of the pile for each combination of hammers and relative densities. The PPV values computed by using an APE D70-52, ICE 120-S, and DELMAG D36-32 hammers are presented in Figures 6-2a, 6-2b, and 6-2c, respectively. The energies used to compute the scaled distance for each hammer correspond to the rated energies presented in Table 5-2. Notice that for distances very close to the pile (i.e., highly disturbed zones affected by pile driving presented in Section 5.3) the looser the material the higher the computed PPV values. As the distance from the pile increases, the scatter of the PPV values tends to reduce. The FDOT PPV limit of 0.5 in/s (i.e., red dashed line in the figures) is shown as the reference line and was reached at scaled distances of approximately 2 $ft/\sqrt{kip-ft}$, regardless of the considered relative densities of the sand. It is concluded that the relative density of the sand does not have a significant influence on the computed ground vibrations in terms of PPVs or on the influence zone of the pile driving operation, especially for the attenuation range necessary to exceed the FDOT PPV limit.

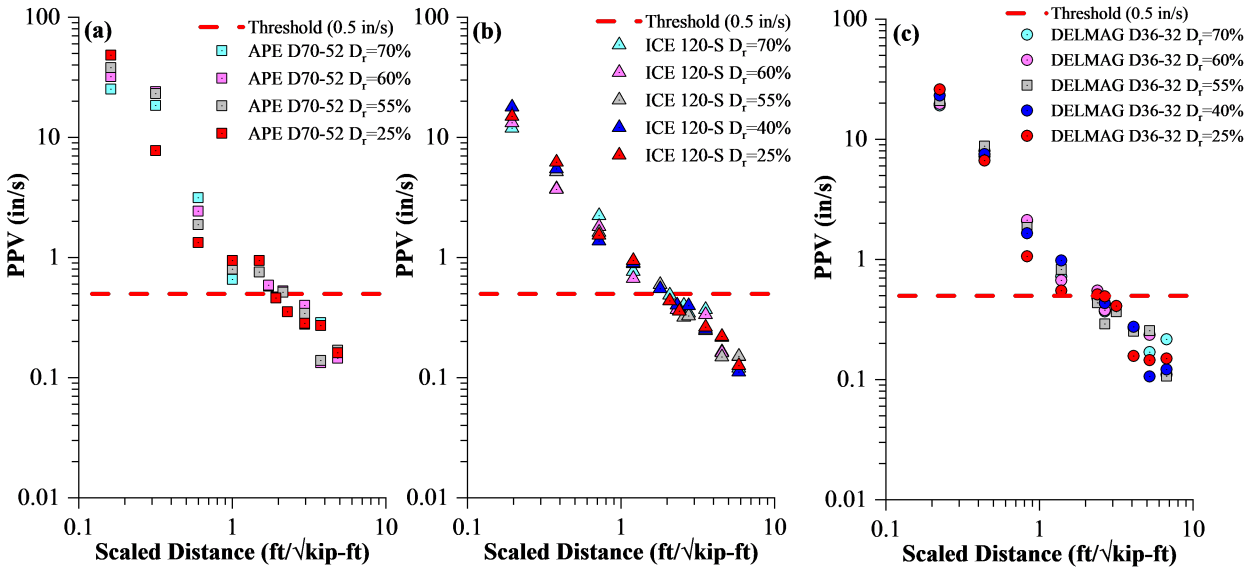

Figure 6-2. Effect of relative density of the sandy soils on the computed PPV attenuation curves during pile driving for the hammer types: (a) APE D70-52, (b) ICE 120-S, and (c) DELMAG D36-32.

6.1.3. Pile Driving-Induced Ground Deformations

Figure 6-3 presents the maximum computed ground surface deformations during the pile driving operation for each combination of hammers (i.e., input energy) and relative densities. Both computed maximum heave and settlement are presented in the figure as positive and negative values, respectively. The ground deformation values computed using an APE D70-52, ICE 120-S, and DELMAG D36-32 hammers are presented in Figures 6-3a, 6-3b, and 6-3c, respectively. In general, the lower the relative density the larger the computed settlements for the considered hammers. This trend is not clear for those distances close to the pile (e.g., within 10-15 ft of the pile) for the ICE 120-S and DELMAG D36-32 hammers, which is related to the higher disturbances and mobilized soil shear strength in that zone as well as the computed characteristics of the forces applied by each hammer. On the other hand, larger heave values were computed for the higher soil relative densities. Notice that the zone of influence for heave is smaller than the one corresponding to settlements. Heave is mostly a result of soil volumetric expansion caused by the *in situ* soil density. Settlement is a soil mechanism mostly associated with particle rearrangement of soil particles and vibration-induced densification.

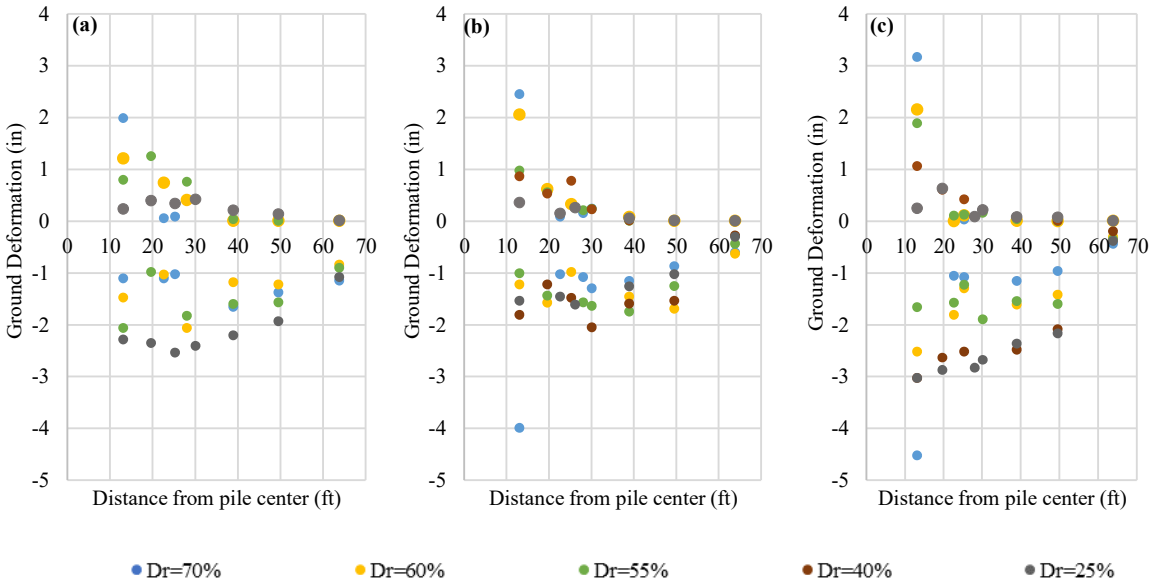

Figure 6-3. Effect of relative density of the sandy soils on the maximum computed ground settlement (negative) and heave (positive) during pile driving conducted using hammer types: (a) APE D70-52, (b) ICE 120-S, and (c) DELMAG D36-32.

6.2. EFFECT OF INPUT ENERGY

6.2.1. Vertical Pile Penetration

Figure 6-4 presents the computed vertical pile penetration during the pile penetration for selected relative densities (i.e., 25%, 60%, and 70%) representing loose, medium-dense, and dense sand conditions. The vertical pile penetration as the hammer blows applied is presented in the figure. The relative density was kept constant in each subfigure so that only the effect of input energy on the pile penetration is elucidated. Three hammer types having different input energies (see Figure 5-1) were selected for the analyses: APE D70-52, DELMAG D36-32, and ICE 120-S. The selected pre-drilling length (i.e., 30 ft) was constant for all the piles. The vertical pile penetration value was reset to zero. As expected, the "effort" required to install each pile is highly dependent on the input energy. Figure 6-4a shows the results obtained for the loose sand conditions. A total of 500 hammer blows were necessary to drive the pile 60 ft through the loose soil using an APE D70-52 but using the ICE 120-S and DELMAG D36-32 hammers, it was only possible to drive the piles 50 ft and 43 ft, respectively. Figure 6-4b presents the same type of analysis of vertical pile penetration versus hammer blows when the relative density of the soil was 60%, while Figure 6-4c presents the analysis for the soil having a D_r of 70%. A similar conclusion is reached for D_r values of 60% and 70%. More hammer blows were required to drive the pile when DELMAG D36-32 was used, since the input energy of the DELMAG D36-32 hammer is lower than the other two hammers. When comparing the results computed with the APE D70-52 hammer in relation to the other hammers, more vertical penetration was obtained for the same number of hammer blows since the input energy of the APE D70-52 hammer is higher than the other two shown in the figures.

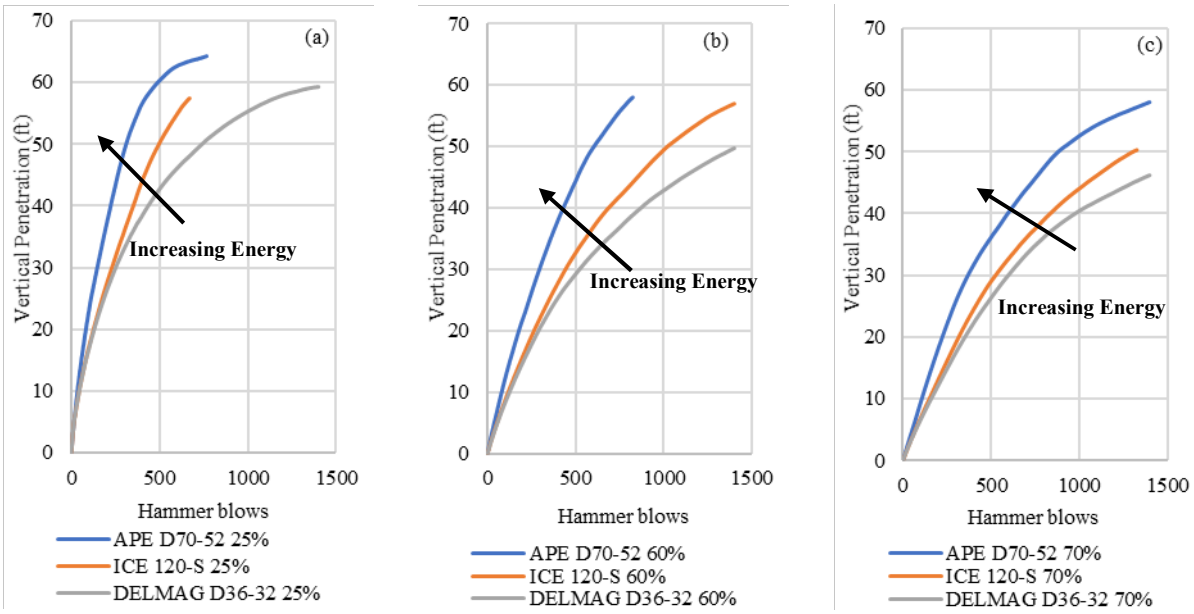

Figure 6-4. Computed vertical pile penetration versus hammer blows during driving by using three selected hammers for three selected relative densities: (a) loose sands, (b) medium-dense sands, and (c) dense sands.

6.2.2. Pile Driving-Induced Ground Vibrations (PPVs)

Figure 6-5 presents computed PPV values in the soil cluster for the three selected input energies and three relative densities (i.e., 25%, 60%, and 70%) representing loose, medium-dense, and dense sands, respectively. A horizontal red dashed line is shown once again to illustrate the FDOT acceptable PPV value of 0.5 in/s. Figure 6-5a shows the results obtained for the loose sand conditions. Observe how PPV values are the highest for the zone close to the pile when the applied energy is given by the APE D70-52 hammer. This is a function of scaled distance which is different for every hammer. Figures 6-5b and 6-5c present the results obtained for the medium-dense and dense sand conditions, respectively. PPV values are higher with the APE D70-52 hammer than the ICE120-S and DELMAG D36-32 up to a distance of approximately 0.3 times the square root of the rated energy. Beyond that value, the scatter in the attenuation curves reduces. These curves for the entire set of parameters considered in this research will be compared in the final section of this report in relation to those presented by Bayraktar et al. (2013).

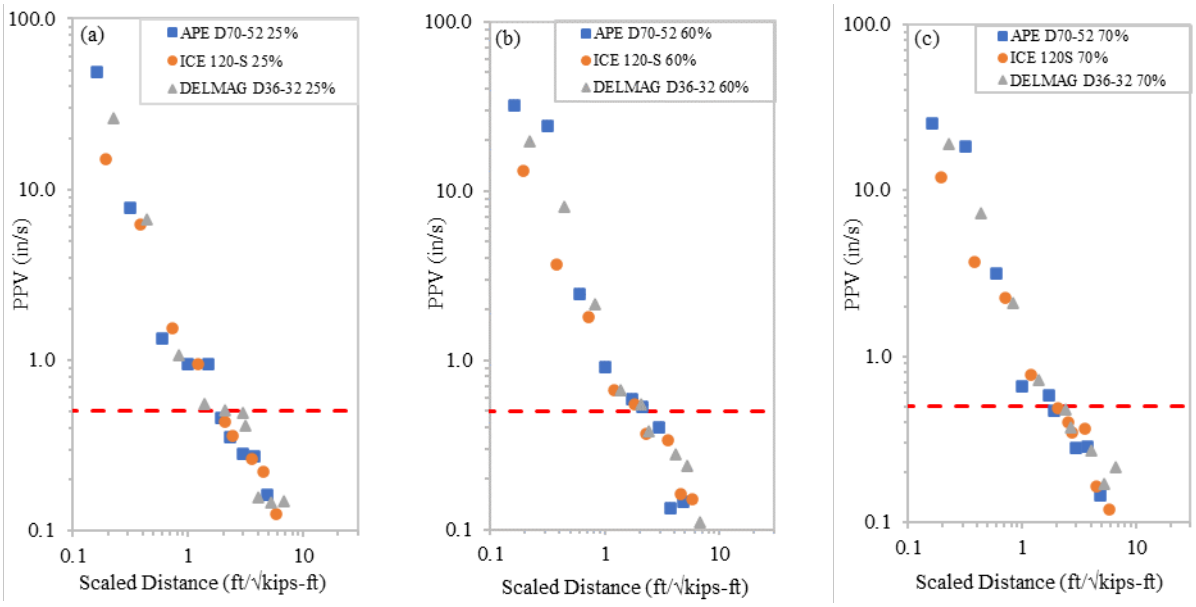

Figure 6-5. Computed PPV versus scaled distance by using three selected hammers during pile driving for piles installed in: (a) loose, (b) medium-dense, and (c) dense sands.

Figure 6-6 presents computed PPV values in the soil cluster for the same input energies and relative densities that were presented in Figure 6-5, but in this case, the PPV values are presented versus distance away from the center of the pile instead of scaled distance which varies depending on the hammer type. This type of plotting the PPV attenuation is also included in order to understand the extension of the influence zone. Figure 6-6a shows the results obtained for the loose sand conditions. Notice that at a distance of approximately 2 to 4 ft away from the center of the pile, the PPV values resulting from input energies computed with APE D70-52 hammer are higher than those computed with ICE120-S and DELMAG D36-32. This confirms the relationship between PPV, distance from the source, and input energy described before. Figure 6-6b-c presents the results obtained for the medium-dense and dense sand conditions, respectively. For these cases, similar trends were observed in the zone close to the pile, but the extension of the influence zone (defined in terms of the 0.5 in/s FDOT reference value) slightly varied with the relative density. In general, PPV values attenuated below the FDOT limit after a distance of approximately 30ft away from the center of the pile regardless of the considered input energy and relative density. Even though the computed values increased up to extreme values (i.e., more than 10 in/s) very close to the pile in all the soil conditions the PPV values attenuated below the FDOT limit after a distance of approximately 28 ft away from the center of the pile regardless of the considered input energy.

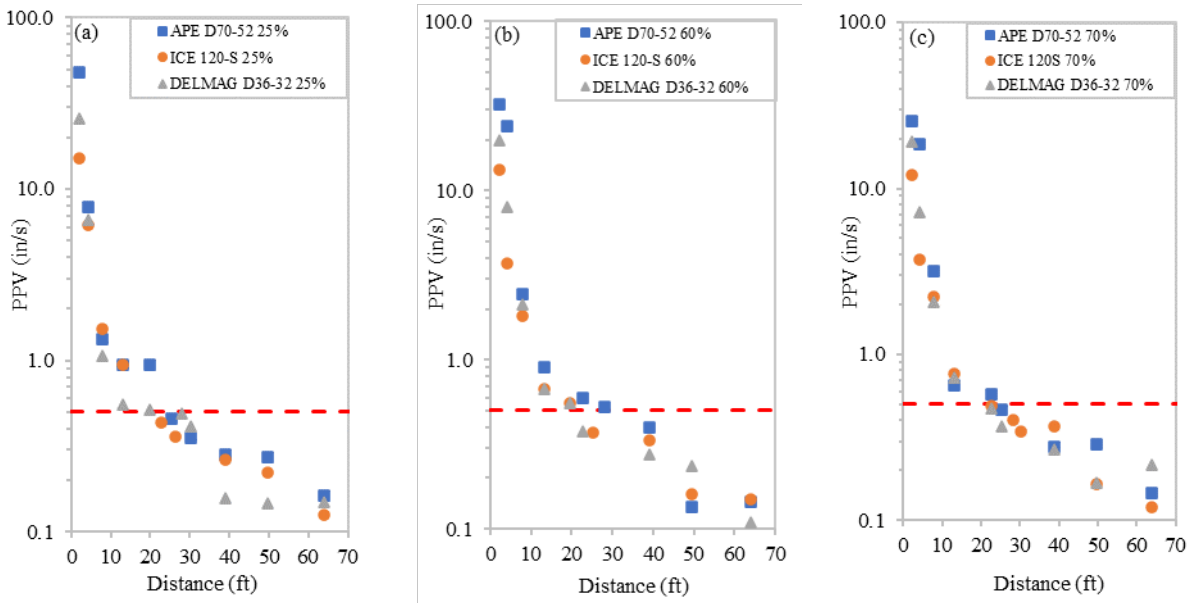

Figure 6-6. Computed PPV versus distance by using three selected hammers during pile driving for piles installed in: (a) loose, (b) medium-dense, and (c) dense sands.

6.2.3. Pile Driving-Induced Ground Deformations

Figure 6-7 presents the maximum ground surface deformations versus scaled distance computed at the ground surface during the pile driving operation for each relative density group. In the figures, the input energy is varied to study its influence on the problem. Recall that maximum heave and settlement are presented in the figure as positive and negative values, respectively. Data points in the figure do not necessarily exceed the maximum PPV requirement by FDOT of 0.5 in/s. The ground deformation "attenuation" as shown in the figure with the scaled distance is presented as an attempt to understand the influence zones of each selected rated energy. The maximum computed ground deformations (heave and settlement are shown) induced by driving through loose, medium-dense, and dense sands are presented in Figures 6-7a, 6-7b, and 6-7c, respectively. Notice that in general, the largest input energy (i.e., that applied with APE D70-52) caused the largest ground surface settlements during driving through the dense sandy soil (Figure 6-7c). However, this trend is not as clear for the remaining hammers (see for instance that the largest ground deformations on loose soils occurred when driving the pile with the DELMAG D36-32 hammer which in fact provides the lowest, but still significant, input energy). The pile penetration previously shown in Figure 6-4c for the dense sands was modeled to the same amount of hammer blows (i.e., approximately 1300 blows) which explains a more reasonable trend in the ground deformation "attenuation" curves for the dense soils. Pile driving-induced ground deformations are highly dependent on the rated energy of the hammer as well as the type of sandy soil in terms of its relative density. The authors considered in this chapter as many variations of those variables to derive an accurate representation of the variation of ground deformations for the selected hammers used in this analysis and for a wide range of relative densities that can be readily used in practice.

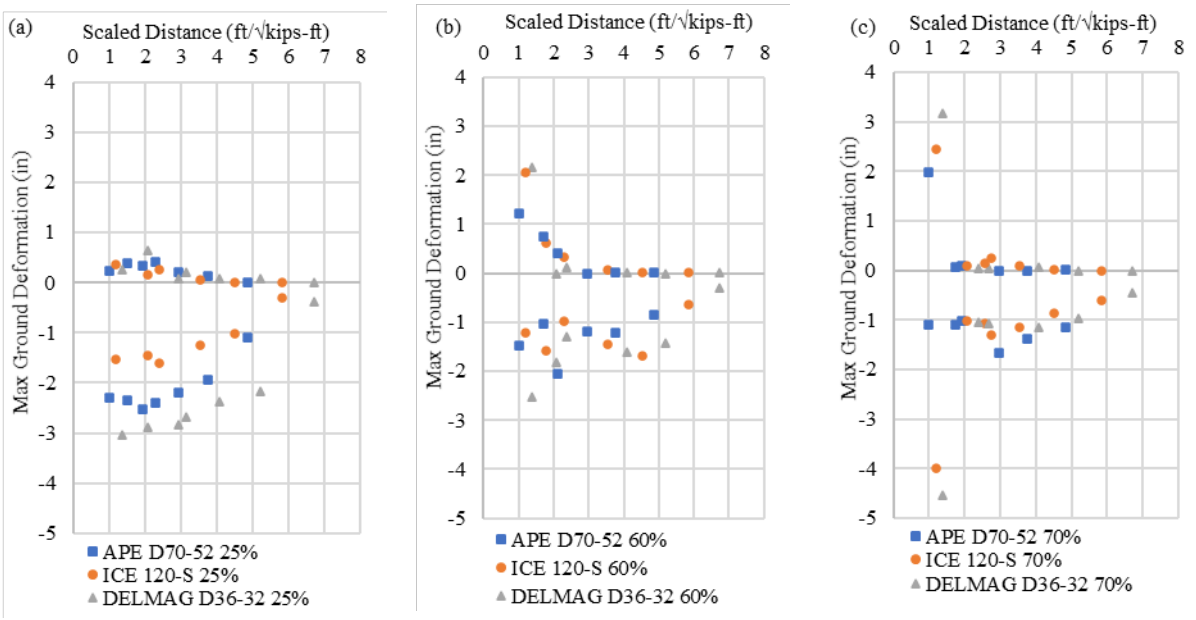

Figure 6-7. Maximum computed ground settlement (negative) and heave (positive) versus scaled distance by using three selected hammers during pile driving for piles installed in: (a) loose, (b) medium-dense, and (c) dense sands.

Figure 6-8 presents the same results but this time plotting in the horizontal axis the distance in "feet" for each combination of relative density and hammer. Recall that data points do not necessarily exceed the maximum PPV requirement by FDOT of 0.5 in/s as it was in Figure 6-7. The ground deformations plotted versus distance as opposed to scaled distance are shown to visualize the extension of the influence zone caused as a result of three selected input energies. Notice that regardless of the soil density the zone of influence of the APE D70-52 (i.e., largest energy) is wider than the one caused by the other two hammers. In conclusion, the extension of the influence zone is determined proportionally to the magnitude of the rated energy.

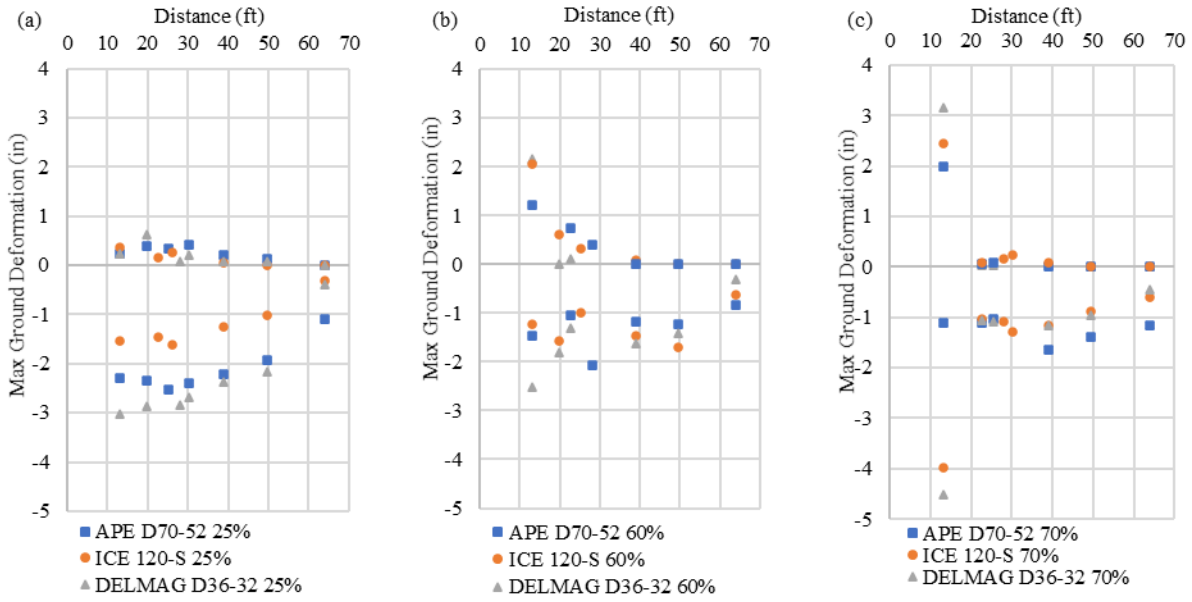

Figure 6-8. Maximum computed ground settlement (negative) and heave (positive) versus distance in ft by using three selected hammers during pile driving for piles installed in: (a) loose, (b) medium-dense, and (c) dense sands.

6.3. EFFECT OF PRE-DRILLING DEPTH

This section analyzes the effect of pre-drilling on the ground response due to pile driving activities in terms of the pile penetration (i.e., the evolution of vertical pile penetration versus applied hammer blows), ground vibrations (i.e., PPV), and maximum ground deformations (both maximum heave and settlement). The results are also compared against current FDOT standards expressed in FDOT (2021a). The FDOT standards established that "holes might be pre-drilled up to a depth of 10 ft or 20% of the length of the pile, whichever is greater." The standards do not specify a minimum pre-drilling depth in order to avoid pile driving-induced vibrations and deformations.

Table 6-1 presents a summary of the different pre-drilling configurations considered in the numerical analyses presented in this report. A total of three pre-drilling depths were selected based on commonly used pre-drilling depths mostly on precast concrete piles observed during field visits that the authors conducted to different construction sites in Central Florida in the course of this research. Observe that pile length is the same for the baseline models (i.e., the initial model explained in Chapter 5.2) and for model M1, but note that their pre-drilling depths are different. M2 and M3 models are presented to vary both pile length and pre-drilling depth and to analyze the effect of both variables on the final response. The results of M2 and M3 models are discussed in further sections. It was common in the field testing sites to have pre-drilling depths deeper than 20% of the pile length, which is the reason for selecting those values reported in the table. Piles corresponding to models M1, M2, and M3 were driven by selected hammers APE D70-52, ICE 120-S, and DELMAG D36-32 to study predrilling depth effects.

Table 6-1. Summary of analyses performed in this report to elucidate pre-drilling depth effects on ground response.

Analysis	Pile Length (ft)	Pre-Drilling Length (ft)	Pre-Drilling Length/ Pile Length
Baseline*	90.0	30.0	33%
M1	90.0	23.0	26%
M2	131.0	39.0	30%
M3	131.0	46.0	35%

* This model corresponds to the initial model explained in Chapter 5.2.

The complete range of relative densities mentioned in Section 5.2.1 (i.e., 25%, 40%, 50%, 55%, 60%, 70%, and 75%) were numerically modeled for the conditions outlined in Table 6-1. This section only discusses the effects of pre-drilling on the ground response for a selected D_r of 55% since it is a typical and representative relative density value to explain the effects of pre-drilling depth in light of the numerical results summarized in this report.

6.3.1. Vertical Pile Penetration

Figure 6-9 presents the change in pile tip depth measured from the ground surface as the hammer blows are applied for the selected input energies and pre-drilling depths of 30 ft and 23 ft (i.e., predrilling-to-pile length ratios of 33% and 26%, respectively). Notice that the curves in the vertical axis start from each selected pre-drilled depth. The numerical analyses were stopped if one of the following conditions were met: the pile tip reached the bearing stratum, 1,400 hammer blows were applied, or due to FE model lack of convergence or excessive computational time. It can be observed that a larger driving "effort" was required as the pre-drilling depth increased for hammer types APE D70-52 and DELMAG D36-32 (see Figures 6-9a and 6-9c, respectively). The slope of the curves (i.e., representing the penetration rate) tends to become horizontal more rapidly as the pre-drilling is decreased. Flattening of the curve implies that a marginal increase in pile penetration is achieved only if a larger amount of hammer blows are applied. This is also related to the densification of the nearby sandy soil when the pile driving operation starts at a shallower depth (i.e., shallower soils are less confined and are easily densified by the pile driving process). A slightly different trend is computed in the case of the ICE 120-S hammer (see Figure 6-9b) but notice that only 362 hammer blows were applied with that hammer beginning at the pre-drilling depth of 23 ft. In general, these results indicate that the type of hammer and its corresponding input force time histories have a large influence on the ground response in terms of the studied evolution of the pile penetration process.

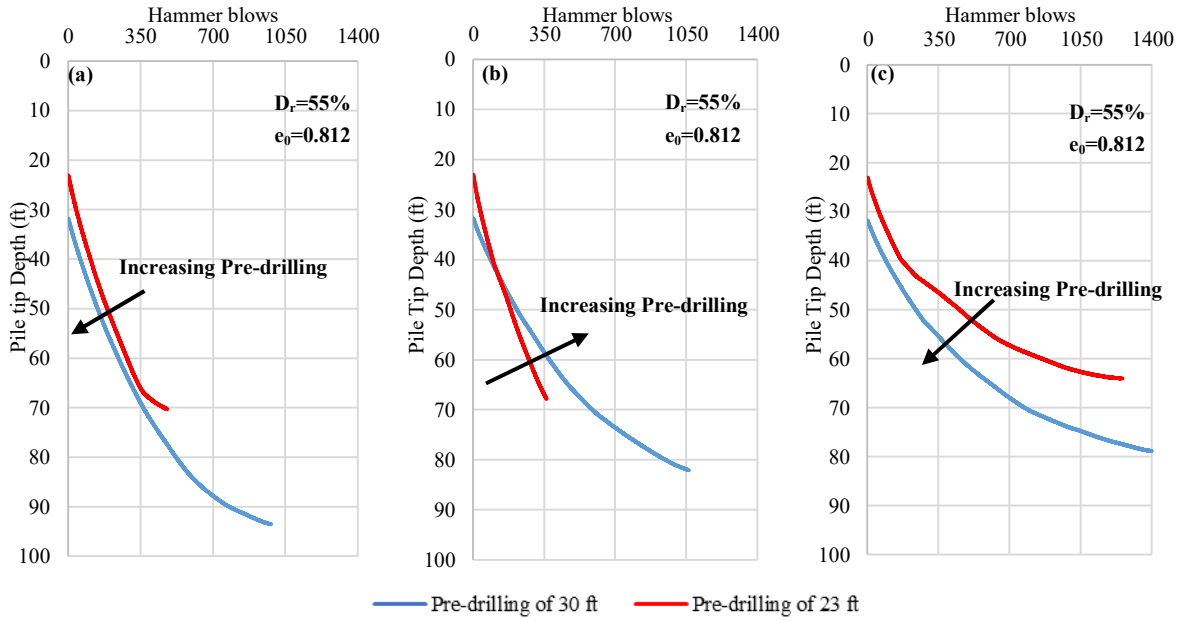

Figure 6-9. Effect of pre-drilling on the computed vertical pile penetration through a sandy soil with a relative density of 55% by using hammer types: (a) APE D70-52, (b) ICE 120-S, and (c) DELMAG D36-32.

6.3.2. Pile Driving-Induced Ground Vibrations (PPVs)

Figure 6-10 presents the computed PPV attenuation curves on the ground surface for each type of hammer and pre-drilling depths of 30 ft and 23 ft. The PPV attenuation curves computed by using an APE D70-52, ICE 120-S, and DELMAG D36-32 hammers are presented in Figures 6-10a, 6-10b, and 6-10c, respectively. It is interesting to note in these figures that the importance of pre-drilling is reflected in the fact that PPV decreases as the pre-drilling depth increases. This is particularly noticeable when driving the piles using the ICE 120-S hammer (see Figure 6-10b). The effect of pre-drilling depth is not as significant for those scaled distances corresponding to PPV values beyond the FDOT limit of 0.5 in/s. The overall trend computed for the three hammers showed that the deeper the pre-drilling, the lower the pile driving-induced ground vibrations.

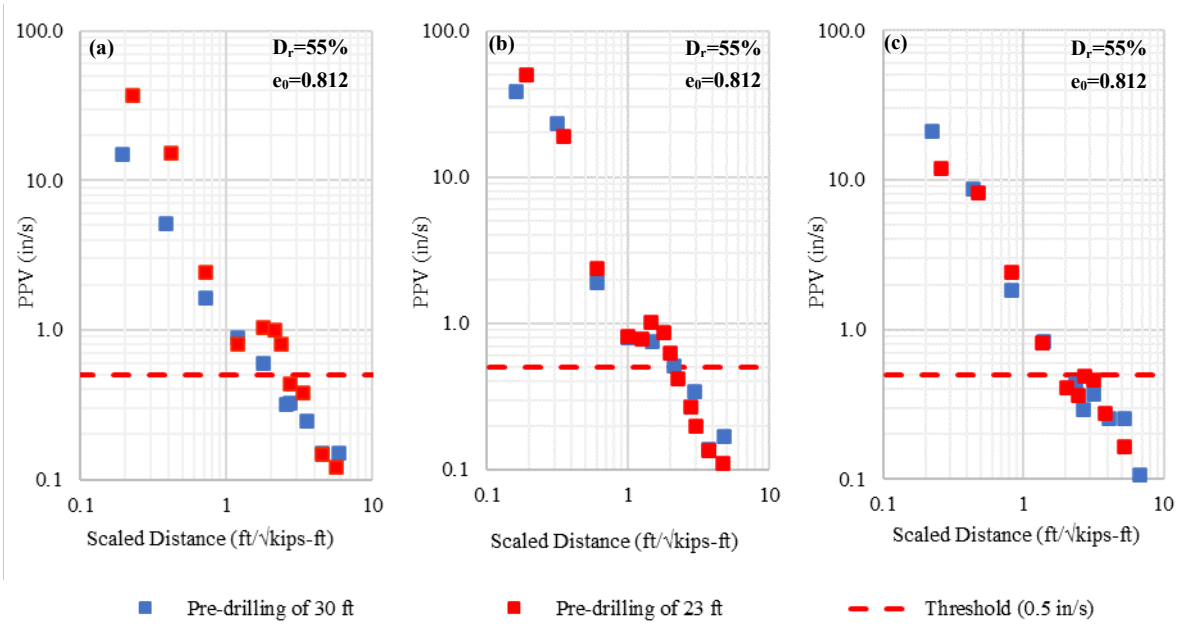

Figure 6-10. Effect of pre-drilling depth on the computed PPV attenuation curves during pile driving through a sandy soil with a relative density of 55% and for the hammer types: (a) APE D70-52, (b) ICE 120-S, and (c) DELMAG D36-32.

6.3.3. Pile Driving-Induced Ground Deformations

Figure 6-11 presents the maximum computed ground surface deformations during the pile driving for the selected hammers and pre-drilling depths. The ground deformation values computed by using APE D70-52, ICE 120-S, and DELMAG D36-32 hammers are presented in Figures 6-11a, 6-11b, and 6-11c, respectively. Notice that similar ground deformation patterns were obtained for both pre-drilling depths when using hammers APE D70-52 and DELMAG D36-32 (see Figures 6-11a and 6-11c, respectively). Slightly larger deformations were computed as the pre-drilling increased for these two hammers. Recall that for the case of hammers APE D70-52 and ICE 120-S fewer hammer blows were able to be applied with a pre-drilling of 23 ft than 30 ft (see Figure 6-9), thus the computed ground deformations are influenced by that effect. A more reasonable comparison can be made for the case of DELMAG D36-32 (see Figure 6-11c) since similar hammer blows were applied for both pre-drilling depths. Note that as an overall trend in our field measurements, pre-drilling did not appear to have any effect on settlements induced by pile driving. Selection of the pre-drilling depth is a decisive factor to attenuate potential detrimental dynamic or vibration effects caused by pile driving operations, as it was described in terms of PPVs in the previous section, but analyses show that ground deformations are not as affected by such variable.

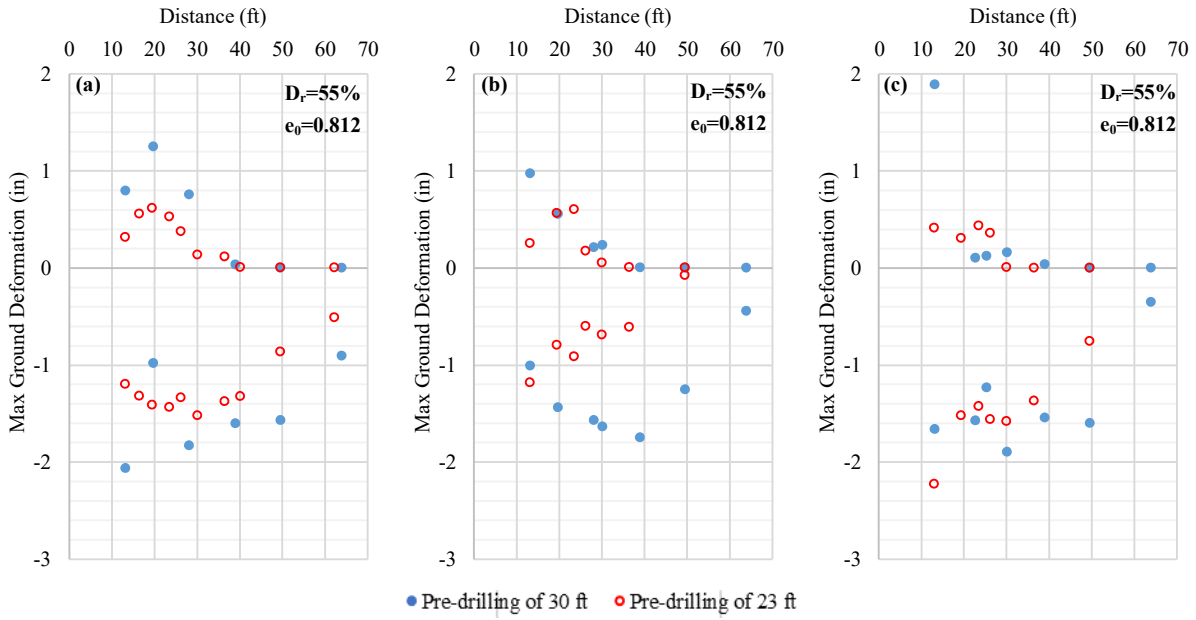

Figure 6-11. Effect of pre-drilling depth on the maximum computed ground settlement (negative) and heave (positive) during pile driving through a sandy soil with a relative density of 55% and for the hammer types: (a) APE D70-52, (b) ICE 120-S, and (c) DELMAG D36-32.

7. SUMMARY TRENDS ON PILE PENETRATION VIBRATIONS AND GROUND DEFORMATIONS

This section presents the summarized numerical results for the entire set of analyses performed in this research, which were summarized in Table 5-6. The study of the variables involved in the problem of pile driving-induced ground vibrations and deformations are presented in this section. These numerical models present the final analyses of the influence of relative densities, input energies, and pre-drilling depths, which cannot be fully tested in the field, but as more data is collected, the proposed envelopes and correlations will be tested even beyond the end of this project. The selected relative densities were grouped into three categories to facilitate the practical use of these charts. Relative densities were grouped as: loose (i.e., 25% and 40%), medium-dense (i.e., 50%, 55%, and 60%), and dense (i.e., 70% and 75%) sands (Meyerhof, 1956). The results are presented for three geometrical configurations: (i) the baseline model, (ii) M1, (iii) M2, and (iv) M3. The baseline model corresponds to the initial model explained in Section 5.2 and models M1, M2, and M3 correspond to different geometric configurations that were presented in Table 5-6. The results are presented for the entire set of input energies for the baseline models, but only input energies APE D70-52, ICE 120-S, and DELMAG D36-32 were selected for the set of models M1, M2, and M3.

7.1. VERTICAL PILE PENETRATION

Figure 7-1 presents the computed change in pile tip depth during the pile driving using the hammers and soil conditions listed in Table 5-6. Figure 7-1a-c presents the results for loose, medium-dense, and dense sands, respectively. The pre-drilling depths defined in the analyses are considered in the figures. The change in pile tip depths corresponding to the baseline models, M1, M2, and M3 started from 30 ft, 23 ft, 40 ft, and 46 ft respectively. The figures show how highest input energies (i.e., those applied by hammers APE D70-52 and DELMAG D62-22) when compared to those applying the lowest input energies (i.e., ICE I-19, ICE80-S, ICE100-S, DELMAG D30-02, DELMAG D30-32, and DELMAG D36-32) elucidate the effect of the effort required to install the piles quantified in terms of the number of hammer blows corresponding to a given target penetration depth. For example, in the case of an APE D70-52, a total of 770 hammer blows were necessary to drive the pile through the loose soil as opposed to for example DELMAG D62-22 where a total of 856 hammer blows were required to drive the pile given that the soil has the same relative density. Also, more than 1400 hammer blows were required to drive the pile and reach the same depth (approximately 70 ft) when DELMAG D36-32 was used to drive the pile in the same loose sand deposit. This shows the effect of the lower input energy of DELMAG D36-32 in relation to the APE D70-52 and DELMAG D36-32 (see Figure 7-1a). When Figures 7-1b and c are investigated, similar trends of pile driving operations in the medium-dense and dense sands can be obtained. As expected, less driving "efforts" were required to drive piles when the highest input energies were employed (e.g., 800 hammer blows were necessary to drive the pile 60 ft through the soil having D_r of 60% when DELMAG D62-22 was used, whereas more than 1400 blows were required with ICE 80-S for the same vertical penetration). Note also how the "effort" required to install the pile varied depending on the relative density. This is reflected in the variable penetration depth for a given number of hammer blows. See for instance how pile penetrations of 57 ft, 41 ft, and 31 ft were reached for 400 hammer blows by using APE D70-52

in loose, medium-dense, and dense sands, respectively. For the study of pile-driving ground deformations, which is the main goal of this research, a significant amount of scenarios were considered (11 input energies, 7 relative densities, 4 pre-drilling depths, and ground deformations computations varying away from the pile), so that a comprehensive envelope of settlement or heave can be derived as a result of this study as shown in the following sections.

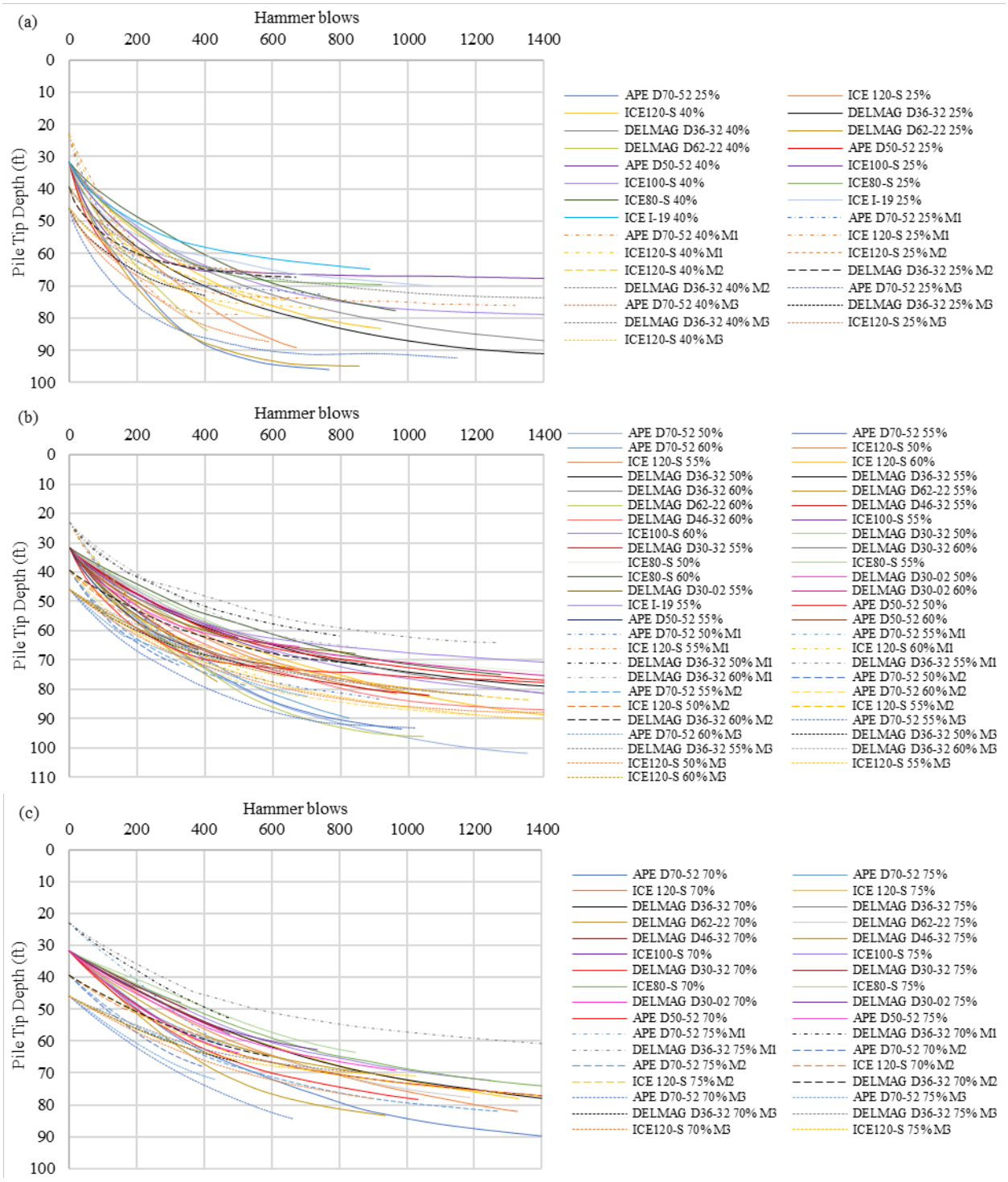

Figure 7-1. Summarized results of change in pile tip depth (ft) during pile driving for the entire set of hammer types, geometrical configurations (i.e., baseline model, M1, M2, and M3), and relative densities considered in this study: (a) loose, (b) medium-dense, and (c) dense sands.

7.2. PILE DRIVING-INDUCED GROUND VIBRATIONS (PPVs)

A summary of ground vibrations quantified in terms of PPVs computed for the entire set of analyses is presented in this section. These results are presented in relation to current FDOT limit and case histories found in past FDOT-sponsored research projects. According to FDOT (2021b), Article 108-2.1.2, "survey and monitor for settlements should be performed within a distance, in ft, of 0.5 times the square root of the impact hammer energy, in foot-pounds" (which is approximately a scaled distance of 16 $ft/\sqrt{kip-ft}$). Thus, this is another limit that can be evaluated in light of the results presented herein. Historical records of PPV attenuation curves proposed by Bayraktar et al. (2013) were also used as a comparison source. These PPV attenuation records were taken from different construction sites along Florida´s Turnpike where the upper limits for the PPV values measured at each site were presented in the form of linear envelopes on a log-log scale. A total of five sites were presented by Bayraktar et al. (2013) and are described as Z.1 through Z.5 herein.

Figures 7-2, 7-3, and 7-4 present a summary of computed PPV values versus scaled distance for precast concrete piles in loose, medium-dense, and dense sands, respectively. For the calculation of scaled distance, recall that the rated energy of the hammer was provided in Table 5-2. Note that using the scaled distance normalization technique, the computations showed a very good match with the PPV values previously measured by Bayraktar et al. (2013) regardless of the different hammer types and soil relative densities, particularly for the zone beyond the horizontal red dashed line illustrating the FDOT acceptable PPV value of 0.5 in/s. At the zones close to the pile (i.e., labeled as a highly disturbed zone), observe how PPV values resulting from this research slightly exceed those reported in the past. A reasonable value of the scaled distance to exceed the FDOT PPV requirement (i.e., 0.5 in/s) ranges approximately from 4 to 5 $ft/\sqrt{kips-ft}$ based on the data points regardless of the considered input energy and relative density.

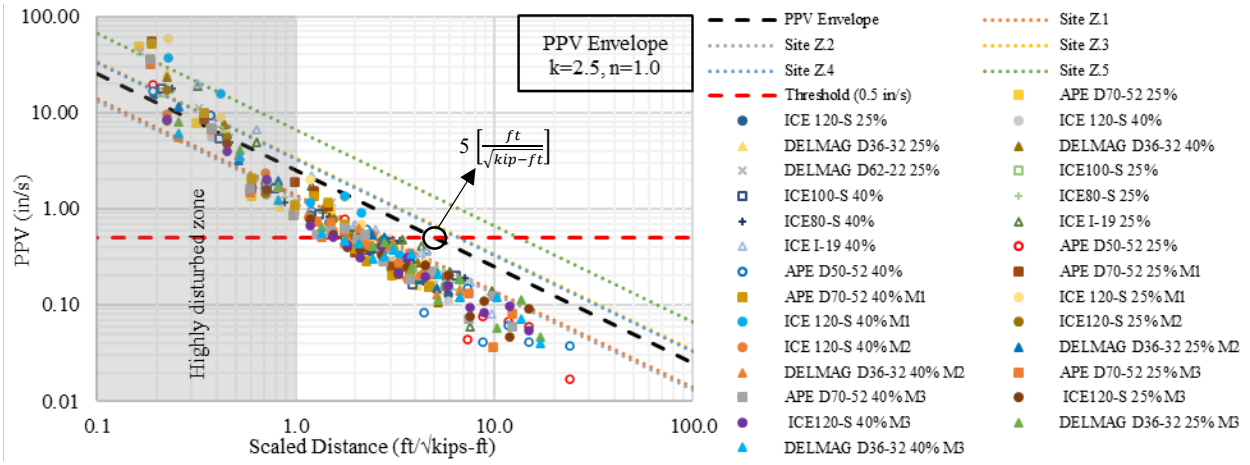

Figure 7-2. Summarized results of PPV attenuation curves (i.e., envelopes) computed for prestressed concrete piles installed in loose sands in relation to those reported boundaries by Bayraktar et al. (2013).

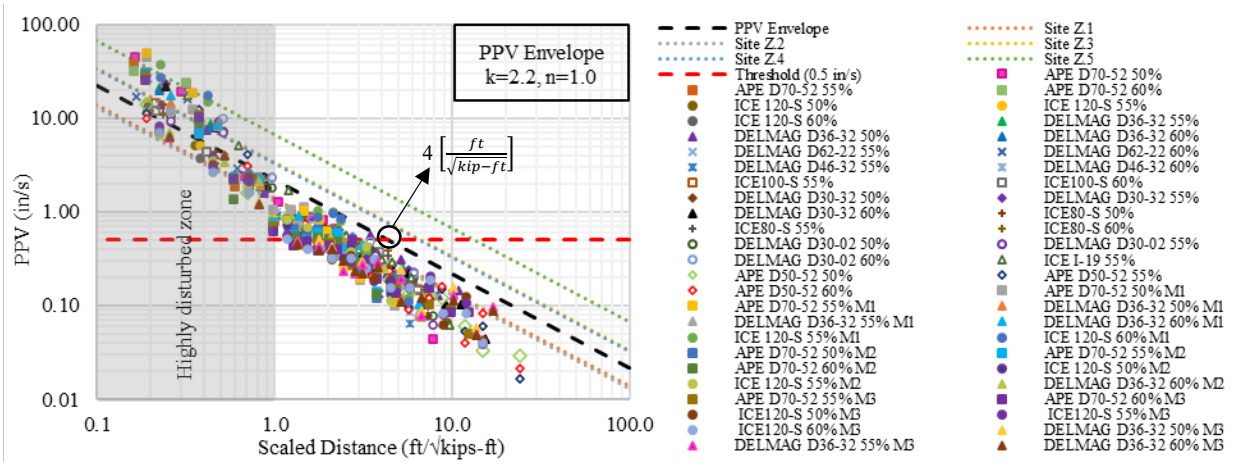

Figure 7-3. Summarized results of PPV attenuation curves (i.e., envelopes) computed for prestressed concrete piles installed in medium-dense sands in relation to those reported boundaries by Bayraktar et al. (2013).

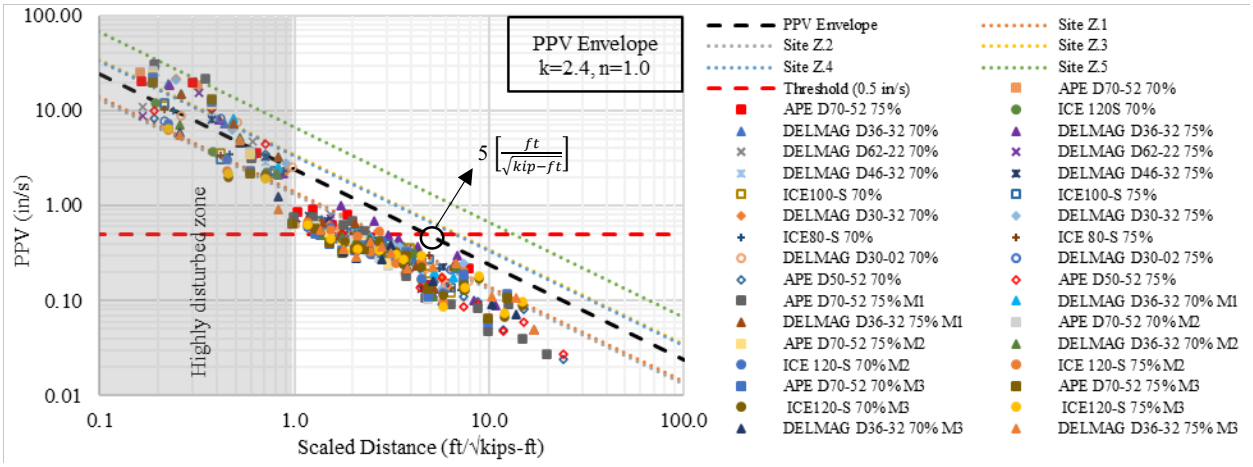

Figure 7-4. Summarized results of PPV attenuation curves (i.e., envelopes) computed for prestressed concrete piles installed in dense sands in relation to those reported boundaries by Bayraktar et al. (2013).

7.3. PILE DRIVING-INDUCED GROUND DEFORMATIONS

A summary of design charts and equations to determine pile-driving induced ground surface deformations (i.e., settlement or heave) is presented in this section. Figure 7-5 presents the summarized maximum ground surface deformations (negative representing settlement and positive heave) computed at distances where PPV values are equal to or less than the 0.5 in/s FDOT limit (FDOT, 2021a) for the considered relative densities. This PPV reference value was met at different distances from the pile, input energies, and relative densities since typical PPV attenuation curves vary as a function of those variables. The results for the three groups of relative densities (i.e., loose, medium-dense, and dense) are presented. The practitioner must respect first

the limit stipulated by FDOT of 0.5 in/s, and then an estimate of the maximum ground deformations (i.e., settlement or heave) as a function of the soil relative density can be extracted from the figure or computed with the equations. Computed ground deformations in the vertical axis were obtained from multiple time histories along the soil continuum at the ground surface for all the considered input energies in this study. Settlement (S) and heave (H) envelopes are shown in the figure. Observe how the magnitude of maximum ground surface settlement decreases as the relative density increases. Larger settlements were computed for the loose sand group (i.e., from 25% to 40%) than for the dense sand group (i.e., from 60% to 75%). The opposite is observed for the case of maximum heave values. This can be explained by the phenomenon of soil dilation (i.e., particles rolling over each other along the shear failure plane) caused by the shear mechanism at the tip and shaft of prestressed concrete piles as they are being driven in the medium-dense to dense sands and potentially triggers volumetric expansion reflected in heave to the ground surface. A total of 884 data points were used for this computation.

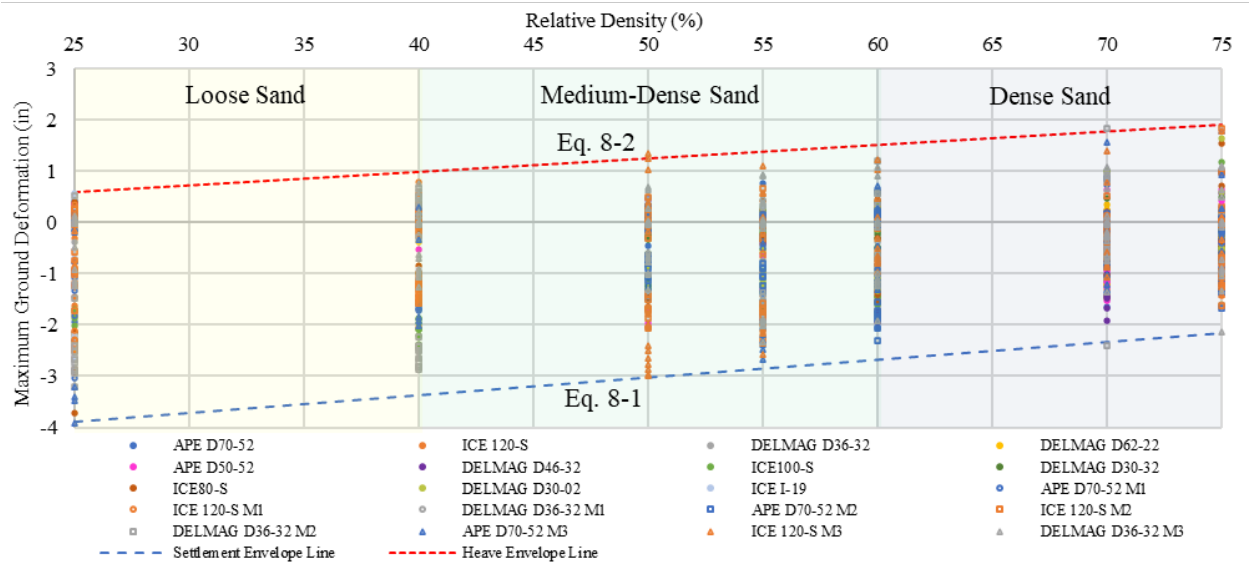

Figure 7-5. Maximum computed ground deformations (i.e., settlement and heave) for the various relative densities and rated energies after the condition of max. PPV of 0.5 in/s stipulated by FDOT is satisfied.

Figures 7-6, 7-7, and 7-8 present maximum ground deformation (i.e., settlement and heave) attenuation curves for piles installed in loose, medium-dense, and dense sands, respectively. The findings are presented in terms of scaled distance ($ft/\sqrt{kips-ft}$) for each relative density group. The results are shown both in terms of maximum settlement and maximum heave for all the considered input energies, thus two data points are shown for each input energy. The figures show how maximum settlement and heave values reduce as one moves away from the pile. Settlement and heave are referred to herein as "envelopes" of the computed values and are not intended to be used to compute normally expected settlement or heave troughs. The equations that represent these envelopes mathematically are presented in Chapter 8. The attenuation curves are also presented with Confidence Intervals (CI) of 95% and 70%. These CIs are given for both settlement and heave envelopes for each relative density group. Not every point presented in the figure satisfies the

FDOT PPV reference value of 0.5 in/s. The authors suggest the contractors to initially guarantee that the FDOT PPV limit of 0.5 in/s is not exceeded and then use the proposed figures to estimate ground deformations. The proposed attenuation curves for maximum ground deformations in Florida sandy soils arising from impact pile driving in prestressed concrete piles have not been presented before in the technical literature and can practically guide future designs. Recall that FDOT (2021b) Article 108-2.1.2 requires monitoring structures within an influence zone of 16.0 $ft/\sqrt{kip-ft}$, which compared to the computed influence zone of 10.0 $ft/\sqrt{kip-ft}$ can be deemed as a good practical approach.

The results were also compared with the two methods that are available in the technical literature. The calculated settlement values, which were presented in Table 5-8 by using the method proposed by Massarsch (2004) and in Table 5-9 by using Drabkin et al. (1996), are also presented in Figures 7-6, 7-7, and 7-8 for loose, medium-dense, and dense sands, respectively. Figure 7-6 presents an overly conservative average settlement value of 8.6 in, which was computed by using the method proposed by Massarsch (2004) for loose sands. Recall that Massarsch's method provides an average settlement value within the influence zone, thus it is independent of the scaled distance. Two maximum settlement values of 3.7 in and 4.5 in, which were computed using the Drabkin et al. (1996) method, are also presented in the figure corresponding to vibration levels of 0.5 in/s and 0.7 in/s, respectively. Observe how the maximum values of the proposed settlement envelopes matched relatively well the values obtained using Drabkin et al. (1996) in loose sands. In medium-dense sands, the method proposed based on experience by Massarsch (2004) again overpredicted the settlements in medium-dense sands with an average settlement value of 5.8 in. The proposed maximum settlement envelope matched well the values computed using Drabkin et al. (1996) for medium-dense sands. Observe also how the proposed maximum settlement envelope matched well the settlement values computed by using Drabkin et al. (1996) and Massarsch (2004) in dense sands. Neither methods provide insight into potential heave (either temporary or residual) that can be extracted from the pile driving-induced ground deformation time histories. Heave is an important mechanism observed typically in medium to dense sands caused by volumetric expansion of the soil due to shearing. It is important to note that heave has also been reported in the past as a result of pile driving operations by Bozozuk et al. (1978), Oostveen and Küppers (1985), Hwang et al. (2001), and Wersäll and Massarsch (2013).

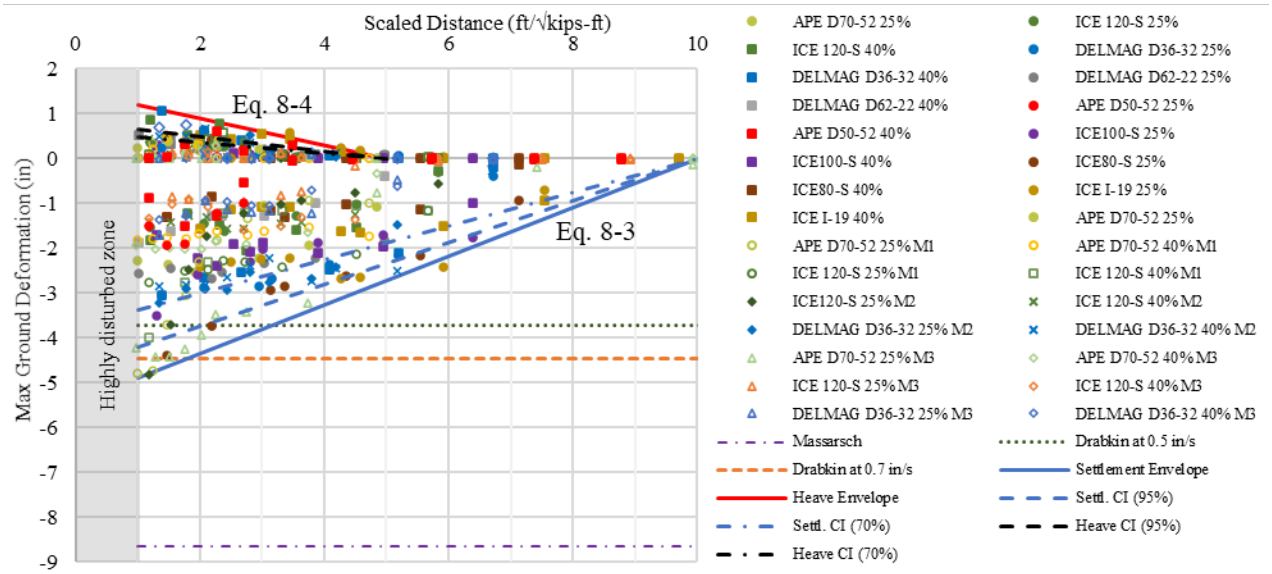

Figure 7-6. Computed maximum ground deformations (in) for prestressed concrete piles installed in loose sands. The figure also shows the values calculated following the methods by Massarsch (2004) and Drabkin et al. (1996). The results are presented in terms of scaled distance $(ft/\sqrt{kips-ft})$.

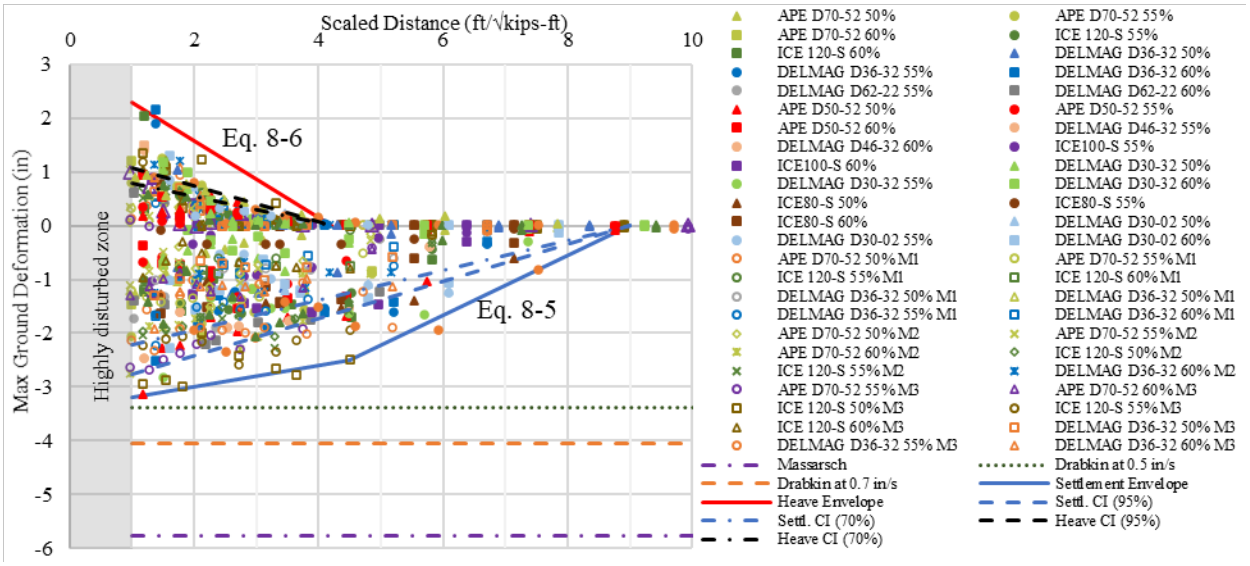

Figure 7-7. Computed maximum ground deformations (in) for prestressed concrete piles installed in medium-dense sands. The figure also shows the values calculated following the methods by Massarsch (2004) and Drabkin et al. (1996). The results are presented in terms of scaled distance $(ft/\sqrt{kips-ft})$.

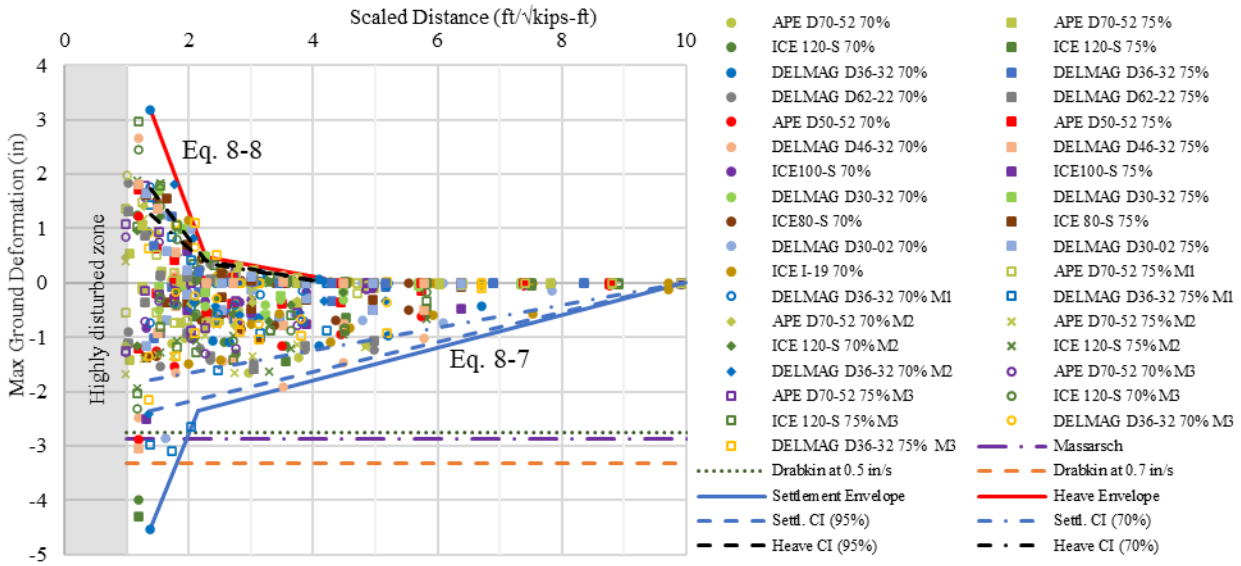

Figure 7-8. Computed maximum ground deformations (in) for prestressed concrete piles installed in dense sands. The figure also shows the values calculated following the methods by Massarsch (2004) and Drabkin et al. (1996). The results are presented in terms of scaled distance ($ft/\sqrt{kips-ft}$).

Figure 7-9 presents the final summarized settlement and heave envelopes for the loose, medium-dense, and dense relative density groups beyond a reasonable scaled distance of 1.0 $ft/\sqrt{kips-ft}$. Computations are beyond the highly disturbed nearby zones of very large deformations and excess pore water pressures caused by the pile driving operation (as it was shown in Chapter 5.3) and where the authors can confidently assure that the computer models are generating accurate and reliable results that can also be safely measured in the field at a prudent safe distance from the pile. Observe how maximum settlements are higher in the loose sands than in the dense sands, whereas the opposite is observed for the case of maximum heave because of volumetric expansion at higher relative densities. Those results match general fundamental soil mechanics principles. Also, the magnitude of maximum ground surface deformations decreases (i.e., or attenuate or fade) as one moves away from the pile. At a reference value of a scaled distance of 1.0 $ft/\sqrt{kips-ft}$, the maximum settlement was approximately 5.0 in (loose sands) and became negligible at scaled distances beyond 10.0 $ft/\sqrt{kips-ft}$. For the dense sands, a maximum heave of 4.0 in was computed at a scaled distance of 1.0 $ft/\sqrt{kips-ft}$, and became zero at scaled distance of approximately 4.2 $ft/\sqrt{kips-ft}$.

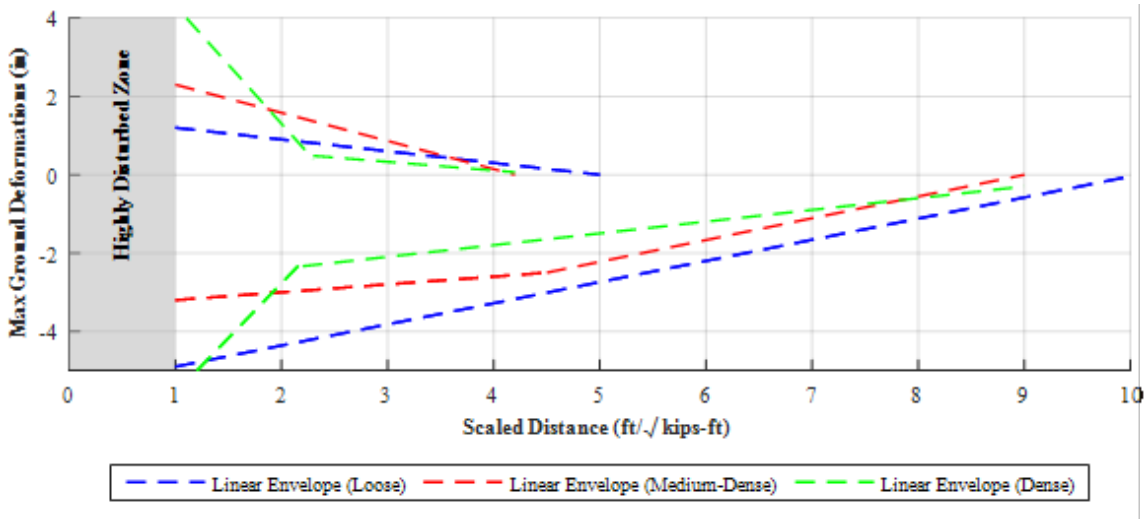

Figure 7-9. Summary of maximum ground deformation envelopes (i.e., settlement and heave) versus scaled distance in $ft/\sqrt{kips-ft}$ for loose, medium-dense, and dense relative density groups. Envelopes were obtained for multiple input energies and pre-drilling depth models considered in this research. These envelopes are a product of 140 numerical simulations, 884 data points, and accounting for 3500 hours of computational effort.

The summarized subsurface conditions in Chapter 3.3 showed that predominant soil conditions are mainly characterized by the granular materials around the medium-dense relative density group. A comparison was performed in Figure 7-10 including the field measurements (i.e., settlement and heave) presented in Chapter 3.6 and computed data points only for the medium-dense relative density group which were presented in Figure 7-7. These ground deformations are presented beyond the vicinity of the pile (i.e., a scaled distance of 1.0 $ft/\sqrt{kips-ft}$) where large deformations occur. Settlement and heave envelopes for the medium-relative density group presented in Figure 7-9 are also given alongside the datapoints. Observe how computational datapoints were more conservative than the field measurements, especially in terms of settlement whereas the scaled distances at which ground deformations became negligible were similar. This degree of conservatism of the proposed numerical modeling framework is normally desirable since some recommendations, charts, and equations proposed in this report are derived from parametric analyses presented in the following chapter of conclusions and recommendations.

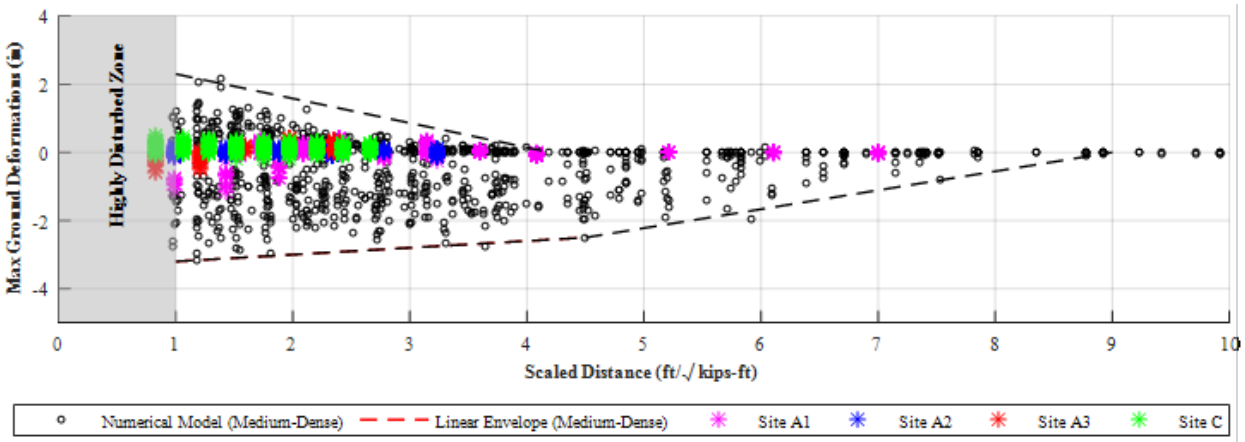

Figure 7-10. Summary of maximum ground deformation envelopes (i.e., settlement and heave) versus scaled distance in $ft/\sqrt{kips-ft}$ for the medium-dense relative density group alongside the ground deformation field measurements.

8. CONCLUSIONS AND RECOMMENDATIONS

8.1. RESEARCH SUMMARY

This report presented a comprehensive analysis of the state of the art of pile driving-induced ground deformations and vibrations. A combination of field measurements performed in Central Florida and numerical analyses were used to elucidate the effects of the key variables that cause these ground deformations. The results of the numerical analyses and the field measurements were used to develop charts and equations to estimate ground deformations as a function of relative density of the soils, rated energy of the driving hammer, and distance away from the pile.

A total of eleven bridge construction sites in Central Florida are presented in this report. Deep foundations in these sites were installed using impact pile driving methods. This provided the opportunity to perform measurements of deformations and vibrations at the ground surface as well as to take advantage of acceleration and strain measurements within the pile that are typically performed during dynamic pile tests. Information corresponding to the field sites given in this report consists of: (i) type and size of the piles, (ii) type of hammer and driving accessories used, (iii) pile driving sequence and procedure, and (iv) soil conditions. The subsurface conditions were characterized for most of the sites as sandy soils with varying relative densities from the loose to the medium-dense range. Ground deformation measurements were analyzed to obtain envelopes of maximum ground deformations and vibration attenuation curves using as a reference the existing FDOT criterion of limiting PPVs to 0.5 in/s.

A series of finite element analyses were performed using PLAXIS 2D to model several driving scenarios based on the most common conditions found at the construction sites. An idealized soil profile consisting of a sandy soil layer with varying relative density from loose to dense was modeled to derive the equations and correlations presented in this chapter. The UBC3D-PLM model was used to investigate the geotechnical mechanisms due to liquefaction of the highly disturbed zone in the close proximity to the pile and the hypoplasticity model for sands was selected to model the ground deformation behaviors of the soils, since it provided the possibility to track changes in void ratios (or relative densities) as the pile is driven into the ground. A parametric study was performed to analyze the effect of the variables involved on the pile driving-induced ground deformations. Conclusions regarding the effect of each variable on the maximum ground deformations are drawn herein.

8.2. CONCLUDING REMARKS AND RECOMMENDATIONS

The following conclusions and recommendations can be drawn from this study:

1. The authors found based on the field measurements performed in several construction sites that it is important to accurately define the transmitted energy to the pile in order to predict future ground deformations. This must include the effects of the pile cushions

and other appurtenances as well as the fuel settings of the hammer applied in the field, particularly when numerical models are expected to match measured responses.

2. Field data also showed that most of the ground surface deformations occurred during the initial stages of pile driving, which can be attributed to the radial distance from the pile tip to the measured points. Spherical waves emanating from the pile tip have less influence at the ground surface as the pile penetration increases This finding is in agreement with other case histories reported in the literature that observed the same correlation between radial distance from the tip of the pile and pile driving-induced vibrations and deformations (e.g., Brunning and Joshi, 1989; Chen et al., 1997; Grizi et al., 2016; Heung et al., 2007).

3. Pile driving-induced vibration and ground deformation measurements next to sheet pile walls and cofferdams showed that these geo-structures provide a protection barrier that caused energy absorption of the cylindrical and spherical waves emanating from the pile.

4. It was observed at construction sites where multiple piles were driven that larger ground deformations occurred during installation of the first pile than driving the subsequent piles. This was attributed to soil densification in loose to medium dense sands that took place during the installation of the first pile affecting the stiffness and final response of the soils during installation of the remaining piles in a bent. Those effects were also observed in terms of ground vibration measurements since changes in the PPV attenuation characteristics were noted after consecutive pile installations. From a numerical modeling standpoint, this highlights the importance of using a robust numerical model capable of tracking changes in soil density as the pile is installed to accurately predict pile driving-induced ground deformations.

5. Based on the comparative analysis of the existing pile driving numerical approaches available in the technical literature, it was concluded that a continuous pile driving modeling approach is necessary to accurately model pile driving induced ground deformations and vibrations. This is because such approach accounts for the accumulation of stresses and strains during pile driving allowing soil contractive or dilative mechanisms to develop and change as the pile is installed, while a discontinuous approach starts from at-rest *in situ* conditions and unrealistic *in situ* void ratios that cause misleading results.

6. Advanced numerical models provided the authors with a robust methodology to analyze ground deformations induced by pile driving under numerous scenarios used to evaluate the main factors that affect pile driving-induced ground deformations: rated energy of the driving hammer, distance away from the pile, soil density, and pre-drilling depths. The following was concluded from the parametric studies:

    - The larger the rated hammer energies the larger the ground deformations. The type of hammer and driving appurtenances change the shape of the force time

history applied at the top of the pile leading to different ground deformations even if the same rated hammer energies are applied.

- Larger settlements were computed when impact pile driving operations were modeled through loose sands than in dense sands due to the densification process observed in contractive soils. Larger heave was computed in dense sands than in loose sands due to the phenomenon of volumetric expansion.
- Pre-drilling operations are beneficial since they reduce ground deformations and vibrations due to an increase in the radial distance between the ground surface and pile tip.

7. The authors concluded based on the presented PPV attenuation curves that a reasonable value of the scaled distance to exceed the FDOT PPV requirement of 0.5 in/s is approximately from 4 to 5 $ft/\sqrt{kips-ft}$ regardless of the considered input energy and relative density.

8. Charts relating the main variables involved in the vibration-induced ground deformation were given as a result of the 140 numerical simulations performed in this study and the measurements taken in eleven construction sites. Equations (8-1) and (8-2) provide ground deformation envelope relationships with the relative density of the soils (D_r). The equations were obtained from analyzing maximum computed settlements (S) and heave (H) caused by pile driving in cases when vibration levels did not exceed with the PPV limit of 0.5 in/s provided by FDOT (i.e., initially guarantee that the FDOT PPV limit of 0.5 in/s is not exceeded and then use the proposed figures to estimate ground deformations). These equations are applicable for a wide range of relative densities between 25% and 75%.

$$S\ (in) = \frac{3.5}{100}\ D_r(\%) - 4.8 \tag{8-1}$$

$$H\ (in) = \frac{2.6}{100}\ D_r(\%) \tag{8-2}$$

The authors concluded based on the envelopes represented by Equations (8-1) and (8-2) that even if the PPV limit of 0.5 in/s is satisfied ground deformations can still occur due to soil densification in loose sands (i.e., settlement) and volumetric expansion in dense sands (i.e., heave).

9. Charts relating ground deformations and scaled distance ($D/\sqrt{E}$) in ft/√kips-ft from the pile are also presented as a result of this research (see Section 7.3). E in the equation stands for the rated energy of the hammer. Ground deformation envelopes based on those charts are shown in Equations (8-3) through (8-8) for different groups of relative densities (i.e., loose, medium-dense, and dense sands). The rated energy of the driving hammer (E) was used to develop the following equations.

   - Loose sands ($25\% < \mathrm{Dr} \leq 40\%$):

$$S = 0.54\, D/\sqrt{E}\ - 5.44 \qquad \text{for } 1.00 < D/\sqrt{E} \leq 10.00 \qquad \text{(8-3)}$$

$$H = -0.30\, D/\sqrt{E}\ + 1.50 \qquad \text{for } 1.00 < D/\sqrt{E} \leq 5.00 \qquad \text{(8-4)}$$

- Medium-dense sands ($40\% < \text{Dr} \leq 60\%$):

$$S = \begin{cases} 0.20\, D/\sqrt{E}\ - 3.40 & \text{for } 1.00 < D/\sqrt{E} \leq 4.50 \\ 0.56\, D/\sqrt{E}\ - 5.00 & \text{for } 4.50 < D/\sqrt{E} \leq 9.00 \end{cases} \qquad \text{(8-5)}$$

$$H = -0.72\, D/\sqrt{E}\ + 3.01 \qquad \text{for } 1.00 < D/\sqrt{E} \leq 4.20 \qquad \text{(8-6)}$$

- Dense sands ($60\% < \text{Dr} \leq 75\%$):

$$S = \begin{cases} 2.80\, D/\sqrt{E}\ - 8.37 & \text{for } 1.00 < D/\sqrt{E} \leq 2.15 \\ 0.30\, D/\sqrt{E}\ - 2.99 & \text{for } 2.15 < D/\sqrt{E} \leq 10.00 \end{cases} \qquad \text{(8-7)}$$

$$H = \begin{cases} -3.01\, D/\sqrt{E}\ + 7.33 & \text{for } 1.00 < D/\sqrt{E} \leq 2.27 \\ -0.22\, D/\sqrt{E}\ + 0.99 & \text{for } 2.27 < D/\sqrt{E} \leq 4.20 \end{cases} \qquad \text{(8-8)}$$

10. Negligible ground deformations were found for the considered relative density groups beyond a scaled distance value of 10.0 $ft/\sqrt{kip-ft}$. Recall that FDOT (2021b) Article 108-2.1.2 requires monitoring structures within an influence zone of 16.0 $ft/\sqrt{kip-ft}$.

11. The authors emphasize the importance of understanding that these equations provide maximum expected ground deformations (i.e., envelopes) and are not intended to be used as settlement troughs (i.e., shapes of settlement profiles to be used to compute differential settlements or angular distortions).

9. REFERENCES

Arboleda-Monsalve, L. G., and Chopra, M. (2020). *Comparison of Standard Penetration Test (SPT) N-value with Alternative Field Test Methods in Determining Moduli for Settlement Predictions*. Draft Final Report, Florida Department of Transportation, Tallahassee, FL, 263 pp.

Arboleda-Monsalve, L. G., Mercado, J. A., Sover, A., and Zapata-Medina, D. G. (2017). "Liquefaction Analyses of the Port of Long Beach Using the UBC3D-PLM Constitutive Soil Model." *Geotechnical Frontiers 2017*, American Society of Civil Engineers, Reston, VA, 369–378.

Athanasopoulos, G. A., and Pelekis, P. C. (2000). "Ground vibrations from sheet pile driving in urban environment: measurements, analysis and effects on buildings and occupants." *Soil Dynamics and Earthquake Engineering*, 19(5), 371–387.

Bathe, K. J. (1982). *Finite Element Procedures in Engineering Analysis*. Prentice-Hall, New Jersey.

Bauer, E. (1996). "Calibration of a Comprehensive Hypoplastic Model for Granular Materials." *Soils and Foundations*, 36, 13–26.

Bayraktar, M. E., Kang, Y., Svinkin, M., and Arif, F. (2013). *Evaluation of Vibration Limits and Mitigation Techniques for Urban Construction*. Florida Department of Transportation, Tallahassee, FL, 128 pp.

Beaty, M. H., and Byrne, P. (1998). "An Effective Stress Model for Predicting Liquefaction Behaviour of Sand." *Geotechnical Earthquake Engineering and Soil Dynamics III, ASCE Geotechnical Special Publication,* 766–77.

Beaty, M. H., and Byrne, P. M. (2011). UBCSAND Constitutive Model, Version 904aR. Bouassida Geotechnics (website). https://bouassidageotechnics.files.wordpress.com/2016/12/ubcsand_udm_documentation.pdf

Beaty, M. H., and Perlea, V. (2012). "Effect on ground motion characteristics on Liquefying sand Dams." *GeoCongress*, (503), 2108–2117.

Bornitz, G. (1931). *Uber die Ausbreitung der von Großkolbenmaschinen erzeugten Bodenschwingungen in die Tiefe*. *Springer, Berlin, Germany*.

Bozozuk, M., Fellenius, B. H., and Samson, L. (1978). "Soil disturbance from pile driving in sensitive clay." *Can. Geotech. J.*, 15, 346–361.

Brandenberg, S. J., Coe, J., Nigbor, R. L., and Tanksley, K. (2009). "Different Approaches for Estimating Ground Strains from Pile Driving Vibrations at a Buried Archeological Site." *Journal of Geotechnical and Geoenvironmental Engineering*, 135(8), 1101–1112.

Brenner, R. P., and Viranuvut, S. (1977). "Measurement and prediction of vibrations generated by drop hammer piling in Bangkok subsoils." *5th Southeast Asian Conference on Soil Engineering*, Southeast Asian Geotechnical Society, Khlong Luang, Thailand, 105–119.

Brinkgreve, R. B. J., Engin, E., and Engin, H. K. (2010a). "Validation of empirical formulas to derive model parameters for sands." *Numerical Methods in Geotechnical Engineering*, Taylor & Francis, London, UK, 137–142 pp.

Brinkgreve, R. B. J., Swolfs, W. M., Engin, E., Waterman, D., Chesaru, A., Bonnier, P. G., and Galavi, V. (2010b). *Plaxis 2D User Manual*. Plaxis bv, Delft, Netherlands.

Brunning, D. F., and Joshi, R. C. (1989). "Vibrations due to pile driving—a case study." *Canadian Geotechnical Journal*, 26(4), 745–747.

Chen, C. H., Yang, W. H., and Sutu, Y. W. (1997). "Ground Responses Induced by Pile Driving." *14th International Conference on Soil Mechanics and Foundation Engineering*, International Society for Soil Mechanics and Geotechnical Engineering, London, UK, 457–460.

Cleary, J. C., Gillis, A. S., and Steward, E. J. (2015). "A Case Study of Ground Vibrations Due to Pile Driving in Mobile, Alabama." *Forensic Engineering 2015*, American Society of Civil Engineers, Miami, Florida, 132–142.

Clough, G. W., and Chameau, J. L. (1980). "Measured effects of vibratory sheetpile driving." *Journal of the Geotechnical Engineering Division, ASCE*, 106(GT10), 1081–1099.

Dobry, R., Ladd, R. S., Yokel, F. Y., Chung, R. M., and Powell, D. (1982). *Prediction of pore water pressure buildup and liquefaction of sands during earthquakes by the cyclic strain method*. Building Science Series 138, National Bureau of Standards, Department of Commerce, Washington D.C, 168.

Drabkin, S., Lacy, H., and Kim, D. S. (1996). "Estimating Settlement of Sand Caused by Construction Vibration." *Journal of Geotechnical Engineering*, 122(11), 920–928.

Farshi Homayoun Rooz, A., and Hamidi, A. (2017). "Numerical Analysis of Factors Affecting Ground Vibrations due to Continuous Impact Pile Driving." *International Journal of Geomechanics*, 17(12), 04017107.

FDOT. (2021a). "Section 455: Structures Foundations." *Standard Specifications for Road and Bridge Construction*, Florida Department of Transportation (FDOT), Tallahassee, FL, 552–619.

FDOT. (2021b). "Section 108: Monitor Existing Structures." *Standard Specifications for Road and Bridge Construction*, Florida Department of Transportation (FDOT), Tallahassee, FL, 552–619.

Galavi, V., Petalas, A., and Brinkgreve, R. B. J. (2013). "Finite Element Modelling of Seismic Liquefaction in Soils." *Geotechnical Engineering Journal of the SEAGS & AGSSEA*, 44(3), 55–64.

Grizi, A., Athanasopoulos-Zekkos, A., and Woods, R. D. (2016). "Ground Vibration Measurements near Impact Pile Driving." *Journal of Geotechnical and Geoenvironmental Engineering*, 142(8), 04016035.

Grizi, A., Athanasopoulos-Zekkos, A., and Woods, R. D. (2018). "H-Pile Driving Induced Vibrations: Reduced-Scale Laboratory Testing and Numerical Analysis." *IFCEE 2018*, American Society of Civil Engineers, Orlando, Florida, 165–175.

Gudehus, G., Amorosi, A., Gens, A., Herle, I., Kolymbas, D., Masin, D., Muir Woods, D., Nova, R., Niemunis, A., Pastor, M., Tamagnini, C., and Viggiani, G. (2008). "The soilmodels.info project." *International Journal for Numerical and Analytical Methods in Geomechanics*, 32(12), 1571–1572.

Hardin, B. O., and Drnevich, V. P. (1972). "Shear Modulus and Damping in Soils: Design Equations and Curves." *Journal of the Soil Mechanics and Foundations Division*, 98(7), 667–692.

Hendricks, R. (2002). *Transportation Related Earhtborne Vibrations*. California Department of Transportation, Sacramento, CA, 31.

Heung, W., Morgan, K., Yoon, Y. H., Gobin, R., and Gollamudi, S. (2007). "Vibration due to Driving Concrete Piles Using Open-Ended Diesel Hammer in Central and South Florida." *7th FMGM 2007*, American Society of Civil Engineers, Boston, MA, 1–12.

Hudson, M., Idriss, I. M., and Beikae, M. (1994). *QUAD4M - A Computer Program to Evaluate the Seismic Response of Soil Structures Using Finite Element Procedures Incorporating a Compliant Base*. Center for Geotechnical Modeling, Department of Civil and Environmental Engineering, University of California, Davis, CA.

Hwang, J. H., Liang, N., and Chen, C. H. (2001). "Ground Response during Pile Driving." *Journal of Geotechnical and Geoenvironmental Engineering*, 127(11), 939–949.

Hyodo, M., Tanimizu, H., Yasufuku, N., and Murata, H. (1994). "Undrained cyclic and monotonic triaxial behaviour of saturated loose sand." *Soils and Foundations*, 34(1), 19–32.

Kaliakin, V., and Dafalias, Y. (1989). "Simplifications to the bounding surface model for cohesive soils." *International Journal for Numerical and Analytical Methods in Geomechanics*, 13(1), 91–100.

Khoubani, A., and Ahmadi, M. M. (2014). "Numerical study of ground vibration due to impact pile driving." *Proceedings of the Institution of Civil Engineers - Geotechnical Engineering*, 167(1), 28–39.

Kim, D.-S., and Lee, J.-S. (2000). "Propagation and attenuation characteristics of various ground vibrations." *Soil Dynamics and Earthquake Engineering*, 19(2), 115–126.

Kim, T. (2011). "Incrementally Nonlinear Responses of Soft Chicago Glacial Clays." Northwestern University, Evanston, IL.

Kulhawy, F. H., and Mayne, P. W. (1990). *Manual on estimating soil properties for foundation design*. Electric Power Research Institute (EPRI), Palo Alto, CA.

Lade, P. V., Liggio, Jr, C. D., and Yamamuro, J. A. (1998). "Effects of Non-Plastic Fines on Minimum and Maximum Void Ratios of Sand." *Geotechnical Testing Journal*, 21(4), 336–347.

Lambe, T. W., and Horn, H. M. (1965). "The Influence on an Adjacent Building of Pile Driving for the MIT Materials Center." *VI International Conference on Soil Mechanics and Foundation Engineering*, 280–284.

Lewis, M. R., and Davie, J. R. (1993). "Vibrations Due to Pile Driving." *Proceedings of the Third International Conference on Case Histories in Geotechnical Engineering*, St. Louis, MO, 649–655.

Likitlersuang, S., Teachavorasinskun, S., Surarak, C., Oh, E., and Balasubramaniam, A. (2013). "Small strain stiffness and stiffness degradation curve of Bangkok Clays." *Soils and Foundations*, 53(4), 498–509.

Linehan, P. W., Longinow, A., and Dowding, C. H. (1992). "Pipeline Response to Pile Driving and Adjacent Excavation." *Journal of Geotechnical Engineering*, 118(2), 300–316.

Liu, G. R., and Jerry, S. S. Q. (2003). "A non-reflecting boundary for analyzing wave propagation using the finite element method." *Finite Elements in Analysis and Design*, 39(5–6), 15.

Mabsout, M. E., Reese, L. C., and Tassoulas, J. L. (1995). "Study of Pile Driving by Finite-Element Method." *Journal of Geotechnical Engineering*, 127(7), 535–543.

Mallard, D. J., and Bastow, P. (1980). "Some observations on the vibrations caused by pile driving." *Recent Developments in the Design and Construction of Piles*, Thomas Telford Publishing, 261–284.

Massarsch, K. R. (2004). "Vibrations Caused by Pile Driving." *The Magazine of the Deep Foundations Institute*, Summer and Fall Articles.

Massarsch, K. R., and Fellenius, B. H. (2008). "Ground Vibrations Induced by Impact Pile Driving." *International Conference on Case Histories in Geotechnical Engineering*, Arlington, VA, 39.

Massarsch, K. R., and Fellenius, B. H. (2014). "Ground vibrations from pile and sheet pile driving. Part 1 Building Damage." *Proceedings of the DFI-EFFC International Conference on Piling and Deep Foundations*, Stockholm, 131–138.

Massarsch, K. R., and Fellenius, B. H. (2015). "Engineering Assessment of Ground Vibrations Caused by Impact Pile Driving." *Geotechnical Engineering Journal*, 46(2), 54–63.

Meyerhof, G. G. (1956). "Penetration tests and bearing capacity of cohesionless soils." *Journal of the Soil Mechanics and Foundations Division*, American Society of Civil Engineers, 82(1), 1–19.

Mohamad, R., and Dobry, R. (1987). "Settlement of cohesionless soils due to piling vibrations." *Ninth Southeast Asian Geotechnical Conference*, Bangkok, Thailand, 7-23-7–31.

Moore, P. J., Styles, J. R., and Ho, W.-H. (1995). "Vibrations Caused by Pile Driving." *International Conference on Recent Advances in Geotechnical Earthquake Engineering and Soil Dynamics*, St. Louis, MO, 737–741.

Niemunis, A., and Herle, I. (1997). "Hypoplastic Model for Cohesionless Soils with Elastic Strain Range." *Mechanics of Cohesive-frictional Materials*, 2, 279–299.

Obrzud, R. F. (2010). "On the Use of the Hardening Soil Small Strain Model in Geotechnical Practice." *Numerics in Geotechnics and Structures*, Elmepress International, 1–17.

Oostveen, J. P., and Küppers, J. A. G. (1985). "Pile driving of soil-displacing piles through soft soils." *Proceedings of the Eleventh International Conference on Soil Mechanics and Foundation Engineering*, San Francisco, CA, 1455–1458.

Puebla, H., Byrne, P. M., and Phillips, R. (1997). "Analysis of CANLEX liquefaction embankments: prototype and centrifuge models." *Canadian Geotechnical Journal*, 34(5), 641–657.

Seed, H. B., and Idriss, I. M. (1970). *Soil Moduli and Damping Factors for Dynamic Response Analyses*. EERC, 41.

Seo, H., Safaqah, O., and Gudavalli, S. R. (2014). "Ground Vibration Levels Due to Impact Pile Driving in Sands." *Tunneling and Underground Construction*, American Society of Civil Engineers, Shanghai, China, 25–34.

Shen, S.-L., Han, J., Zhu, H.-H., and Hong, Z.-S. (2005). "Evaluation of a Dike Damaged by Pile Driving in Soft Clay." *Journal of Performance of Constructed Facilities*, 19(4), 300–307.

Smith, E. A. L. (1960). “Pile-Driving Analysis by the Wave Equation.” *Journal of the Soil Mechanics and Foundations Division*, 86(4), 35–61.

Surarak, C., Likitlersuang, S., Wanatowski, D., Balasubramaniam, A., Oh, E., and Guan, H. (2012). “Stiffness and strength parameters for hardening soil model of soft and stiff Bangkok clays.” *Soils and Foundations*, 52(4), 682–697.

Thandavamoorthy, T. S. (2004). “Piling in fine and medium sand—a case study of ground and pile vibration.” *Soil Dynamics and Earthquake Engineering*, 24(4), 295–304.

Tsegaye, A. B. (2010). “Liquefaction Model (UBC3D).”

Turkel, B., Orozco-Herrera, J. E., Arboleda-Monsalve, L. G., Nam, B. H., and Jones, L. (2021). “Comparative Analysis of Pile Driving Numerical Modeling Approaches.” *International Foundations Congress and Equipment Expo 2021*, American Society of Civil Engineers, Dallas, TX, 484–495.

Van Langen, H., and Vermeer, P. A. (1991). “Interface elements for singular plasticity points.” *International journal for numerical and analytical methods in geomechanics*, Wiley Online Library, 15(5), 301–315.

Wersäll, C., and Massarsch, K. R. (2013). “Soil Heave Due to Pile Driving in Clay.” *Sound Geotechnical Research to Practice*, American Society of Civil Engineers, San Diego, California, United States, 480–498.

Wichtmann, T., Fuentes, W., and Triantafyllidis, T. (2019). “Inspection of three sophisticated constitutive models based on monotonic and cyclic tests on fine sand: Hypoplasticity vs. Sanisand vs. ISA.” *Soil Dynamics and Earthquake Engineering*, 124, 172–183.

Wiss, J. F. (1981). “Construction vibrations: State-of-the-art.” *Journal of Geotechnical Engineering Division*, 107(2), 167–181.

von Wolffersdorff, P. A. (1996). “A hypoplastic relation for granular materials with a predefined limit state surface.” *Mechanics of Cohesive-Frictional Materials*, 1, 251–271.

Wong, I. H., and Chua, T. S. (1999). “Ground movements due to pile driving in an excavation in soft soil.” *Canadian Geotechnical Journal*, 36, 152–160.

Zapata-Medina, D. G., Vergara, C. Y., Vega-Posada, C. A., and Arboleda-Monsalve, L. G. (2019). “On the use of Fredlund gas–fluid compressibility relationship to model medium-dense gassy sand behavior.” *Canadian Geotechnical Journal*, 56(8), 1070–1079.

APPENDIX A: SURVEY RESULTS OF THE CURRENT PRACTICE IN FLORIDA

A survey was developed using the Qualtrics platform available through the University of Central Florida. It was then disseminated as a link to a list of geotechnical engineers compiled using the attendance at GRIP meetings and other sources for contact information for consultants in Florida.

A total of 44 consultants participated in the survey. Some of the respondents did not answer all questions; thus, the total number of responses varies for each question. A report was generated based on the responses. The survey results are presented in this report.

The survey is presented below:

Question 1. Have you experienced in any past designs or construction projects; any problem associated with ground surface settlement induced by pile driving installations?

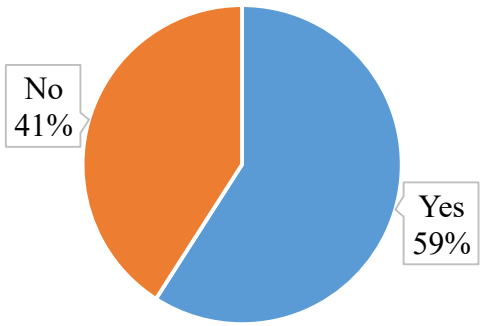

Figure A-1. Responses regarding experience associated with ground surface settlement induced by pile driving installations.

Question 2. If your answer to **Question 1** was "Yes", did you observe or experience any type of damage to adjacent infrastructure during pile driving because of high vibration levels (quantified in terms of high peak particle velocities) or large ground settlements or structural distortions?

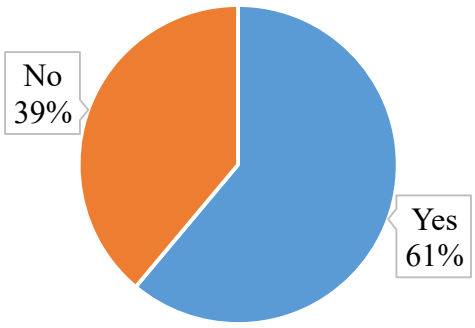

Figure A-2. Responses regarding experience on damage to adjacent infrastructure during pile driving because of high vibration levels or large ground settlements or structural distortions.

Question 3. If your answer to **Question 1** was "Yes", at what distance from the pile driving source did the previously reported settlement occur?

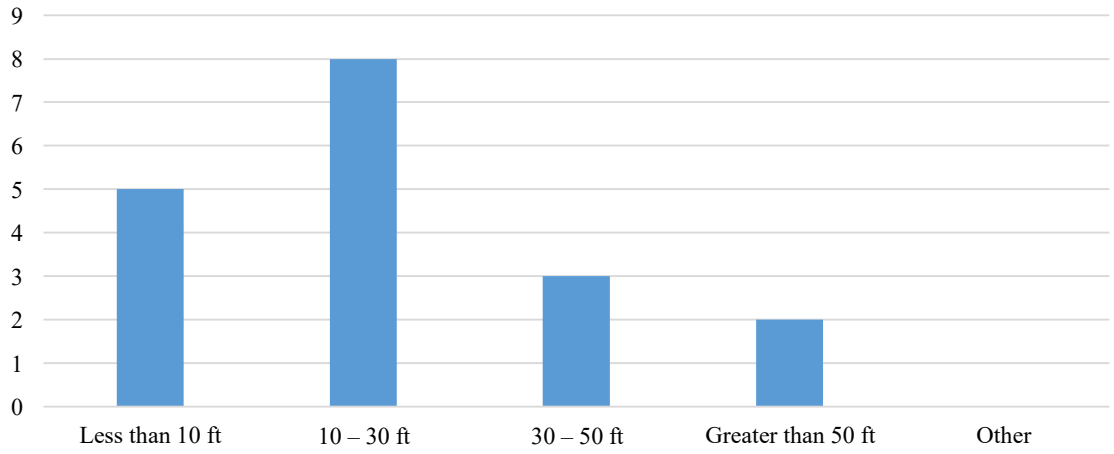

Figure A-3. Responses regarding distance from the pile driving source of reported settlement.

Question 4. If your answer to **Question 1** was "Yes", could you provide a brief description of the geotechnical conditions of the site? (e.g., mostly sandy soils at shallow depth, about 50 ft of soil and bedrock found at 70 ft, etc.)?

Answers:

- Miami Limestone, near surface. Settlement was negative (i.e. heave).
- Sandy soils to 50 ft with silty sands/hardpans below.
- Sandy soils.
- Mostly sandy soils to 30 feet then intermittent clay soils and sand/silty soils to greater than 80 feet then weathered limestone.
- Sandy soils with loose to medium relative densities.

- Mostly sandy.
- Shallow foundations bearing on sandy soils.
- Shallow foundation adjacent to pile driving with shallow limestone.
- Mostly clays.
- Sands and silty sands.
- Sandy soils; mostly A-3 clean sand.
- Sandy soils with intermittent layers of organics to great depths.
- Sand.
- Sand over limestone.

Question 5. Do you consider monitoring ground vibrations due to pile driving an important issue during the design phase of any deep foundation system?

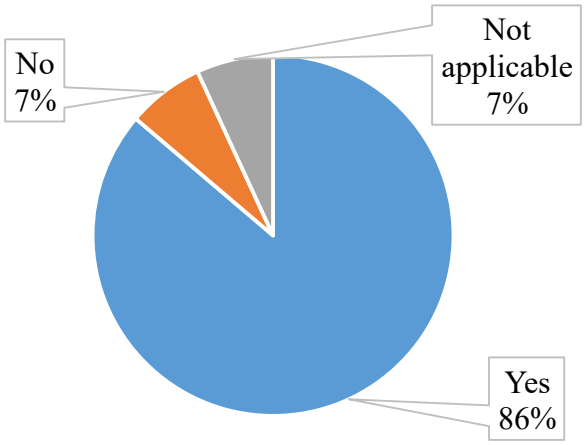

Figure A-4. Responses regarding importance of considering ground vibration monitoring during the design phase of deep foundations.

Question 6. If your answer to **Question 5** was "Yes", what was the approximate level of ground settlements experienced in the project?

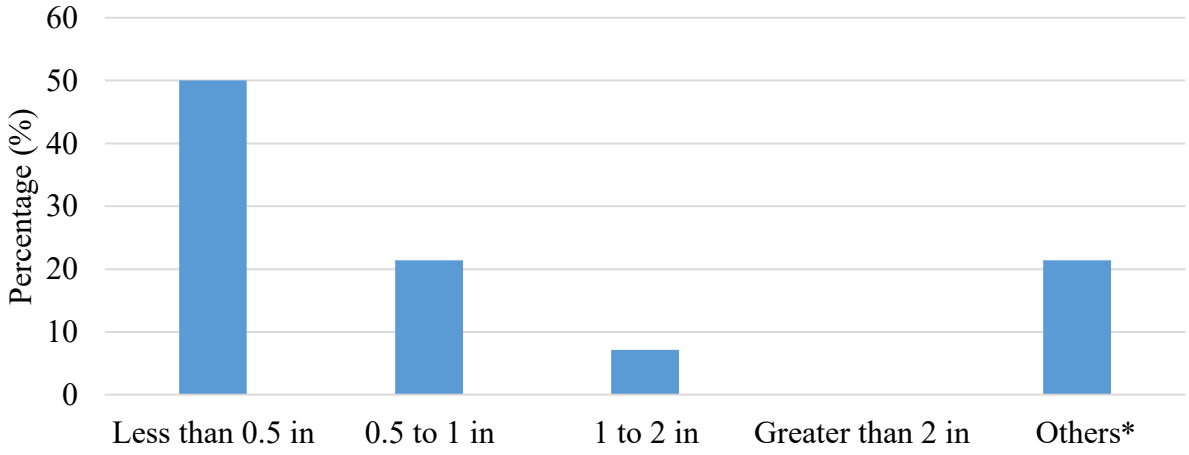

Figure A-5. Responses regarding the approximate level of ground settlements experienced in the project.

*Answers for others:

- Depending on the type of structures and foundations, shallow foundations on loose to medium dense sandy soils are susceptible for more settlements and structures damage.
- Enough to cause cracks on the nearby structure. The actual settlement that took place is unknown, but it was probably less than an inch.

Question 7. How much time do you think is necessary to monitor ground vibrations and soil settlements induced by pile driving?

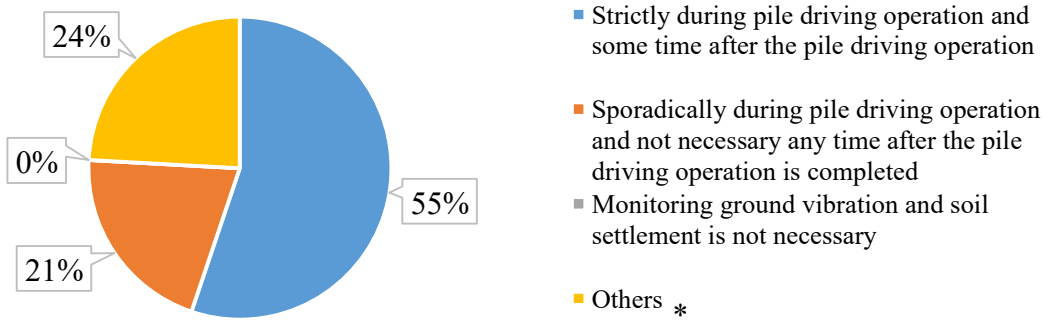

Figure A-6. Responses regarding the time necessary to monitor ground vibrations and soil settlements induced by pile driving.

*Answers for others:

- For sensible brick structures, especially historic buildings monitor before and during pile installing is necessary. The monitors include vibration and settlements are essential.

- A monitoring program should be project specific and generally developed based on Site Conditions, subsurface profile, scope of work, duration of driving and proximity to settlement sensitive structures.
- Vibration monitoring continuously and settlement readings before and after pile driving.
- Initial readings, during pile driving and limited post-driving final survey.
- Most of the time it should only be necessary during pile driving. In some instances where the nearby bridge is either on shallow foundations or on short piles, the monitoring should extend for a long enough period of time that ensures no settlement occurs under normal service conditions.

Question 8. From your experience, do you think monitoring ground vibration due to deep foundation installations at multiple locations is important?

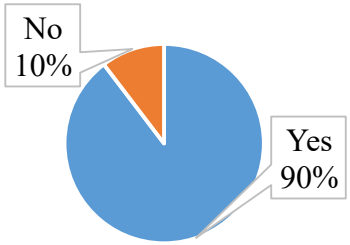

Figure A-7. Responses regarding the importance of monitoring ground vibration due to deep foundation installations at multiple locations.

Question 9. If your answer to **Question 8** was "Yes", from your experience what should be the location of the farthest sensor? (typically a geophone or settlement transducer)

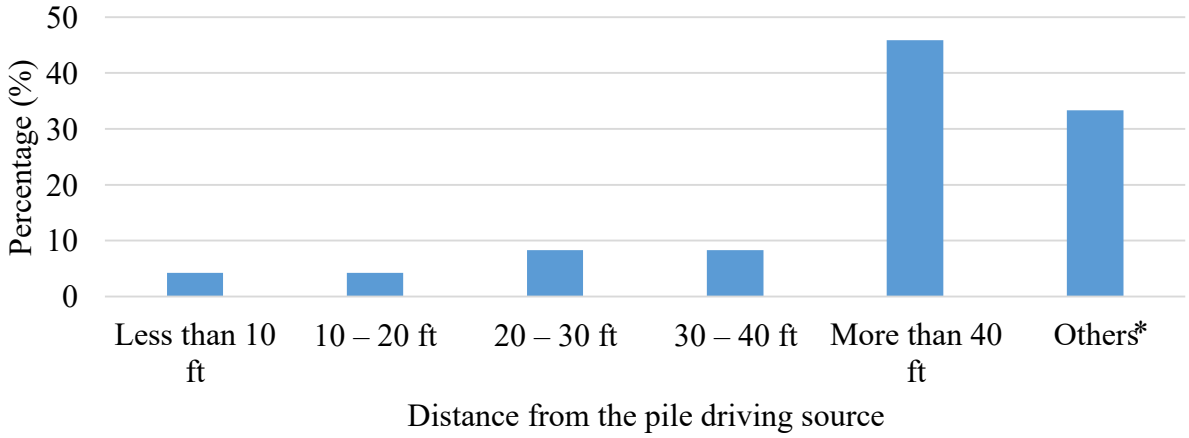

Figure A-8. Responses regarding the location from the pile driving source of the farthest sensor.

*Answers for others:

- It will depend on soil conditions but 40 feet or less may work in most cases.
- Depend on the distance from pile to existing structure.

- Depends on subsurface information and proximity and foundation of structures.
- Site specific. depending on many variables.
- Unless it is for research purpose, vibration monitoring should be conducted at the closest structure of concern. By experience, we have not noticed very high vibration level or settlement exceeding approx. 200 feet and this appears to be conservative with the exception when we are dealing with sensitive electronic equipment.

Question 10. From your experience what are the type(s) of driven pile(s) that you commonly use for your projects? (You can select more than one choice.)

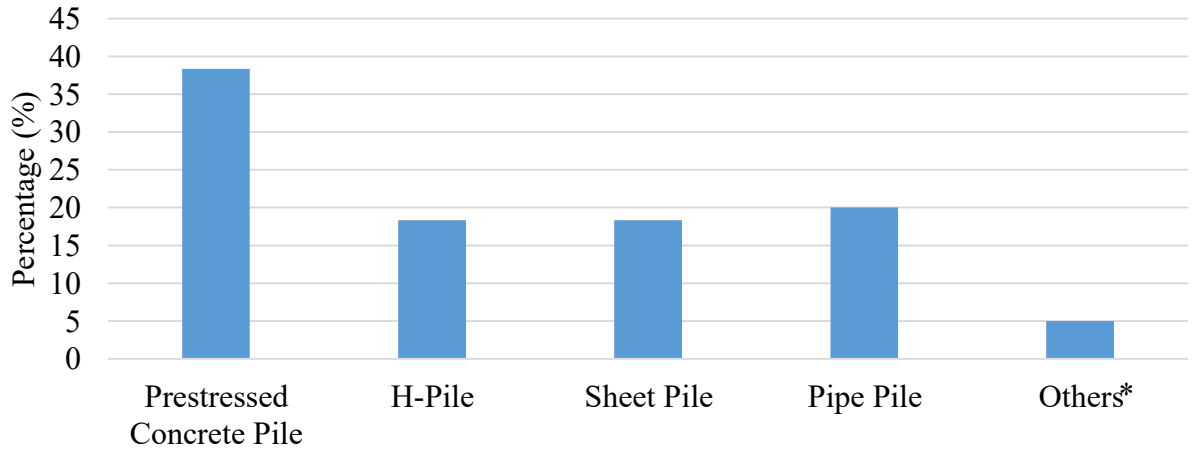

Figure A-9. Responses regarding most common types of driven piles used for projects in Florida.

*Answer for others:

- Vibratory hammer of drilled shaft casing, also vibratory roller for earthwork.

Question 11. Do you think measuring the impact characteristics of the pile driving source is necessary?

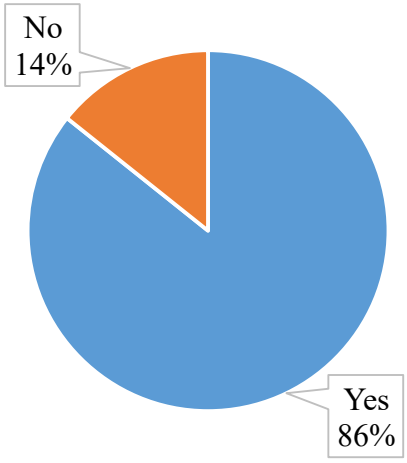

Figure A-10. Responses regarding importance of measuring impact characteristics of the pile driving source.

Question 12. Do you think performing a pre-construction survey of adjacent infrastructure before pile driving installations is necessary?

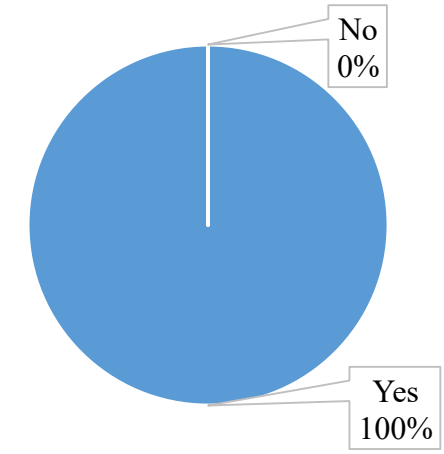

Figure A-11. Responses regarding importance of a pre-construction survey of adjacent infrastructure before pile driving installations.

Question 13. If your answer to **Question 12** was "Yes", from your experience, what is the maximum distance from the pile driving source at which infrastructure (e.g., buildings, public utilities, bridges, etc.) is not affected by pile driving?

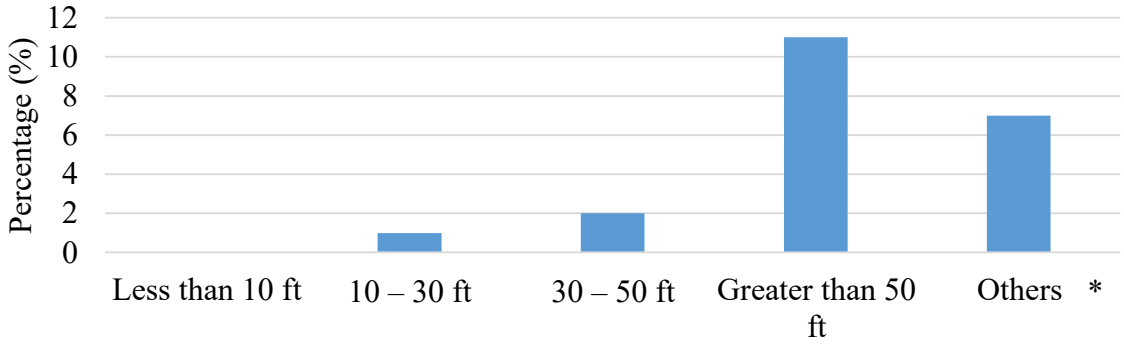

Figure A-12. Responses regarding the maximum distance from the pile driving source at which infrastructure is not affected.

*Answer for others:

- This should be on a case by case. But surely also greater than 50'.
- Depends on what type of impact and how much is considered acceptable. In typical highway construction, worst case distress may occur within 50 feet or so. However, if we consider annoyance of surrounding neighbors, it may extend to approx. 200 feet.
- Depends on type of pile driving, subsurface conditions and sensitivity of structures.
- Claims have been received for damages at distances > 50 feet.

Question 14. Which of the following methods and/or models do you use to estimate dynamic soil displacement due to pile driving and/or to determine the impact of construction vibrations? (You can select more than one choice.)

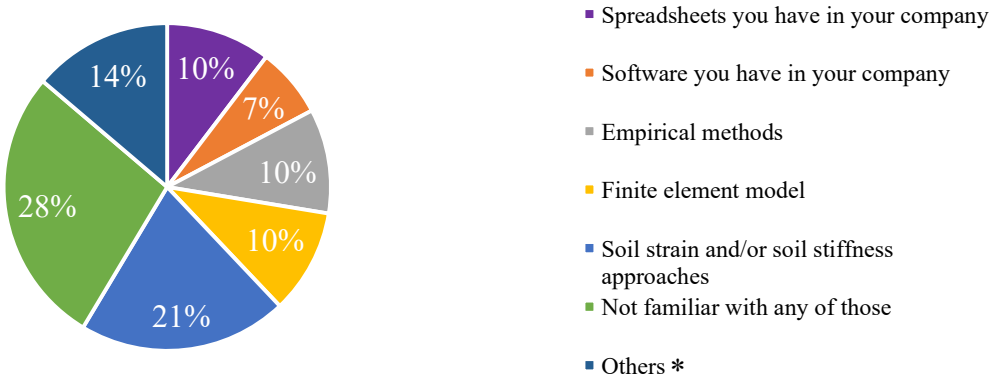

Figure A-13. Responses regarding the methods and/or models used to estimate dynamic soil displacement due to pile driving and/or to determine the impact of construction vibrations.

*Answer for others:

- Past experience.
- Not common practice to do that.

- No calculation is performed.
- I am yet to see a single consultant provide a settlement vs. vibration analysis.

Question 15. Rating from 0 to 10, do you have any experience or knowledge on the relationship between peak particle velocity (PPV), pile-driving induced settlement, and distance from the driving source? (0 meaning you do not have any experience or knowledge in these relationships)

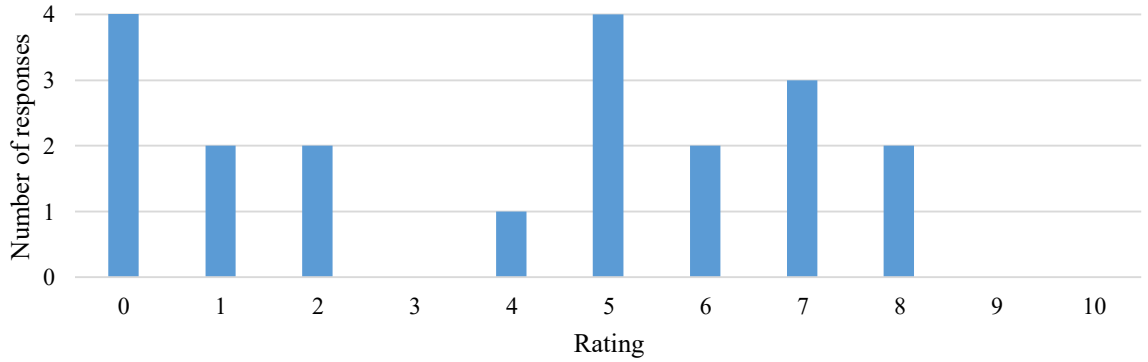

Figure A-14. Responses regarding experience on the relationship between peak particle velocity (PPV), pile-driving induced settlement, and distance from the driving source (Rating from 0 to 10).

Question 16. What is your experience, rated from 0 to 5, on the analysis, design, interpretation, or installation of any of the following sensors? (0 means no previous experience)

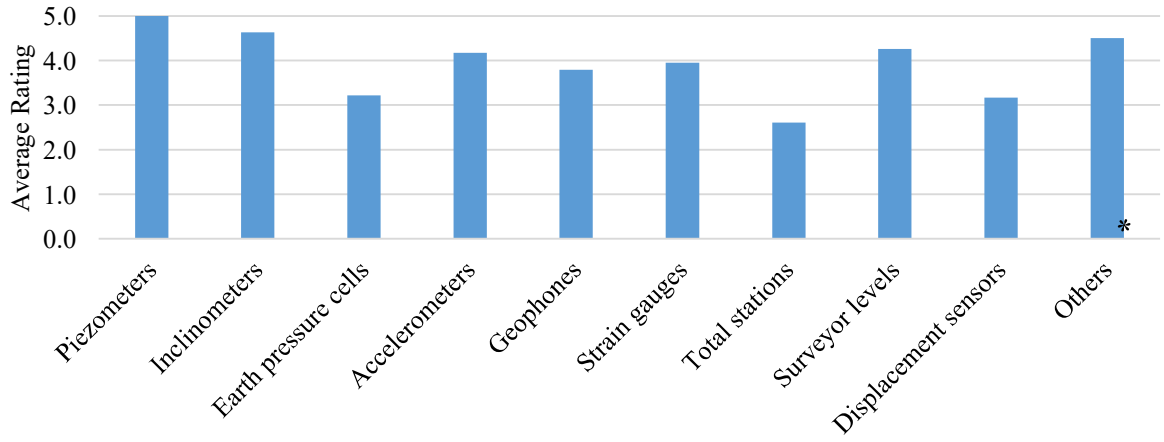

Figure A-15. Responses regarding experience on the analysis, design, interpretation, or installation of field sensors (Rating from 0 to 5, zero means no experience).

*Answer for others:

- Tiltmeters, crackmeters.
- Shape array, fiber optics strain measurements (e.g., Bragg grating) and laser scanning.

Question 17. From your experience, the installation of what type of deep foundation system would potentially cause more damage to adjacent urban infrastructure?

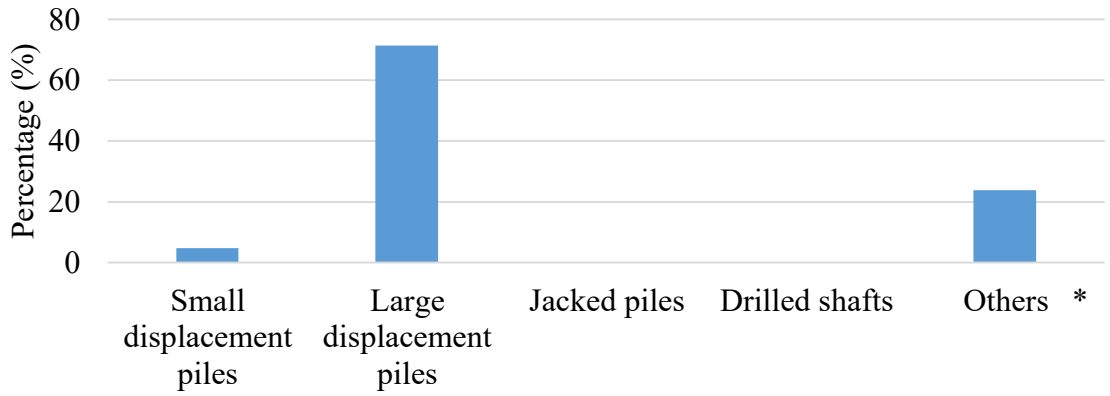

Figure A-16. Responses regarding comparison of damage to adjacent urban infrastructure due to installation of different types of deep foundations.

*Answer for others:

- Vibratory pile driving.
- Cantilever sheet piles used for temporary excavation support.
- Using vibratory hammer (typically steel sheet pile and occasionally steel H-piles).
- Vibratory methods of casing installation for drilled shafts.

Question 18. From your experience, rating from 0-5 please provide what type of material is the most adequate to develop the least amount of settlement associated to pile driving installations: (0 means the soil with the least settlement)

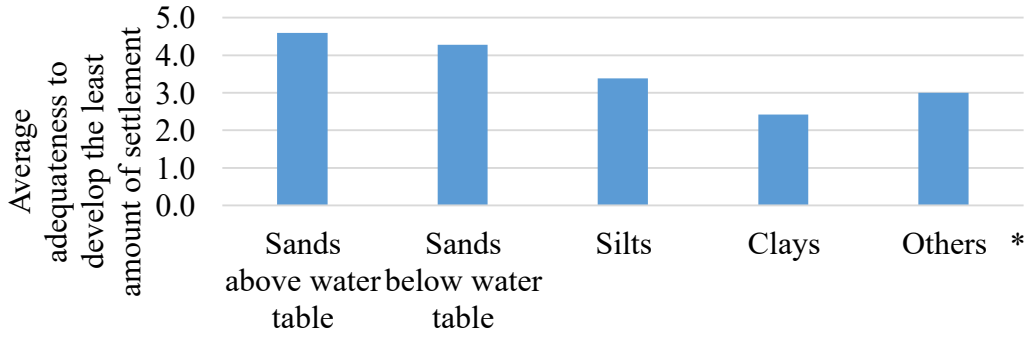

Figure A-17. Responses regarding average adequateness to develop the least amount of settlement by different types of soil conditions (Rating from 0 to 5, zero means the soil with the least settlement).

*Answer for others:

- Limestones and rocks.
- Clays, we experienced heave.

Question 19. From your experience, what are the main sources of pile-driving induced settlements? (You can select more than one choice.)

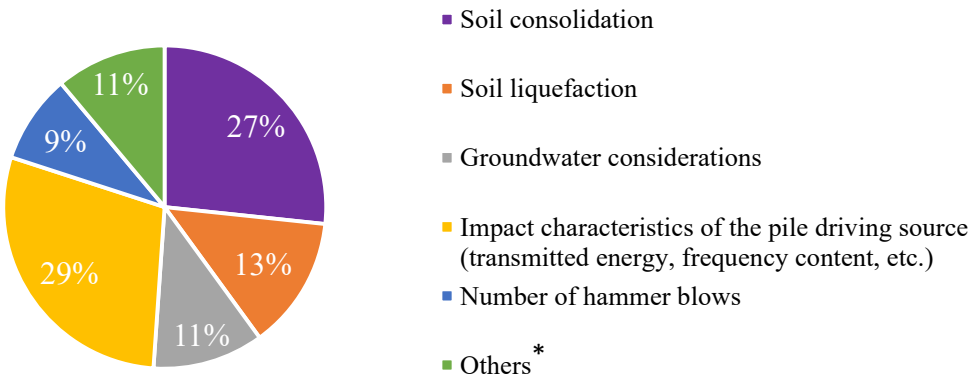

Figure A-18. Responses regarding main sources of pile-driving induced settlements.

*Answer for others:

- Grain re-arrangement.
- Duration of pile driving.
- Relative density of sand and choice of pile driving equipment.
- Wave amplitude, length and frequency, and soil relative density/stiffness.

Question 20. Do you consider numerical modeling of ground vibrations due to pile driving an important issue during the design phase of any deep foundation installation?

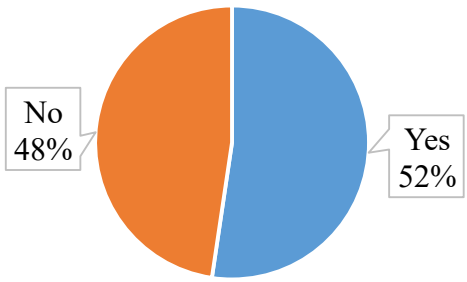

Figure A-19. Responses regarding the importance of numerical modeling of ground vibrations due to pile driving during the design phase of any deep foundation installation

APPENDIX B: PILE DRIVING VIBRATIONS AND GROUND DEFORMATIONS CASE HISTORIES DATABASE

Table B-1. Pile driving case histories database.

Case History Information											Vibration Measurements		Attenuation	Ground Movement		
Reference	Location	Type of Pile	Number of Piles	Distance between Piles (m)	Pile Specifications	Pile Length (m)	Type of Hammer	Type of soil	Water Table (m)	Depth of penetration (m)	Distance from Pile (m)	PPV (mm/s)	Geophone Depth (m)	Type of Displacement	Distance from Pile (m)	Measurement (mm)
Grizi et al., 2016	Niles, Michigan	H-Pile	-	-	360x109 mm*kg/m	16.8	Pileco D30-32 Diesel Hammer	Loose to medium-dense sand	-	16.2			0	-		
	Constantine, Michigan	H-Pile	-	-	360x109 mm*kg/m	16.8	Delmag D30-32 Diesel Hammer	Surficial Loose to medium-dense sand and hard sandy clay	-	13.1			0	-		
Wersäll and Massarsch, 2013	Gothenburg, Sweden	Driven Concrete Pile		1.3	275 mm	52.0		Soft Clay	-	52.0			-	Heave	25	12
Hwang et al., 2001	Chiayi-Taipo, Taiwan	Driven Hollow Concrete Pile	13	2.4	Outer Diameter 800 mm; Inner Diameter 560 mm	34.0	Delmag D100 Diesel Hammer	Surficial soft clay and medium-dense sand	1.0	34.0			-	Heave	2.4	39
Bozozuk et al., 1978	Contrecoeur, Quebec	Driven Concrete Pile	116	1.5	300 mm	26.0	-	Marine Clay		26				Heave	3	110
Wong and Chua, 1999	Singapur Island, Singapur	Driven Concrete Pile	-	-	350 x 350 mm		-									
Brunning and Joshi, 1989	Calgary, Alberta	H-Pile	6	2	300 x 300 mm	11	D-22 Diesel Hammer	Dense Gravel		11	2.1	22	0			
Mallard and Bastow, 1980	North Yorkshire, England		7	-	-	-	Delmag 30.02 Diesel Hammer									
	North Yorkshire, England	Driven Concrete Pile	10	-	400 x 400 mm	23	6T Drop Hammer or Kobe 35 Diesel Hammer									
Cleary et al., 2015	Mobile, Alabama	Driven Concrete Pile	-	-	914.4 x 914.4 mm	27	Delmag D-62-22 Diesel Hammer	Medium-Dense Sand		24	15	20.8	0			
	Mobile, Alabama	H-Pile	-	-	HP14X117	32	APE D30-42 Diesel Hammer	Medium-Dense Sand		29	15	4.6	0			
	Mobile, Alabama	H-Pile	-	-	HP12X53	21	APE D30-42 Diesel Hammer	Medium-Dense Sand		18	15	5.8	0			
Drabkin et al., 1996	Back Bay Site, Boston	Driven Concrete Pile	180	-	360 x 360 mm	29-39	ICE 640 Diesel Hammer	Medium-Dense Sand	0	29-39	-	6.4-15	0	Settlement	-	18-54
	Southern Brooklyn Site, New York City	Close-end Pipe Pile	>100	-	273.1 mm	40	Vulcan 08 Impact Hammer	Medium-Dense Fine Sand	6	40	-	2.5-23	0	Settlement	-	70
	Cedar Creek Site, New York	Sheet Pile	-	-	PZ22	-	ICE 812 Vibratory Hammer	Loose to medium-dense sand	0	9	3.1-7.6		0	Settlement	1	13-19
	Tri-Beca Site, New York City	Pipe Pile	-	-	178 mm	30	-	Medium Compact to Medium Sand			1.5-15	2.5-18	0	Settlement	1.5-15	38-69
Shen et al., 2005	Bailianjing, Shanghai	Driven Concrete Pile	-	1	200 x 200 mm	9	Piston Type Diesel Hammer	Silty Clay	1-2	9				Settlement	-	141-281

Case History Information											Vibration Measurements		Attenuation	Ground Movement		
Reference	Location	Type of Pile	Number of Piles	Distance between Piles (m)	Pile Specifications	Pile Length (m)	Type of Hammer	Type of soil	Water Table (m)	Depth of penetration (m)	Distance from Pile (m)	PPV (mm/s)	Geophone Depth (m)	Type of Displacement	Distance from Pile (m)	Measurement (mm)
Athanasopoulus and Pelekis, 2000	Patras, Greece (A)	Sheet Pile	-	-	LARSSEN III	7	MGF RBH 60M Vibratory Hammer	Sandy Silt and Low Plasticity Clay	1	7	21	0.45	0			
	Patras, Greece (B)	Sheet Pile	-	-	ARBED PU16	10	MS-5H14 Vibratory Hammer	Sandy Silt	3	10	6.8	4	0			
	Patras, Greece (C)	Sheet Pile	-	-	LARSSEN III	8	MGF RBH 60M Vibratory Hammer	Silty Sand	3	8	3.6	5.5	0			
	Patras, Greece (D)	Sheet Pile	-	-	LARSSEN 22	8	ABI RE 10000/3 Vibratory Hammer	Sandy Silt	3	8	5.5	2.2	0			
	Patras, Greece (E)	Sheet Pile	-	-	LARSSEN III	8	MGF RBH 60M Vibratory Hammer	Silty Sand and Gravel	1	8	3.4	7.5	0			
	Patras, Greece (F)	Sheet Pile	-	-	LARSSEN III	7	ICE 416 Vibratory Hammer	Surficial Sandy clay and Silty Sand	3	7	3.6	6	0			
	Patras, Greece (G)	Sheet Pile	-	-	LARSSEN III	8	MGF RBH 60M Vibratory Hammer	Silty Sand with Gravel	2	8	4.4	20	0			
	Patras, Greece (H)	Sheet Pile	-	-	LARSSEN III	8	ICE 416 Vibratory Hammer	Surficial Sandy clay and Silty Sand	3	8	11.4	1.25	0			
	Patras, Greece (I)	Sheet Pile	-	-	LARSSEN III	8	ABI RE 10000/3 Vibratory Hammer	Surficial Sandy clay and Silty Sand	3	8	1	35	0			
Thandavamoorthy, 2003	Chennai, India	Close-end Pipe Pile	-	6.25	Outer 600 mm; Inner 575 mm	16.4	Impact Hammer	Clayey Sand, fine to medium Sand and Silty Sand	-	16.4	15	126.2	0			
Oostveen and Kuppers, 1985	The Hague, Netherlands	-	14	-	600 mm	12	-	-		12				Heave	2.5	4
Massarsch and Fellenius, 2008	Skövde, Sweden	Driven Concrete Pile	-	-	270 x 270 mm	29.3	Hydraulic Hammer Type Banut	Surficial Fill, Clay and Sand	3-4	25	10	6.2	0			
Clough and Chameau, 1980	San Francisco Bay E1	Sheet Pile	-	-	-	-	Vibratory Hammer	Surficial Fill followed by alternating layers of dense sand and clay	-	-				Settlement	2	40
	San Francisco Bay E2	Sheet Pile	-	-	-	-	ICE 812 Vibratory Hammer	Surficial Fill followed by alternating layers of dense sand and clay	-	-				Settlement	2	80
Chen et al., 1997	Changhua Coastal Industrial Park, Taiwan	Driven Concrete Pile	5	3.2	800 mm	24	KOBELO 80 Diesel Hammer	Sandy Soil with Silt	2.5-5	24				Settlement	5	50
Seo et al., 2014	Fort McMurray, Alberta Location1	H-Pile and Pipe Pile	1 H-Pile 3 Pipe Pile		HP 360 X 174 Outer 406 mm Inner 393.3 mm	18-21	Junttan HHK9S Hydraulic Hammer	Medium dense to very dense Silty Sand	-	18-21	2	29				
	Fort McMurray, Alberta Location 2	H-Pile and Pipe Pile	1 H-Pile 3 Pipe Pile		HP 360 X 174 Outer Diameter 406 mm Inner Diameter393.3 mm	18-21	Junttan HHK9S Hydraulic Hammer	Very dense Silty Sand	-	18-21	2	80				
Moore et al., 1995	Hallam Road, Melbourne, Australia	-	-	-	-	-	Impact Hammer	Fine Sand	-	-	-	<10				
	Footscray Park, Melbourne, Australia	-	-	-	-	-	Impact Hammer	Soft to Firm Silty Clay	-	-	-	<10				

Case History Information											Vibration Measurements		Attenuation	Ground Movement		
Reference	**Location**	**Type of Pile**	**Number of Piles**	**Distance between Piles (m)**	**Pile Specifications**	**Pile Length (m)**	**Type of Hammer**	**Type of soil**	**Water Table (m)**	**Depth of penetration (m)**	**Distance from Pile (m)**	**PPV (mm/s)**	**Geophone Depth (m)**	**Type of Displacement**	**Distance from Pile (m)**	**Measurement (mm)**
Heung et al., 2007	Orange County, Florida	Driven Concrete Pile	-	-	455 mm x 455 mm	-	ICE 100-S Diesel Hammer	Sand, Silty Sand, Clay and Silts	-	-						
	Orange County, Florida	Driven Concrete Pile	-	-	455 mm x 455 mm	-	ICE 100-S Diesel Hammer	Sand, Silty Sand, Clay and Silts	-	-						
	Orange County, Florida	Driven Concrete Pile	-	-	610 mm x 610 mm	-	Delmag D62-22 Diesel Hammer	Sand, Silty Sand, Clay and Silts	-	-						
	Orange County, Florida	Driven Concrete Pile	-	-	455 mm x 455 mm	-	ICE 120-S Diesel Hammer	Sand, Silty Sand, Clay and Silts	-	-						
	Orange County, Florida	H-Pile	-	-	HP 360 X 132	-	ICE 80-S Diesel Hammer	Sand, Silty Sand, Clay and Silts	-	-						
	Orange County, Florida	Driven Concrete Pile	-	-	610 mm x 610 mm	-	ICE 100-S Diesel Hammer	Sand, Silty Sand, Clay and Silts	-	-						
	Osceola County, Florida	Driven Concrete Pile	-	-	455 mm x 455 mm	-	D30-32 & D36-32 Diesel Hammer	Sand, Silty Sand, Clay and Silts	-	-						
	Osceola County, Florida	H-Pile	-	-	HP 360 X 132	-	ICE I-19 Diesel Hammer	Sand, Silty Sand, Clay and Silts	-	-						
	Osceola County, Florida	Driven Concrete Pile	-	-	455 mm x 455 mm	-	Delmag D46-32 Diesel Hammer	Sand, Silty Sand, Clay and Silts	-	-						
	Osceola County, Florida	Driven Concrete Pile	-	-	610 mm x 610 mm	-	Delmag D46-32 Diesel Hammer	Sand, Silty Sand, Clay and Silts	-	-						
	Palm Beach, Florida	Driven Concrete Pile	-	-	455 mm x 455 mm	-	ICE 80-S Diesel Hammer	Clean Medium to fine Sand	-	-						
	Palm Beach, Florida	Driven Concrete Pile	-	-	455 mm x 455 mm	-	ICE 80-S Diesel Hammer	Clean Medium to fine Sand	-	-						
	Palm Beach, Florida	Driven Concrete Pile	-	-	455 mm x 455 mm	-	D30-32 & D36-32 Diesel Hammer	Clean Medium to fine Sand	-	-						
	Broward County, Florida	Driven Concrete Pile	-	-	455 mm x 455 mm	-	Delmag D36-32 Diesel Hammer	Clean Medium to fine Sand	-	-						
	Broward County, Florida	Driven Concrete Pile	-	-	455 mm x 455 mm	-	Delmag D36-32 Diesel Hammer	Clean Medium to fine Sand	-	-						
	Broward County, Florida	Driven Concrete Pile	-	-	455 mm x 455 mm	-	Delmag D36-32 Diesel Hammer	Clean Medium to fine Sand	-	-						
	Broward County, Florida	Driven Concrete Pile	-	-	455 mm x 455 mm	-	Delmag D36-32 Diesel Hammer	Clean Medium to fine Sand	-	-						
	Broward County, Florida	Driven Concrete Pile	-	-	455 mm x 455 mm	-	Delmag D36-32 Diesel Hammer	Clean Medium to fine Sand	-	-						
	Broward County, Florida	Driven Concrete Pile	-	-	455 mm x 455 mm	-	Delmag D36-32 Diesel Hammer	Clean Medium to fine Sand	-	-						
	Broward County, Florida	Driven Concrete Pile	-	-	455 mm x 455 mm	-	Delmag D30-02 Diesel Hammer	Clean Medium to fine Sand	-	-						
	Broward County, Florida	Driven Concrete Pile	-	-	455 mm x 455 mm	-	Delmag D30-02 Diesel Hammer	Clean Medium to fine Sand	-	-						
	Broward County, Florida	Driven Concrete Pile	-	-	455 mm x 455 mm	-	Delmag D30-02 Diesel Hammer	Clean Medium to fine Sand	-	-						

Case History Information											Vibration Measurements		Attenuation	Ground Movement		
Reference	Location	Type of Pile	Number of Piles	Distance between Piles (m)	Pile Specifications	Pile Length (m)	Type of Hammer	Type of soil	Water Table (m)	Depth of penetration (m)	Distance from Pile (m)	PPV (mm/s)	Geophone Depth (m)	Type of Displacement	Distance from Pile (m)	Measurement (mm)
Massarsch and Fellenius, 2015	Lak Si, Bangkok, Thailand	Driven Concrete Pile	–	–	Cross Section 0.0675 m2	18	Impact Hammer	Soft Clay		18-28	18	5				
	EGAT, Bangkok, Thailand	Driven Concrete Pile	–	–	Cross Section 0.180 m2	25	Impact Hammer	Soft Clay		18-28	20	3				
Lewis and Davie, 1993	Site 1	Driven Concrete Pile	–	–	350 x 350 mm	24.4	ICE 640 Diesel Hammer	Loose to dense sands and silty sands	1.22	24.4	914.40	0.03				
	Site 2	Raymond Step Taper	–	–	305 mm Shells, 000BR	23.8	Vulcan 80c Impact Hammer	Fill, Soft Clayey Silt and medium clayey Sand	2.13	23.8	24.38	2.54				
	Site 3	Sheet Pile	–	–	PZ-27	9.1	Delmag D-15 Diesel Hammer	Medium to dense sands	0.00	9.1	0.91	25.40				
	Site 4	Raymond Step Taper	–	–	307 mm Shells, 000BR	12.2	Vulcan 80c Impact Hammer	Fill, Soft Silts and clay, dense to medium dense sands	0.61	12.2	30.48	1.27				
	Site 5	Close-end Pipe Pile	–	–	Outer Diameter 270 mm Inner Diameter 265 mm	9.1	Vulcan 06 Impact Hammer	Loose to Medium Sand, Soft Clay, Very dense sand	0.00	9.1	21.34	1.78				
	Site 6	H-Pile	–	–	14 x 117	9.1	Vulcan 06 Impact Hammer	Medium dense to dense sand	3.05	9.1	0.91	25.40				
	Site 7	Raymond Step Taper	–	–	310 mm Shells, 0BR	24.4	Vulcan 06 Impact Hammer	Loose sand, soft clayey silt and medium dense to dense sand	3.05	24.4	12.19	12.70				
	East Coast United States	Driven Concrete Pile	–	–	350 x 350 mm	24.4	ICE 640 Diesel Hammer	Loose to very dense fine Sand and Silty Fine Sand	–	24.4				Settlement	3.05	50.8
Kim and Lee, 2000	Busan, South Korea	Pipe Pile	–	–	600 mm	40	Hydraulic Hammer	Gravel Fill, Silty Sand and Clay	–	16-28	4	0.5				
Heung et al., 2007	Miami-Dade County, Florida	Driven Concrete Pile	–	–	760 mm x 760 mm	–	ICE 120-S Diesel Hammer	Clean Sand underlain by hard limestones	–	–						
	Miami-Dade County, Florida	Driven Concrete Pile	–	–	455 mm x 455 mm	–	Delmag D36-32 Diesel Hammer	Clean Sand underlain by hard limestones	–	–						
	Miami-Dade County, Florida	Driven Concrete Pile	–	–	760 mm x 760 mm	–	ICE 120-S Diesel Hammer	Clean Sand underlain by hard limestones	–	–						
Lambe and Horn, 1965	M.I.T, Massachusetts	Driven Concrete-filled Steel Shell Pile	537	–	Outer Diameter 325 mm; Inner Diameter 320 mm	43	–	Boston Blue Clay	2.44	43				Settlement	–	9.1
Brandenberg et al., 2009	San Joaquin County, California	Pipe Pile	80		600 mm	20	Impact Hammer	Fill and Alluvium	–	20	40	4.1	4.6			
Brenner and Viranuvut, 1977	Bangkok, Thailand	Driven Concrete Pile	7	8	350 mm	18	Drop Hammer	–	–	18						
Linehan et al., 1992	–	Sheet Pile and H-Pile	–	–	PZ40 HP14X73	6.10	Vibratory Hammer and Diesel Impact Hammer	Dense Gravel, peat, Very dense sand		4.6	6	10.2	–	Settlement	–	38.1

APPENDIX C: PAPERS PRESENTED TO DATE AT IFCEE AND GEOCONGRESS-ASCE

- **Comparative Analysis of Pile Driving Numerical Modeling Approaches**
- **Continuous Impact Pile Driving Modeling to Elucidate Settlement-PPV-Soil Density-Input Energy Relationships**

Comparative Analysis of Pile Driving Numerical Modeling Approaches

Berk Turkel, S.M.ASCE,[1] Jorge E. Orozco-Herrera, S.M.ASCE, [2]
Luis G. Arboleda-Monsalve, Ph.D., M.ASCE,[3] Boo Hyun Nam, Ph.D., A.M.ASCE,[4]
and Larry Jones[5]

[1]Graduate Research Assistant, Dept. of Civil, Environmental, and Construction Engineering, University of Central Florida, Orlando, FL 32816, USA; e-mail: TurkelBerk@knights.ucf.edu
[2]Graduate Research Assistant, Dept. of Civil, Environmental, and Construction Engineering, University of Central Florida, Orlando, FL 32816, USA; e-mail: Jeorozcoh@knights.ucf.edu
[3]Assistant Professor, Dept. of Civil, Environmental, and Construction Engineering, University of Central Florida, Orlando, FL 32816, USA; e-mail: Luis.Arboleda@ucf.edu
[4]Associate Professor, Dept. of Civil, Environmental, and Construction Engineering, University of Central Florida, Orlando, FL 32816, USA; e-mail: BooHyun.Nam@ucf.edu
[5]State Geotechnical Engineer, Florida Department of Transportation, 605 Suwannee St, Tallahassee, FL, 32399, USA; e-mail: Larry.Jones@dot.state.fl.us

ABSTRACT

Driven piles have been commonly used as a suitable deep foundation alternative to the soil conditions in central Florida. Pile driving is a complex dynamic soil-structure interaction problem that induces vibrations and settlements in the surrounding soils. Numerical models need to be capable of accurately simulating pile dynamics so that the response of soil during the pile installation can be properly assessed. In this paper, numerical analyses were conducted using the finite element platform PLAXIS 2D to compare different modeling approaches used in the technical literature (i.e. continuous vs. discontinuous) for the pile driving process. A parametric study was performed to elucidate the role of plastic zones in the process of pile penetration. The constitutive soil model used was the hardening soil model enhanced with small strains (i.e., HS small). Subsurface conditions were determined using laboratory and field-testing data collected from a project site. Input parameters were estimated from subsurface exploration data and processed using GRLWEAP, which is a wave equation analysis program. The concept of a plastic zone with reduced stiffness and strength was introduced around the pile to model the continuous process of pile installation. Based on the results, a continuous pile driving approach matched well with field measurements and provided better insight into the pile-dynamic behavior than a discontinuous modeling approach based on a single blow at various depths. The continuous and discontinuous numerical modeling approaches are compared and discussed associated with pile penetration and velocities at the top of the pile.

INTRODUCTION

Driven piles are a compelling deep foundation alternative in geotechnical engineering designs to transfer structural loads to deep competent strata and also to avoid serviceability issues associated with shallow compressible soil layers. In central Florida where the subsurface conditions consist mainly of sandy sedimentary soil deposits, driven piles are a commonly used method. The design

of such elements consists of not only bearing capacity calculations, but also potential construction issues related to the driving process; thus, its effects on nearby structures must be considered.

The wave equation analysis originally proposed by Smith (1960) transformed the analysis and design of deep foundations by incorporating in the design process the production of bearing graphs, driveability studies, and enhanced the understanding of pile dynamics in terms of velocities, forces, and displacements that occur as a result of the driving process. Software such as GRLWEAP (PDI, 2003) and CAPWAP (PDI, 2000) use the wave equation analysis to estimate engineering demands triggered during the driving process and are also used to analyze dynamic testing of piles for the determination of *in situ* capacity.

Despite having numerous features that can be used to guide deep foundation designs and installation processes, those wave equation analysis programs do not provide insight into the effects of pile driving on the surrounding soil or nearby structures (e.g., settlements and vibrations). To overcome this issue, several authors have modeled the pile driving process in finite element programs by using different approaches. Some studies such as Grizi et al. (2018) and Mabsout et al. (1995) performed a "discontinuous model" by installing the pile at different "wished-in-place" depths and applying a single hammer blow at the top of the pile for each depth. This approach has been used to compute Peak Particle Velocities (PPV) and excess pore water pressure build-up at different depths and distances from the pile. Authors such as Khoubani and Ahmadi (2014), and Farshi Homayoun Rooz and Hamidi (2017) modeled a continuous pile driving process, referred to as "continuous model" hereafter, in which the pile was driven without any interruption up to a final depth. These authors focused mainly on the vibrations generated as the pile was driven.

In this paper, Pile Driving Analyzer (PDA) data were used to model a continuous pile driving process in the finite element (FE) program PLAXIS 2D, and the results were compared with the reported pile driving records. Additionally, the discontinuous model was performed at a selected depth to compute pile penetration and induced PPV caused by a single hammer blow. A comparison between both modeling approaches (i.e., continuous or discontinuous pile driving) is presented and discussed. The FE models are validated with CAPWAP/iCAP and GRLWEAP program outputs for a single blow to compare computed pile dynamics.

PROJECT DESCRIPTION

The selected project for the proposed analysis involves the construction of a bridge at the intersection between Florida's Turnpike and the I-4 highway (see Figure 1a). Foundation reports including driving records were provided by the Florida Department of Transportation (FDOT). Figure 1b shows a Google Earth view of the project location with soil borings performed at the site (TB-63) and in nearby sites (B1-B7).

A 640 m long bridge was designed to have two traffic lanes consisting of thirteen spans built over fifteen piers and two end bents. As part of the foundation construction, numerous dynamic pile tests were performed on the northeast bridge pier (i.e., pier 11RT). The installation of a prestressed precast square concrete test pile for one of the north-east bridge piers is

investigated for this paper. The 27.4 m long, 0.61 m width prestressed concrete pile was installed by using an APE D 70-52 open-ended diesel (OED) hammer. This hammer model has a ram weight of 68.7 kN with a maximum rated energy of 235.5 kJ. A plywood hammer cushion with a 381 mm thickness was used but it was later changed during the driving process for a 457 mm thick plywood. The pile cushion consisted of 25.4 mm Micarta (i.e., capblock material made out of plastics that are impregnated with fiber compounds) and 12.7 mm aluminum materials.

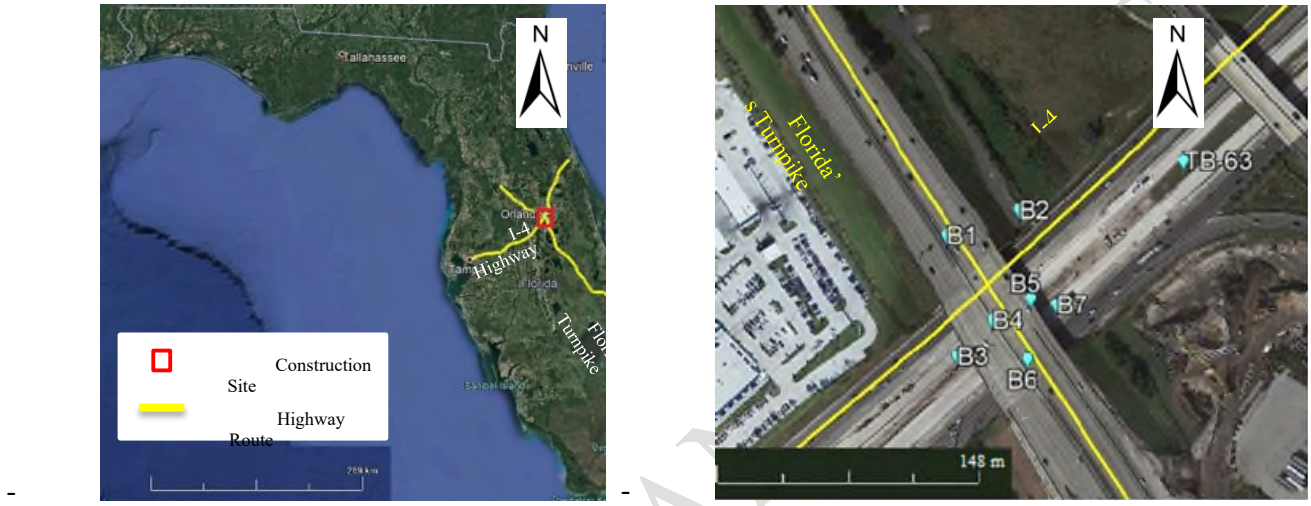

Figure 1. Location of: (a) bridge at the intersection between Florida's Turnpike and I-4 highway and (b) soil borings relative to the construction site. (Map data © 2020 Google.)

Figure 2 presents the results of the subsurface exploration conducted for the project. The soil profile was defined mainly based on SPT borings and index properties performed at the project site. Additional SPTs performed in nearby sites were also added in the figure. Index properties consisting of fine contents, water contents (w), liquid limits (LL), and plastic limits (PL) are shown in the figure. The relative density (D_r) of sand layers and the undrained shear strength (S_u) of an interbedded clay layer was determined by using correlations with the SPT blow counts presented by Kulhawy and Mayne (1990). The summarized soil conditions shown in the figure consist of three sand strata having various relative densities (D_r) mostly in the loose to medium-dense range and an interbedded clay layer of medium-stiff consistency. The medium dense sand layer, which extends from the ground surface level to a depth of 6.19 m, is underlaid by a 7 m thick medium stiff clay layer. A 15 m thick loose to medium dense sand with a 45% relative density is followed by a dense sand of 85% in relative density. The figure shows the approximate location of the shallow groundwater table at the project site.

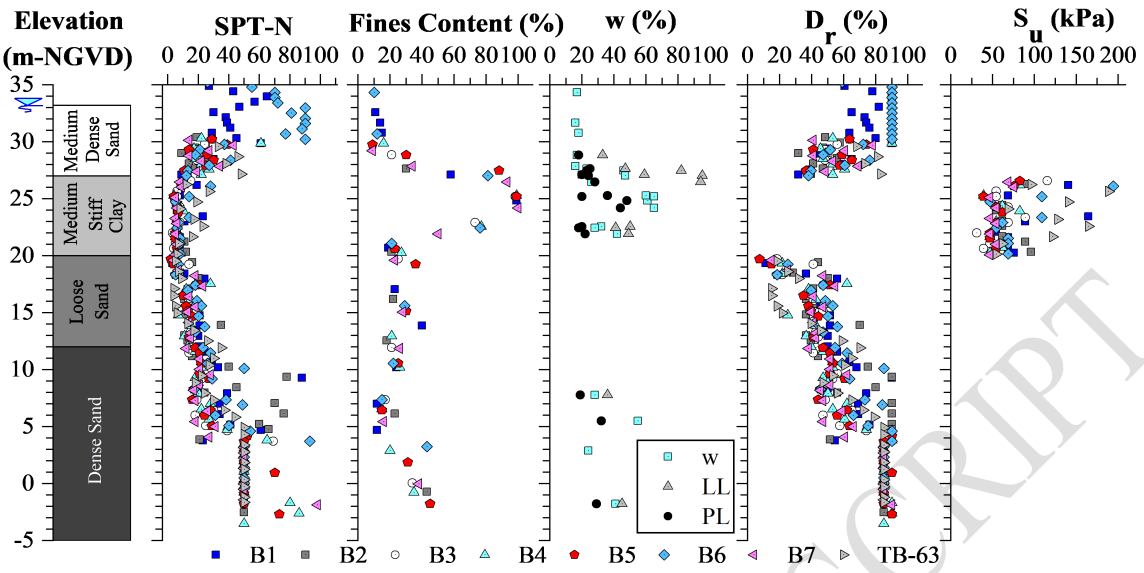

Figure 2. Summarized subsurface conditions at the project site.
Note: NGVD=National Geodetic Vertical Datum.

NUMERICAL PILE DRIVING MODELS

GRLWEAP Pile Driving Model

The pile driving process was numerically simulated using GRLWEAP. In this program, the soil profile was generated based on SPT-N values for each stratum. Soil parameters such as quake and damping for the shaft and toe resistances were obtained from the CAPWAP results presented in the project foundation reports. The hammer model and pile dimensions used in the analyses were defined from actual pile driving conditions and as-built dimensions. “Used” plywood properties were selected for the pile cushion since the dynamic test was performed at an advanced stage of the driving process, thus the cushion was used more than once. A thickness of 38.1 mm for hammer cushion and 381 mm for pile cushion were used.

A GRLWEAP driveability analysis was performed for a penetration depth of 26.9 m for the pile with a load-bearing capacity of 8109.1 kN in order to obtain a forcing function, which is comparable to the one measured with the PDA. Figure 3 presents a comparison between the GRLWEAP model and the field measurements processed by CAPWAP. Since the applied force history at the top of the pile obtained with GRLWEAP well matched with the one measured with PDA, especially in terms of peak magnitude and overall shape, the forcing function was converted into a stress function to be applied along the width of the pile in PLAXIS 2D.

A second driveability analysis was performed in GRLWEAP to compare the results of the discontinuous model with the continuous pile driving analysis. In order to define the “wished-in-place” pile penetration depth, the 667th hammer blow was selected, which corresponds to a penetration depth of 23.2 m with an ultimate capacity of 1112.1 kN. This pile penetration depth was modeled in GRLWEAP and PLAXIS 2D to compare the results of pile dynamics in light of the measured field data.

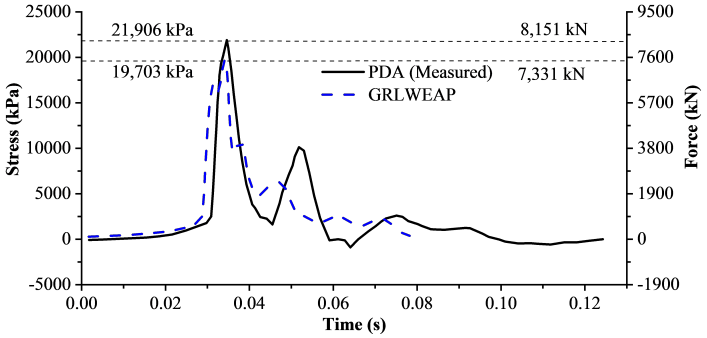

Figure 3. Stress function at the top of the pile.

Finite Element Pile Driving Model

The numerical model was performed under axisymmetric conditions. Figure 4a shows the model geometry, indicating the groundwater table and the soil profile used for the continuous model. The model mesh had a height and width of 44.2 m and 54.0 m, respectively. Boundary conditions in the model were defined as normally fixed for the right and left and fully fixed for the bottom. To avoid wave reflections, viscous boundaries were placed at the right and bottom ends. Fifteen-node triangular elements and a medium-mesh option were used. Figure 4b presents a detailed view of the tip of the pile for the continuous model and the "plastic zone" clusters, which were defined to represent the soil-pile interaction. Since the pile was first pre-drilled up to a depth of 9.7 m in the field before the pile driving process started, the pile cluster was activated in the model at that depth instead of beginning the driving process from the ground surface. The water table was placed at the ground surface. For the discontinuous model, the only parameter changed was the initial depth of pile penetration from 9.7 m to 26.9 m.

The HS small model available in PLAXIS 2D was used as the constitutive soil model since it provides small-strain soil stiffness, adequate hysteretic soil behavior and it has been successfully used in various types of soils (e.g., Grizi et al., 2018; Obrzud, 2010). Correlations with the D_r of the sand layers presented by Brinkgreve et al. (2010) were used to calculate HS small parameters of the granular layers. The parameters for the clay layer that underlies the top sand layer were based on an S_u of 110 kPa corresponding to a medium-stiff clay. HS small soil parameters for similar soils have been proposed in the technical literature (e.g., Likitlersuang et al. 2013; Surarak et al. 2012).

The soil-pile interaction was modeled by introducing a plastic zone around the pile with reduced strength (R) and shear wave velocity (R_s) parameters instead of defining an interface element between soil and pile. This alternative was proposed by Grizi et al. (2018) to overcome issues with interface elements in PLAXIS 2D when a dynamic stage is conducted. The radius of the plastic zone was defined to be twice the diameter of the pile (i.e., 1.2 m), which is the same ratio used by Grizi et al. (2018) that used a plastic zone of 150 mm for a laboratory test performed in a pile of 76 mm in diameter. However, instead of defining an R value of 0.5 and an R_s of 0.2 as suggested by Grizi et al. (2018), this paper used factors of 0.4 and 0.12 for R and R_s, respectively.

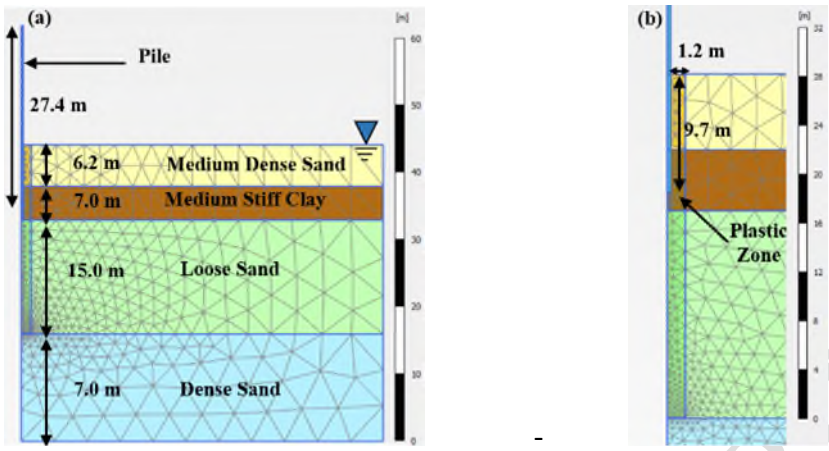

Figure 4. Continuous pile driving model in PLAXIS 2D: (a) model geometry and (b) detailed view of the pile initial penetration depth.

Table 1 presents the input parameters used in the model for both the plastic zone and the zone of soil continuum away from the plastic zone as it approaches free field conditions, labeled as "free-field zone" just for simplicity hereafter. Only the strength and stiffness parameters were affected by the plastic zone. Rayleigh damping was also applied to both zones in terms of the Rayleigh mass (α) and stiffness (β) proportional damping coefficients. They were defined for each layer, thus a damping ratio (ξ) of 5% was applied. As proposed by Hudson et al. (1994), α and β were determined by estimating the natural frequency of the soil layers.

Table 1. Soil layers properties used for the HS small model in PLAXIS 2D.

		Free-Field Zone				Plastic Zone			
Parameter	Units	Medium Dense Sand	Medium Stiff Clay	Loose Sand	Dense Sand	Medium Dense Sand	Medium Stiff Clay	Loose Sand	Dense Sand
Thickness	m	6.2	7.0	15.0	16.0	6.2	7.0	15.0	16.0
SPT-N	-	30.0	10.0	20.0	50.0	30.0	10.0	20.0	50.0
D_r	(%)	60.0	-	45.0	85.0	60.0	-	45.0	85.0
R	-	-	-	-	-	0.4	0.4	0.4	0.4
R_s	-	-	-	-	-	0.12	0.12	0.12	0.12
γ_{sat}	kN/m^3	20.0	19.0	19.7	20.4	20.0	19.0	19.7	20.4
ϕ'	º	35.5	28.0	33.6	38.6	14.2	11.2	13.5	15.5
ψ	º	5.5	-	3.6	8.6	2.2	-	1.5	3.5
c'	kPa	1.0	11.5	1.0	1.0	0.0	11.5	0.0	0.0
S_u	kPa	-	110.0	-	-	-	44.0	-	-
E_{50}^{ref}	kPa	36000	9500	27000	51000	518	137	389	734
E_{oed}^{ref}	kPa	36000	12000	27000	51000	518	173	389	734
E_{ur}^{ref}	kPa	108000	30000	81000	153000	1555	432	1166	2203
G_0^{Ref}	kPa	100800	70000	90600	117800	1452	1008	1305	1696
m	-	0.5	0.7	0.6	0.4	0.5	0.7	0.6	0.4
ν'_{ur}	-	0.3	0.2	0.3	0.3	0.3	0.2	0.3	0.3
$\gamma_{0.7}$	x10^{-4}	1.40	9.95	1.55	1.15	1.40	9.95	1.55	1.15
α	-	2.7	2.6	1.9	2.0	0.7	0.6	0.3	0.3
β	x10^{-4}	9.4	9.2	6.7	6.9	2.6	1.9	1.0	1.1
R_f	-	0.9	1.0	0.9	0.9	0.9	1.0	0.9	0.9

The forcing function of the hammer blows that were obtained from GRLWEAP was input as the stress function on top of the pile (see Figure 3). The continuous pile driving analysis consisted of three stages in PLAXIS 2D. The first stage was applied to initialize the stress field of the soil layers so that representative K_0-conditions of the *in situ* conditions can be simulated before the pile driving process started. In the second stage, the pile cluster was activated at the pre-drilling elevation described in the foundation reports. The third stage included the activation of the plastic zone and the application of a total of 1824 hammer blows at the top of the pile using the stress forcing function. Each blow in the third phase was separated by a time of 1.0 sec. For the discontinuous model, the first two stages remained the same but instead, the installation depth was defined at 23.2 m. However, the third stage only involved a single hammer blow.

RESULTS OF THE NUMERICAL MODEL

Table 2 presents four different sets of reduction factors (R and R_s) defined in this study to parametrically investigate the influence of the plastic zone on the pile driving process. The *model A* set of parameters is considered as a baseline model in this study. Both *models B* and *C* varied in just one reduction factor compared with *model A* in order to check their separate effects. *Model D* used the same reduction factors presented by Grizi et al. (2018).

Table 2. Reduction factors for the plastic soil adjacent to the pile.

PLAXIS 2D Model Number	Strength Reduction Factor (R)	Shear Wave Velocity Reduction Factor (R_s)
Model A	0.4	0.12
Model B	0.4	0.2
Model C	0.5	0.12
Model D	0.5	0.2

The numerical model, configured as a continuous pile driving process, was validated by comparing the results versus actual pile driving records from the foundation reports in terms of vertical displacements at the top of the pile as a result of 1,824 hammer blows. Figure 5a presents the computed and measured number of blows versus pile penetration. Observe in the measured data how after 1,173 blows the penetration depth increased suddenly. This is attributed to changes in the fuel settings of the hammer reported in the pile driving record log of the project. The numerical models were not defined to allow for changes in the stress forcing function to perfectly match the final pile penetration depth. A comparison of the numerical results is presented in terms of pile penetration for the different sets of parameters adopted for the plastic zone. This is to highlight its importance in the numerical modeling framework. It is observed that the *model A*, selected as the base model, matches very well the measured data up to the point of change in the fuel setting. As expected, it is found that as the reduction factors decreased, the pile penetration increased. Comparing *model D* with *models B* and *C*, it is concluded that the shear wave velocity factor has a greater effect on the driveability of the pile than the strength reduction factor.

Figure 5b presents parametrically the influence of the size of the plastic zone (r) on the pile penetration process. The reduction factors for *model A* were used for further comparisons since they matched well the field measurements. Observe in the figure how an increase in the width of the plastic zone increased the pile penetration as well. The assumption of having a plastic zone radius of twice the diameter of the pile is in good agreement with the measured penetration. This matches the value proposed by Grizi et al. (2018). The definition of the properties and size of this plastic zone is key in the study of pile driving induced geotechnical mechanisms (e.g., settlements, excess pore water pressures, peak particle velocities, etc.) that occur in the soil continuum since the actual pile penetration process needs to be properly characterized in the numerical model. The selection of numerical input parameters for this highly disturbed zone near the pile, idealized in this finite element model as a plastic zone, must be performed as a function of the type of soil, pile properties (i.e., geometric and material), and characteristics of the input source.

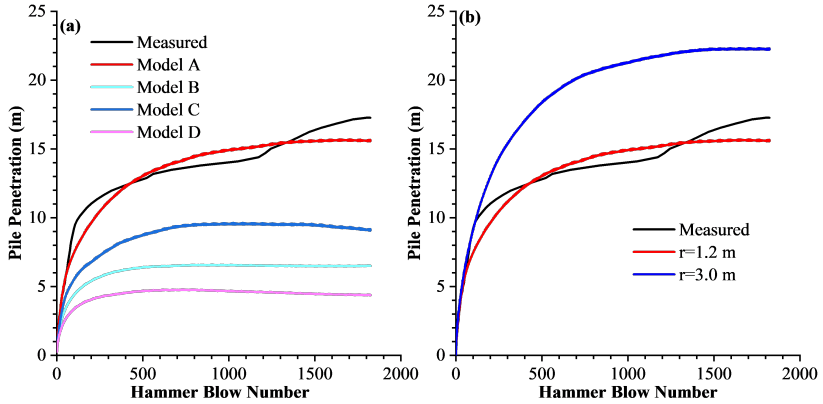

Figure 5. Effects of: (a) definition of plastic zone parameters on the pile driving process compared with field measurements and (b) size of the plastic zone on the pile penetration.

After the continuous model was validated using the driving records in the foundation reports (see Figure 5), the discontinuous model was also performed in PLAXIS 2D at the desired depth of 23.2 m. In this analysis, the same set of parameters corresponding to *model A* and the size of the plastic zone of 1.2 m were used. The comparison between the two modeling approaches in PLAXIS 2D in relation to the results computed with GRLWEAP for a single blow applied at the top of the pile is presented in Figure 6. The time history of vertical velocities at the top of the pile for the 667th hammer blow is shown in Figure 6a. The three approaches have approximately the same peak velocity of 2.5 m/s. However, a better representation of the signal computed with GRLWEAP was obtained using the continuous modeling approach as opposed to the discontinuous model. Figure 6b presents time versus vertical displacements computed with GRLWEAP and both PLAXIS 2D modeling approaches. Only the continuous model was able to represent the magnitude of residual vertical displacements as a result of a single hammer blow. These differences in the discontinuous approach accumulate and ultimately provide misleading results when the entire pile driving process is modeled (e.g., 1824 blows for the pile in this paper). Despite differences in the shape of the time history results of vertical displacements, the continuous

model provides very similar results that GRLWEAP in terms of both displacements and velocities. This is attributed to the accuracy in the numerical representation of the state of stresses generated during the driving process when continuous pile driving models are used.

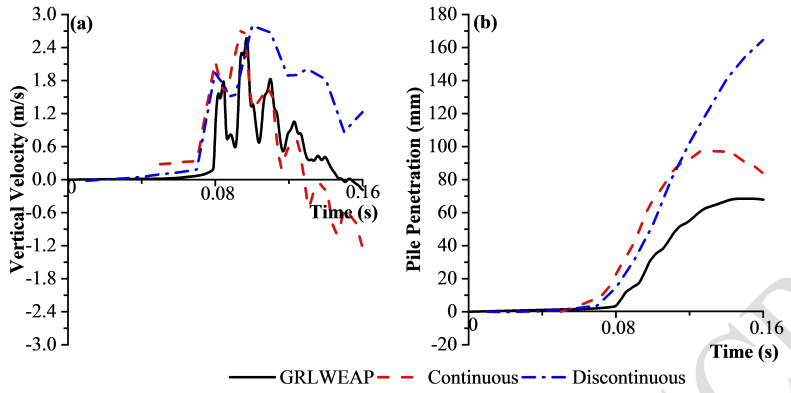

Figure 6. Comparison of the continuous and discontinuous numerical approaches compared with results from GRLWEAP in terms of: (a) vertical velocity at the top of the pile and (b) vertical displacement at the top of the pile.

CONCLUSIONS

Numerical analyses were performed in this paper to compare the two finite element modeling approaches (i.e., continuous vs. discontinuous) of pile driving with field measurements from pile driving records. Those models were parametrically studied in terms of displacements and vibrations in the pile by varying the properties and size of the plastic zone. The following conclusions were drawn from this paper:

1. A continuous pile driving process can be modeled in PLAXIS 2D by introducing a plastic zone around the pile with reduced parameters. The reduction factors in the disturbance zone had a large effect on the final computed response since they represent the soil-pile interaction. A decrease in the reduction factor R_s, related to the shear wave velocity, increases more the penetration of the pile than the parameter R that represents a strength reduction. The numerical analyses also indicated that a size of the plastic zone of twice the diameter of the pile might be used for the large displacement pile of this study, which matches well with other published values in the technical literature.
2. A continuous pile driving model matches better the computed pile driving response (i.e., displacements and velocities) with GRLWEAP/CAPWAP for a single hammer blow than a discontinuous model. The change in the state of stresses during the pile driving process is considered explicitly in a continuous pile driving modeling approach. Results computed by assuming “wished-in-place” locations of the pile at different elevations along the process, applying a single hammer blow at those locations, and accumulating those values (i.e., “discontinuous” modeling approach) do not constitute an accurate method to study pile driving dynamics and can produce misleading results in the soil continuum.

ACKNOWLEDGEMENTS

This study was funded by the Florida Department of Transportation (FDOT). The authors would like to thank Mr. Michael Byerly at FDOT District 5 and Dr. Roger Gobin at the Turnpike for their help in providing the field data presented in this paper.

REFERENCES

Brinkgreve, R.B.J., Engin, E., and Engin, H. K. (2010). "Validation of Empirical Formulas to Derive Model Parameters for Sands". *Numerical Methods in Geotechnical Engineering*, 137-142.

Farshi Homayoun Rooz, A., and Hamidi, A. (2017). "Numerical Analysis of Factors Affecting Ground Vibrations due to Continous Impact Pile Driving". *International Journal of Geomechanics, 17*(12), 1-15.

Grizi, A., Athanasopoulus-Zekkos, A., and Woods, R. D. (2018). "H-Pile Driving Induced Vibrations: Reduced-Scale Laboratory Testing and Numerical Analysis". *Proc., IFCEE 2018: Advances in Geomaterial Modeling and Site Characterization*, 165-175.

Hudson, M., Idriss, I., and Beikae, M. (1994). *QUAD4M: A Computer Program to Evaluate the Seismic Response of Soil Structures Using Finite Element Procedures and Incorporating a Compliant Base.* Davis, California: Center for Geotechnical Modeling Dept. of Civil and Environmental Engineering University of California Davis.

Khoubani, A., and Ahmadi, M. M. (2014). "Numerical Study of Ground Vibration Due to Impact Pile Driving". *Proc., of the ICE - Geotechnical Engineering, 167*(1), 28-39.

Kulhawy, F. H., and Mayne, P. W. (1990). *Manual on Estimating Soil Properties for Foundation Design.* Ithaca, NY: Cornell University.

Likitlersuang, S., Teachavorasinskun, S., Surarak, C., Oh, E., and Balasubramaniam, A. (2013). "Small Strain stiffness and Stiffness Degradation Curve of Bangkok Clays". *Journal of Soils and Foundations, 53*(4), 498-509.

Mabsout, M. E., Reese, L. C., and Tassoulas, J. L. (1995). "Study of Pile Driving by Finite-Element Method". *Journal of Geotechnical Engineering, 121*(7), 535-543.

Obrzud, R. F. (2010). "On the Use of the Hardening Soil Small Strain Model in Geotechnical Practice". *Proc., Numerics in Geotechnics and Structures*, 16.

Pile Dynamics, Inc. (2000). *CAPWAP for Windows Manual Version 2000-1.* Renaissance Parkway, Cleveland, Ohio: <www.pile.com> (Jul.14, 2020).

Pile Dynamics, Inc. (2003). *GRLWEAP Procedures and Models Version 2003.* Renaissance Parkway, Cleveland, Ohio: <www.pile.com> (Jul.14, 2020).

Smith, E. A. (1960). "Pile-Driving Analysis by the Wave Equation". *J. Soil Mech. and Found. Div., 86(4)*, 35-61.

Surarak, C., Likitlersuang, S., Wanatowski, D., Balasubramaniam, A., Oh, E., and Guan, H. (2012). "Stiffness and Strength Parameters for Hardening Soil Model of Soft and Stiff Bangkok Clays". *Journal of Soils and Foundations, 52*(4), 682-697.

Continuous Impact Pile Driving Modeling to Elucidate Settlement-PPV-Soil Density-Input Energy Relationships

Jorge E. Orozco-Herrera,[1] S.M.ASCE, Berk Turkel, S.M.ASCE, [2]
Luis G. Arboleda-Monsalve, Ph.D., M.ASCE,[3] Boo Hyun Nam, Ph.D.,[4] and Larry Jones[5]

[1]Graduate Research Assistant, Dept. of Civil, Environmental, and Construction Engineering, University of Central Florida, Orlando, FL 32816, USA; e-mail: Jeorozcoh@knights.ucf.edu

[2]Graduate Research Assistant, Dept. of Civil, Environmental, and Construction Engineering, University of Central Florida, Orlando, FL 32816, USA; e-mail: TurkelBerk@knights.ucf.edu

[3]Assistant Professor, Dept. of Civil, Environmental, and Construction Engineering, University of Central Florida, Orlando, FL 32816, USA; e-mail: Luis.Arboleda@ucf.edu

[4]Associate Professor, Dept. of Civil, Environmental, and Construction Engineering, University of Central Florida, Orlando, FL 32816, USA; e-mail: BooHyun.Nam@ucf.edu

[5]State Geotechnical Engineer, Florida Department of Transportation, 605 Suwannee St, Tallahassee, FL, 32399, USA; e-mail: Larry.Jones@dot.state.fl.us

ABSTRACT

The geotechnical conditions in Central Florida consist predominantly of medium-dense silty-sands that allow the installation of deep foundations using pile driving methods to carry large infrastructure loadings to the limestone bedrock. This process generates vibrations in the surrounding soils that could trigger ground deformations and possible damage to nearby structures. The process is a complex dynamic soil-pile interaction problem that involves many variables including the transmitted energy of the driving hammer, the length, material, and cross-sectional properties of the pile, and the dynamic properties of the surrounding and supporting soils, among others. This paper presents a numerical model developed in PLAXIS 2D for the continuous driving process of a prestressed concrete pile. The constitutive soil model used was the critical-state based hypoplasticity model for sands enhanced with the intergranular strain concept. A parametric study was performed to elucidate the effect of the above-mentioned variables on the vibrations and ground deformations in the vicinity of the pile. A wide range of relative void ratios varying from 25% to 70% is presented. The effects of type of hammer on soil response at the ground surface are also examined. Conclusions are drawn regarding the geomechanical characteristics of these soils to trigger large pile-driving induced ground deformations.

INTRODUCTION

Driven piles are a suitable deep foundation alternative in geotechnical engineering designs to transfer structural demands to competent strata and to avoid serviceability issues associated with shallow compressible soil layers. This foundation type is commonly used in Central Florida due to the soil conditions in the area that consist mainly of granular soil deposits. The pile driving process generates ground vibrations and ground deformations (e.g., settlement or heave) which can affect nearby structures. According to Massarsch and Fellenius (2014), damage to structures induced by construction vibrations may occur from four different causes such as i) static movements (mostly heave) due to volume displacement after installation of large displacement piles, ii) ground distortions due to propagation of surface waves subjecting the structures to cycles

of upward and downward movements, iii) ground deformations caused by dynamic compaction effects in loose materials, and iv) vibrations in the structures and their dynamics effects. The geotechnical practice and design standards have focused mainly on limiting vibrations to a certain limit or threshold. For example, the Florida Department of Transportation (FDOT) establishes an acceptable vibration threshold of 12.7 mm/s (0.5 in/s) for road and bridge construction projects (FDOT, 2021). In current studies, these vibration criteria are not linked to the amount of settlement or heave that the soils may experience due to pile driving induced vibrations. This paper aims to analyze the pile driving-induced settlements as an additional variable that should be considered during the design stage.

This study aimed at not only selecting the most adequate numerical approaches and constitutive soil models to study ground deformations arising from pile driving but also at understanding via wave equation analysis the soil-pile interaction for the ground settlement assessment. Software such as GRLWEAP and CAPWAP use wave equation analyses to estimate engineering demands generated during the pile driving process. The pile driving demands applied to the models (i.e., forcing function on top of the pile) were numerically simulated using the wave equation analysis program GRLWEAP. Wave equation-based programs such as GRLWEAP have countless positive features that can be used for deep foundation designs, but engineering demands such as ground deformations and ground vibrations cannot be retrieved from these programs. GRLWEAP only allows the calculation of a detailed time history of displacements, velocities, forces, and input energy in the pile for a single hammer blow. To overcome this issue, the pile driving process was also modeled herein using the finite element (FE) platform PLAXIS 2D to conclude about the relationships between input energy, ground deformations, peak particle velocities, distance from the source, and soil properties. Input parameters for the critical-state based hypoplasticity model for sands enhanced with the intergranular strain concept were estimated based on Zapata-Medina et al. (2019).

Turkel et al. (2021) used Pile Driving Analyzer (PDA) data to model a continuous pile driving process using an APE D70-52 hammer in PLAXIS 2D and then compared the results with the reported pile driving records. The FE models were validated with CAPWAP/iCAP and GRLWEAP program outputs for a single blow to compare computed pile dynamics. In this study, the continuous pile driving modeling approach was adopted in the analyses since this modeling approach is capable of accurately representing the accumulation of stresses during the pile driving process. The analyses are presented using a combination of numerical analyses conducted in GRLWEAP and PLAXIS 2D. A parametric study was performed to investigate the effect of various relative void ratios (as defined by Herle and Gudehus, 1999) for the predominant soil conditions (i.e., sandy soils) and various hammer types commonly used in Central Florida during the continuous pile driving process of a prestressed concrete pile.

NUMERICAL PILE DRIVING MODELS

GRLWEAP Pile Driving Model

Driveability analyses for the pile were first conducted in GRLWEAP before running the FE models to obtain input forcing functions for the various models. The driving process of a 610 mm-wide square precast concrete pile was modelled for a final penetration depth of 27.5 m and a pre-drilling depth of 9.7 m. The total length of the pile was 27.50 m. A thickness of 38.1 mm for the hammer cushion and 381 mm for a “used” plywood pile cushion were used. The soil profile was

defined in GRLWEAP using two layers consisting of a 30.5 m thick granular strata and an underlying 53.4 m thick very dense competent granular soil strata.

Heung et al. (2007) presented a study of pile-driving induced ground vibrations in several projects along Florida's Turnpike. The most common hammer types were the DELMAG D36-32 and the ICE 120-S. These two hammers were selected for the parametric study to compare the results with the APE D70-52 hammer used by Turkel et al. (2021). Thus, forcing functions were obtained for three typical hammer types in Florida. Figure 20a presents the forcing functions at the top of the pile created by a single blow of the various hammers by using GRLWEAP. Based on this analysis, the APE D70-52 and D36-32 hammers apply the highest and lowest peak forces at the top of the pile, respectively. Figure 20b presents the energy transmitted to the top of the pile by a single hammer blow for each type of hammer. Similar to the results for the forcing function at the top of the pile, the APE D70-52 and D36-32 hammers transmit the highest and lowest energies at the top of the pile, respectively. The APE D70-52 hammer had the maximum peak and residual transmitted energies. The forcing function of the hammer blows that were obtained from GRLWEAP was input in PLAXIS 2D as a stress function distributed on top of the pile by diving the forcing function by the area of the pile (see Figure 20a).

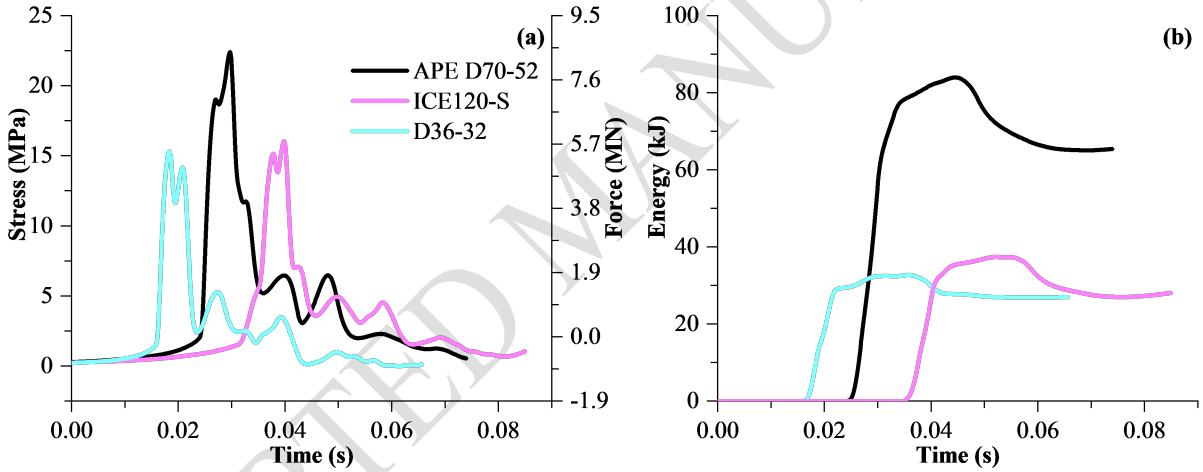

Figure 20. Analysis of different hammers used in Central Florida in terms of: (a) forcing functions at the top of the pile, and (b) transmitted energy functions at the top of the pile.

Finite Element Pile Driving Model

The selected hammers (i.e., APE D70-52, DELMAG D36-32, and ICE 120-S) and their respective forcing functions were used to conduct finite element analyses in PLAXIS 2D and investigate the pile-driving induced effects on the surrounding soils. Since the subsurface conditions in Central Florida are mainly characterized by the presence of granular materials varying with relative void ratios from loose to medium dense conditions (Heung et al. 2007, Bayraktar et al., 2013, and Turkel et al., 2021) the numerical study was developed to investigate the effect of relative void ratios (r_e) of the soils (25%, 40%, 55%, 60%, and 70%) on the final response.

The hypoplasticity model for sands developed by von Wolffersdorff (1996) and enhanced with the intergranular strain concept by Niemunis and Herle (1997) was used for the proposed analyses. This constitutive soil model is selected because accurate relationships between the variables

involved can be established given its capabilities to perform dynamic analyses (Gudehus et al., 2008). The formulations of the hypoplasticity model consider the influence of the void ratio (e) that enhances the computational capabilities to study the geomechanical response of soils to dynamic loadings for a wide range of relative void ratios and confining pressures (Wichtmann et al., 2019).

The numerical model was performed under axisymmetric conditions in PLAXIS 2D. Figure 5-2a shows the model geometry, groundwater table, and idealized soil profile. The finite element mesh had a height and width of 84.2 m and 94.0 m, respectively. Normally fixed boundary conditions were defined for the right and left boundaries and fully fixed for the bottom boundary. Viscous boundaries were also placed at the right and bottom ends to avoid wave reflections. Fifteen-node triangular elements were used and a soil cluster with a refined mesh having a height of 21.2 m and width of 20.0 m was created around the pile to improve the accuracy of the numerical results close to the pile. Figure 5-2b presents a detailed view of this refined soil cluster which had a mesh coarseness factor of 0.25 in PLAXIS 2D. The mesh coarseness factor describes the ratio of the mesh refinement at the given soil cluster to the overall mesh coarseness of the model. The large deformation of the mesh given the continuous nature of the pile driving process was modeled by enabling the updated mesh option in PLAXIS 2D. A staged construction process consisting of three main stages was followed in this study. The first stage was applied to initialize the stress field of the soil layers. Then, a pre-drilling depth of 9.7 m before starting the driving operation was defined by activating the pile cluster in the model. In the last stage, the driving operation was initiated by applying a total of 1400 hammer blows at the top of the pile. The stress forcing function was applied with a time interval of 1 second between blows. The water table was kept constant at the ground surface during the entire simulation.

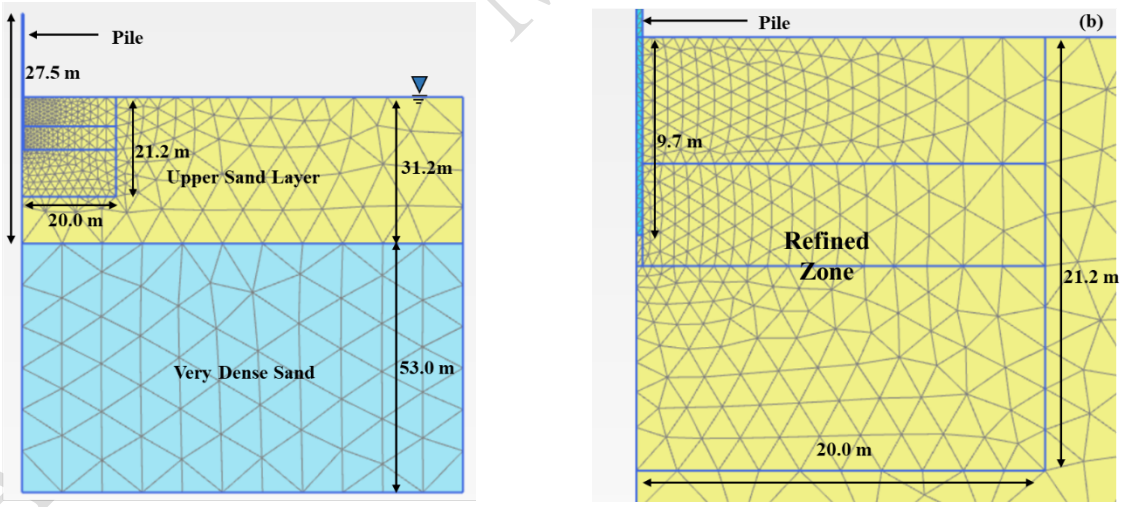

Figure 21. Pile driving model used in the parametric study in PLAXIS 2D: (a) model geometry and (b) detailed view of the refined zoned and initial pile penetration depth.

The model consists of a 31.2 m thick idealized sand layer with variable relative void ratios on top of a 53.0 m thick very dense competent sand layer. The finite element model matched the soil conditions defined also in the GRLWEAP model. A relative density of approximately 90% was assigned to the very dense bottom sand layer that was selected to represent a firm layer where the pile driving processes is completed since the pile reached a competent bearing stratum.

The analyses were finalized when the pile reached the bottom competent stratum or due to excessive computational time when approximately 1400 blows were applied. It was typical to complete the pile driving process for a given combination of hammer type and soil conditions at a different number of hammer blows.

Definition of the Soil Parameters

A relative void ratio varying between 25% and 70% was assigned to the upper soil layer in this parametric study. The methodology conducted by Kim (2011) was followed to calculate the secant shear modulus degradation curves of the upper sand layer on monotonic triaxial tests for each relative void ratio. Figure 5-4 presents the computed secant shear modulus degradation with the selected parameters for the upper sand layer at selected relative void ratios (i.e., 25%, 40%, 60%, and 70%). The nonlinear behavior of the upper sand layer at the laboratory scale level was studied to computationally match expected dilative or contractive responses. Stress-controlled undrained triaxial compression tests consolidated to K_0 conditions ($CK_0U - TXC$) on the soil test module available in PLAXIS 2D were conducted to determine hypoplasticity model parameters. An initial cell pressure of 100 kPa and a K_0 of 0.5 were applied following monotonic undrained triaxial tests conducted by Hyodo et al. (1994) on saturated loose Toyoura sand. Thus, a mean confining pressure (p_s) of 133 kPa was applied. Based on the numerically simulated triaxial test results using the hypoplasticity sand model for the upper sand layer, the secant shear modulus degradation curves for each relative void ratio were computed. The definition of soil parameters was conducted so that the computed secant shear modulus degradation curves for each void ratio (e_0) matched other published degradation curves presented by Hardin and Drnevich (1972), and Seed and Idriss (1970). Since the void ratio at the specified p_s is required to plot the reference degradation curves, the equation developed by Bauer (1996), which is based on the granular hardness (h_s) and an exponent for the grain skeleton (n), was used to calculate the void ratio-applied pressure relationships.

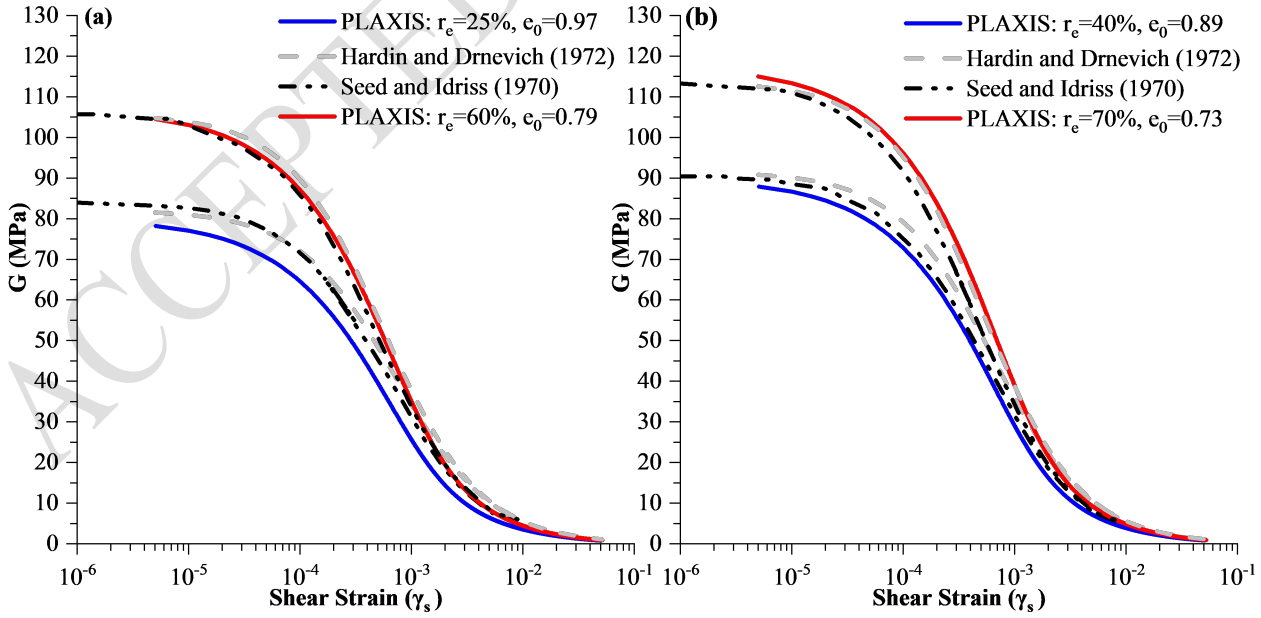

Figure 22. Secant shear stiffness degradation curves for the relative void ratios of: (a) 25% and 60% (b). 40%, (c) 40%, and (d) 70%.

The adopted set of parameters for the upper sand layer based on the numerically simulated triaxial tests are listed in Table 5-4. The same reference values proposed by Zapata-Medina et al. (2019) for minimum void ratio at zero pressure (e_{d0}), critical void ratio at zero pressure (e_{c0}), and maximum void ratio at zero pressure (e_{i0}) were used. The remaining basic hypoplastic model parameters (i.e., h_s, n, α, β), and the size of the elastic range (R_{max}) and material constant representing stiffness degradation (β_r) were obtained by fitting the secant shear modulus degradation curves to the reference curves. The remaining intergranular strain concept parameters (i.e., $m_R, m_T, \chi,$) were also proposed by Zapata-Medina et al. (2019). An input Rayleigh damping ratio of 5% was defined throughout the analyses.

Table 2. Soil properties used for the Hypoplasticity sand model in PLAXIS 2D.

No.	Parameter	Description	Value	Unit
1	f_c	Critical state friction angle	31	°
2	pt	Shift of the mean stress due to cohesion	0	kPa
3	h_s	Granular hardness	1200	MPa
4	n	Exponent for pressure sensitive of a grain skeleton	0.37	-
5	e_{d0}	Minimum void ratio at zero pressure (ps = 0)	0.58	-
6	e_{c0}	Critical void ratio at zero pressure (ps = 0)	1.096	-
7	e_{i0}	Maximum void ratio at zero pressure (ps = 0)	1.315	-
8	a	Exponent for transition between peak and critical stresses	0.05	-
9	β	Exponent for stiffness dependency on pressure and density	1.4	-
10	m_R	Stiffness increase for 180° strain reversal	5	-
11	m_T	Stiffness increase for 90° strain reversal	2	-
12	R_{max}	Size of elastic range	5.00×10^{-5}	-
13	β_r	Material constant representing stiffness degradation	0.1	-
14	χ	Material constant for evolution of intergranular strains	1.0	-

Numerically simulated $CK_0U - TXC$ results using the selected parameters are presented in Figure 5-3. Deviatoric stress (Δq) and excess pore water pressures (Δu) are presented versus axial strains (ϵ_a) for various relative void ratios. A dilative response to soil shearing was the main characteristic for the medium-dense sands (i.e., r_e=60% and 70%). A more contractive response was computed for the loose sands (i.e., r_e= 25% and 40%). The overall computed sand response to shearing investigated herein generally matches the results of $CK_0U - TXC$ tests conducted by Hyodo et al. (1994).

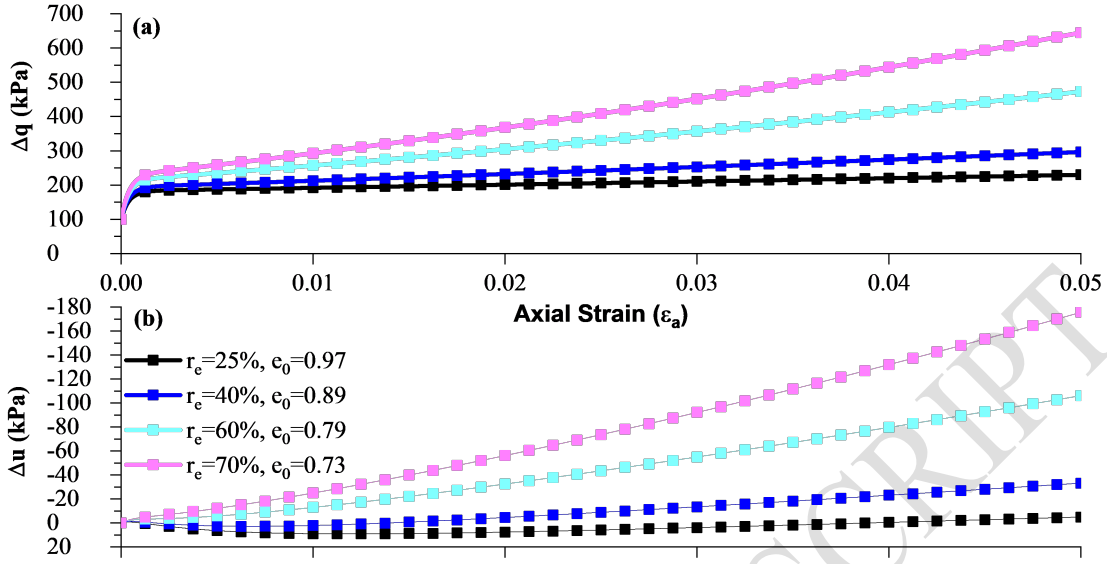

Figure 23. Computed Triaxial Test Results ($CK_0U - TXC$) a) Δq versus ϵ_a, b) Δu versus ϵ_a.

The constitutive soil model used for the very dense competent sand layer was HS small. Correlations with r_e presented by Brinkgreve et al. (2010) were used to calculate HS small parameters for this stratum. The selected parameters are given in Table 5-5.

Table 3. Soil layer properties used for the very dense sand in PLAXIS 2D.

Parameter	ϕ' (°)	Ψ (°)	c' (kPa)	E_{50}^{ref} (x10⁶ kPa)	E_{oed}^{ref} (x10⁶ kPa)	E_{ur}^{ref} (x10⁶ kPa)	G_0^{ref} (x10⁶ kPa)	m	ν'ur	$\gamma_{0.7}$ (x10⁻⁴)	R_f
Value	39.3	9.3	1	0.054	0.054	0.16	0.12	0.42	0.3	1.1	0.89

RESULTS OF THE NUMERICAL MODEL

Figure 24 presents the computed vertical pile penetration during the pile driving process for various relative void ratios (i.e., 25%, 40%, 55%, 60%, and 70%). The pile penetration due to the applied hammer blows is presented. The pre-drilled length (i.e., 9.7 m) is constant for all the piles, therefore, it is not shown in the figure (i.e., initial pile penetration value was reset to zero). As expected, the effort required to install each pile, reflected in the variable hammer blows necessary to reach a given penetration depth target, is highly dependent on the relative void ratio of the soil. Figure 24a shows the results obtained using an APE D70-52 hammer. A total of 770 hammer blows were necessary to drive the pile completely through the soil having a r_e of 25%. Conversely, 1400 hammer blows were necessary to drive the pile to reach the target 18.3 m depth when the r_e was 70%. Figure 24b presents the same type of analysis of pile penetration versus hammer blow when the ICE 120-S hammer was used. When comparing the analyses versus those obtained with the APE D70-52 hammer, more hammer blows were required to drive the pile to reach the same vertical penetration since the input energy of the ICE 120-S hammer is lower than the one from the APE D70-52 hammer (see Figure 20b). Figure 24c presents pile penetrations when the D36-

32 hammer was used. Similar results were reached with this hammer than those computed with the ICE 120-S hammer.

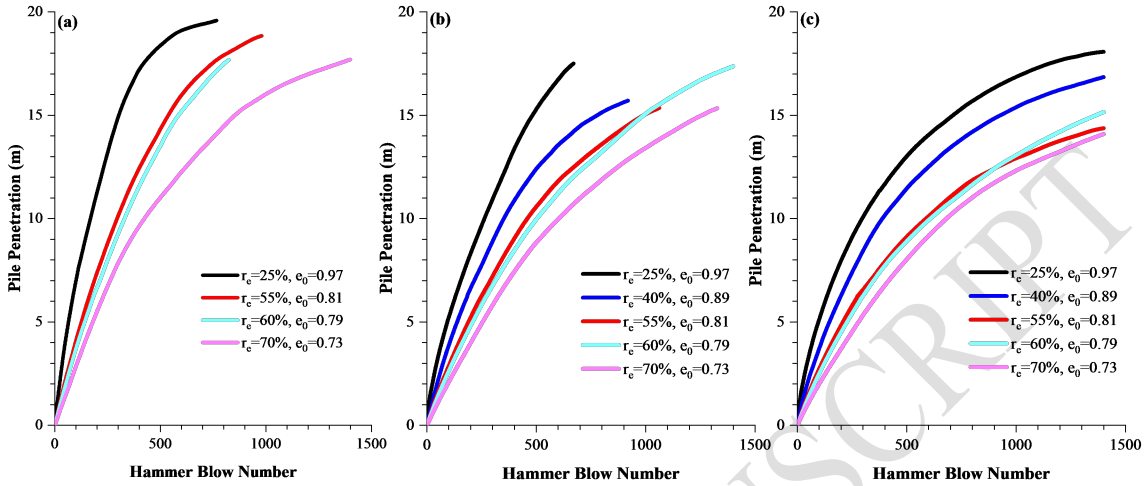

Figure 24. Comparison of the vertical penetration during the pile driving process for different hammer types and relative void ratios: (a) APE D70-52 (b) ICE 120-S (c) D36-32.

Figure 25 presents the PPV values computed at the ground surface versus distance away from the pile. These data are compared with historical records of PPVs along five construction sites in Central Florida's Turnpike collected by Bayraktar et al. (2013). The PPV attenuation curves derived for each project by Bayraktar et al. (2013) are presented in the figure. The normalization factor for the scaled distance in the horizontal axis was defined using the maximum transferred energy of the hammers. The figure shows how the computed PPVs from the numerical model reasonably match the attenuation curve boundaries provided by Bayraktar et al. (2013). A horizontal red dashed line is shown in the figure to illustrate the reference value of 12.7 mm/s (0.5 in/s). Even though the computed values went up to 1230 mm/s very close to the pile, observe how a minimum scaled distance of approximately 1.0 $m/\sqrt{kJ}$ can be defined regardless of the hammer type and relative void ratio considered in the numerical model since PPVs beyond that point lie within the maximum acceptable threshold.

Figure 7-5 presents the maximum computed settlements (S) during the pile driving at distances where PPV values satisfied the 12.7 mm/s (0.5 in/s) FDOT threshold (FDOT, 2021) for different relative void ratios. This PPV value was met at different distances from the pile, input energies, and relative void ratios since typical PPV attenuation curves vary as a function of those variables. These maximum settlements were obtained from the settlement time history during the pile driving operations. A settlement linear trendline for each hammer type is shown in the figure; APE D70-52 and D36-32 trends were similar. Lower settlements were computed with ICE 120-S. Approximately 38 to 76 mm of maximum settlement associated with PPV 12.7 mm/s (0.5 in/s) were observed at the relative void ratio of 25%, which decreased to approximately 25 mm for denser soil profiles (i.e., r_e= 70%).

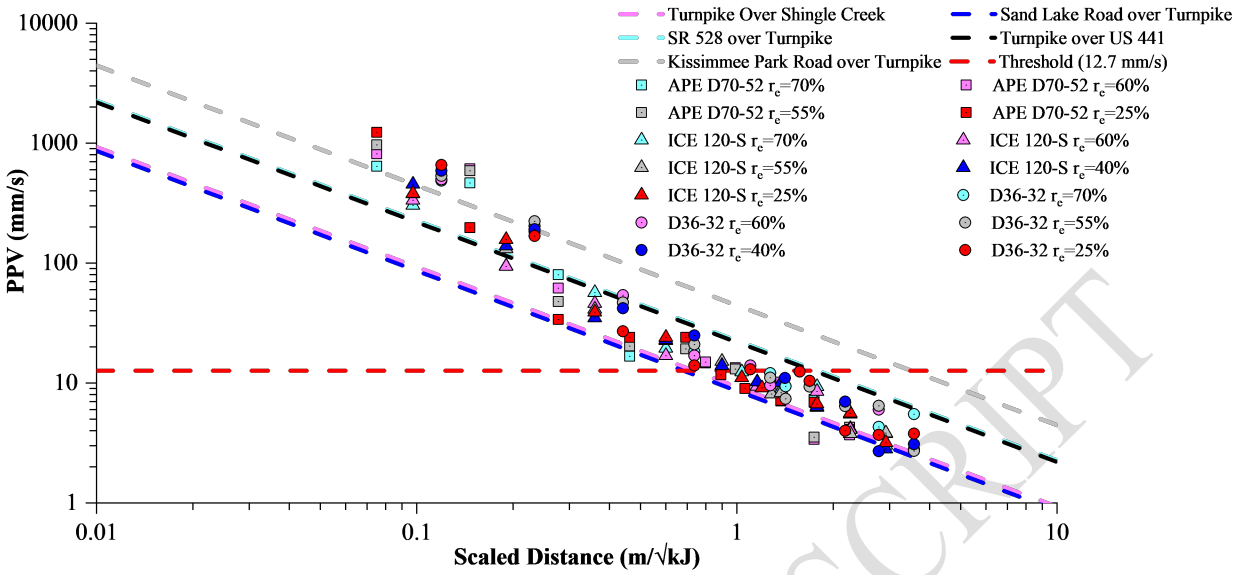

Figure 25. Computed PPV versus scaled distance with the numerical model in relation to reported boundaries by Bayraktar et al. (2013).

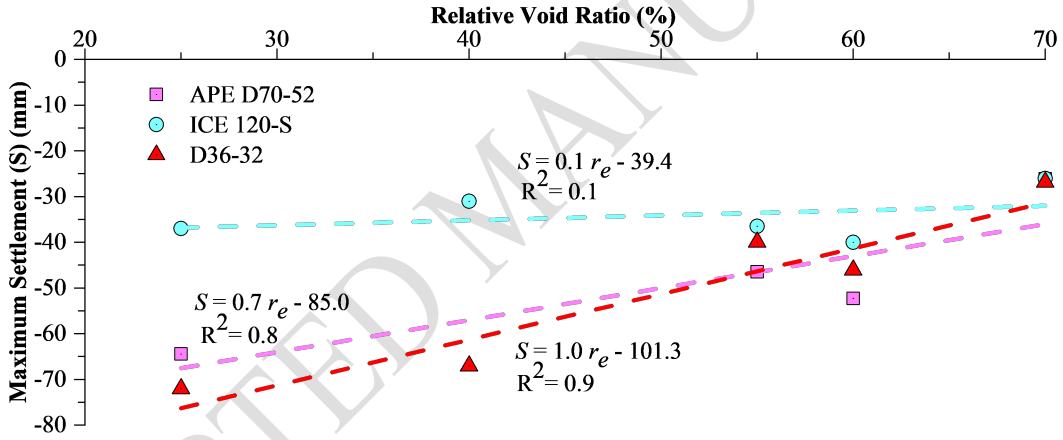

Figure 26. Maximum computed settlement associated with PPV of 12.7 mm/s (0.5 in/s) for the various relative void ratios and input energies.

SUMMARY AND CONCLUSIONS

A continuous pile driving process was successfully modeled in PLAXIS 2D by using critical-state based hypoplasticity model for sands enhanced with the intergranular strain concept. Numerical analyses were performed to investigate the influence of the hammer type and relative void ratio of the soils on the ground surface settlements induced by pile driving operations. The following conclusions are drawn from this paper:

1. Larger ground surface settlements were computed for loose sandy soils (i.e., r_e = 25% and 40%) than denser sandy soils due to dynamic soil densification.
2. The amount of ground surface settlement experienced during the pile driving largely depends on the maximum transmitted energy of the hammer and the type and shape of forcing function,

which directly depends on the hammer accessories used for the driving process, and the relative void ratio of the soils that implicitly affects the dynamic properties of the surrounding soils.

3. Significant values of ground surface settlements were computed even if the PPV threshold of 12.7 mm/s (0.5 in/s) established by the FDOT was satisfied. A minimum scaled distance of approximately 1.0 $m/\sqrt{kJ}$ was defined regardless of the hammer type and relative void ratio considered in the numerical model since PPVs beyond that point lie within the maximum acceptable threshold.

ACKNOWLEDGEMENTS

Financial support was provided by the Florida Department of Transportation, Project No. BDV24 TWO 977-33. The opinions, findings, and conclusions expressed in this publication are those of the authors and not necessarily those of the State of Florida Department of Transportation.

REFERENCES

Bauer, E. (1996). "Calibration of a Comprehensive Hypoplastic Model for Granular Materials." *Soils and Foundations*, 36, 13–26.

Bayraktar, M. E., Kang, Y., Svinkin, M., and Arif, F. (2013). *Evaluation of Vibration Limits and Mitigation Techniques for Urban Construction*. Florida Department of Transportation, Tallahassee, FL, 128.

Brinkgreve, R. B. J., Engin, E., and Engin, H. K. (2010). "Validation of empirical formulas to derive model parameters for sands." *Numerical Methods in Geotechnical Engineering*, Taylor & Francis, 137–142.

FDOT. (2021). "Section 455: Structures Foundations." *Standard Specifications for Road and Bridge Construction*, Florida Department of Transportation (FDOT), Tallahassee, FL, 552–619.

Gudehus, G., Amorosi, A., Gens, A., Herle, I., Kolymbas, D., Masin, D., Muir Woods, D., Nova, R., Niemunis, A., Pastor, M., Tamagnini, C., and Viggiani, G. (2008). "The soilmodels.info project." *International Journal for Numerical and Analytical Methods in Geomechanics*, 32(12), 1571–1572.

Hardin, B. O., and Drnevich, V. P. (1972). "Shear Modulus and Damping in Soils: Design Equations and Curves." *Journal of the Soil Mechanics and Foundations Division*, 98(7), 667–692.

Herle, I., and Gudehus, G. (1999). "Determination of parameters of a hypoplastic constitutive model from properties of grain assemblies." *Mechanics of Cohesive-frictional Materials*, 4(5), 461–486.

Heung, W., Morgan, K., Yoon, Y. H., Gobin, R., and Gollamudi, S. (2007). "Vibration due to Driving Concrete Piles Using Open-Ended Diesel Hammer in Central and South Florida." *7th FMGM 2007*, American Society of Civil Engineers, Boston, MA, 1–12.

Hyodo, M., Tanimizu, H., Yasufuku, N., and Murata, H. (1994). "Undrained cyclic and monotonic triaxial behaviour of saturated loose sand." *Soils and Foundations*, 34(1), 19–32.

Kim, T. (2011). "Incrementally Nonlinear Responses of Soft Chicago Glacial Clays." Northwestern University, Evanston, IL.

Massarsch, K. R., and Fellenius, B. H. (2014). "Ground vibrations from pile and sheet pile driving. Part 1 Building Damage." *Proceedings of the DFI-EFFC International Conference on Piling and Deep Foundations*, Stockholm, 131–138.

Niemunis, A., and Herle, I. (1997). "Hypoplastic Model for Cohesionless Soils with Elastic Strain Range." *Mechanics of Cohesive-frictional Materials*, 2, 279–299.

Seed, H. B., and Idriss, I. M. (1970). *Soil Moduli and Damping Factors for Dynamic Response Analyses*. EERC, 41.

Turkel, B., Orozco-Herrera, J. E., Arboleda-Monsalve, L. G., Nam, B. H., and Jones, L. (2021). "Comparative Analysis of Pile Driving Numerical Modeling Approaches." *International Foundations Congress and Equipment Expo 2021*, American Society of Civil Engineers, Dallas, TX, 484–495.

Wichtmann, T., Fuentes, W., and Triantafyllidis, T. (2019). "Inspection of three sophisticated constitutive models based on monotonic and cyclic tests on fine sand: Hypoplasticity vs. Sanisand vs. ISA." *Soil Dynamics and Earthquake Engineering*, 124, 172–183.

von Wolffersdorff, P. A. (1996). "A hypoplastic relation for granular materials with a predefined limit state surface." *Mechanics of Cohesive-Frictional Materials*, 1, 251–271.

Zapata-Medina, D. G., Vergara, C. Y., Vega-Posada, C. A., and Arboleda-Monsalve, L. G. (2019). "On the use of Fredlund gas–fluid compressibility relationship to model medium-dense gassy sand behavior." *Canadian Geotechnical Journal*, 56(8), 1070–1079.